



HAL
open science

**Electrospinning of chitosan based polymeric systems for
the production of nanostructured scaffolds.
Characterization and potential application in tissue
engineering**

Christian Enrique Garcia Garcia

► **To cite this version:**

Christian Enrique Garcia Garcia. Electrospinning of chitosan based polymeric systems for the production of nanostructured scaffolds. Characterization and potential application in tissue engineering. Chemical and Process Engineering. Université Grenoble Alpes [2020-..]; Universidad de Guadalajara (Mexique), 2022. English. NNT : 2022GRALI049 . tel-03789645

HAL Id: tel-03789645

<https://theses.hal.science/tel-03789645v1>

Submitted on 27 Sep 2022

HAL is a multi-disciplinary open access archive for the deposit and dissemination of scientific research documents, whether they are published or not. The documents may come from teaching and research institutions in France or abroad, or from public or private research centers.

L'archive ouverte pluridisciplinaire **HAL**, est destinée au dépôt et à la diffusion de documents scientifiques de niveau recherche, publiés ou non, émanant des établissements d'enseignement et de recherche français ou étrangers, des laboratoires publics ou privés.



THÈSE

Pour obtenir le grade de

DOCTEUR DE L'UNIVERSITÉ GRENOBLE ALPES

Spécialité : MEP : Mécanique des fluides Energétique, Procédés

Arrêté ministériel : 25 mai 2016

Présentée par

Christian Enrique GARCIA GARCIA

Thèse dirigée par **Frédéric BOSSARD**, Professeur des Universités, Université Grenoble Alpes
et codirigée par **J. Félix Armando SOLTERO MARTINEZ**, CUCEI

préparée au sein du **Laboratoire Laboratoire Rhéologie et Procédés**
dans l'**École Doctorale I-MEP2 - Ingénierie - Matériaux, Mécanique, Environnement, Energétique, Procédés, Production**

Electrofilage de systèmes polymères à base de chitosane pour la production de substrats nanostructurés. Caractérisation et application potentielle en ingénierie tissulaire

Electrospinning of chitosan based polymeric systems for the production of nanostructured scaffolds. Characterization and potential application in tissue engineering

Thèse soutenue publiquement le **14 juin 2022**,
devant le jury composé de :

Monsieur Frédéric BOSSARD

PROFESSEUR DES UNIVERSITES, Université Grenoble Alpes,
Directeur de thèse

Monsieur Jean-Luc SIX

PROFESSEUR DES UNIVERSITES, Université de Lorraine, Rapporteur

Monsieur Patrick CAÑADAS

MAITRE DE CONFERENCE HDR, Université de Montpellier, Rapporteur

Monsieur Franz BRUCKERT

PROFESSEUR DES UNIVERSITES, Grenoble INP, Examineur

Monsieur J. Félix Armando SOLTERO MARTÍNEZ

PROFESSEUR, Universidad de Guadalajara, Directeur de thèse

Madame Emma Rebeca MACÍAS BALLEZA

PROFESSEUR ASSOCIE, Universidad de Guadalajara, Présidente



THÈSE

Pour obtenir le grade de

DOCTEUR DE L'UNIVERSITE GRENOBLE ALPES

**préparée dans le cadre d'une cotutelle entre
l'Université Grenoble Alpes et l'Universidad de
Guadalajara**

Spécialité : **Mécanique des fluides, énergétique, procédés**

Arrêté ministériel : le 25 mai 2016

Présentée par

« Christian Enrique / GARCÍA GARCÍA »

Thèse dirigée par « **Frédéric/BOSSARD** »

codirigée par « **J. Félix Armando/SOLTERO MARTÍNEZ** »

co-encadrée par « **Marguerite/RINAUDO** » et

« **Bernard/LARDY** »

préparée au sein du **Laboratoire Rhéologie et Procédés (LRP)**
et **Laboratorio de Reología**

dans l'École Doctorale **Ingénierie - Matériaux, Mécanique,
Environnement, Énergétique, Procédés, Production (I-MEP-2)**
et l'École Doctorale de **Génie Chimique**.

Électrofilage de systèmes polymères à base de chitosane pour la production de substrats nanostructurés. Caractérisation et application potentielle en ingénierie tissulaire

Thèse soutenue publiquement le « **Mai 2022** », devant le jury composé
de :

Mr. Patrick CAÑADAS

Associate professor, Université Montpellier

Reviewer

Mr. Jean-Luc SIX

Professor, Université de Lorraine

Reviewer

Mr. Franz BRUCKERT

Professor, Université Grenoble Alpes

Examiner

Mr. Eduardo MENDIZABLA MIJARES

Professor, Universidad de Guadalajara

Examiner

Mme. Emma Rebeca MACIAS BALLEZA

Professor, Universidad de Guadalajara

Examiner

Mr. Gabriel LANDÁZURI GÓMEZ

Professor, Universidad de Guadalajara

Examiner

Mr. J. Félix Armando SOLTERO MARTÍNEZ

Professor, Universidad de Guadalajara

Co-director

Mr. Frédéric BOSSARD

Professor, Université Grenoble Alpes

Director



RESUME

L'ingénierie tissulaire représente une approche potentielle pour promouvoir la réparation du cartilage, en utilisant une matrice extracellulaire (ECM) artificielle 3D pour générer de nouveaux tissus. Aucune des procédures actuelles de rénovation du cartilage n'a réussi à obtenir une régénération durable et le tissu a une tendance faible à s'auto-réparer.

Les ECM natives peuvent être efficacement imitées par des membranes de nanofibres électrofilées, notamment en utilisant des polymères d'origine naturelle. Dans ce travail, des systèmes à base de chitosane (CS) (CS et CS/Hyaluronan (HA)) sont transformés, par électrofilage, en matrices nanofibreuses biocompatibles et biodégradables adaptés au développement des chondrocytes. Les matériaux à base de CS sont censés favoriser l'adhésion et la croissance des cellules, fournissant le microenvironnement adéquat pour la préservation du phénotype des chondrocytes.

Des solutions homogènes de CS, HA et du complexe polyélectrolyte CS/HA sont préparées à différents rapports de charge, en utilisant des mélanges acide formique/eau comme solvant. La stabilité du complexe est améliorée par traitement thermique à 120°C. Après ce traitement, les échantillons du complexe CS/HA plus rigides sont obtenus. La cristallisation du matériau et la formation de ponts amides sont liées aux modifications des propriétés.

Pour permettre l'électrofilage, de l'oxyde de polyéthylène (PEO) est incorporé aux solutions de CS et HA. La teneur en PEO dans le mélange est fixée à 30 % en masse et des fibres électrofilées CS/PEO et CS/HA/PEO sont produites, avec des diamètres compris entre 100 et 200 nm. Plusieurs types de collecteurs permettent la production de matrices nanofibreuses avec un arrangement spécifique de fibres visible selon la structure du collecteur. Ces membranes de fibres sont appliquées comme bio-substrat pour la culture de chondrocytes et l'observation de la morphologie cellulaire.

Les mesures effectuées par microscopie à force atomique entre des chondrocytes individuels et le film et les fibres de CS, permettent de comparer la force d'adhésion en fonction de la topographie du substrat. La force d'adhésion cellule-substrat est légèrement supérieure dans le cas du film de CS par rapport aux fibres. Néanmoins, l'adhésion est plus efficace sur les dernières, étant donné que la cellule est en contact avec quelques fibres, compte tenu d'une surface de contact effective plus faible (porosité du support ~40%), alors qu'elle est en contact total avec le film.

Pour la culture cellulaire, l'importance de la stabilisation des fibres de CS, par neutralisation, est mise en évidence. Des tests de prolifération cellulaire, réalisés sur des matrices de fibres de CS, ont révélé que les fibres conduisent à des taux de prolifération plus élevés par rapport aux films.

La topographie des membranes de nanofibres de CS électrofilées pourrait avoir un impact sur les modèles de colonisation cellulaire. L'alignement des cellules dans certaines zones des échantillons de fibres alignées est détecté. De même, une concentration des cellules est observée sur des zones du substrat plus densément chargées en fibres.

En comparant le développement des chondrocytes sur les substrats de CS et CS/HA, on constate que la confluence cellulaire est atteinte plus tôt sur le complexe CS/HA que sur les fibres de CS. Le développement cellulaire pourrait être amélioré par la présence de HA dans le support étant un composant naturel de l'ECM, favorisant l'adhésion cellulaire. Dans les deux cas, des valeurs élevées de viabilité cellulaire (>90%) sont enregistrées.

En ce qui concerne la morphologie cellulaire, les chondrocytes primaires sont contenus individuellement dans le cartilage, conservant une forme ovoïdale. Cette forme est également observée lorsque les chondrocytes sont cultivés sur des matrices fibreuses de CS et CS/HA. Au contraire, les cellules deviennent adhérentes lors de cultures en monocouche sur des surfaces planes telles que des films de même composition et des boîtes de Pétri. La préservation de la morphologie pourrait indiquer la conservation des caractéristiques des cellules natives.

Comme procédure alternative pour l'implantation de cellules/substrats, la faisabilité d'injections intra-articulaires de suspensions de cellules/fibres est étudiée. Les profils de prolifération diffèrent significativement de ceux sur des fibres de CS, différence principalement attribuée à la surface limitée disponible pour le développement des cellules sur la suspension de fibres fragmentées, contrairement à des supports fibreux continus.

En conclusion, l'optimisation du processus d'électrofilage et la caractérisation du matériau ont permis l'utilisation de matrices de nanofibres stables pour le développement des chondrocytes dans le but d'applications de réparation tissulaire. La compatibilité des fibres à base de CS est confirmée et l'efficacité du substrat est comparée en fonction de la topographie du matériau.

Compte tenu des résultats prometteurs obtenus ici, les nanofibres CS et CS/HA peuvent être considérés comme des substrats potentiels conservant la forme native des cellules et des profils de prolifération adéquats. Comme certains patients ne sont pas aptes à subir une intervention chirurgicale, l'approche injectable proposée vise à devenir un traitement réalisable pour la régénération du cartilage.

Electrospinning of chitosan based polymeric systems for the production of nanostructured scaffolds. Characterization and potential application in tissue engineering.

ABSTRACT

Tissue engineering represents a potential approach to improve cartilage mending, where an artificial 3D extracellular matrix (ECM) is essential to generate new tissues. No current procedures for cartilage renovation have successfully achieved long-lasting regeneration and, the tissue shows little tendency for self-repair.

Native ECMs can be effectively mimicked by electrospun nanofiber membranes, specially using natural sourced polymers. In this work, chitosan (CS)-based systems (CS and CS/HA) are transformed, by electrospinning, into biocompatible and biodegradable nanofibrous mats adapted for chondrocyte development. CS materials are claimed to favor cell adhesion and growth, providing the microenvironment adequate for chondrocyte phenotype preservation.

Homogeneous CS, HA, and CS/HA polyelectrolyte complex solutions are prepared at different charge ratios, using formic acid/water mixtures as solvent. Stability of the complex is improved by thermal treatment at 120°C. After this treatment, more rigid samples of CS/HA complex are obtained. Material crystallization and amide bond formation are related to the property modifications.

Enabling electrospinning, 1000 kg/mol polyethylene oxide (PEO) is incorporated to the CS and HA solutions. The PEO content in the blend is set at 30 % w/w and electrospun CS/PEO and CS/HA/PEO fibers are obtained, with diameters ranging between 100-200 nm. Several collector types allow the production of nanofibrous mats with a visible fiber arrangement depending on the collector structure. Patterned fiber mats are produced and applied as a bio-substrate for chondrocyte culture and cell morphology observation.

Atomic force microscopy measurements between single chondrocytes and CS film and fibers, help to compare the adhesion strength as a function of the substrate topography. The cell-substrate adhesive force is found slightly higher in the case of CS film compared to the mat. Nevertheless, adhesion is more effective on the mats given that the cell is in contact with several fibers, considering a lower effective contact area (porosity of the support ~40%), whereas in full contact with the film, the cell expands. For cell culture, the importance of CS fiber stabilization, by neutralization is highlighted. Cell proliferation tests, performed on CS fiber mats, revealed that fiber mats lead to higher proliferation rates compared to casted films.

Topography of electrospun CS nanofiber membranes could impact cell colonization patterns. Cell alignment in certain zones of aligned fiber samples is detected. In the same way, concentration of cells is observed on zones of the mat denser in fibers.

When comparing chondrocyte development on CS and CS/HA substrates, it is found that cell confluency is achieved earlier on the complex CS/HA than on CS fibers. Cell development could be improved by the presence of HA in the support which is a natural component of the ECM, favoring cell adhesion. In both cases, high chondrocyte viability values (>90%) are detected.

Regarding the cell morphology, primary chondrocytes are individually packed in cartilage, maintaining an ovoidal shape. This form is also observed when chondrocytes are cultured on CS and CS/HA fibrous mats. On the contrary, cells become adherent and expanded during monolayer cultures on flat surfaces such as films and Petri dish. Morphology preservation could indicate native cell characteristics maintaining.

As an alternative procedure for cell/substrate implantation, the feasibility of intra-articular injections of cell/fiber suspensions is studied. Proliferation profiles differ significantly from CS fiber mats, mainly attributed to the limited available surface for cell development on the fragmented fiber suspension in contrast with continuous fibrous supports.

In conclusion, electrospinning process optimization and material characterization allowed the use of stable nanofiber mats for chondrocyte development in pursuit of tissue repair applications. The compatibility of CS-based fiber mats is confirmed and substrate efficiency compared as a function of material topography (films, fibers, patterned mats).

Considering the promising results herein obtained, CS and CS/HA nanofibrous mats can be considered as potential scaffolds maintaining native cell shape and adequate proliferation profiles. Since some patients do not fit for surgery, the proposed injectable approach aims to become a valuable treatment for cartilage regeneration.

Mots clés : Électrofilage, chitosane, acide hyaluronane, développement cellulaire, cartilage, régénération tissulaire.

Key words: Electrospinning, chitosan, hyaluronan, cell development, tissue engineering, cartilage.

Laboratoire Rhéologie et Procédés, Domaine Universitaire
363, Rue de la Chimie, 38 610 Gières, France

Laboratorio de Reología,
Centro Universitario de Ciencias Exactas e Ingenierías (CUCEI), Universidad de Guadalajara
3313, Boulevard Marcelino García Barragán, Quartier Olympique, 44430 Guadalajara, Jalisco, Mexique

Thesis contributions

- García García, C. E., Verdier, C., Lardy, B., Bossard, F., Soltero Martínez, J. F. A., & Rinaudo, M. (2022). Chondrocyte cell adhesion on chitosan supports using single-cell atomic force microscopy. *International Journal of Polymer Analysis and Characterization*, 27(1), 71-85.
- Garcia, C. E. G., Lardy, B., Bossard, F., Martínez, F. A. S., & Rinaudo, M. (2021). Chitosan based biomaterials for cartilage tissue engineering: chondrocyte adhesion and proliferation. *Food Hydrocolloids for Health*, 1, 100018.
- Garcia Garcia, C. E., Bossard, F., & Rinaudo, M. (2021). Novel Nanofibers Made of Chitosan/Hyaluronan Electrostatic Complex. *NanoWorld J*, 7(1), 8-12.
- Garcia Garcia, C. E., Bossard, F., & Rinaudo, M. (2021). Electrospun biomaterials from chitosan blends applied as scaffold for tissue regeneration. *Polymers*, 13(7), 1037.
- Garcia Garcia, C. E., Soltero Martínez, F. A., Bossard, F., & Rinaudo, M. (2020). Production of Chitosan/Hyaluronan Complex Nanofibers. Characterization and Physical Properties as a Function of the Composition. *Polymers*, 12(9), 2004.

Manuscript Contents

Introduction to Tissue Engineering. Multidisciplinary tool for specific tissue regeneration.....	10
Chapter I. Literature review	15
1. Cartilage and characteristics	15
1.1. Composition, functioning and pathology	15
1.2. Osteoarthritis	17
1.3. Current treatments and approaches for cartilage repairing	18
1.3.1. Non-pharmacological treatments.....	19
1.3.2. Pharmacological treatments.....	19
2. Polymer-based systems	22
2.1. Chitosan characteristics and properties.....	22
2.2. Hyaluronan characteristics and properties	23

2.3. Polyelectrolyte complex	24
3. The electrospinning technique	26
3.1. Electrospinning mechanism	27
3.2. Process affecting parameters	28
3.3. Electrospinning of chitosan-based systems for tissue engineering	32
Chapter II. Materials and Methods.....	35
1. Obtention and characterization of polymer fibers and films.....	35
1.1. Polymer solution preparation	35
1.1.1. Reagents	35
1.1.2. Studied systems, individual solutions and blend composition	35
1.1.2.1. System CS/PEO	35
1.1.2.2. System CS/HA.....	35
1.2. Fiber production by electrospinning.....	36
1.2.1. Micro-structured collectors	37
1.2.2. Rotatory cylinder	37
1.3. Casting of polymer films.....	38
1.4. Substrate stabilization	38
1.4.1. CS Neutralization	38
1.4.2. Thermal treatment	38
1.4.3. Two-phases fibers by stabilization in Ca ²⁺ bath	39
1.4.4. Solubility and swelling degree	39
1.5. Fiber structure characterization	39
1.5.1. Nuclear Magnetic Resonance (NMR) material characterization	39
1.5.2. X-ray Diffraction	40
1.5.3. Scanning Electron Microscopy (SEM)	40
1.6. Tensile Tests.....	40
1.7. Cell-substrate adhesion strength and energy characterization.....	41
1.7.1. Single cell force spectroscopy	41
1.7.2. Substrate preparation.....	41
1.7.3. Substrate fixation	41
1.7.4. AFM measurements	42
1.7.4.1. Experimental approach.....	42
1.7.4.2. Cell binding	43
1.7.4.3. Analysis of AFM response	44

1.7.5.	Statistical analysis for AFM.....	45
2.	Cell Development on Chitosan-based substrates	45
2.1.	Substrate conditioning	46
2.2.	Cell seeding.....	46
2.3.	Cell detachment.....	46
2.4.	Cell quantification.....	46
2.4.1.	Brightfield/Fluorescence counting	46
2.4.2.	Colorimetry.....	46
2.5.	Cell adhesion protocol.....	47
2.6.	Cell proliferation protocol	47
2.7.	Cell observation.....	48
2.7.1.	Viability test by redox agents.....	48
2.7.2.	Fluorescence staining	48
2.7.2.1.	Markers	48
2.7.2.2.	Cell staining process.....	50
2.7.2.3.	Staining verification by Flow cytometry-FACS	51
2.7.2.4.	Fluorescence microscopy	51
Chapter III. Production, physicochemical properties and cell-interactions of electrospun CS-based nanofibrous materials.....		53
1.	Nanofiber production	53
1.1.	Operating Conditions.....	53
1.1.1.	Optimization of CS/PEO system	53
1.1.2.	Optimization of CS/HA/PEO system.....	56
1.1.3.	Fiber obtention as a function of the collector.....	59
1.2.	CS/PEO and PEC/PEO fiber characteristics	63
2.	Material properties.....	66
2.1.	Solubility and swelling degree.....	66
2.1.1.	System CS/PEO	66
2.1.2.	System CS/HA.....	67
2.2.	NMR Analysis on PEC systems	71
2.2.1.	Film Composition by NMR and Influence of Thermal Treatment.....	71
2.2.2.	Film Made of Complex and Influence of Thermal Treatment	74
2.3.	Behavior under uniaxial tension.....	75
2.3.1.	CS and PEC for thermal stabilization	75

2.3.2.	CS/PEO and PEC/PEO fiber mats.....	77
2.4.	Substrate stability in biological solutions.....	80
2.5.	Cell-substrate adhesion strength and energy	81
2.5.1.	AFM response for cell detachment	82
2.5.2.	Adhesion Energy of chondrocytes on chitosan substrates.....	87
3.	Conclusion.....	89
Chapter IV. Chondrocyte development on chitosan-based electrospun materials.		91
1.	Cell compatibility and viability.....	91
2.	Chondrocyte adhesion.....	93
1.1.	Chondrocyte adhesion kinetics.....	93
1.2.	Parameters influencing cell adhesion	95
2.	Proliferation of chondrocytes on CS fibrous mats.....	96
2.1.	Neutralization step and fiber diameter influence	96
2.2.	Effect of solvent and composition of the blend	98
2.3.	Influence of CS fiber structuration on cell development	100
2.4.	Proliferation measured by colorimetry.....	101
2.5.	Fluorescence staining	102
2.5.1.	Staining assessment by FACS.....	103
2.5.2.	Fluorescence Microscopy.....	104
3.	Proliferation of chondrocytes on PEC fibrous mats.....	110
4.	Conclusion.....	113
Chapter V. Proposed clinical approach. Fiber suspension as an injectable system for cartilage regeneration treatments.....		115
1.	Electrospinning for fiber production.....	115
2.	Fiber stabilization and fragmentation	116
3.	Fiber suspension conditioning and cell culture	118
3.1.	Conditioning.....	119
3.2.	Cell culture, viability and proliferation	119
3.3.	Injection characteristics	122
4.	Evaluation of the approach.....	123
General Conclusions and Perspectives		127
1.	Conclusions	127
2.	Perspectives.....	131
Bibliography.....		133

Introduction to Tissue Engineering. Multidisciplinary tool for specific tissue regeneration.

Tissue engineering is an interdisciplinary field that comprises applying principles of life sciences and material engineering to heal, regenerate and restore the tissue damage. The main purpose is the repairing and creation of tissues and/or organs for the restoration of native functions (Askari et al., 2020). By the early 1990s, the concept of applying engineering for biological tissue repairing resulted in the fast growth of tissue engineering as a wide domain with the potential to revolutionize important areas of medicine (Rogers, 2018).

As part of regenerative medicine, the use of cells, growth factors or signaling molecules, and biologically compatible and active materials are considered tissue engineering guidelines (Rajpoot et al., 2020). By harvesting cells from a patient (or other sources) and seeding onto a tissue scaffold, the cell-scaffold ensemble tends to maturation to become a functional structure. Thus, it could be implanted into the patient to help repair or heal the damaged zone.

The understanding of scaffold composition and organization strongly influences the design of functional constructs. Accordingly, appropriate material architecture and convenient biomaterial/cell set should be carefully selected in order to reproduce the main tissue properties (Bakhshandeh et al., 2017; Mazzoni et al., 2021). In this regard, a wide variety of cells, biomaterials and other supporting components have been investigated to create efficient structures.

Regenerative medicine and tissue engineering have been developed in order to overcome current limitations and find revolutionary therapies. However, scaffold-based strategies have often failed to imitate the complex structures of native tissues.

Most of the mammalian cells are adherent and require a matrix to attach and proliferate. To be successfully used for tissue regeneration, scaffolds should exhibit basic characteristics, such as (i) support cell adhesion, proliferation and differentiation in specific cell lines; (ii) provide the diffusion of oxygen and nutrients from the surrounding environment; and (iii) show clear biocompatibility and do not promote any rejection or inflammation (Biswal, 2019).

Nowadays, biomaterials of very different nature, including ceramics, bio-glasses, polymers, and related composites, are investigated and tested for regeneration of tissues (Mazzoni et al., 2021). In the case of polymers, as a vast and practical material source, the development of composites has enabled the association of natural and

synthetic polymers to develop scaffolds for both, soft and hard tissue repair. In particular, composite biomaterials have been extensively studied for several applications involving skin tissue engineering (Chaudhari et al., 2016), nerve (Shafei et al., 2017), and cardiovascular tissue repair (Ahmed, 2013).

Polymer characteristics are often complemented with the material morphology. Several cell-supporting construct types have been proposed according to the target tissue, final application and structure efficiency. In the context of the scaffold design criteria, the main conventional and advanced fabrication techniques include 3D-bioprinting, additive manufacturing, preparation of porous scaffolds and hydrogel development (Eltom et al., 2019).

Among these technologies, porous ECM-like scaffolds are suitable for regenerating tissues and are frequently produced by electrospinning (Dersch et al., 2005; Wade & Burdick, 2014; Xie et al., 2020).

As an efficient way adopted to build fibrous mats, electrospinning allows the fabrication of non-woven polymer fiber membranes. The relevance of electrospun materials rests mainly on their morphology, since fibers acquire diameters ranging from the nano to micro scales (Balagangadharan et al., 2017). Electrospinning offers some unique advantages, such as a large surface-to-volume proportion (Tong et al., 2012), surface flexibility, high and adjustable porosity of the nanofiber mats (Smith & Ma, 2004), interconnected pores (Jiang et al., 2005) and superior mechanical performance compared to other known forms of the material (Mondésert et al., 2021).

Nanofiber membranes have been applied to understand *in vitro* cell growth for the regeneration of organic tissues. Although they have been investigated as scaffolds for multiple tissue types, nanofibrous matrices for musculoskeletal tissue application is probably the most studied. Included in this category, it is found skin, muscular, bone, nerve and cartilage repairing approaches (S. Chen et al., 2018; dos Santos et al., 2020; Gangolphe et al., 2021; Malik et al., 2020).

Related to cartilage regeneration, a major challenge is faced considering that cartilage shows little tendency for self-repair, injuries remain unhealed for years and can lead to further degeneration. The more common diseases of this tissue, affecting millions on people worldwide, are trauma surgery, rupture or detachment, rheumatoid arthritis, and osteoarthritis (Rai et al., 2017; Y. Wang et al., 2015; Wei et al., 2021).

Several approaches, mainly based on hydrogels and intra-articular injections, to improve cartilage natural mending response have been proposed and tested (Dantas et al., 2021; Maumus et al., 2018; Mohan et al., 2017; Rai et al., 2017; Varady & Grodzinsky, 2016). However, no current pharmacological procedures for cartilage renovation have successfully regenerated long-lasting hyaline tissue to repair lesions, leading to surgical interventions as the viable option (Dantas et al., 2021). Considered as an alternative therapy for articular cartilage defects, artificial three-dimensional (3D) fibrous ECMs have been considered as one of the most promising therapeutic approaches. ECM can be effectively mimicked by electrospun fiber mats, acting as a scaffold adapted for cells to adhere and grow, while cells maintain their original functions and differentiation process is minimized.

To this end, in this project it is proposed to transform, by electrospinning, two chitosan-based polymeric systems: chitosan/polyethylene-oxide (CS/PEO) and chitosan/hyaluronan/polyethylene-oxide (CS/HA/PEO). The produced nanostructured materials, owing to their properties, could favor cell adhesion and growth (Balagangadharan et al., 2017; H. Liu et al., 2017). The electrospinning processing of CS and its blends with different polymers and biopolymers (collagen, alginate, hyaluronan), is frequently proposed in the literature, to produce materials, especially for biomedical application purposes (J.-P. Chen et al., 2012; Z. G. Chen et al., 2010; Haider et al., 2015; Jalaja et al., 2016; Jayakumar et al., 2010; Y. Zhang et al., 2010).

It has been described that the CS/HA hybrid support serves as an ideal biomaterial to create a three-dimensional scaffold with adequate strength, high cellular adhesivity, and excellent support for chondrogenesis, preserving the phenotype and enhancing production of type II collagen (Yamane et al., 2005). Data obtained on CS/HA hybrid fibers indicate that materials including HA provide excellent adhesivity for seeded chondrocytes and enhance their biological behavior on the 3D scaffolds with different pore sizes (Majima et al., 2007; Yamane et al., 2007).

It has been shown that CS presents the microenvironment favoring osteoblast and chondrocyte phenotype preservation, as well (Ching et al., 2021). This character is one of the main concerns about chondrocyte treatments since original cell functions are modified out of the native tissue ECM. It was also found that topography of electrospun membranes of CS nanofibers enhanced attachment, and proliferation during chondrocyte cultivation (Shim et al., 2008). Moreover, the porous material obtained favors cell development due to large surface available allowing also oxygen diffusion and metabolites migration.

Chitosan-based electrospun materials with promising characteristics for satisfactory acceptance in the human body have been in observation, considering antimicrobial and healing properties for use as support in tissue repair (Tonda-Turo et al., 2017). This polymer can induce low biodegradability rates in the body depending on its degree of acetylation (DA) (Yang et al., 2007). Then, chitosan can be considered as a long-term biodegradable material in the body.

Nevertheless, chitosan solutions exhibit some difficulties in terms of electrospinning processing due to their high viscosity and chitosan polycationic nature in acidic solutions, where CS is soluble. Such properties leads to jet break up during the electrospinning procedure (Pakravan et al., 2011).

Avoiding these processing difficulties, without compromising biocompatibility, CS nanofiber fabrication has been attempted using blends with easy spinnable polymers, such as poly(ethylene oxide) (PEO) (Bhattacharai et al., 2005; Corrello et al., 2007; Pratap et al., 2020; Varnaitė-Žuravlioiva et al., 2019). The interaction of the CS/PEO blend has been observed to influence the solution viscosity and interfacial tension, affecting directly the blend spinnability (Lemma et al., 2016; Ridolfi et al., 2017; Varnaitė-Žuravlioiva et al., 2019).

The realization of this work seeks to deepen the understanding of the electrospinning technique, and find the optimal conditions for the obtention of nanofibers of the systems CS/PEO and CS/HA/PEO. In this way, it is necessary to adopt the correct polymer proportions and the appropriate solvent(s) to favor processing. In the case of the CS/HA blend, the choice of solvent should also limit phase separation, a current problem when preparing opposite charged polymer blends.

Aiming to produce stable and durable materials, a high yield of polysaccharides in the blends is maintained. The stability of chitosan-based materials (under fiber and film forms) in aqueous solutions, emulating the physiological environment, is covered in this work. Neutralization step to get pure chitosan fibers is applied in order to assure chitosan stability, this treatment is sometimes neglected when transforming CS in acidic conditions. Considering the relevance of the physicochemical properties on the substrate performance, characterization of the materials in terms of the swelling degree, partial solubility and uniaxial mechanical behavior are carried out.

The main interest of producing chitosan-based fibers stands on the utilization as a biodegradable natural substrate for chondrocyte proliferation and potential cartilage regeneration strategy. In this manner, it is important i) to evaluate the biocompatibility of chondrocytes with the chitosan fiber mat, ii) to observe and assess proliferation rates on the substrates and iii) to study the effect of the matrix topography on chondrocytes attachment, migration, and expansion, in terms of the fiber arrangement in the mat and polymer films as control surface.

The subject is developed in 2 main sections. In chapters I and II, the literature review and materials and methods are presented, Then, in Chapters III-V, the research findings are reported and discussed accordingly to the field of interest: Material preparation and characterization, biological application and treatment strategies for repairing of the target tissue: Cartilage.

Chapter I. Literature review

1. Cartilage and characteristics

In this project, research is focused on an articular cartilage repairing approach. Cartilage is an important tissue in the body with key biomechanical and structural functions. There are three major types of cartilage found in humans: hyaline, fibrous and elastic cartilage. Hyaline (articular) cartilage has a glassy appearance and is the most common form of cartilage in the human body. It is the firm but flexible tissue that covers the ends of the bones in a joint as it is depicted in figure 1.1. This cartilage also gives shape and support to other parts of the body such as the ribs, nose, trachea, bronchi, larynx, and growth plate (Hoemann et al., 2012; Krishnan & Grodzinsky, 2018).

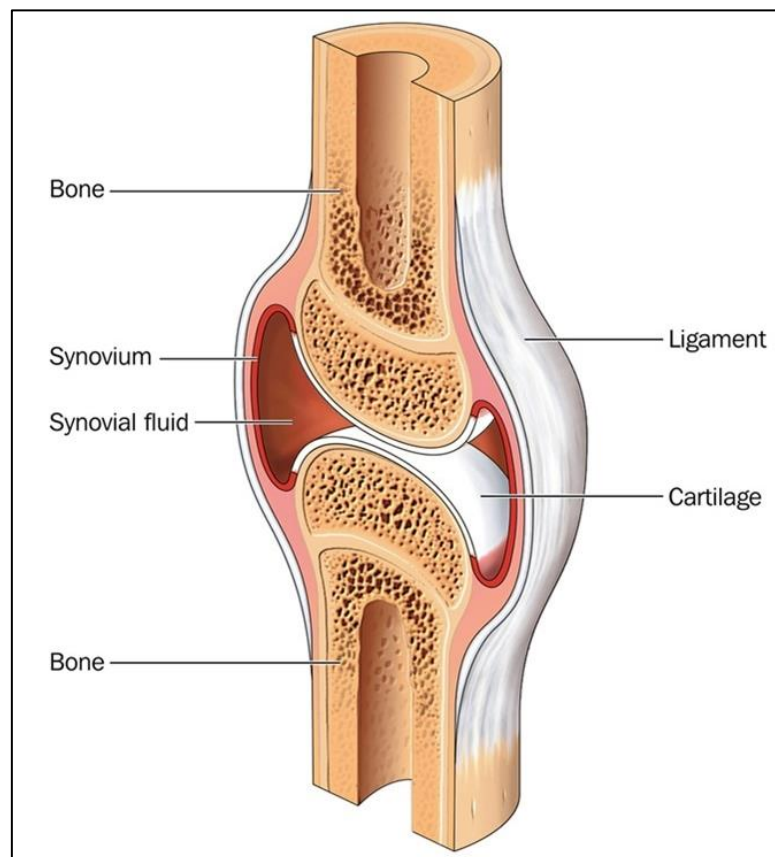


Figure 1.1. Articular joint elements. *Image Credit: Blamb / Shutterstock*

1.1. Composition, functioning and pathology

Cartilage is a non-innervated and non-vascularized connective tissue that helps to distribute the forces of locomotion onto the underlying bone, providing a smooth low-friction surface for joint articulation (C. H. Wu et al., 2010). These properties are furnished by the expanded and highly specialized extracellular matrix. ECM is

predominantly formed by a dense and highly hydrated network of type II collagen fibers and a high content of proteoglycans, mainly with attached hyaluronic acid and chondroitin sulfate (glycosaminoglycans GAG) (Bosworth & Downes, 2011). In general, the fibrillar collagenous network resists tensile and shear forces while the interfibrillar aggrecan resists compression loads and interstitial fluid flow (Hoemann et al., 2012). Considering cartilage composition, water represent the majority of the volume, the rest of component proportions are presented in table 1.1.

Table 1.1 Articular cartilage composition (Bhosale & Richardson, 2008; Krishnan & Grodzinsky, 2018).

Component	Percentage
Collagen (type II collagen mainly)	10-20%
Proteoglycans	10-20%
Chondrocytes	1-5%
Water	65-80%

Articular cartilage is composed of a single cell type, the chondrocytes, which are specialized cells embedded in the ECM, giving them structural and biochemical support (Gao et al., 2014). The main function of chondrocytes is to synthesize and degrade the various elements of the extracellular matrix such as proteoglycans and collagen. Chondrocytes are regarded as mature cells that maintain the cartilage-specific matrix phenotype under low turnover conditions (Mary B Goldring et al., 1994).

The fact that hyaline cartilage, as an aneural and avascular tissue, lacks the ability to generate a typical tissue response to injuries, provokes that cartilage affections remain undiagnosed and unhealed for years. Then, stages such as inflammation, repair and scar remodeling are inexistent and after any overstress or damage, the intrinsic reparative ability of cartilage is very low (Krishnan & Grodzinsky, 2018; Mandl, 2019).

Considering the variety of cartilage diseases, two categories can be identified based on the affected components of the tissue. They involve from extremely common conditions such as osteoarthritis to rare genetic disorders (Krishnan & Grodzinsky, 2018). From one hand, we have direct mechanical trauma to the ECM without damaging the cells, the ability of chondrocytes to synthesize new proteoglycan molecules is not exceeded and cartilage can be restored. From the other hand, the second category involves mechanical destruction of the ECM and cells, which is the

most commonly seen situation in clinical practice and tissue repair depends on external medical factors (Bhosale & Richardson, 2008).

1.2.Osteoarthritis

Worldwide, the most recurrent articular cartilage disease is osteoarthritis, causing substantial personal and health care costs (Murray & Azari, 2015). It is considered as a degenerative rheumatic illness leading to the destruction of the cartilage of one or more joints (Mora et al., 2018; Rai et al., 2017). The joints most frequently affected are the knee, hip, spine and hands. The osteoarthritis physiopathology shows that it is mainly related to an imbalance between the synthesis and degradation of cartilage proteins (Mary B Goldring, 2000; Umlauf et al., 2010), however other factors may also cause the illness, as it is discussed thereafter. Overall, it can be considered as a disease of chondrocytes since they are the main actors in the evolution of this condition. It affects the whole joint, causing synovial inflammation, cartilage damage, bone remodeling, and osteophyte formation (Emery et al., 2019; Loeser et al., 2012).

The prevalence of osteoarthritis has dramatically risen in recent years due to many factors such as the progressive aging of the population, obesity, abnormal physical constraints, but also genetic issues (Dantas et al., 2021). Typical symptoms include pain, muscle weakness, joint instability, brief morning stiffness, and functional limitations (Lawson et al., 2020a; Mandl, 2019). According to epidemiology studies, 654.1 million individuals (40 years and older) were affected by knee osteoarthritis up to 2020 worldwide (Cui et al., 2020), which places this disease as a real public health problem, mostly in developed countries. Osteoarthritis develops in 3 different stages described in table 1.2.

Table 1.2. Main phases of osteoarthritis articular disease (Dantas et al., 2021; Krishnan & Grodzinsky, 2018).

<i>Initial stage</i>	<i>Second Stage</i>	<i>Final stage</i>
----------------------	---------------------	--------------------

<p>It is characterized by an increase in the anabolic and catabolic activity of chondrocytes.</p> <p>Hyperhydration and softening of the cartilage is caused by an overproduction of proteoglycan and small collagen X.</p>	<p>Superficial cracks in the cartilage due to matrix proteolysis are observed.</p> <p>This is caused by a catabolic hyperactivity of chondrocytes which leads to the inhibition of cartilage natural components synthesis. Under these conditions, chondrocytes will proliferate to become hypertrophic and then die by apoptosis.</p>	<p>All the cartilage is destroyed and the subchondral bone is visible, and completely exposed to friction.</p>
---	--	--

1.3. Current treatments and approaches for cartilage repairing

Multiple efforts to fully understand osteoarthritis have been attempted in the last decades. Despite the extensive amount of research regarding this topic, there are still marked controversies but also new findings. Nowadays, osteoarthritis is considered as a multifactorial disease involving aspects like trauma, mechanical forces, inflammation, biochemical reactions, and metabolic disorders (Ayhan et al., 2014). Cartilaginous and non-cartilaginous tissues are concerned at early and advanced stages of the disease, being the source of pain, swelling and then, evident damage.

Osteoarthritis is a progressive and degenerative condition, with low tendency to regress and restore the damaged structures. Big part of the existing treatments aims to control the symptoms unless a clear need of surgical intervention with articulation replacement (Dantas et al., 2021).

Academic and professional associations, such as the Osteoarthritis Research Society International (OARSI), American College of Rheumatology (ACR) and American Academy of Orthopedic Surgeons (Jevsevar, 2013; Kolasinski et al., 2020; McAlindon et al., 2014), have developed standard guidelines in order to suggest the appropriate and available medical actions.

Key treatments against this cartilage disorder are categorized in (i) non-pharmacological and (ii) pharmacological, as a function of the type of management selected (Abramoff & Caldera, 2020; Dantas et al., 2021).

1.3.1. Non-pharmacological treatments

In current clinical practice, non-pharmacological therapies conform the first line treatment for osteoarthritis as suggested by the experts. It mainly includes education, exercise and weight loss (when needed). However, less than 40% of patients with knee osteoarthritis receive this kind of intervention.

Inactivity and disuse are lethal for the health of the joint, the absence of mechanical stimulation induces a more rapid cartilage degeneration due to cartilage softening/thinning, decrease of glycosaminoglycan content, impaired joint mechanics and flexibility (DeFrate et al., 2019; Kloppenburg & Berenbaum, 2020).

Exercise routines should be tailored to every patient's needs/tolerance and preferences. High impact activities should be avoided, and long-term adherence should be maximized to increase success. It is proved that physical activity prevents superior damage and decreases pain, while increasing joint functionality and patient quality life (Maly et al., 2020; Mora et al., 2018). Any other procedure based on manual therapies are included in this category.

1.3.2. Pharmacological treatments

Pharmacological strategies aim to control pain and inflammation, the main symptoms in osteoarthritis. Interactions and side effects are of special attention since the majority of patients are elderly (Mora et al., 2018). In table 1.3, several types of systemic medications, proposed nowadays as treatment for osteoarthritis, are presented and briefly described.

Table 1.3. Pharmacological strategies currently applied for osteoarthritis therapy (Dantas et al., 2021; Kloppenburg & Berenbaum, 2020; Mora et al., 2018).

Approach	Characteristics
Non-steroidal anti-inflammatory drugs	<p>Strongly recommended by OARSI and ACR.</p> <p>Most commonly used medications</p> <p>Long-term oral administration limited due to possible affectation to gastrointestinal, renal and cardiac systems.</p> <p>Topical application is safer with minimal adverse effects.</p> <p>Suggested with glucocorticoid injections.</p>
Corticoid injections	<p>Acts as an anti-inflammatory agent directly on nuclear receptors.</p>

	<p>Corticoids approved for intra-articular injections: Methylprednisolone Acetate, Triamcinolone Acetate, Triamcinolone Hexacetonide, Betamethasone Acetate, Betamethasone Sodium Phosphate, and Dexamethasone. Corticoids have similar performance in terms of pain relief. The latter is related to the drug dosage. More than 3 injections in a year should be avoided.</p>
Opioids	<p>Considered as potent pain-relievers. Produce serious adverse effects. Have small effect on pain and patient physical function.</p>
Extended-release triamcinolone acetate	<p>Aims to prolong pain relief benefit and decrease adverse effects. Triamcinolone Acetate is contained in PLGA microspheres. Analgesic effect lasting up to 24 weeks after dosage.</p>
Nutraceuticals	<p>Food supplements thought to benefit health. Glucosamine and Chondroitin sulphate are commonly used by patients with osteoarthritis. Not recommended by associations guidelines. Low efficacy and effects of insufficient clinical relevance.</p>
Visco-supplementation with hyaluronic acid	<p>It provides viscous lubrication, high absorbing capacity and possible anti-inflammatory/anti-oxidant functions. Effect lasting up to 6 months. Recommendation by drug societies is conflicting. The treatment might be more effective in patients with higher levels of knee pain, younger and with lower cartilage erosion. First single-injection Synvisc-One® approved in 2009 (Muzzarelli et al., 2012).</p>

Since osteoarthritis provokes different reactions and have multiple causal factors, a wide variety of pharmaceutical procedures against the symptoms are available in our days, as can be seen in table 1.3. The recommendation of each treatment is still questionable considering the affectations to other organs and its level of efficiency and acceptance. Besides, all treatments are not long-term solutions to the cartilage disease and chirurgical interventions are considered as last alternative in severe cases.

The surgical procedures performed in osteoarthritis mainly include:

Arthroscopy: Removal of damaged tissues from the joint.

Arthroplasty (Articular Endoplasty): Replacement of the joint surface, removal of the damaged joint and replacement with new plastic or metal implant.

Osteotomy: Correction of the placement of joint surfaces and bones.

Corrective surgeries: In case of extensive joint damage, corrective surgeries are performed to fix the placement of bones and ligaments, improving the function of the limb.

From these options, arthroscopic surgery, specifically knee joint lavage, is the most common procedure performed (Siemieniuk et al., 2017). Nevertheless, it has been demonstrated that arthroscopy presents a low efficacy in terms of pain relief and function improvement in patients suffering from knee osteoarthritis (Reichenbach et al., 2010; Thorlund et al., 2015). Some other disadvantages of this surgery are the increasing possibility of subsequent knee replacement surgery (Rongen et al., 2017) and multiple complications associated with the procedure, including venous thrombosis, infection, pulmonary embolism, and in some cases, death (Thorlund et al., 2015). Clinical practice guidelines strongly recommend against the use of arthroscopy in nearly all patients with degenerative knee disease (Thorlund et al., 2015).

Articular endoplasty is another popular surgery in individuals with advanced knee osteoarthritis. It is a cost-efficient procedure, considered when all non-surgical treatment options were unsuccessful after 6 months of therapy (Higashi & Barendregt, 2011). Although joint replacement is a successful treatment for relieving many symptoms of individuals with knee osteoarthritis, persistent pain after surgery is reported by some patients (Wylde et al., 2011). Individuals with severe osteoarthritis are most likely to report considerable improvements in pain and function after knee replacement, with a recuperation time around 8 weeks (Dowsey et al., 2012).

Even though research in osteoarthritis has been documented for more than 100 years, there are still no successful therapies to stop or reduce the progression of joint degeneration. However, with technological advancements, new approaches and therapies are emerging to aid osteoarthritis patients.

From one hand, domains such as computer technology, could help to reinforce and facilitate data analysis. Consistent databases could provide possible relationships between variables to then propose specific prediction models and design effective personalized therapies (Dantas et al., 2021). Modern technology can help to advance in imaging techniques, analytical electronic devices and sample analysis to obtain real-time data and monitor patients by using mobile equipment (Deveza et al., 2019; M. B. Goldring, 2000; Jamshidi et al., 2019).

From the other hand, biomaterials such as scaffolds, hydrogels, microspheres, and nanofibers associated with cutting-edge advances in cell-based approaches that focus primarily on cartilage regeneration, hold promise in the regeneration of the osteoarthritic joint (M. B. Goldring, 2000; Lawson et al., 2020b). However, robust evidence still scarce regarding this topic.

2. Polymer-based systems

The main properties of the polymers and composites, studied during this research work, are described in the next section. As it has been introduced, tissue engineering is mainly based in 3 aspects; scaffold design, cell line selection and grow factors (active molecules) incorporation. Related to the scaffold preparation, several polymer systems have been proposed for medical applications. The 3D scaffold is critical to preserve cells' properties and constitute a structural template to support new tissue. In this context, systems based on chitosan are claimed to favor cell adhesion and development in tissue engineering models (Balagangadharan et al., 2017; Bhattarai et al., 2005; H. Liu et al., 2017).

2.1. Chitosan characteristics and properties

Chitosan is a partially deacetylated derivative of chitin, consisting of random mixtures of β -(1-4)-linked D-glucosamine and N-acetyl-D-glucosamine in the polymer chain, as it is illustrated in figure 1.2.

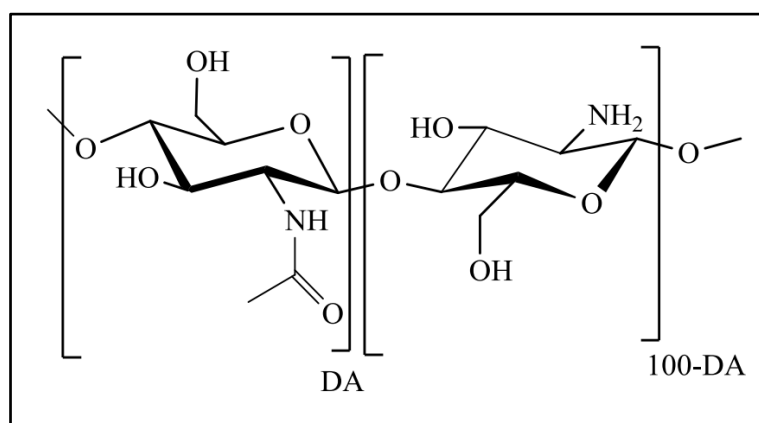


Figure 1.2. Structure of repeat units involved in Chitosan, DA = degree of acetylation (%).

The fraction of the N-acetyl-D-glucosamine units in chitosan determines the degree of acetylation (DA); it is also expressed in percentage of acetylated units. DA has been shown to play an important role on the physicochemical and biological properties of

chitosan. Unlike most of other polysaccharides, the amino groups on the D-glucosamine units are protonated in aqueous acidic solution forming a cationic polyelectrolyte soluble in aqueous medium at $\text{pH} < 6.5$ (Younes & Rinaudo, 2015).

One advantage of CS, compared to other polymers, is that it is obtained from a natural source, and it is a biodegradable and biocompatible polymer with bacteriostatic and antifungal properties (Ridolfi et al., 2017; Rinaudo, 2006). Moreover, under unprotonated form, CS is stabilized by a network of hydrogen bonds in the solid state, which provides good mechanical properties under film or fiber morphology (C. E. Garcia et al., 2020; Garcia Garcia et al., 2018). Chitosan materials with promising characteristics for satisfactory acceptance in the human body have been observation, considering antimicrobial and healing properties for use as support in tissue repair (Tonda-Turo et al., 2017). Chitosan fibrous membranes have been also developed into wound dressings due to its excellent hemostatic properties, antimicrobial activity, and anti-inflammatory responses (Sapkota & Chou, 2020).

Chitosan biological activity studies have revealed that it promotes cartilage matrix compounds expression and reduces the production of inflammatory and catabolic mediators by chondrocytes. In matrix enriched with chitosan, a homogeneous distribution was observed, as well as direct contact between the polymer chains and chondrocytes. It has been observed that chondrocyte homeostasis could be restored after 4 weeks of encapsulation in chitosan matrix (Comblain et al., 2017).

From behavior in solution, protonated chitosan allows the molecular chains to form electrostatic complexes or multilayered structures with other polymers having negatively charged groups. In addition, the presence of amine groups on chitosan makes it possible for specific modifications on C-2 to include functional groups for biomedical applications (Sapkota & Chou, 2020).

2.2.Hyaluronan characteristics and properties

Hyaluronan, also called hyaluronic acid, is an abundant polysaccharide, component of the extracellular matrix of living organisms, widely used in biomedical applications for tissue engineering and regenerative medicine (G. Ma et al., 2012; Petrova et al., 2019; Sandri et al., 2019). HA is a large linear glycosaminoglycan, with typical molar mass of a few million Daltons (Toole, 2001). HA is composed of units of D-glucuronic acid and N-acetyl-D-glucosamine joined alternately by -1,3 and -1,4 anhydroglycosidic bonds (Creuzet et al., 2006; Petrova et al., 2019), as it is shown in represented 1.3.

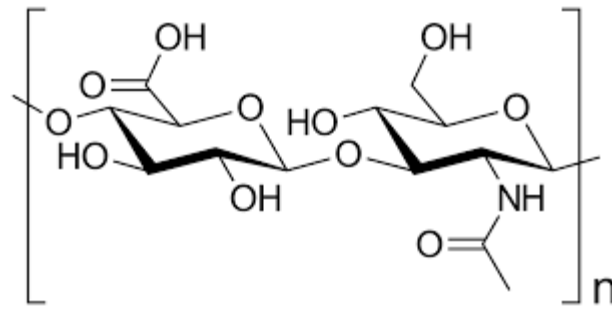


Figure 1.3. Structure of Hyaluronan ($C_{14}H_{21}NO_{11}$)_n

A relevant point of similarity between hyaluronan and partially deacetylated chitin is the N-acetylglucosamine repeating unit present in both polysaccharides. Due to the carboxyl group of the glucuronic acid, hyaluronan is highly negatively charged at physiological pH, and behaves in solution as an anionic polyelectrolyte, with viscoelastic behavior (Almond, 2007; Hillel et al., 2007). HA is highly soluble in water, under the sodium salt form, favored by the disaccharide structure, strongly adsorbing a large number of water molecules, generating intra- and inter-molecule hydrogen bonds, and interactions with aqueous solvents. This provides solutions of entangled HA chains with extraordinarily high viscosity at low concentrations, as well as shear-thinning behavior (Creuzet et al., 2006; Yao et al., 2013).

Hyaluronan can either be secreted by the cells to the ECM or associated with the plasma membrane. As an ECM component hyaluronan is involved in mediating and modulating ECM physical properties, cell adhesion as well as in maintaining osmotic balance and reducing friction in tissues such as the synovium, vitreous humor, and cartilage (Creuzet et al., 2006; Petrova et al., 2019).

Hyaluronan can enhance or block cell adhesion, depending on whether it is present on the cell surface, on the substrate, or on both. It is also involved in the activation of signaling pathways that control cell proliferation, differentiation, adhesion, migration and the entire cell cycle, as well as in processes such as morphogenesis, and inflammation. (Hosseini et al., 2020; Murano et al., 2011; Schaefer & Schaefer, 2010).

2.3. Polyelectrolyte complex

Polyelectrolyte complex (PEC) represents an interesting type of macromolecular materials formed by the association of a polycation and a polyanion (Rusu-Balaita et al., 2003). The formation of PECs is mainly driven by the electrostatic attraction between polymer chains carrying opposite charges (Meng et al., 2017). A strong PEC is obtained if the polyions reach their fully ionized forms. Although other intra- or inter-molecular forces including hydrogen bonding and van der Waals forces may also play minor roles in the complexation process (Cai et al., 2018). In this consideration,

PEC systems are usually difficult to process due to phase separation related to the electrostatic interactions (Iwasaki et al., 2011; Meng et al., 2017; Petrova et al., 2019).

PECs generally contain two distinctive polyelectrolytes, and integrate the respective virtues of both components, offering competitive advantages in their physicochemical properties, enhanced from any single constituent polyelectrolyte (Cai et al., 2018).

PECs made from natural ionic polysaccharides are generally non-toxic, biocompatible and bioresorbable. These properties are valuable for their use in medicine and pharmacy (Cai et al., 2016; Ji et al., 2012). Intensifying attentions on PECs study are aroused in academia and industry since PEC-related fabrication process is mild and materials are ideal vectors for susceptible drugs and macromolecules (D. Wu et al., 2020). They present a wide range of applications, such as encapsulation of substances, drug delivery systems, and waste-water treatment, medical prosthetics, environmental sensors and protein separation systems (Lehmann et al., 2005; Tsao et al., 2011).

PEC scaffolds, have been fabricated by several methods such as gas foaming (Barbetta et al., 2010), phase separation (Nam & Park, 1999), freeze drying (Sadeghi et al., 2008) and electrospinning (Yu et al., 2020). With the integration of a nanostructure, electrospun nanofibers have gained increasing interest as well.

Chitosan, with its unique cationic character, has been used for the preparation of various PECs with natural polyanions such as carboxymethylcellulose, alginic acid, dextran sulfate, carboxymethyl-dextran, hyaluronan, heparin, collagen, pectin, gelatin and xanthan (Bernabé et al., 2005; J. Xu et al., 2013) highlighting potential biomedical applications. For instance, according to *Iwasaki et al.*, chitosan combined with glycosaminoglycans may be a novel class of polyion complex effective for cartilage specific scaffolds (Iwasaki et al., 2011). PECs fibrous mats have been produced from sulfated dextran sulfate sodium-chitosan PEC membranes for high separation performance and hydration ability (X. S. Wang et al., 2015), and chitosan/gelatin nanofiber membranes for wound dressing (J. Xu et al., 2013).

The PEC composed of CS/HA, has been successfully prepared in water/formic acid 20/80 w/w as solvent, and electrospun to produce nanofibers at several $\text{NH}_3^+/\text{COO}^-$ charge ratios (G. Ma et al., 2012). A bilayer chitosan/hyaluronan CS-HA-PEO material was produced by sequential electrospinning of HA-PEO onto a freshly formed CS-PEO layer, with a CS/HA layer thickness ratio of 2:1 (Petrova et al., 2019).

3. The electrospinning technique

Electrospinning is a broadly applied technology for electrostatic fiber formation. It is founded on the application of electrical forces to produce fibers, from both natural and synthetic polymer, with diameters ranging from 2 nm to several micrometers, recovered on a metallic collector (Bhardwaj & Kundu, 2010). A tremendous increase in research and commercial attention on the electrospinning process of polymer solutions has been reached the last two decades, since the first use of this term to describe the phenomenon in 1995 (Doshi & Reneker, 1995; Haider et al., 2018).

In regenerative medicine, polymeric electrospun nanofibers that mimic the structure and function of the natural ECM got interest as potential scaffolding materials with innumerable applications (S. Chen et al., 2018; Malik et al., 2020). Electrospinning has been widely accepted as the simplest and least expensive way to fabricate ultrafine fibers, via a contactless procedure, compared to mechanical drawing, self-assembly and phase separation methods (Garg & Bowlin, 2011). Throughout a simple setup, it involves a practical manipulation, and it allows production of highly porous scaffolds, spun into a variety of shapes and sizes (Garg & Bowlin, 2011). It is considered as an efficient method to produce fibrous mats for cell development (Balagangadharan et al., 2017).

Currently, vertical and horizontal electrospinning setups are the most commonly used. With the constant expansion of this technology, more sophisticated arrangements have been adapted to fabricate complex nanofibrous structures, and to control operating parameters. The typical electrospinning setup consists of three major components: a high voltage power supply, a conducting spinneret and a grounded collecting plate (usually a metal plate, or rotating cylinder) separated at a defined distance (Haider et al., 2018), as depicted in figure 1.4.

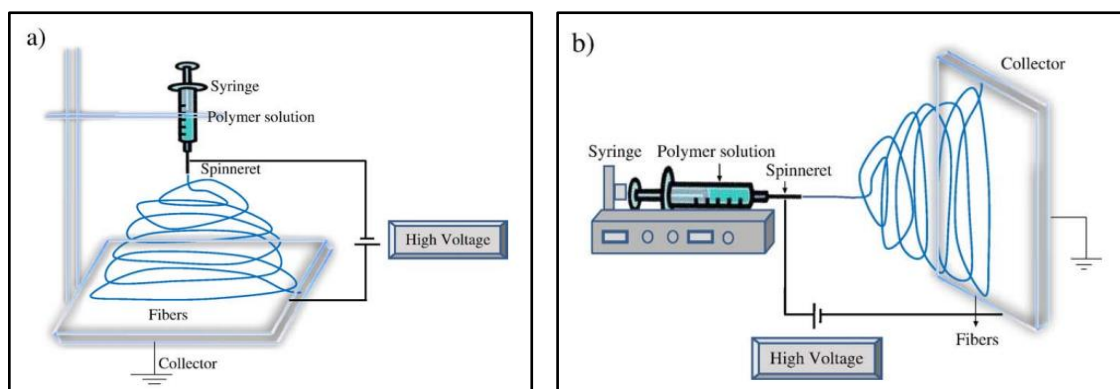


Figure 1.4. Diagram of electrospinning equipment. (a) Vertical setup and (b) horizontal setup (Bhardwaj & Kundu, 2010).

In laboratory, a syringe serves as polymer solution container and the needle tip acts as spinneret. In this way, the system can be fed at a constant and controllable rate with the use of a syringe pump, as it is illustrated in figure 2.1 (*Materials and methods*).

3.1. Electrospinning mechanism

Electrospinning is considered as an electrodynamic process. It is initiated by the application of a high voltage, in the range of 5-30kV, which creates an electric field between the needle of the polymer solution container and the metallic collector (Haider et al., 2018). Then, electric charges move into the polymer solution causing instability due to the induction of charges on the solution droplet, as depicted in figure 1.5A.

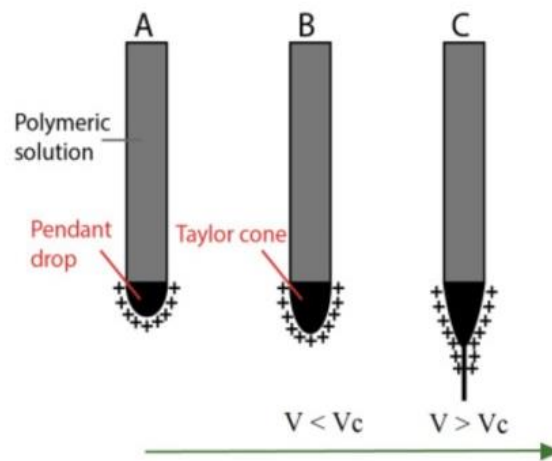


Figure 1.5. Schematic illustration of the Taylor cone and jet formation: (A) surface charges in the polymeric solution; (B) drop elongation; (C) polymeric jet formation (Casasola, 2016). V_c = critical voltage.

With the increasing voltage, the pendant drop, formed at the needle tip, elongates, undergoing two electrostatic forces: electrostatic repulsion between the surface charges and Coulombic force exerted by the external electric field. Then, electrostatic forces in the charged drop will overcome the surface tension, and a conical shape (Taylor cone) will be formed at the nozzle, ejecting a liquid jet once achieving the critical voltage (figure 1.5B-C) (Theron et al., 2004).

The stable jet travels from the droplet to the metallic collector. In this trajectory, internal and external charge forces cause liquid jet whipping, which provokes polymer chains stretching and slipping. After strong elongation and jet thinning, dry polymeric

fibers with diameters in the nanoscale are deposited onto the collector (Haider et al., 2018; Theron et al., 2004).

3.2.Process affecting parameters

Even though electrospinning process has become popular because of its relatively simple setup, smooth fiber formation by electrospinning involves the optimization of several processing factors, solution parameters and environmental conditions (Haider et al., 2018) that influence the complex physicochemical behavior of the system.

The applied electric field, spinneret-collector gap and polymer solution flow rate are considered electrospinning processing. In table 1.4, a description of the process affecting variables is presented.

Table 1.4. Summary of processing parameters and their effect on the electrospinning process.

Parameter	Description
Voltage	<ul style="list-style-type: none"> • Voltage plays a key role in electrospinning, modulating Taylor cone formation. It causes the stretching of a liquid jet during fiber formation. Ultrafine fibers are formed at a critical voltage which varies for each system (Laudenslager, M.J., Sigmund, 2012). • At low voltages, only small beads reach the collector. Further increase of voltage ($>V_c$) might lead to Taylor cone reduced size, reducing the diameter of fibers (Sill & von Recum, 2008). • For too high electric tension, Taylor cone instability and jet break-up are observed, resulting in an irregular fiber morphology (Deitzel et al., 2001).
Tip-to-collector distance	<ul style="list-style-type: none"> • The distance between metallic needle tip and collector influences the force of the electric field, applied during fiber formation, which is indirectly proportional to the electrode separation (Haider et al., 2018). • When increasing the tip-to-collector distance, the electric field strength will decrease, as well as the fiber diameter (Bhardwaj & Kundu, 2010). • Other factors such as evaporation, jet stretching and fiber deposition time could be also affected. Therefore, fiber morphology and diameter might be also disturbed.

Solution feed rate	<ul style="list-style-type: none"> • The flow rate of the polymer from the syringe is an important process parameter as it influences the jet velocity and the material transfer rate (Bhardwaj & Kundu, 2010). • For diluted solutions, by increasing the feed rate, bead size will increase, and no fibers will be formed. • Normally, by increasing the feed rate, the fiber diameter will increase as well, all due to the increased solution volume drawn out of the spinneret.(Z. Li & Wang, 2013). A minimum flow rate is preferred to maintain a balance during fiber obtention.
---------------------------	---

Processing parameters are adjusted for optimal electrospinning and uniform fiber production. Solution properties are equally important for the process and define spinnability of the system. This category involves polymer concentration and molecular weight, viscosity, surface tension, and solvent type, which effect is described in table 1.5.

Table 1.5. Summary of solution properties effect on the electrospinning process.

Parameter	Description
Polymer concentration	<ul style="list-style-type: none"> • For fiber formation, a minimum solution concentration is required and an optimum should be found. At low concentrations, a blend of beads and fibers is obtained. With the increasing polymer concentration, beads transform into uniform fibers. However, high concentration provoke an instable solution flow leading to larger fibers (Bhardwaj & Kundu, 2010). • According to the critical entanglement concentration (C_e) definition, a concentration of around $1-2C_e$ is needed for stable jet maintaining during electrospinning (Chi Wang et al., 2011).
Molecular weight	<ul style="list-style-type: none"> • Polymer molecular weight significantly influences the rheological and electrical properties of the system. In general, high molecular weight polymers are used for fiber fabrication (Bhardwaj & Kundu, 2010) but chain entanglement is also important to consider. • The molecular weight of the polymer reflects the number of entanglements of polymer chains in a solution, thus solution viscosity.

	<ul style="list-style-type: none"> • Too low molecular weight polymers tend to form beads instead of fibers.
Solution viscosity	<ul style="list-style-type: none"> • Viscosity is determining for fiber size and morphology. It is correlated to polymer concentration and molecular weight. Viscosity helps to determine the range of concentrations from which continuous fibers can be obtained (Bhardwaj & Kundu, 2010). • With very low viscosity there is no continuous fiber formation, while very high viscosity results in difficult jet ejection from polymer solution. • The study on the effect of the concentration/viscosity on fiber morphology has reported an optimum viscosity for the generation of PEO nanofibers of 800–4000 cp (Doshi & Reneker, 1995), this range varies for each system.
Surface Tension	<ul style="list-style-type: none"> • Surface tension is a critical factor for electrospinning process. It can be considered as a function of the solvent and the composition of the solution. • Generally, the high surface tension of a solution inhibits the electrospinning process because of jet instability and generation of sprayed droplets. A lower surface tension of the spinning solution helps electrospinning to occur at a lower electric field (Haghi & Akbari, 2007). • Basically, surface tension determines the upper and lower boundaries of the electrospinning window if all other variables are held constant.
Conductivity	<ul style="list-style-type: none"> • When exposed to an applied voltage, polymer jet solutions with high conductivity, show greater tensile force. • Generally, it has been observed that an increase in solution conductivity results in a substantial decrease in nanofiber diameter (Pillay et al., 2013). • By increasing the net charge density of the jet solution, a decrease in the resistivity of the solution is observed (increase of spinnability), as uniformity of nanofibers increases. • Charge density can be improved by adding salts, polyelectrolytes or surfactants to the electrospinning solution.
Solvent	<ul style="list-style-type: none"> • The selection of the solvent is another vital factor for the formation of electrospun nanofibers, since the solvent

	<p>nature and its evaporation kinetics directly influence the fiber morphology and possible pore formation (Haider et al., 2018).</p> <ul style="list-style-type: none"> • For solvent selection, it must be considered that, the preferred solvents are those enabling complete polymer solubilization and have a moderate boiling point. • For consideration, highly volatile solvents are mostly avoided because their high evaporation rates cause the drying of the jet at the needle tip, blocking the needle tip. • Similarly, less volatile solvents are also avoided because their high boiling points prevent their drying during the nanofiber jet flight. The deposition of solvent-containing nanofibers on the collector will cause the formation of beaded nanofibers (Pillay et al., 2013).
--	--

Besides processing and solution parameters, environmental factors such as relative humidity and temperature also affect the diameter and morphology and surface texture of the obtained nanofibers.

Depending on the chemical nature of the polymer, humidity cause changes in the nanofibers diameter by controlling the solidification process of the charged jet. (Haider et al., 2018). A high increase in humidity could led to bead fiber formation and a decrease in spinnability. On the opposite, at very low humidity, a volatile solvent may dry rapidly as the evaporation of the solvent is faster. Sometimes the evaporation rate is so fast than compared to the removal of the solvent from the tip of the needle and this would create a problem with electrospinning (Bhardwaj & Kundu, 2010).

Humidity also plays an important role in the creation of porous nanofibers when a binary solvent system is used. However, a more significant effect is observed in the pore formation during electrospinning of hydrophobic polymers while minor influence is related to hydrophilic polymers (Lancuski, 2013).

Related to temperature variations, it causes two opposing effects to change the average diameter of the nanofibers: (i) it increases the rate of evaporation of solvent and (ii) it decreases the viscosity of the solution. The increase in the evaporation of the solvent and the decrease in the viscosity of the solution work by two opposite mechanisms, however, both lead to decrease in the mean fiber diameter (Bhardwaj & Kundu, 2010; Haider et al., 2018)

3.3. Electrospinning of chitosan-based systems for tissue engineering

Introduced in the past section, electrospinning of chitosan and its blends with other polymers has been widely studied. Applications of the electrospun materials comprise from industrial to medical domains, taking advantage of the valuable properties of chitosan.

Systems based on chitosan materials are claimed to favor cell adhesion and growth for tissue engineering (Bhattarai et al., 2005). Nevertheless, chitosan solutions exhibit some difficulties in terms of electrospinning processing due to their high viscosity and the polycationic nature of chitosan in acidic solutions, leading to jet break up during the spinning procedure (Pakravan et al., 2011). In order to achieve the electrospinning process of chitosan systems, this biopolymer is blended with other synthetic polymers, mainly polyethylene oxide (PEO) and polyvinyl alcohol (PVA), influencing the solution viscosity and chain interactions which affects directly the blend spinnability (Ridolfi et al., 2017; Varnaitė-Žuravliova et al., 2019).

In relation with the main objective of this project, studying cartilage regeneration, a major issue is faced, since generating well-integrated, stable cartilage, presents a real challenge to tissue engineering. In that effort, scaffolds play a key role recreating the extracellular matrix, directing cells to appropriate phenotyping and location. Several approaches and characterization protocols of chitosan-based biomaterials have been proposed in this subject.

CS/PEO electrospun fibers were fabricated using 5000 kg/mol PEO and have been evaluated in terms of chondrocyte gene expression modification as a function of the topography of the substrate. Fiber diameter (from 300 nm to 1 μ m in the obtained fibers) and substrate structure were considered relevant for phenotype preservation, since cells are responsive to their environment once extracted from their native EMC (Noriega et al., 2012). CS/PEO fiber alignment has also been highlighted, since it could lead to pore orientation and promote control load transfer onto the scaffold, for better performance in the articulation (Subramanian et al., 2005). Electrospun CS/Ethylene glycol fibers, forming a 3D-scaffold with nanofibrous walls and micro-sized pores, are claimed to provide a great microenvironment for chondrocyte proliferation towards regeneration therapy (In et al., 2009). Other systems have been studied towards chondrocyte dedifferentiation process and mechanical scaffold enhancement in cartilage tissue engineering, such as electrospun CS-Polycaprolactone scaffolds (W. J. Li et al., 2003) and genipin crosslinked CS/PEO nanofibers (Ching et al., 2021).

Regarding polyelectrolyte complex, a synergic effect is observed on the final material characterization, from physicochemical to biological properties (J. Xu et al., 2013). The PEC obtained from the blend CS/HA is claimed to enhance cell adhesion during cell culture. Moreover, it was demonstrated a significantly higher number of living cells on the surface of the CS/HA compared with CS with a better biocompatibility. However, few references are found related to electrospun CS/HA, reporting better spinnability of the solution at higher contents of CS in the blend (G. Ma et al., 2012). Avoiding phase separation for the system CS/HA, co-axial (H. Ma et al., 2017; Chongyang Wang et al., 2017) and bilayer CS-HA (Petrova et al., 2019) electrospun fiber mats have been proposed in literature, as viable scaffolds for drug delivery and tissue engineering, respectively, as it is presented in *Chapter I, Section 2.3*.

Otherwise, chitosan/hyaluronan hybrid biomaterials proposed in cartilage tissue engineering have been formed by wet-spinning of chitosan solubilized in 2% Acetic acid immersed in presence of calcium solution and coated with hyaluronan (Iwasaki et al., 2011; Kasahara et al., 2008; Yamane et al., 2005). Accordingly with *in vitro* studies, it has been shown that the CS/HA hybrid support serves as an ideal biomaterial to create a three-dimensional (3D) scaffold with adequate strength, high cellular adhesivity, and excellent support for chondrogenesis, preserving the phenotype and enhancing production of type II collagen (with increase of type II/ type I collagen ratio) (Yamane et al., 2005).

Data obtained on CS/HA hybrid fibers indicate that materials including HA provide excellent adhesivity for seeded chondrocytes and enhance their biological behavior on the 3D scaffolds with different pore sizes (see Table 4 of (Iwasaki et al., 2011)). In addition, it is shown that large pores (400 nm) in the structured 3D materials have much better mechanical properties and better cartilage regeneration (Iwasaki et al., 2011; Yamane et al., 2007).

Different from electrospun CS and PEC fibers, cartilage reconstruction has been approached by applying CS-based hydrogels (García-López et al., 2015; Rai et al., 2017; Wei et al., 2021) and scaffolds prepared from other techniques such as wet spinning (Yamane et al., 2005), freeze-drying (Tan et al., 2007; TIĞLI & Gumüşderelioğlu, 2009), lyophilization (Rogina et al., 2021) and recently, bioprinting (Askari et al., 2020).

In this application domain, CS-based electrospun materials are developed towards the production of adapted scaffolds, promoting cartilage healing defects in patients and avoiding illness progression which leads to joint replacement surgery.

Chapter II. Materials and Methods

1. *Obtention and characterization of polymer fibers and films*

1.1. Polymer solution preparation

1.1.1. Reagents

The chitosan (CS) sample was obtained from Northern cold-water shrimp (*Pandalus borealis*) and bought from Primex Ehf (ChitoClear®, Batch TM4778, code 42010, Siglufjordur, Iceland). The CS molecular weight (MW) was measured around 160 kg/mol and a degree of acetylation (DA) of 0.05 was determined using ¹H NMR.

Hyaluronan (HA) sample from Soliance (Pomacle, France) has a weight-average molecular weight MW= 540 kg/mol.

Poly (ethylene oxide) (PEO) with two different molecular weights, 1000 kg/mol and 5000 kg/mol, respectively, were used to prepare the fibrous mat. Acetic acid (AcOH) (≥99.7%) and formic acid (FA) (ACS reagent >98%) from Sigma-Aldrich (Product of Finland, lot #STBJ3705) were utilized as solvent for both polymers.

For substrate treatments, ethanol (EtOH) and K₂CO₃ were purchased from Sigma-Aldrich (France). Similarly, Dulbecco's Phosphate Buffered Saline (PBS), with a pH = 7.4 (ref. 14190-094, Lot 2118924) from Gibco (Made in UK). Deionized water was utilized to prepare the solutions. All reagents and polymers were used as received without further purification.

1.1.2. Studied systems, individual solutions and blend composition

1.1.2.1. System CS/PEO

For this system, two series of polymer solutions were studied at different stages of the research work, based on the influence of the solvent.

Initially, CS and PEO (MW= 1000 kg/mol and 5000 kg/mol) homogeneous solutions were prepared separately at 5% (w/w) in 0.5 M acetic acid, at room temperature with slow stirring for 4 days. CS and PEO solutions were mixed at CS/PEO weight ratios (in %) of 90/10, 80/20, 70/30 and 60/40. The weight ratios are expressed as weight of CS or PEO normalized by the total polymer content.

The same polymer blend was studied using Water/Formic acid (W/FA) as solvent. CS and PEO (MW=1000 kg/mol) homogeneous solutions were prepared separately at 4% (w/w) in W/FA at ratios 25/75, 50/50 and 75/25 (v/v) to obtain stable solutions. Similarly, CS and PEO solutions were mixed at CS/PEO weight ratios (in %) of 90/10, 80/20, 70/30 and 60/40.

1.1.2.2. System CS/HA

The polyelectrolyte complex (PEC) formed with chitosan and hyaluronan was prepared from individual solutions of both polymers. The choice of a convenient

solvent is essential hence W/FA mixtures were selected as previously proposed (G. Ma et al., 2012). Using W/FA 25/75, 50/50 and 75/25 (v/v) as solvents, CS and HA were dissolved to separately get 4% w/w polymer solutions. In these conditions, the total functional group contents were 0.233 $[-NH_2]/L$ in chitosan and 0.1 $[-COOH]/L$ in hyaluronan, respectively. Subsequently, HA and CS solutions were mixed, under stirring, getting a homogeneous blend at several volume ratios corresponding to $-NH_2/-COOH$ charge ratios, $R_c = 0.5, 1, 1.8, 2.35$ and 3.0 .

In order to favor PEC spinnability, the addition of a 4% PEO w/w solution was needed for fiber production. Using the same solvent as for the corresponding biopolymer mixture, final contents in PEC/PEO equal to 80/20 and 70/30 (w/w) were selected such as to preserve a high yield in polysaccharides in the fibers.

1.2. Fiber production by electrospinning

The nanofibrous scaffolds were fabricated by using a conventional vertical electrospinning arrangement, as shown in figure 2.1.

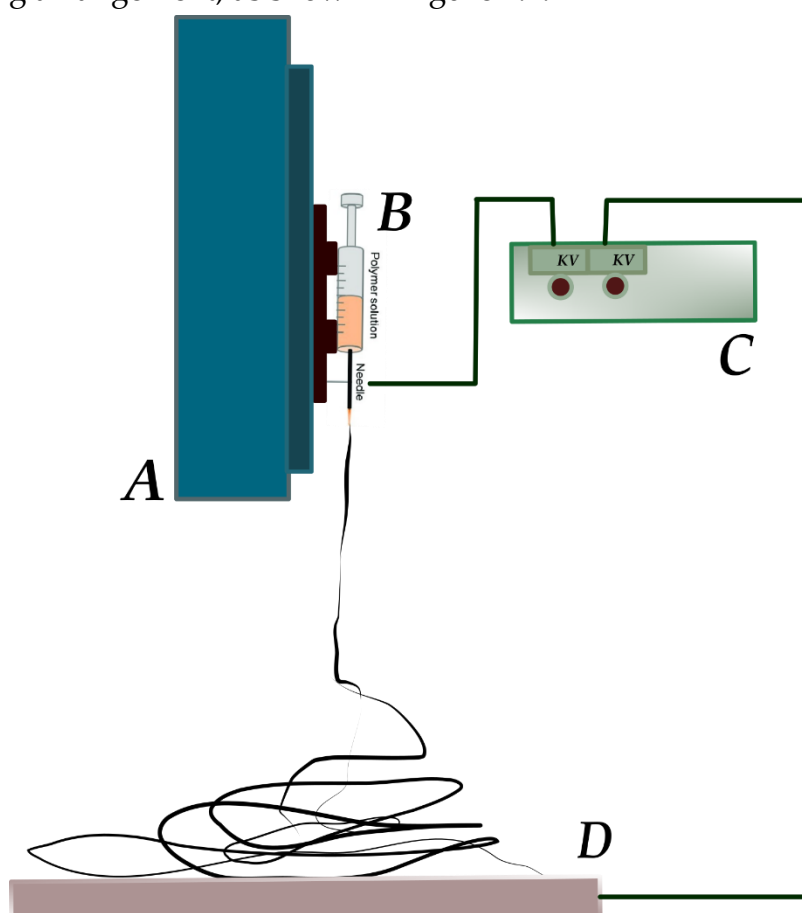


Figure 2.1. electrospinning device for chitosan nanofiber production. (A) Syringe pump, (B) plastic syringe and metallic needle, (C) power supply and (D) metallic collector.

The polymer blend solutions were placed in a 5 mL plastic syringe (figure 2.1B) fitted with a 21-gauge stainless steel needle with an internal diameter of 0.510 mm. The

syringe pump (KDS Legato 200, KD Scientific, Holliston, MA, USA) (figure 2.1A) delivered the polymer solution at a specified flow rate. The electrospinning process was carried out with an applied voltage around 25 kV between the electrodes using a homemade dual high voltage power supplier (figure 2.1C) (± 20 kV, iseq GmbH, Radeberg, Germany).

Nanofibers were recovered on aluminum foil on metallic collectors (figure 2.1D). During electrospinning, A gap of 15-17 cm was left the tip of the needle and the collector surface. Flow rates varying from 0.05 to 1.5 mL/h were applied during electrospinning processing considering the system in study.

Experiments were carried out at room temperature in closed Plexiglas® box with relative humidity ranging between 20% and 60%. The produced nanofibers matrices were left in ambient conditions to evaporate excess of acid and water and reserved for further analyses.

1.2.1. Micro-structured collectors

Several collector types were used for fiber recovery according to further biological analysis proposed. Squared and hexagonal patterned metallic plates utilized for electrospinning are illustrated in figure 2.2.

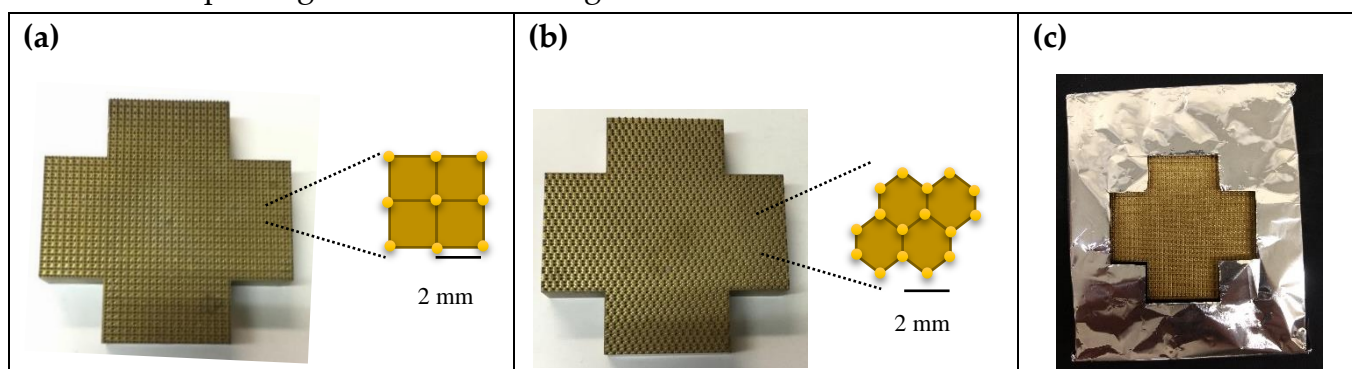


Figure 2.2 Micro-structured metallic collectors assisting fiber collection during electrospinning. (a) Square pattern, (b) hexagonal pattern and (c) collector plus aluminum foil for sample

The metallic micro-structured collectors are composed of regularly distributed peak arrays, forming a particular pattern, as it is shown in figure 2.2. This type of 3D collectors is fabricated by electro-erosion.

Aluminum foils cut in cross have been chosen to remove the mat after processing, avoiding sticking to the metallic support, as shown in Figure 2.2c. In these conditions, the probes for further tests are easy to take out.

1.2.2. Rotatory cylinder

In this study, a cylindrical collector was used for fiber orientation and recovery (Figure 2.3). High speed rotation of the disk (in rpm) can be set by a revolution-counter.

Conductive contact during rotation is maintained by a metallic sheet assuring conductivity between the power supply and the disk surface.

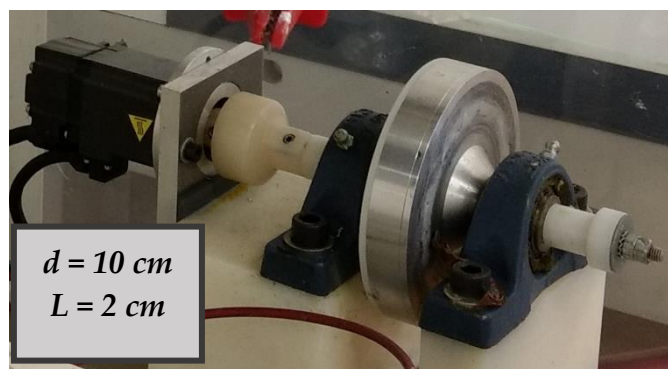


Figure 2.3. Rotatory metallic collector, d = diameter, L = length.

1.3. Casting of polymer films

A constant amount (~1.0 g) of chitosan solution and each of the PEC mixtures was placed in a Teflon mold to obtain uniform polymer films with nearly the same thickness between 40-50 μm (measured with a *Mitutoyo Digimatic* micrometer, with precision of 0.001mm). The probes were stored at room temperature for 3 days until complete evaporation of the solvent until measuring constant dried weight.

Different samples were taken from the films (CS and PEC) for application in cell culture and future measurements of solubility, swelling degree in aqueous medium and cell-substrate adhesion strength measurements. For mechanical properties, rectangular samples were prepared for analysis in wet and dried states.

1.4. Substrate stabilization

Materials based on chitosan and PEC need stabilization steps in order to reduce partial solubilization and render the substrate suitable for application.

1.4.1. CS Neutralization

As-spun nanofiber mats samples were weighted and cut before being immersed in alkaline ethanol/water 80/20 v/v mixture, prepared by dissolving K_2CO_3 until achieving a pH value around 12. This step helps to neutralize the amino groups ($-\text{NH}_2$) in the chitosan chains that are protonated when dissolving CS in acidic conditions (Rinaudo, 2006), eluding solubility thanks to high yield of ethanol. Further, nanofibers membranes were washed during 3 days, four times in a day, with deionized water until neutral pH to remove the salt formed from chitosan solutions, K_2CO_3 excess and PEO. At last, the membranes were dried at room temperature for further stability observations and cell culture tests. The stabilization step was followed for CS/PEO and CS/HA/PEO fibers.

1.4.2. Thermal treatment

As proposed in literature, amide linkage is formed between $-\text{NH}_2$ and $-\text{COOH}$ under controlled thermal treatment (Peniche et al., 1999; Recillas et al., 2011). Chitosan and

CS/HA complex (fibrous mats and films) were treated at 120°C during 4 hours in air conditions for structural stabilization. In electrospun fibers, the heating process was carried out in presence of PEO. On films, as model, the procedure allowed physicochemical characterization.

1.4.3. Two-phases fibers by stabilization in Ca²⁺ bath

In the case of fibers based on two polyelectrolytes, also named hybrid biomaterials, chitosan fiber coating with hyaluronan in the presence of calcium salt has been studied (Dumont et al., 2018; Iwasaki et al., 2011; Majima et al., 2007; Yamane et al., 2005). After electrospinning, CS/PEO nanofibers were immersed in HA solution (1 g/L) during 24 hours and passed through CaCl₂ saturated solution in EtOH/water (80/20 v/v) and washed in deionized water.

The yield in hyaluronan is determined from the weight increase in the dried state. It comes that the mass ratio CS/HA = 1.38, corresponding to a PEC charge ratio R_c = 3.44 (C. E. Garcia et al., 2020). These fibers were swollen in aqueous medium and found fully insoluble. Due to easier control of the polymer composition, homogeneous PEC biomaterials were preferred and no extensive work was performed on core-shell fibers.

1.4.4. Solubility and swelling degree

Stability and swelling degree of the biomaterials (fiber mats and films) were determined at equilibrium in phosphate buffer saline (PBS), at pH = 7.4. For characterization of the complex CS/HA, these properties were also measured at pH=3 and pH=12.

Final dried weight (W_d) compared with the initial dried weight (W_i) allows to control the eventual partial solubility (%). Measurement of material swelling was examined in terms of water loss between swollen state in PBS and final dried weight at room temperature. The wet swollen samples were weighed (W_w) after blotting with tissue paper to remove excess surface water. Accordingly, the dried samples were also weighted repeatedly until the mass became constant (W_d) at room temperature. The measured values correspond to the first swelling and were carried out three times each. The average data were taken for the determination of swelling ratio S, expressed as mass (g) of retained water per gram of dried material, using the following equation:

$$S(\text{g H}_2\text{O/g}) = \frac{W_w - W_d}{W_d}$$

For swelling degree determination, density values of inner solvent and buffer are considered close to density of water.

1.5. Fiber structure characterization

1.5.1. Nuclear Magnetic Resonance (NMR) material characterization

Analysis of the spectra allows the determination of PEC, CS nanofibers and films composition, as well as the presence of PEO and remaining solvent on selected

samples. The yield of PEO remaining in the samples before and after extraction in different conditions (Lemma et al., 2016; Vasiliu et al., 2005) is of especial interest. The weight ratio of chitosan and hyaluronan are also obtained for each PEC studied once solubilized in D₂O. Protons NMR spectra were recorded on a Bruker Avance III 400 spectrometer (Billerica, MA, USA), operating at a frequency of 400.13 MHz for ¹H, processing 5 mg samples, solubilized in 1 mL of D₂O/DCl. Residual signal of the solvent was used as internal standard: HOD at 4.25 ppm at 353 K. Proton spectra were recorded with a 4006 Hz spectral width, 32,768 data points, 4.089 s acquisition times, 10 s relaxation delay and 32 scans.

1.5.2. X-ray Diffraction

Nanofiber mats of CS/PEO oriented fibers were analyzed on X-ray diffraction to confirm fiber alignment as a function of collector rotational speed. The mat was folded several times along the major orientation direction and taped on a sample holder with a pinhole, and X-rayed with a Ni-filtered Cu K α radiation ($\lambda = 1.542 \text{ \AA}$), using a Philips PW3830 generator operating at 30 kV and 20 mA. Diffraction patterns were recorded on Fujifilm imaging plates placed at about 5 cm from the sample and read with a Fujifilm BAS-1800II bioimaging analyzer with 50 μm resolution.

1.5.3. Scanning Electron Microscopy (SEM)

SEM analyses of the samples were performed at CERMAV(CNRS) and CMTC-INP platforms (Grenoble, France). The morphology of electrospun nanofiber membranes samples were observed with a scanning electron microscope FEI Quanta 250, ThermoFischer Scientific TM in CERMAV, and Zeiss ultra 55 SEM FEG (Oberkochen, Germany) in CMTC, both equipped with a field emission gun and operating at 2.5 kV and 1 kV, respectively. The nanofibers samples were coated with 3-4 nm gold/palladium prior to SEM imaging. The average fiber diameter (AFD) was calculated by randomly selected diameter of 500 nanofibers from each sample.

1.6. Tensile Tests

The measurements were carried out using an ARES-G2 rheometer (TA Instruments, New Castle, DE, USA) equipped with grips dedicated to tensile tests. Samples were cut in rectangular shapes (6 mm x 40 mm) from films and the nanofibrous electrospun matrices (randomly oriented and aligned fibers), in order to maintain a free length/width ratio around 2.69. The results are expressed as the Stress σ (Pa) = Force applied (N)/section area (m²).

Tensile tests were performed starting from a zero-applied force until the material presented a breaking point, with a deformation rate of 0.01 mm/s. The experiments were carried out at constant temperature around 25 °C. For tests in the humid state, a cylindrical device around the sample was adopted to maintain the relative humidity in the surrounding environment of the samples.

The rheometer also allowed obtaining the thickness of the samples by measuring the gap between the two plates when they approach film or fiber mat as close as possible until the detector perceives a minimal axial force (0.001-0.01 N) during compression. This measurement was confirmed with a micrometer (Mitutoyo Digimatic micrometer; -25 mm with precision of 0.001 mm) giving very close values. Both techniques used to determine the thickness are in good agreement with a precision of 1 μm .

1.7. Cell-substrate adhesion strength and energy characterization

In order to show the effect of the electrospun chitosan mat topography on cell adhesion strength for further biological interests, force measurements at the nanoscale provided by atomic force microscopy (AFM) have been performed using single cell-force spectroscopy (SCFS). The behavior on fiber mats is compared with the adhesion response on chitosan films as well as a Bovine Serum Albumin (BSA)-coated Petri dish surface as reference.

1.7.1. Single cell force spectroscopy

The method known as single-cell force spectroscopy consists in the immobilization of a single living cell on an AFM cantilever and the measurement of the interaction forces between the cellular entity and a bio-interface, which can be a tissue, another cell or a surface (Puech et al., 2005; Ungai-Salánki et al., 2019). In SCFS, the cell attached to the cantilever is pushed until contact with the substrate or to the other cell, allowing direct measurement of cell-surface or cell-cell adhesion, respectively. Since both spatial resolution and force sensitivity are high, the AFM was the first method able to measure cell adhesion (Puech et al., 2005; Ungai-Salánki et al., 2019).

1.7.2. Substrate preparation

For AFM analysis, the different substrates were taken from the materials already studied. Firstly, chitosan nanofiber mats were prepared through conventional electrospinning of the system CS/PEO at 70/30 (w/w) polymer proportion. PEO with a MW = 1000 kg/mol was used for the blend and 0.5 M acetic acid as solvent. Nanofibrous scaffolds were collected on a square-patterned metallic collector. The so-formed-mats were left at ambient conditions to evaporate the excess of acetic acid and water.

Chitosan films were prepared by casting of a 5% CS solution. After drying, uniform polymer foils were obtained. Both films and fiber mats, were submitted to a neutralization step for CS stabilization. Finally, the substrates were dried at room temperature before being used in AFM measurements.

1.7.3. Substrate fixation

Substrate samples, covering the majority of the circular surface (9.2 cm²) of the culture Petri dish (Techno-Plastic product AG, Switzerland), were selected.

UV curing NOA 68, Norland Optical Adhesive 68 (Lot 319, Norland Products, INC, Cranbury, NJ, USA), was used to stick the solid substrates to the bottom part of the culture dish. Different adhesion points were created by putting a small amount of the product between the substrate and the dish; NOA 68 was left acting during 15 minutes under UV radiation before AFM tests.

In order to have a reference surface for the adhesion response, a culture dish was treated with a 5 mg/mL BSA solution in PBS buffer during 60 minutes. In such a case, the surface was negatively charged in the presence of the PBS buffer (pH=7.4). As culture plates are frequently treated to improve cell adhesion and spreading (Zeiger et al., 2013), control BSA coated surface represents a substrate where chondrocyte adhesion is partially inhibited.

1.7.4. AFM measurements

1.7.4.1. Experimental approach

In AFM, a minute tip is used as a sensor, and the cantilever serves as a transducer to measure surface and force interactions between the tip and the sample by means of cantilever deflection signals. This optical signal can be converted into an electric response by using a photodiode detector with 4 quadrant phases and recorded on a computer. When the AFM cantilever is bent by an applied force during the scanning topography or force measurement, the angle of the deflected laser beam changes and is reflected onto the photodiode detector (Akai et al., 2005). The position of the laser spot moves on the photodiode detector, inducing voltaic signal changes. These signal changes can be read to quantitatively estimate cantilever bending and force. This technique allowed the investigation of the adhesion response of chondrocytes attached to tipless cantilevers on different chitosan supports using normal force measurement in the process depicted in figure 2.4.

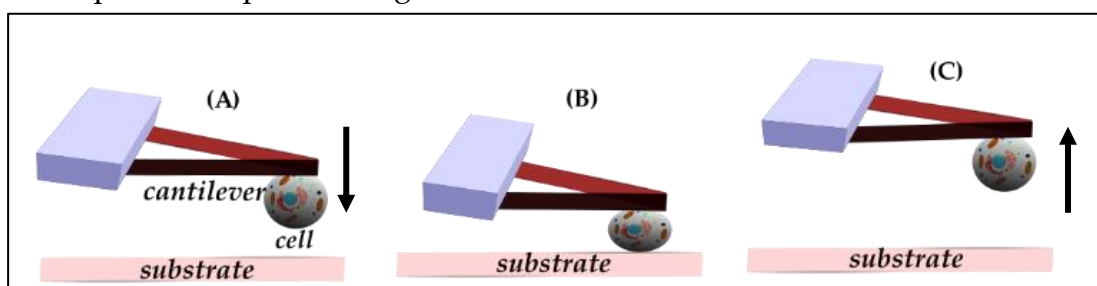


Figure 2.4. Global strategy for the cell adhesion measurements performed in this work. (A) Approach. Chondrocyte is attached to the cantilever and approached to the chitosan substrate at constant velocity. (B) Contact. Chondrocyte is in contact with the substrate during the contact time (t_c) under force (F_c). (C) Retraction. The cantilever is retracted and the cell interaction response is obtained.

The experiments were performed on a Nanowizard II AFM from JPK Instruments (Berlin, Germany). Soft tipless V-shaped commercial cantilevers MLCT-O (Bruker,

France) with a spring constant (k) around 0.01 N/m were used to measure force strength. The spring constant was calibrated following a classical method, first the sensitivity ($\sim 50\text{nm/V}$) was found by contact on a rigid surface, then the method of thermal fluctuations (Hutter & Bechhoefer, 1993) was used to find $k \sim 0.01$ N/m.

1.7.4.2. Cell binding

The global strategy consisted in the attachment of an individual chondrocyte, which was extracted from its original culture medium. The cantilever was pre-treated with several proteins allowing the binding of the cell to the tipless cantilever tip, as depicted in figure 2.5a.

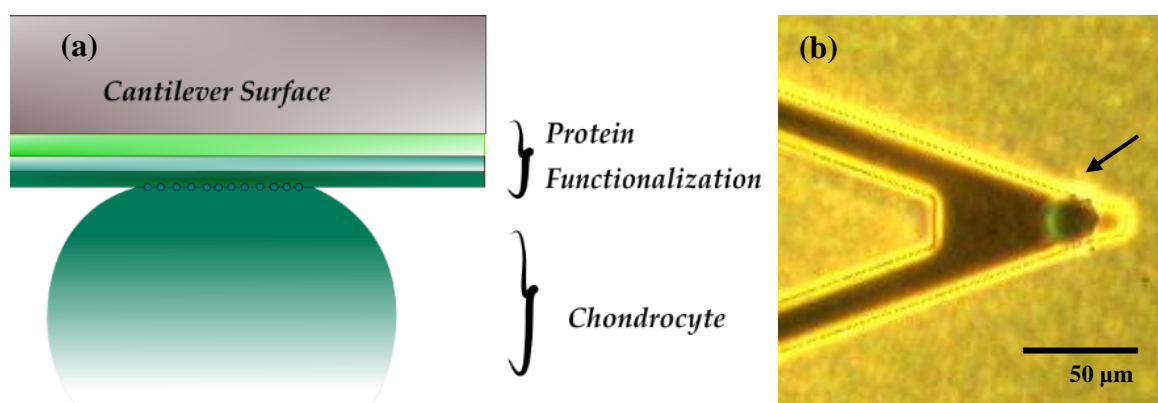


Figure 2.5. (a) Cantilever functionalization for cell attachment prior adhesion measurements. (b) Living chondrocyte adherent to the cantilever tip (as pointed by the black narrow) and placed on the top of chitosan film as substrate. The diameter of the chondrocyte determined by fluorescence cell counting is around 20 μm .

The cantilever functionalization consisted in using Biotin-BSA (an overnight treatment by incubation at 37°C) followed by Streptavidin during 10 minutes under the same conditions, and the final step of the treatment involved the immersion of the tips into a Biotin-conA solution for 10 minutes (Laurent et al., 2014; Sundar Rajan et al., 2017). Intermediate cantilever rinsing with PBS between each step was carried out. The chondrocyte was first captured, as shown in figure 2b, with the cantilever in 2 mL serum-free culture medium at 37°C. Complete culture medium was added and the cell was then approached to the chitosan support which was fixed at the bottom of the Petri dish. During the experiment, physiological conditions (temperature and inner air flow) were maintained. The force set point (F_c) was selected to 500 nN (applied force in the normal direction during the contact time) and the cantilever speed was set to 1 $\mu\text{m/s}$.

As tipless cantilevers are used for this approach, the influence of the cell on the cantilever does not change the cantilever properties (in particular stiffness, k), as shown previously (Laurent et al., 2014). The most important point is that the cell

should be effectively in contact with the fiber mat or chitosan film which is the case according to the force curves obtained by microscopy. Cell membrane damage and deformation were verified after each measured point to avoid adhesive response perturbations.

1.7.4.3. Analysis of AFM response

The system response to the AFM experimental procedure consists in two curves corresponding to the approach and retraction processes. Vertical force F (nN) of the cantilever is represented versus piezo-height (z). The piezoelectric device, placed at height (z) $\sim 15 \mu\text{m}$, moves from its position towards the bottom of the Petri dish until a vertical deflection according to the setpoint is observed. Once the contact time is achieved, the cantilever retracts until the cell is completely detached from the substrate.

When the retraction region is analyzed, we are able to determine the number of significant adhesion events and the forces required to break each adhesion bond. This response could be directly related to the adherent protein distribution (large families of lectins and integrins, for instance) among the cellular membrane. In chondrocytes, they mediate the ability of the cell to develop specific interactions with the ECM and regulate cartilage structure (Changhsun et al., 2008; Toegel et al., 2013).

Each event, representing cell-substrate bond detachments, has a relative position (z) and intensity (Δf). In figure 2.6 a detachment event is exemplified, with a force jump $\Delta f \sim 70 \text{ pN}$ observed at $z = 1.55 \mu\text{m}$ on the retraction curve.

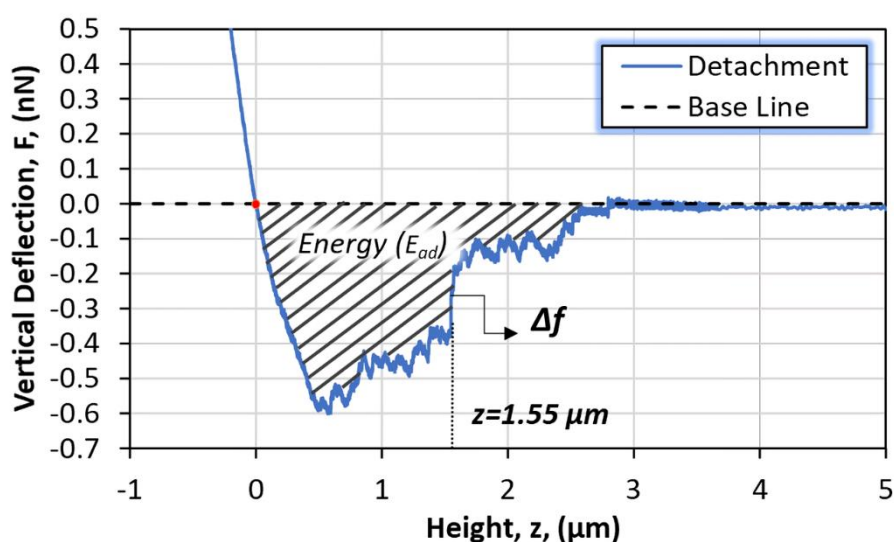


Figure 2.6. Retraction curve analysis. Force jump location (z) and intensity (Δf) for adhesion test of chondrocytes on chitosan supports. Adhesion Energy (shaded area) represented as the integration of force (f) vs. cantilever displacement (z) for the detachment response of chondrocytes on the chitosan film. Contact time = 60 s (García García et al., 2022).

Another relevant aspect, helping to characterize the interaction of chondrocytes to artificial scaffolds, is the adhesion energy (E_{ad}). The adhesion energy represents the detachment work done by the cantilever to completely detach the cell from the substrate. This parameter involves the whole cell contact area and is derived through integration of the area under the force (nN) curve as a function of displacement (z), presented in figure 2.6. In the same context as the other parameters studied, the base line is chosen as the final limiting value, where all bonds are considered detached (Laurent et al., 2014).

Since cell adhesive response can be obtained during short cell-substrate contact time (Laurent et al., 2014; Sundar Rajan et al., 2017); two durations were used at contact times of 60 and 120 seconds. As mentioned before, two chitosan substrates were studied: a casted film as model and an electrospun nanofiber mat with an average fiber diameter around 100-250 nm depending on of the experimental conditions (Garcia Garcia et al., 2018). A reference surface was prepared by coating the plastic Petri dish with BSA. Under the same buffer conditions, zeta-potential indicates that cells are negatively charged.

1.7.5. Statistical analysis for AFM

Data for adhesion assays were generated at three independent experiments, using around 15 contact points on each sample. All results are reported as mean with standard deviation (mean \pm SD) as the error bar. The value $p < 0.01$ was considered statistically significant for comparison between sample groups, and it was obtained by one-way analysis of variance (ANOVA) using Excel.

2. Cell Development on Chitosan-based substrates

For cell culture, the C-20/A4 chondrocyte cell line (Mary B Goldring et al., 1994) was selected as model. Dulbecco's Modified Eagle Medium (DMEM) supplemented with 10% v/v of fetal bovine serum (FBS) and 1% v/v penicillin, streptomycin and a dose of glutamine was used as culture medium. All biological reagents were acquired from Gibco by Life technologies (UK). From the same source, 0.05% Trypsin-EDTA and Phosphate Buffered Saline (PBS) solution with a pH value, measured in laboratory, equal to 7.4 were acquired for cell culture treatments.

Chondrocytes C-20/A4 initial sample was disposed in a culture flask with 20 mL of complete DMEM. Cell sample was preserved into a cell incubator (inCu safe, Panasonic) at 37 °C and 5% CO₂ constant inlet flow during few days until 80-90% of confluence. During incubation, culture medium was renewed every 2 days.

For further cell quantification and seeding on other substrates, cells were detached by trypsinization and resuspended in complete DMEM.

2.1. Substrate conditioning

Samples of fiber mats after neutralization were selected, cut and weighted for cell culture. The nanofiber mats, with a surface of $\sim 1 \text{ cm}^2$, were directly placed in a Petri dish and washed 2 times with the PBS solution to be subsequently hydrated in the DMEM culture solution during 2 days, before cell seeding.

The same procedure was used for cell culture on neutralized CS fibers, CS/HA fibers and CS films as control, depending on the case.

2.2. Cell seeding

From the final cell suspension obtained in DMEM. A volume of $10 \mu\text{L}$ of the suspension with a concentration of $1 \times 10^6 \text{ cell/mL}$, measured by fluorescence (see section *Cell quantification*), was disposed on the substrate (fiber mat or film) followed by the addition of 2 mL of complete DMEM. The samples were preserved into a cell incubator (inCu safe, Panasonic) at $37 \text{ }^\circ\text{C}$ and 5% CO_2 constant inlet flow during few days before cell quantification, the culture solution was renewed every 3 days.

2.3. Cell detachment

For cell detachment, 0.05% Trypsin-EDTA solution was applied. In the case of fibrous substrates, cells were resuspended in DMEM in order to quantify the number of cells as a function of time. The ensemble cell-substrates in culture were placed in a 15 mL conical tube (Falcon™, Fisher-Scientific) and carefully washed twice with 1 mL of in order to remove remaining DMEM solution and unattached cells. Washing was followed by the detachment step consisting in the addition of 0.5 mL of Trypsin-EDTA 0.05% and vortex agitation at 1000 rpm during 60 seconds repeated times. Further addition of DMEM and PBS washings helped to resuspend the extracted cells. Then, cell counting was carried out for adhesion and proliferation analysis.

2.4. Cell quantification

2.4.1. Brightfield/Fluorescence counting

Resuspended detached cells are required to apply this analysis. Therefore, a previous cell detachment step was carried out for the concerned cell-substrate sets. The cell suspension was stained with Acridine Orange/Propidium Iodine fluorescent marker (F230001, Logos biosystems, Villeneuve d'Ascq, France) and cell quantification, in cell/mL, was performed by triplicate, on a dual brightfield and fluorescence cell counter (LUNA-FL, Logos biosystems, Villeneuve d'Ascq, France). This technique allows to identify and quantify the amount of total and living cells, for cell viability calculation. It gives also information about average cell size.

2.4.2. Colorimetry

For cell quantification based on intracellular Iodonitrotetrazolium chloride (INT) reduction, the substrates were disposed in a microtube and washed with $500 \mu\text{L}$ of PBS. PBS rinsing was followed by a 10-second centrifugation cycle at 10000 g. Since

cell detachment from the substrates is not needed, 500 μL of fresh DMEM and 200 μL of the INT solution were added to the sample pellet to be incubated during 1 hour at 37 $^{\circ}\text{C}$.

During incubation, INT is reduced to furazan which is visually identified by its purple-red characteristic color. Then, the culture medium is removed and the substrates washed twice with PBS, alternated with centrifugation cycles. For furazan extraction, 500 μL of DMSO are added. The microtubes are vortexed until complete dissolution of the extract.

Samples were placed on a 96-well microplate by duplicate and absorbance was measured on a UV/Vis microplate spectrophotometer (Thermo Scientific Multiskan Sky Spectrophotometry) at a wave length of $\lambda = 490 \text{ nm}$.

Calibration measurements were performed in order to relate a known number of cells to an absorbance value. One calibration curve was elaborated each measurement to evaluate also repeatability.

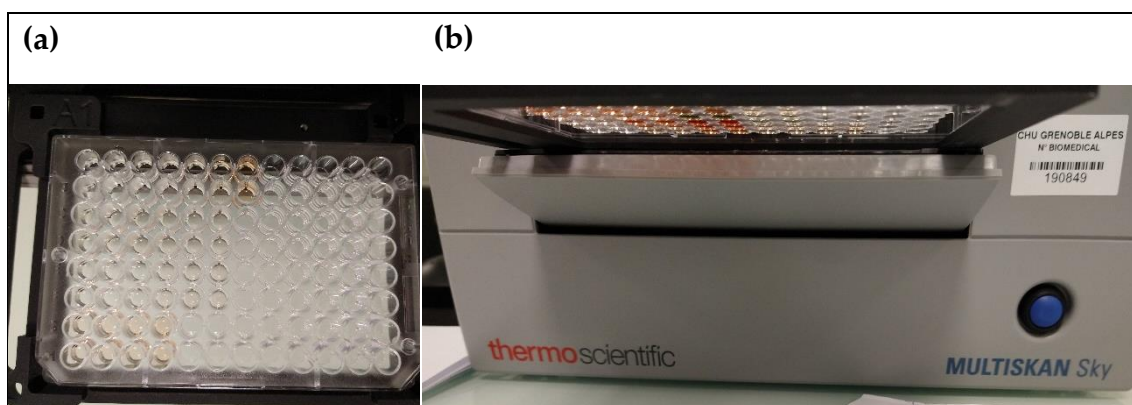


Figure 2.7. Plate schema (a) and spectrophotometer (b) for colorimetry tests.

2.5. Cell adhesion protocol

In order to reduce the quantity of cells out of the substrate, samples for the adhesion analysis were cut following the well shape, with a sample surface around 1 cm^2 . For this study, detachment and counting steps were carried out at times between 1 and 24 hours after cell seeding.

2.6. Cell proliferation protocol

In the case of proliferation analysis, cell counting measurements were performed at longer periods leaving time for cell colonization.

Once cultured, chondrocytes they were detached from the nanofibrous substrates and resuspended in DMEM in order to quantify the number of existent cells as a function of time (t).

Cell counting by fluorescence helped to characterize proliferation rates of chondrocytes attached to chitosan fibers and films. Measurements were performed at

time = 7, 14 and 21 days of culture. Samples were analyzed by duplicate and average values are presented in terms of proliferation rate or detached cells number.

As an improving way for cell development measurements, chondrocyte proliferation by colorimetry was performed. Cell quantities were directly related to absorbance values, by formazan extraction, at different culture times between 1 and 30 days in order to establish the proliferation behavior.

2.7. Cell observation

In order to qualitatively verify cell viability and visualize the presence of cells on CS-based substrates, the samples were treated through several observation techniques and cell development behavior was put in evidence. Procedures are detailed separately in the next sections.

2.7.1. Viability test by redox agents

Cell viability on the surface of the studied substrates was performed by Nitroblue Tetrazolium (NBT) reduction. This specific dye penetrates the cell membrane where reacts with the free oxygen radicals in the cytoplasm. NBT reduction helps to evidence, by coloring, the presence of cell activity and therefore, living cells.

Samples of cell/substrates in culture, were carefully washed twice with PBS and, treated with a 6 mg/mL of NBT solution. Models were observed on a microscope Nikon Eclipse TS100, using magnification 10x and 20x, after 30 minutes of NBT immersion at 37°C in cell incubator.

2.7.2. Fluorescence staining

Adherent cells look transparent in the microscope and are difficult to identify on the substrates. As an auxiliary tool for continuous cell observation, fluorescence staining was applied. Initially, cells were stained with Red-Fluorescent Protein (Red-FP) which apports a fluorescent character in living cells. With the same purpose, cells were marked with Hoechst-33342, which enters in the cell nucleus and emits a blue fluorescence. Details are described in the next sections.

2.7.2.1. Markers

Red-FP staining implies a cell transfection step which is effectuated during cell culture. For this, the defective retrovirus Red-FP is introduced into the cell DNA using the plasmid pLenti-C-tRFP as vector, shown in Figure 2.8.

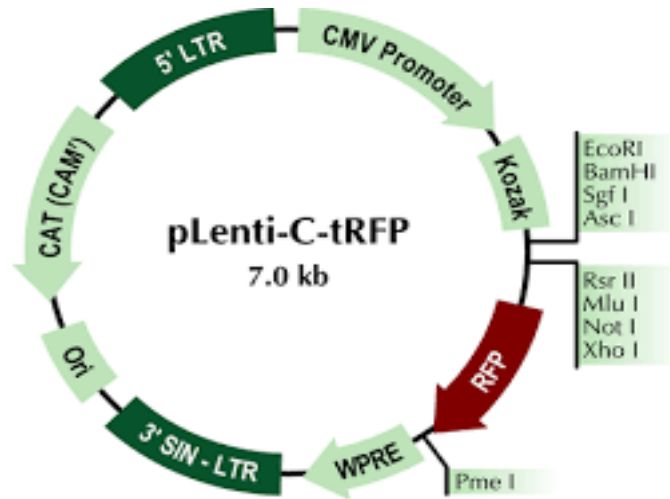


Figure 2.8. Plasmide pLenti-c-tRFP used for Red-FP cell transfection. The incorporated sequence corresponds to 5' LTR → 3'SIN-LTR.

The retrovirus is commercialized by Origen and it encloses a gene that is retro-transcribed in ADN allowing the integration in the hosting cell by the sequences LTR. As a defective virus, a stable transfection is obtained since no more particles of the virus are produced. Once the vector is assimilated and replicated by cells, it allows to express the fluorochrome Red-FP and the cytosol to emit yellow-red fluorescence, when observed under a fluorescence microscope. Red-FP is excited between 488 nm and 532 nm with optimal detection at 588 nm as presented in the excitation/emission spectrum in figure 2.9.

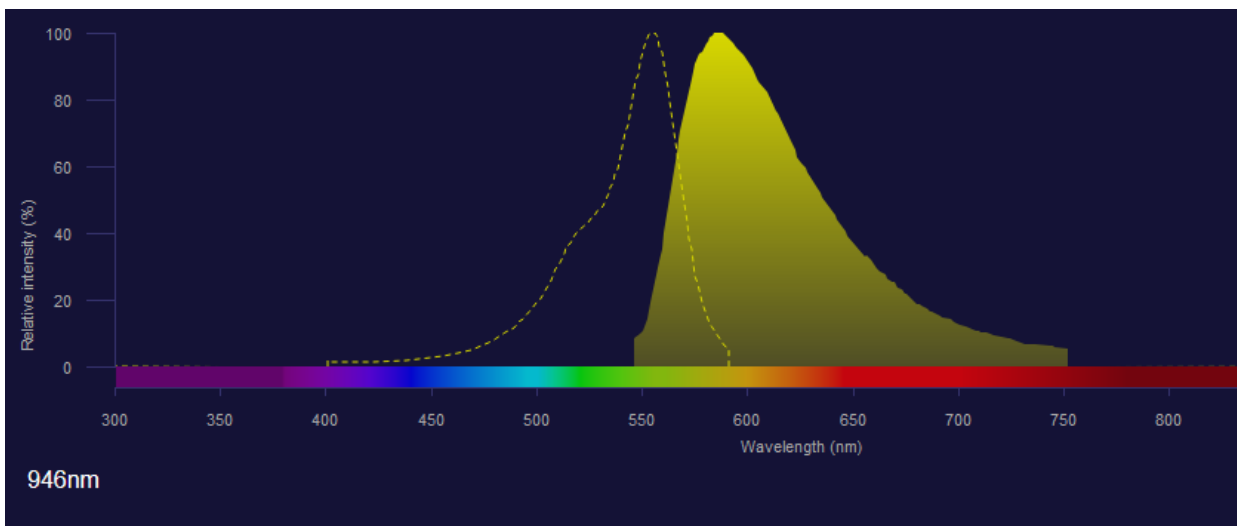


Figure 2.9. Excitation /emission (yellow zone) spectrum of Red-FP fluorochrome.

In order to contrast Red-FP fluorescence, Hoechst marker was incorporated into the cells. It is one of the most popular fluorophores used to stain DNA in living and fixed cells. It binds by specific and non-specific interactions to DNA chain sites. Hoechst

33342 is preferred since it offers greater cell permeability and lower cytotoxicity (Bucevič & Lukinavič, 2018). It is excited at ~360 nm and emits a broad spectrum of blue light with a maximum in the 460 nm region, as shown in figure 2.10.

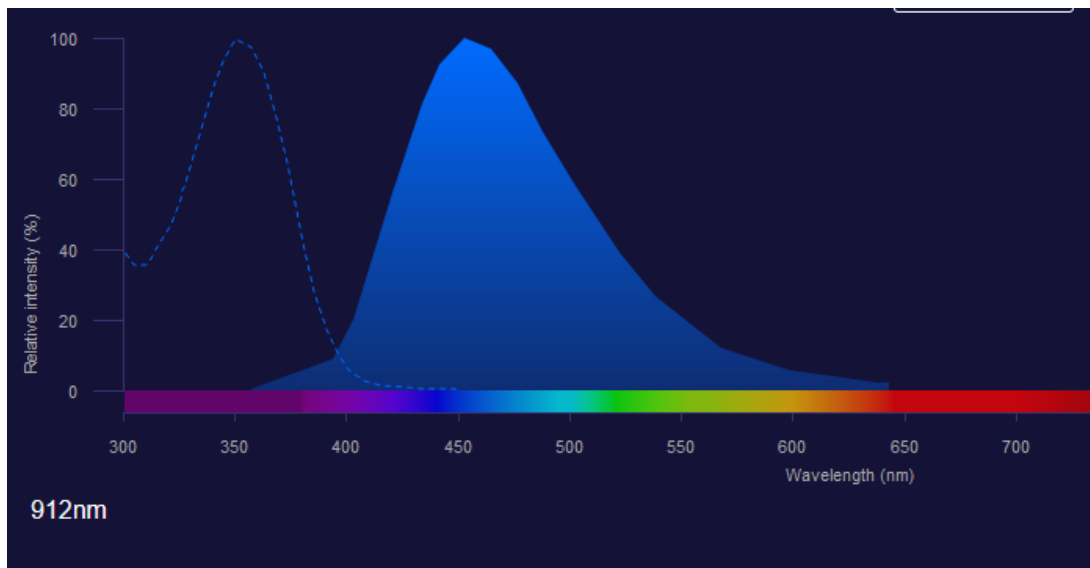


Figure 2.10. Excitation/emission (blue zone) spectrum of Hoechst-33342 fluorochrome.

2.7.2.2. Cell staining process

Initially, Red-FP transfection was effectuated at low cell concentration. Small cell quantity is preferred to favor the integration between the transfecting virus and cells. In this consideration, C20-A4 cells were seeded in a 24-well plate, containing ~ 5000 cell per well. A volume of 10 μL of the pLenti-C-tRFP vector solution, comprising 2×10^7 TU/mL, was incorporated into each of the seeded wells. Then, the ensemble cell/virus was complemented with 500 μL of culture medium DMEM and incubated during 7 days at 37°C and 5% CO_2 inlet flow.

In order to select the wells with the higher proportion of transfected cells, a limit dilution was effectuated. Once identified, transfected cells were seeded in new culture dishes with fresh culture medium until confluence. At the end, cells strongly expressing the Red-FP were harvested and seeded on CS-based substrates for cell observation.

Red-FP staining was coupled with Hoechst dying for microscopy observations. Differently from the former, Hoechst staining is effectuated at the moment of analysis since, with time, the marker can be rejected from the nucleus.

For cell marking, the samples were extracted from the culture medium to be placed in a new culture dish and carefully rinsed with 500 μL of PBS. Then, 1 mL of a Hoechst-

33342 solution diluted 1/1000 was added to the samples and reacted during 7-10 minutes in absence of light before microscopy observations.

Enhancing cell staining with Hoechst 33342, a cell fixation step was included after PBS rinsing. For this treatment, samples were immersed in 1% p-formaldehyde during 30 minutes in an ice bath and in absence of light. Samples were washed with PBS to be stained with the Hoechst dye for further analysis and observations.

2.7.2.3. Staining verification by Flow cytometry-FACS

Flow cytometry was performed in order to assess the transfection process. For this purpose, cell suspensions were prepared from transfected (Red-FP and Hoechst33342) and non-transfected cells. For analysis, the cytometer Becton Dickinson CE-IVD FACSLytic flow cytometer, presented in Figure 2.11, was utilized. It is equipped with 3 lasers having wavelengths of 405, 488 and 640 nm respectively, and allowing the analysis of the fluorescence markers in addition to the size and structure parameters of a cell mixture. Cells are driven by sheath liquid, pass in front of the 3 lasers and the collected fluorescence is then analyzed with the FACSuite software.



Figure 2.11. FACSLytic flow cytometer utilized for cell staining verification.

2.7.2.4. Fluorescence microscopy

For cell visualization, the samples were kept in the well plate and were observed on an inverted fluorescence microscope Nikon Eclipse TS100 corresponding to figure 2.12. Different filters were used conforming to the wavelengths of excitation and emission: Blue. *Excitation:* 325-375 nm/*Emission:* 435-485 nm. Red: *Excitation:* 510-560 nm *Emission:* 590 nm. Images were acquired using the software NIS-Elements (Nikon Instruments).



Figure 2.12. Microscope Nikon Eclipse TS100, used for cell visualization.

Chapter III. Production, physicochemical properties and cell-interactions of electrospun CS-based nanofibrous materials.

The present section is devoted to the production of chitosan-based fibrous substrates as well as a characterization of their mechanical and physicochemical properties up to surface interaction with cells. This could be considered as the first step before material validation and application. Solutions of the polymeric systems CS/PEO and CS/HA/PEO were processed by electrospinning in order to produce homogeneous fiber mats. Blending with PEO is frequently applied to mend low spinnability observed in biopolymers. Stabilization steps of the fiber mats were carried out and verified by analytical techniques. Partial solubility and material morphology, under the further biological environment, were analyzed.

1. Nanofiber production

1.1. Operating Conditions

Fabrication of fibrous substrates by electrospinning is the results of a complete research of the operating parameters of the process. Conditions of electrospinning of the blends CS/PEO and PEC/PEO, were explored in order to fabricate smooth fibers and uniform nanofiber mats with several collector types.

1.1.1. Optimization of CS/PEO system

The system CS/PEO, initially prepared in 0.5 M acetic acid as solvent, was transformed by electrospinning based on previous works and using similar conditions as reference (Lemma et al., 2016). Adequate blend spinnability was observed at several polymer proportions, and fiber mats were produced using PEO with MW = 1000 kg/mol and 5000 kg/mol.

On a second part of the project, it was also found that formic acid could be used as solvent for chitosan and its blends (Iwasaki et al., 2011; Y. Liu et al., 2011). Based on terms of solution preparation, electrospinning of CS/PEO (MW=1000 kg/mol) mixtures was also performed using W/FA 75/25, 50/50 and 25/75 v/v, as solvent. The conditions for electrospinning process of the bends, for both solvents, and the obtained products are presented in table 3.1. and 3.2.

Table 3.1. Summary of global electrospinning conditions for CS/PEO fiber production. PEO MW= 5000 and 1000 kg/mol, solvent: Acetic acid 0.5 M (Garcia Garcia et al., 2018).

CS/PEO	Flow Rate (mL/h)	Tip to Collector Distance (cm)	Applied Voltage (kV)	Electrospun Products
PEO MW= 5000 kg/mol				
60/40	0.7-1.4	15	20-24	<i>Fibers, few beads</i>
70/30	1.4-1.5	15	24-27	<i>Fibers</i>
80/20	0.6-1.0	15	21-24	<i>Fibers</i>
90/10	0.65-0.7	15	20	<i>Fibers</i>
95/5	1.2	15	22	<i>Fibers, few beads</i>
PEO MW= 1000 kg/mol				
50/50	0.06-0.15	14-15	20-22	<i>Fibers</i>
60/40	0.05-0.2	14-15	22-25	<i>Fibers</i>
70/30	0.05-0.2	13-16	24-27	<i>Fibers</i>
80/20	0.05-0.22	13-15	25-28	<i>Fibers, few beads</i>
90/10	0.05-0.2	15-16	26-28	<i>Fibers, beads, droplets</i>

Concerning this polymer blend, when it is prepared with 5000 kg/mol PEO, spinnability was observed to appear at low PEO content, in the range of 5% to 40% w/w compared to 1000 kg/mol PEO. These results are obtained when chitosan of medium molar mass is selected (MW=100-160 kg/mol) (Lemma et al., 2016). High molecular weight polymers are not usually suited for electrospinning process since highly viscous solutions are produced (G. Ma et al., 2012). Working with 5000 kg/mol PEO, allowed the production of fiber mats under elevated polymer flow rates to prevent bead formation. Flow rates are lower in contrast with solutions prepared with 1000 kg/mol PEO as shown in Table 3.1. Nevertheless, fiber production was compromised with solution jet stability and drop falling during electrospinning, then beads and droplets were more commonly found on fiber mats containing 5000 kg/mol PEO.

Table 3.2. Summary of global electrospinning conditions for CS/PEO fiber production. PEO MW= 1000 kg/mol; Solvent: W/FA 75/25, 50/50 and 25/75 v/v.

CS/PEO	Flow Rate (mL/h)	Tip to Collector Distance (cm)	Applied Voltage (kV)	Electrospun Products
Solvent: 75/25 v/v W/FA				

60/40	0.05-0.1	15	28	Fibers
70/30	0.05-0.15	15-17	27	Fibers, few beads
80/20	0.05-0.1	15	28	Fibers, beads
90/10	0.05-0.1	15	28	Fibers, beads, Droplets
Solvent: 50/50 v/v W/FA				
60/40	0.05-0.1	15	28	Fibers
70/30	0.08-0.2	16-17	23-25	Fibers
80/20	0.1-0.2	16-17	21-28	Fibers
90/10	0.05-0.1	15	28	Fibers, beads, Droplets
Solvent: 25/75 v/v W/FA				
60/40	0.05-0.1	15	28	Fibers
70/30	0.08-0.15	16-17	22-25	Fibers
80/20	0.05-0.2	16	24-28	Fibers
90/10	0.05-0.2	15-16	24-28	Fibers, beads, Droplets

Considering the experimental conditions explored for CS/PEO solubilized in W/FA, given in table 3.2, it is constated that PEO 1000 kg/mol favors electrospinning as well as in Acetic acid. Fibers were produced with PEO proportions between 20% and 50% w/w. Because chitosan is soluble in acidic conditions both solvents allowed the obtention of nanofibers at relatively similar electrospinning conditions, especially considering the flow rates.

According to tables 3.1 and 3.2, spinnability increases with the PEO content; drop falling and bead formation reduces as long as the PEO content in the blend is 20% or higher. The uniformity and the presence or absence of beads and spraying on the nanofiber samples was determined by optical and scanning microscopy.

Considering the ensemble of processing conditions and blend composition, it is concluded that the proportions 80/20 and 70/30 w/w CS/PEO were optimal for further fiber production and analysis. A both PEO contents, spinnability is assured and the high yield in polysaccharides in the fibers is preserved. It must be remarqued that more stable jets during electrospinning of CS/PEO solutions were observed when using formic acid as solvent, mainly due to its higher volatility and better

solubilization of the polymers. At the end, the solvent FA was adopted for the electrospinning of the blend CS/PEO.

At last, in order to support the solvent and PEO choice as well as to compare fiber deposition on selected collectors, micro-structured metallic supports were utilized for electrospinning of the blend CS/PEO. The process was carried out under the conditions already described and the mats produced are shown in figure 3.1.

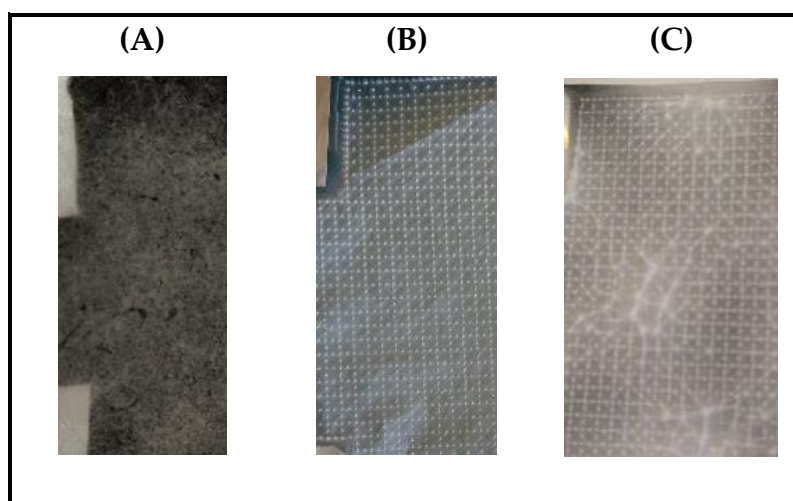


Figure 3.1. Electrospun fiber mats produced from the systems CS/PEO 70/30 w/w using (A) 5000 kg/mol PEO in 0.5 M AcOH, collection time = 60 min (Garcia Garcia et al., 2018) (B) 1000 kg/mol PEO in 0.5 M AcOH, collection time = 35 min (García García et al., 2022) (C) 1000 kg/mol PEO in 50/50 FA/W, collection time = 25 min. Fibers recovered on square patterned collector.

In Figure 3.1, two distinctive results are observed depending on the PEO molecular weight present in the blend. At the macroscale, the pattern of the collector was not strictly replicated by the fibers obtained with solutions containing 5000 kg/mol PEO, thus the fiber mat looked randomly oriented. On the contrary, solutions prepared with PEO 1000 kg/mol (in both solvents, acetic and formic acid) allowed the production of thinner nanofibers. These mats dry more rapidly during jet stretching, permitting to evidence the structure of the corresponding collector used for fiber recovery (figure 2.3). Operation conditions and fiber obtention as a function of the collector type are covered in next sections.

1.1.2. Optimization of CS/HA/PEO system

The system CS/HA is characterized for the formation of a polyelectrolyte complex (PEC) due to electrostatic interactions between the polyanion, HA with -COOH

groups, and polycation, CS with $-NH_3^+$ groups in acidic conditions. Electrospinning of PECs is challenging because of phase separation when the blends are prepared. For this reason, the stability of the mixture was firstly studied in several acidic solvents and homogeneous final blends were observed when using FA for solution preparation.

Electrospinning of the CS/HA complex, in different charge ratios, was possible when PEO, MW=1000 kg/mol, was blended with the prepared PEC solutions. Spinnability of the system appears, and fibers were obtained as long as the proportion of PEO in the final polymeric mixture is equal or larger than 20% w/w. Other characteristics like uniformity (beadless morphology) increased with the chitosan content in the initial PEC solution as it is furtherly presented in Table 4.3. To our knowledge, it is the first time that nanofibers are produced with the CS/HA polyelectrolyte complex with variable controlled charge ratio.

In order to optimize the production of nanofibers at high yield in PEC, different experimental conditions were explored in order to fabricate smooth fibers and uniform mats. In Table 3.3, the range of the more appropriate parameters for the electrospinning process, allowing the obtention of fibers without spraying are presented. Nanofiber formation was studied in solutions using water/formic acid 75/25, 50/50 and 25/75 v/v as solvent for polymer (CS, HA, PEO) solutions. Likewise, the proportion PEC/PEO for fiber production was fixed at 70/30 w/w.

Table 3.3. Experimental conditions for electrospinning process of CS/HA/PEO blends in W/FA as solvent.

Charge Ratio NH ₂ /COOH	Weight Ratio NH ₂ /COOH	Flow Rate (mL/h)	Tip to Collector Distance (cm)	Applied Voltage (kV)	Electrospun Products
Solvent: 75/25 v/v W/FA					
0.5	0.21	0.05– 0.15	15-17	22-27	Fibers, beads, droplets
1.0	0.42	0.09– 0.15	16–17	25-26	Fibers, beads
1.8	0.77	0.11–0.2	17	23-24	Fibers, few beads
2.35	1.0	0.1–0.15	16–17	21–28	Fibers
3.0	1.26	0.09– 0.17	15–17	21–25	Fibers
Solvent: 50/50 v/v W/FA					

0.5	0.21	0.08– 0.12	17	18–25	Fibers, few beads
1.0	0.42	0.15–0.2	16–17	24–26	Fibers
1.8	0.77	0.15–0.2	17	24	Fibers
2.35	1.0	0.10– 0.15	16–17	21–29	Fibers
3.0	1.26	0.12– 0.17	16–17	21–23	Fibers
Solvent: 25/75 v/v W/FA					
0.5	0.21	0.08– 0.13	17	25	Fibers, few beads
1.0	0.42	0.11– 0.15	17	24–27	Fibers
1.8	0.77	0.1–0.14	17	24	Fibers
2.35	1.0	0.12– 0.15	16–17	20–24	Fibers
3.0	1.26	0.14–0.2	16–17	20–25	Fibers

From table 3.3, it is observed that the systems were processed by electrospinning under relatively close parameters for PEC/PEO and CS/PEO in presence of FA. In this research, electric fields of more than 20 kV between electrodes are applied for CS and PEC fiber formation which is relatively high compared to uncharged polymeric systems from which PEO and PVA (Filip & Peer, 2019; Na et al., 2012).

The influence of the solvent resulted important for PEC electrospinning while it was unnoticeable for PEC solutions stability. Water/ Formic acid 50/50 and 25/75 v/v allowed fiber production for the PEC charge ratios proposed between 0.5 and 3.0. On the opposite, when using W/FA 75/25 v/v, more beads of several forms appeared on the fibrous structure of the mat, mainly attributed to Rayleigh stabilities of the jet solution during processing (Zuo et al., 2005).

As applied for CS/PEO electrospinning, the square patterned collector was adopted for PEC/PEO. Fiber matrices were easily recovered from the metallic support helped with aluminum foils cut in cross as presented in figure 3.2. After processing, the mats were removed and samples were possible to handle and prepare for further analysis.

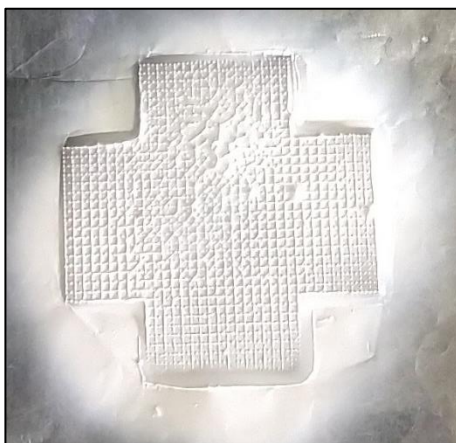


Figure 3.2. CS/HA/PEO nanofibers on metallic collector (square patterned) utilized for the electrospinning process. Yield in PEO = 30% w/w.

From figure 3.2, it could be mentioned that the pattern of the metallic collector was macroscopically visible on the mat. However, when fiber time deposition increases so as the fiber density, the collector structure saturates and the pattern in the mat is slightly lost. It was observed that long fiber collection times (>10 minutes), on a unique spot, could lead to thick fiber mats with random orientation in the upper fiber layers.

For further studies, the electrospinning was carried out with solutions prepared in water/formic acid 50/50 v/v. PEC/PEO solutions in W/FA 25/75 v/v could dry at the tip of the needle and cause syringe blocking, due to extremely high solvent volatility and low flow solution rates during the process.

In terms of composition, the NH_2/COOH ratio in the blend could affect importantly the stability of the final material in aqueous medium. As it is demonstrated in subsequent sections of this chapter, the solubility of the PEC decreases with the increasing of NH_2 groups in the blends i.e., the chitosan content. In this way, electrospinning of fiber mats with higher proportion of CS are preferred. Thus, procedures and analysis are focus on one CS/HA ratio (weight ratio= 1.0, charge ratio = 2.35).

1.1.3. Fiber obtention as a function of the collector

In consideration of the preliminary knowledge of the CS/PEO and PEC/PEO electrospinning, the process was optimized for different collector types in order to contrast final material properties based on fiber arrangement (for final material application). In the overview, the established conditions for further fiber production are presented in table 3.4.

Table 3.4. Set parameters for fiber production based on previous experimentations.

Parameter	Set value/condition
CS/PEO and PEC/PEO composition for electrospinning	70/30 w/w (and 80/20 for some analysis)
Solvent	FA 50/50 v/v
CS/HA = PEC composition	Charge ratio = 2.35

One of the interests of fiber orientation or structuration is the modification of their mechanical performance. In the case of biological applications, our main goal in this project, this specific arrangement of fibers could lead to preferential cell attachment and development.

Fiber mats were prepared directly on aluminum foil where fibers are randomly oriented, two structured collectors, with square and hexagonal patterns, were utilized for fiber deposition as well. Finally, the fiber alignment on a rotatory cylinder as collector was also studied. The ensemble of operating conditions for the electrospinning process is summarize in table 3.5.

Table 3.5. Summary of electrospinning conditions for CS/PEO and PEC/PEO fiber production for each collector utilized.

Collector	Flow Rate (mL/h)	Tip to Collector Distance (cm)	Applied Voltage (kV)	Electrospun Products	Rotational speed
CS/PEO 70/30					
Aluminum foil	0.08-0.12	15-17	22-24	Fibers	NA
Squared pattern	0.08-0.15	15-17	22-25	Fibers	NA
Hexagonal pattern	0.08-0.12	15-17	22-25	Fibers	NA
Rotatory cylinder	0.08-0.1	17	25-28	Fibers	From 700-1500 rpm
PEC/PEO 70/30					

Squared pattern	0.08-0.12	15-17	22-26	Fibers	NA
Rotatory cylinder	0.08-0.1	17	24-28	Fibers	1500 rpm

Homogeneous processing conditions were observed for fiber production on varied metallic collectors with minor deviations for rotatory collector, specifically the voltage applied for electrospinning. Slightly higher electric tension was needed for electrospinning when the rotatory collector was employed.

For the CS/PEO system, during rotatory collection of fibers, their alignment was observed under microscope. At low speed (700 and 1000 rpm) fibers resemble more to a random arrangement, on the contrary at 1500 rpm, they were clearly aligned. It has been established in literature that gradual fiber alignment increases with the rotational velocity (Eslamian et al., 2019; C. Y. Xu et al., 2004), then a maximal orientation is achieved. Those variables are closely related to the fiber diameter and molecular arrangements within the fiber (Baji et al., 2010).

X-Ray Diffraction study was employed to investigate the molecular orientation and degree of crystallinity of fibers recovered on rotatory collector, reflection patterns are shown in figure 3.3.

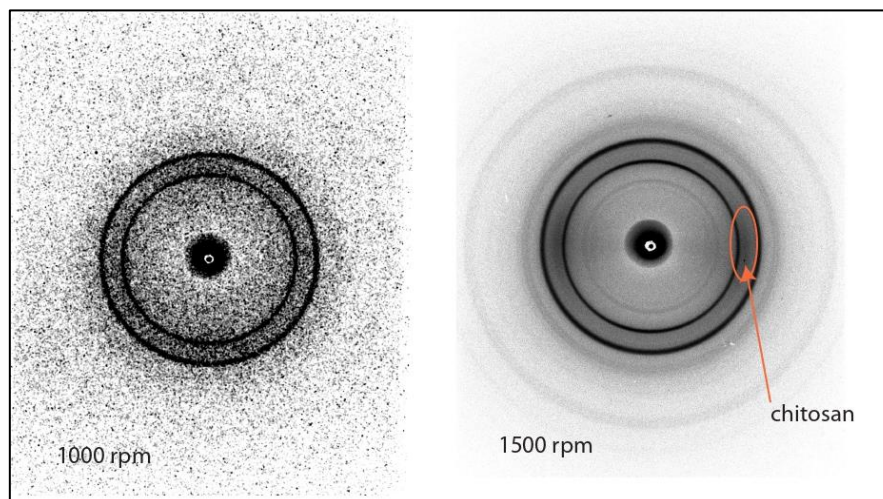


Figure 3.3. Two-dimensional XRD patterns for reflections of 70/30 CS/PEO fibers, aligned at 1000 and 1500 rpm.

From the patterns in figure 3.3, the diffraction arcs of the equatorial reflection (circled in orange) suggest that the crystal planes in the nanofibers are oriented in a specific direction. It is indicated that the degree of crystallinity in the aligned fibers at 15000 rpm was higher than that of their counterparts at 1000 rpm. Therefore, crystals might

be oriented parallel to the fiber axis in the aligned CS/PEO fibers at 1500 rpm, as well as the polymer chains (Alfaro De Prá et al., 2017; X. Wang et al., 2013).

Aligned fiber obtention was fixed at 1500 rpm, considering that too elevated rotational speeds could lead to fiber fragmentation before complete fiber deposition. It has been established that fiber diameter decreases with the increasing collector speed (Thomas et al., 2006).

Regarding the micro-structured collectors, they were observed to define the arrangement of fibers with identifiable patterns in the macroscale in contrast to other collectors such as aluminum foil or rotatory cylinders, as it is shown in figure 3.4.

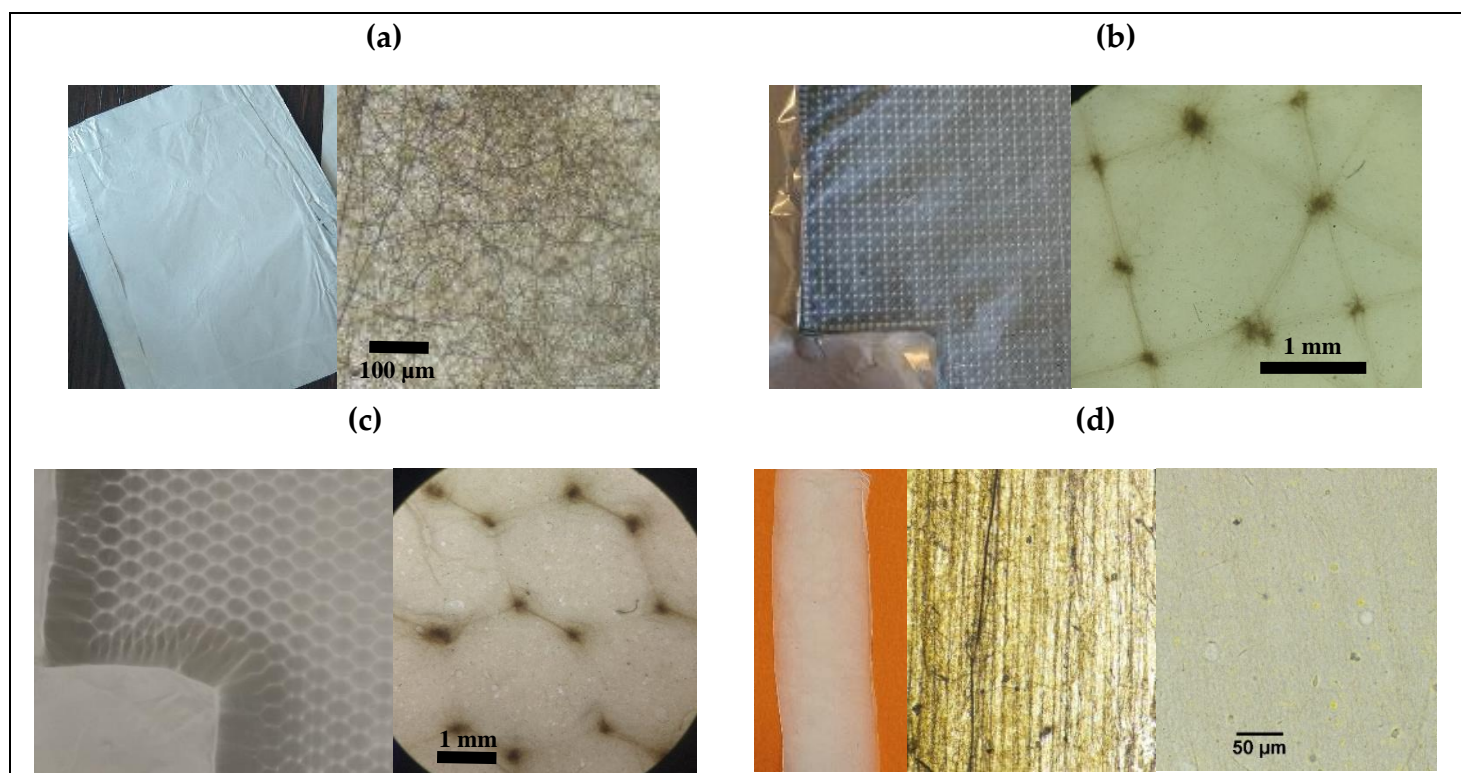


Figure 3.4. CS/PEO 70/30 fiber mats collected on several collectors. (a) Fibers on the aluminum foil (randomly collected fibers), (b) fibers on squared patterned metallic collector, (c) fibers on hexagonal patterned and (d) aligned fibers from rotatory cylinder.

Randomly oriented fibers are the intrinsic result of electrospinning. This is affected just by changing the collector topography as it is contrasted in figure 3.4. On the cylinder, polymer fiber mats are collected accordingly to the rotational speed and cylinder dimensions obtaining visible aligned fibers as previously discussed.

On square and hexagonal patterned collectors (figure 3.4bc), fibers were found more densely deposited on the metallic peaks and between neighboring peaks, according to

collector pattern. However, for both CS/PEO and PEC/PEO systems, fibers are also found covering all the collector available surface. This particular behavior of chitosan-based systems could influence not only the fiber mat mechanical properties but also biological aspects during cell culture.

1.2. CS/PEO and PEC/PEO fiber characteristics

Fiber morphology of chitosan-based mats were analyzed by SEM. Samples of as-spun fiber mats of CS/PEO and PEC/PEO were observed and average fiber diameters (AFD) were calculated by statistical size distribution. Globally, it was found that smooth fibers and homogenous substrates were obtained. On a first step, mats produced on squared-pattern collectors and 20-30% w/w PEO content in the material were analyzed. Then, AFDs of the different fiber arrangements were estimated.

In figure 3.5, SEM images of CS/PEO fibers with a PEO proportion in the blend of 30 and 20 % w/w, are presented. In the same figure, the influence of the two solvents, involved in experiments (AcOH and FA), on the fiber morphology is shown.

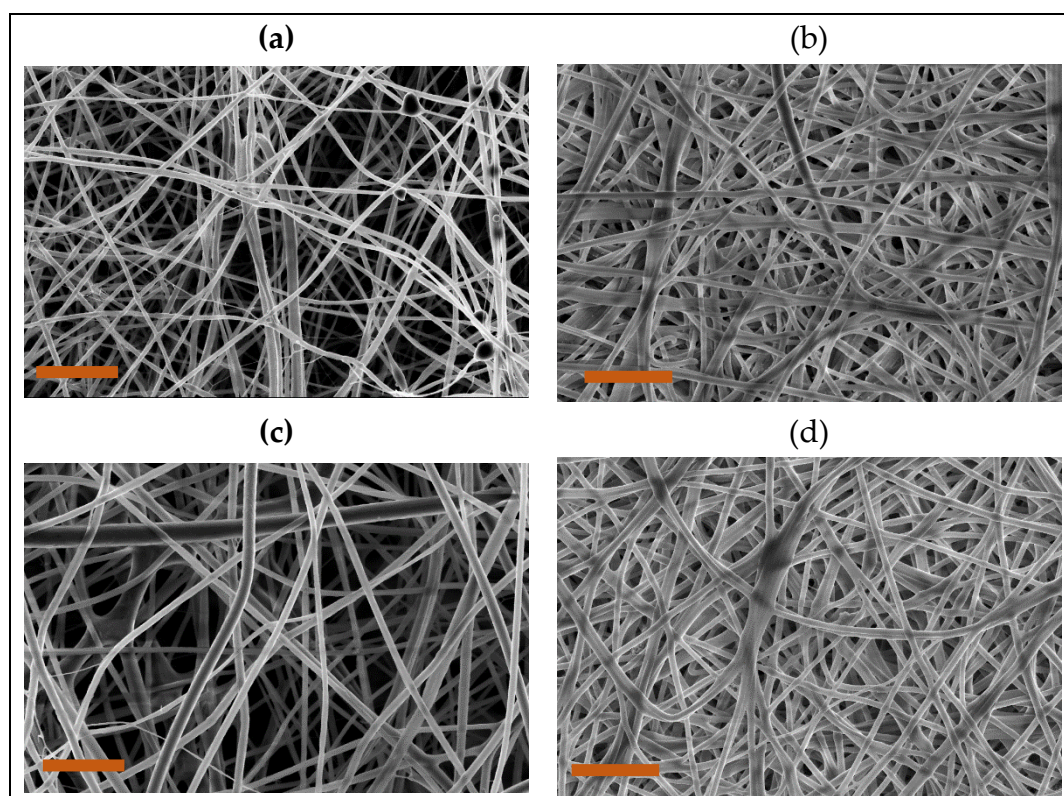


Figure 3.5. Fiber morphology of 70/30 (a, b) and 80/20 (c, d) CS/PEO fibers obtained with acidic solvents. 0.5 M Acetic acid (a, c) and 50/50 v/v W/FA (b, d). Scale bar = 2 micrometers.

Overall, after ADF estimation, close fiber diameter values were observed for CS/PEO fibers. Small differences could be attributed to the solvent and polymer concentration which define the solution viscosity, an important parameter for electrospinning.

Average fiber diameters in the range 112-156 nm for the CS/PEO systems, presented in figure 3.5, were found. It was concluded, in this case, that the composition of the blend slightly influenced the fiber size since 80/20 CS/PEO fibers presented an AFD $\sim 156 \pm 41$ nm and 139 ± 28 nm for AcOH and FA as solvents respectively. In the same way, 70/30 CS/PEO fibers presented an ADF $\sim 118 \pm 36$ nm and 123 ± 26 nm, for both studied solvents.

Similar analysis was effectuated for the system PEC/PEO, based on the images acquired by SEM. Frequency size distributions were obtained and average diameters were calculated from the statistical analysis. To show the influence of the PEC composition (charge ratio) on the fiber characteristics, the average diameters are presented in Figure 3.6, and compared with produced CS/PEO fibers.

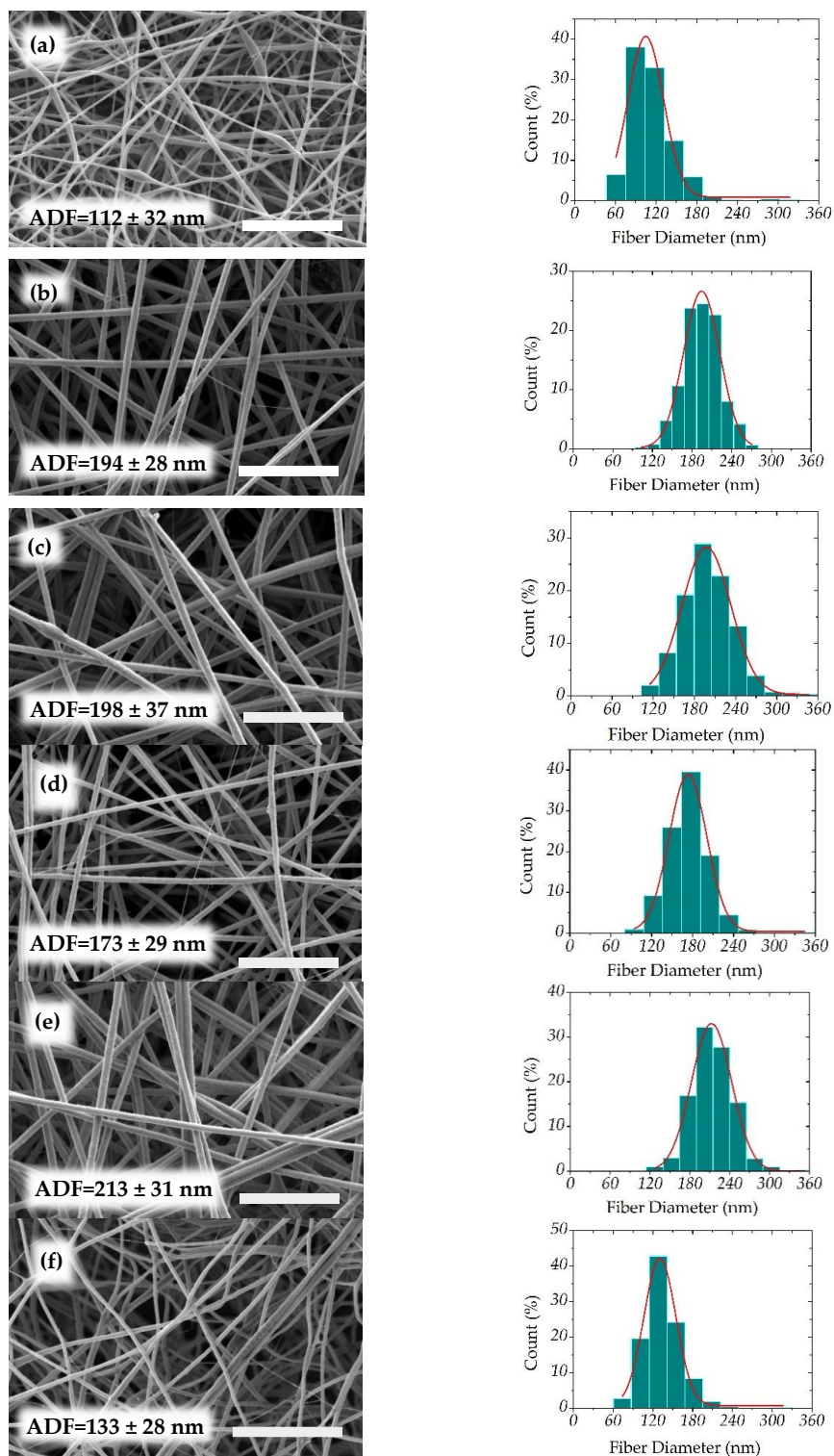


Figure 3.6. Scanning electron microscopy images of nanofibers obtained at different charge ratios and corresponding average fiber diameters (AFD) (nm) together with their diameter distribution. **(a)** $R_c = 0.5$, **(b)** $R_c = 1.0$, **(c)** $R_c = 1.8$, **(d)** $R_c = 2.35$, **(e)** $R_c = 3.0$, and **(f)** CS. Systems prepared in Formic Acid 50/50 v/v (C. E. Garcia et al., 2020). Scale bar = 3 μm .

It is found that, at higher content of HA ($R_c = 0.5$), fibers are thinner due to a lower content in the blend at constant total polymer concentration. Then, the diameter increases when the chitosan yield increases. The average diameter becomes larger than for pure CS in the same experimental conditions. This behavior pointed out the interest of the solvent selected avoiding phase separation between the two oppositely charged polymers. All average diameters for complex nanofibers are close to 200 nm.

2. *Material properties*

An important aspect related to the production of a new material is the ensemble of properties and their relevance for the final application. For biological requests, in addition to biocompatibility, stable and easy handling materials are needed. For this purpose, analysis of the solubility, swelling degree and mechanical performance of the systems CS, CS/PEO, CS/HA and CS/HA/PEO were effectuated. In the same way, the biological behavior and adhesion strength measurements of CS/PEO fibrous materials in contact with culture medium and cells, were investigated. The summary of the results is presented in subsequent sections.

2.1. **Solubility and swelling degree**

Chitosan based materials, in solid state, are stable in neutral (and basic) aqueous media (Rinaudo, 2006). However, since CS is solubilized in acidic conditions for electrospinning, a regeneration step of the protonated groups is needed to obtain insoluble materials from both systems CS/PEO and CS/HA/PEO.

2.1.1. *System CS/PEO*

In the case of CS/PEO systems and their physicochemical properties, the effect of the stabilization step in 80/20 v/v EtOH/Water has already been studied and applied in order to produced stable pure CS fibers (and films) due to deprotonation of the $-NH_3^+$ groups. At the same time, this washing treatment allows the obtention of PEO free fibers since PEO is solubilized during the procedure. Neutralization and washing steps have been verified by RMN and gravimetry (Garcia Garcia et al., 2018). It has been concluded that solubility of chitosan, after stabilization in ethanolic basic solution, is minor and fibers and films can keep its morphology unchanged even after months. Similarly, PEO in the blend can be extracted from electrospun fibers and films with a high efficiency. However, long polymer chains of elevated MW PEO could lead to a less effective PEO extraction (Garcia Garcia et al., 2018; Lemma et al., 2016).

Water retention capacity, at neutral pH, has also been analyzed for CS films and fibers (Garcia Garcia et al., 2018). It was observed that CS films presented swelling degrees, at neutral pH, in the range of 1.2 to 2.5 g Water/g dried substrate, depending on the composition. In contrast, CS fibers produced from the blend CS/PEO, shown capacities

varying between 3.1 and 5.3 g Water/g dried CS regenerated fibers, influenced by the polymer concentration and blend composition (Garcia Garcia et al., 2018) .

2.1.2. System CS/HA

The blend CS/HA is considered an important biopolymeric system with potential in biomedical domains (Petrova et al., 2019). Nevertheless, less information about the polyelectrolyte complex behavior, in dried and wet states, can be found in literature.

Using the same experimental conditions, casted films and electrospun nanofibers were parallelly produced. The use of a film as model allows easier characterization of the material, in order to find the more adapted methods and conditions to produce stable materials for the desired application.

Initially, PEC films were hydrated in PBS (pH=7.4) where partial solubility and high swelling degree were detected. Attributed to the probable presence of remaining solvent, longer evaporation periods were applied, however the same behavior was observed.

Contrary to CS, HA is highly soluble in aqueous solutions, for this reason a different method for PEC stabilization was adopted. The films were submitted to a thermal treatment at 120 °C for 4 h, the time was selected after a study of the weight loss kinetics (Figure 3.7).

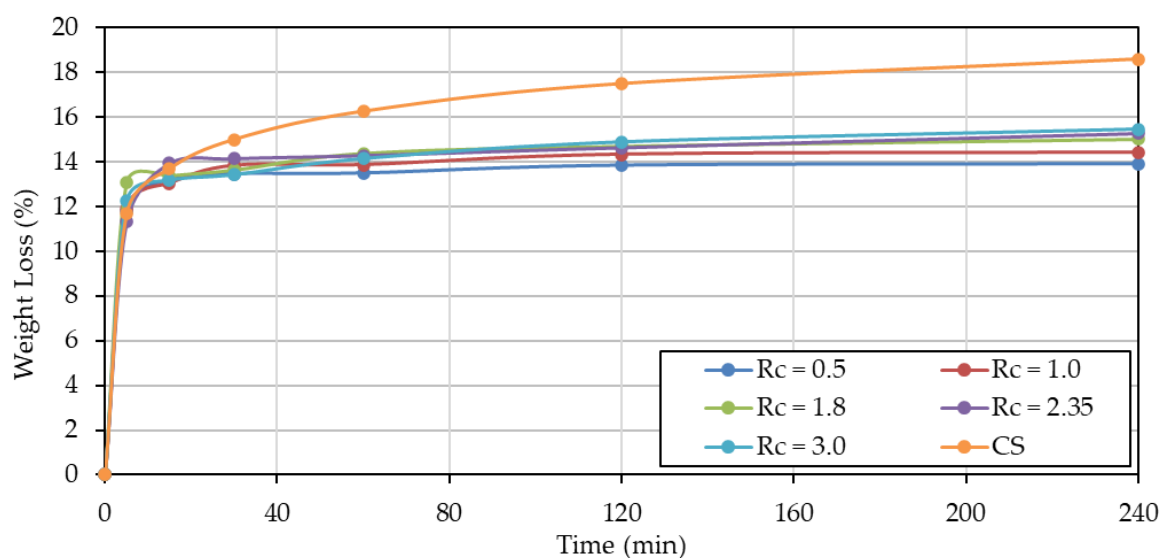


Figure 3.7. Weight loss of polyelectrolyte complex at different CS/HA charge ratios R_c compared with pure chitosan prepared in W/FA 50/50 v/v as a function of time at 120 °C.

Thermal procedure up to 4 hours was considered sufficient for PEC treatment. Even though CS films need more time to reach constant weight, PEC films shown constant weight after 60 minutes of heating.

Over $R_c=1$, the behavior of complexes is similar for the different R_c ratios increasing progressively with the time and chitosan content indicating a larger crosslinkage degree due to H-bonds and probably amide bond formation involving free $-NH_2$.

Comparison with chitosan shows that weight loss is higher for free chitosan than for complexes due to lower interaction between chains (thermal treatment of chitosan induces an increase of crystallinity) and lower degree of reaction with residual formic acid used as solvent.

Firstly, considering partial solubility and swelling degree in aqueous medium, PEC films prepared from three solvent mixtures W/FA 25/75, 50/50 and 75/25 v/v were compared. Nearly the same film characteristics were observed for the solvents studied, as it is shown for solubility in Figure 3.8.

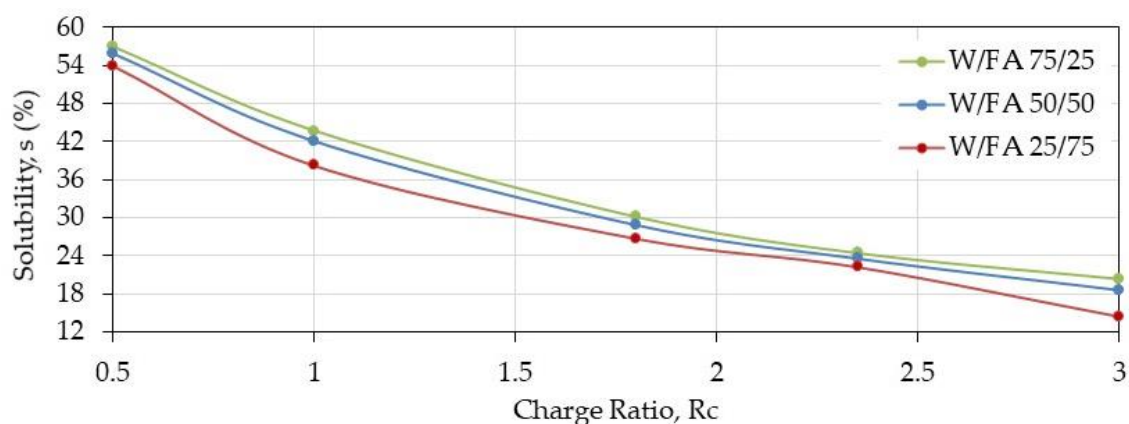


Figure 3.8. Solubility of PEC films at pH = 7.4 after thermal treatment as a function of charge ratio prepared in the solvents: W/FA 25/75, 50/50, 75/25 v/v.

Related to solvent selection, the W/FA 50/50 v/v is preferred for the film tests and electrospinning considering that the processing of PEC solutions was difficult in W/FA 75/25, and due to high volatility of W/FA 25/75 which affected significantly fiber production.

Then, the swelling characteristics of the films prepared from complex solubilized in W/FA (50/50 v/v) are tested before and after thermal treatment as it is presented in figure 3.9.

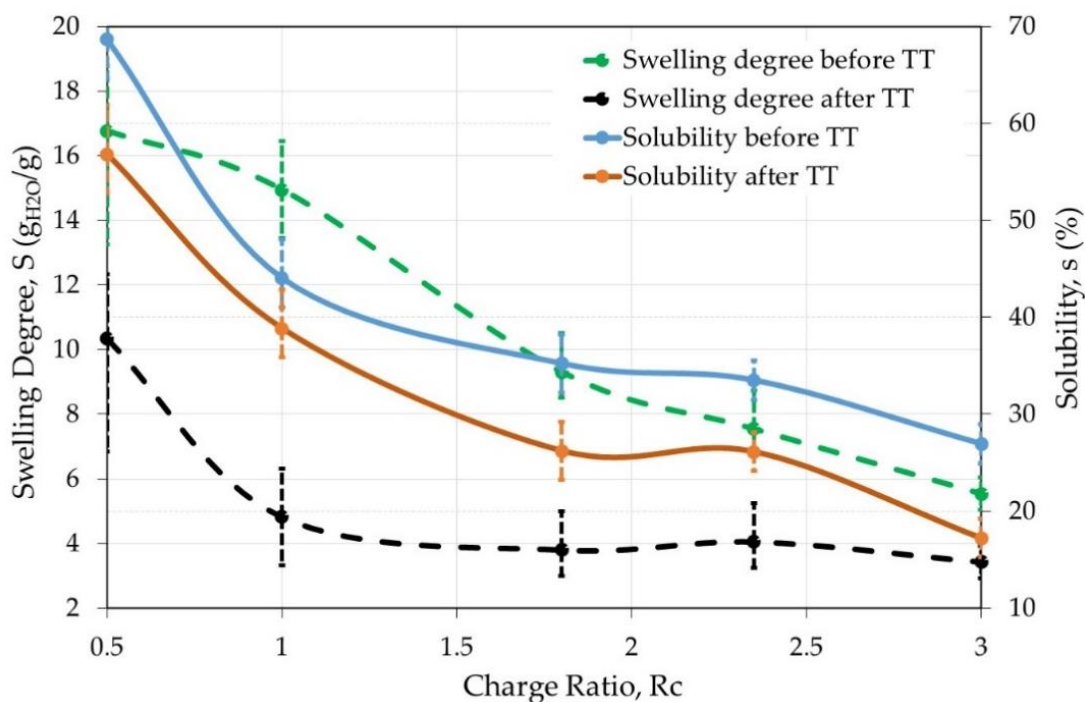


Figure 3.9. Influence of the thermal treatment (4 h at 120 °C) on PEC films solubility (blue and brown) and degree of swelling (green and black) as a function of charge ratio at pH = 7.4. Average values obtained on four independent experiments.

The swelling degree decreases strongly after thermal treatment when the charge ratio is lower than 2. At the same time, the solubility also decreases when the charge ratio increases but with a lower efficiency. Thermal treatment clearly allows to stabilize the PEC films which remain easy to handle even in the wet state. In the following, films after a thermal treatment are tested in different conditions of solvent and pH (Table 3.6).

Table 3.6. Influence of Charge Ratio R_c and pH on Swelling Degree and Solubility before and after Thermal Treatment for Solubilization in W/FA 50/50

Charge Ratio (R_c) NH ₂ /COO H	Weight Ratio NH ₂ /COOH	pH	Swelling Degree (g Water/g) before Thermal Treatment	Solubility (%) before Thermal Treatment	Swelling Degree (g Water/g) after Thermal Treatment	Solubility (%) after Thermal Treatment
0.5	0.21	3	3.2	24.1	4.6	37.2
		7.4	16.8	68.7	10.0	59.3
		11	----	High*	22.6*	69.5*
1	0.42	3	2.6	10.1	3.6	11.5
		7.4	14.9	44.0	4.7	37.7
		11	21.8	61.0	11.4	39.4
1.8	0.77	3	4.5	14.5	3.8	9.8
		7.4	9.3	35.2	3.9	25.1
		11	16.0	45.1	6.8	25.9
2.35	1.0	3	6.6	37.1	3.8	8.4

		7.4	7.6	33.5	4.3	23.2
		11	13.9	35.4	4.3	21.3
3	1.26	3	7.0	46.9	3.4	7.1
		7.4	5.5	26.9	3.6	17.2
		11	12.1	28.5	4.1	21.3

(*) Approximative values due to difficult sample handling.

From Table 3.6, few values are presented in the next figures. In Figures 3.10 and 3.11, the influence of the charge ratio on swelling degree and solubility are represented, respectively, for different pH after thermal treatment when the solvent used was W/FA 50/50 (*v/v*).

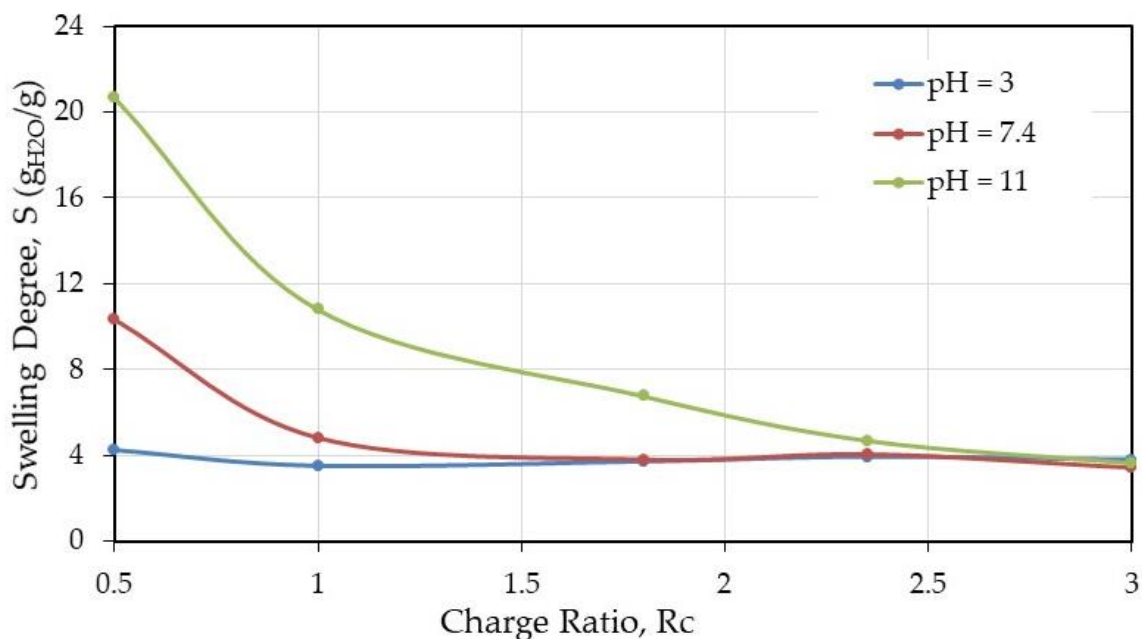


Figure 3.10. Swelling degree (g Water/g dried material) as a function of the charge ratio after thermal treatment.

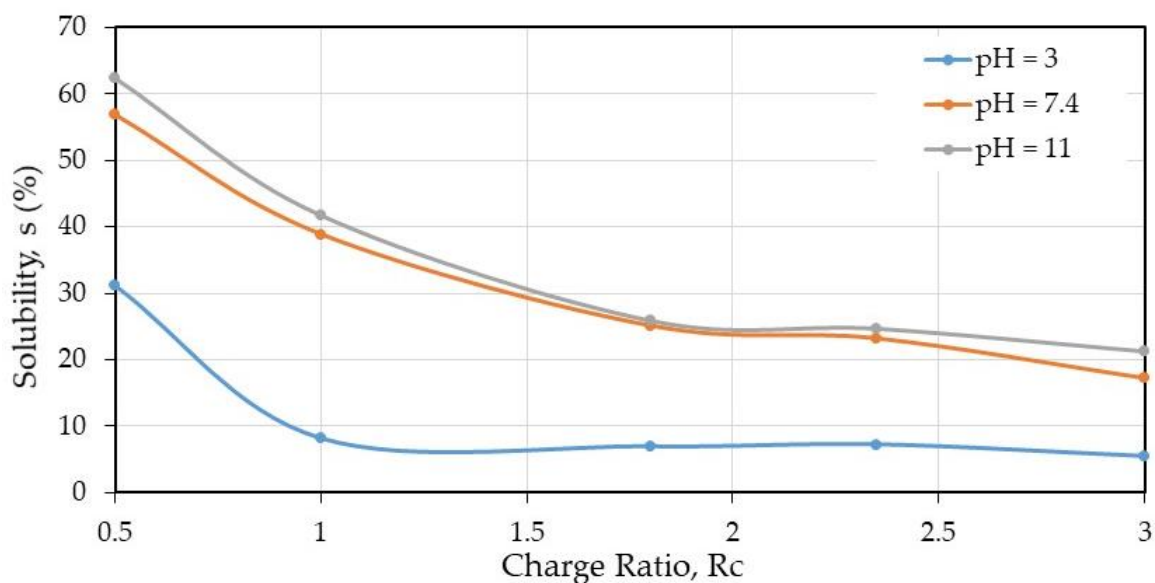


Figure 3.11. Partial solubility at different pH on PEC films prepared in W/FA 50/50 v/v as a function of charge ratio.

From these results, it is shown that the thermal stabilization starts with a ratio NH_2/COOH equal to 1.8, indicating the need of enough chitosan in the blend to complex HA, due to the fact that HA is a polysaccharide highly soluble in aqueous medium in a wide range of values.

It is found that stability is larger at pH = 3 as soon as the charge ratio NH_2/COOH is larger than 0.5 independently of the composition. This condition corresponds to the lower solubility of HA and gel-like behavior (Gatej et al., 2005), preserving the complex formation. Taking care of the material composition, over $R_c = 1.8$, less than 10% is soluble when the material contents 43.3% w/w of chitosan and consequently 56.6% w/w of HA.

At pH = 7.4 and 11, the solubility values are close as shown in Figure 4.10 when chitosan alone becomes insoluble. The solubility is around 22% indicating that the material is and remains a stabilized polyelectrolyte complex.

The study on films as a model allows, after thermal treatment, to conclude that the complex formation stabilized the material taking benefit of HA as well as chitosan biological properties for new applications.

2.2. NMR Analysis on PEC systems

PEC properties modification after thermal treatment led us to investigate changes at the structural level. For this purpose, an NMR analysis of chitosan and PEC samples, under film form as model, was performed. This technique allowed the confirmation of the PEC composition and help validate the solvent selection and thermal treatment application.

2.2.1. Film Composition by NMR and Influence of Thermal Treatment

In a first step, ^1H NMR of chitosan was examined as reference. The spectrum is obtained after dissolution in acidic D_2O of a film prepared in formic acid W/FA 50/50 v/v and presented in figure 3.12.

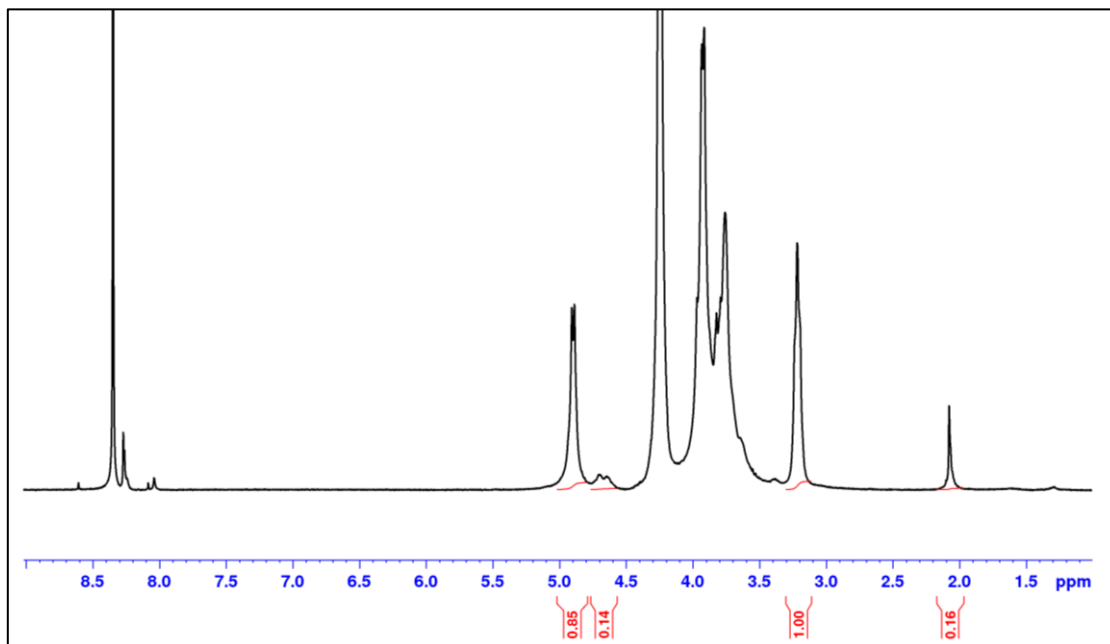


Figure 3.12. ^1H NMR spectrum obtained on a chitosan film casted from chitosan in $\text{D}_2\text{O}/\text{HCl}$ solvent at $85\text{ }^\circ\text{C}$.

This spectrum allows to determine the degree of acetylation of the chitosan obtained from the ratio between the signals of the methyl group at 2.1 ppm and H-2 at 3.2 ppm, which give a DA = 0.05. In addition, it shows that there is some formic acid left (around 8.4 ppm) before thermal treatment (Berregi et al., 2007).

Once thermal treatment is carried out, the film becomes insoluble in acidic medium probably due to H-bond network formation and reinforced by partial crystallization after solvent evaporation as shown by X-rays diffraction (Petrova et al., 2019). Our data agree with the X-rays spectra given in Figure 2 in *Petrova et al.* for chitosan/PEO (Petrova et al., 2019). Furthermore, as proposed in literature, amide bonds involving the solvent may occur, decreasing free NH_2 content and increasing the H-bonds density (Bernabé et al., 2005; Cooper et al., 2011; Zotkin et al., 2004).

It was also demonstrated that the acid used to dissolve chitosan and cast films influences the solubility of films after thermal treatment. A chitosan film dissolved in presence of HCl and dried remains soluble in aqueous medium even after thermal treatment, the NMR spectra are shown in Figure 3.13.

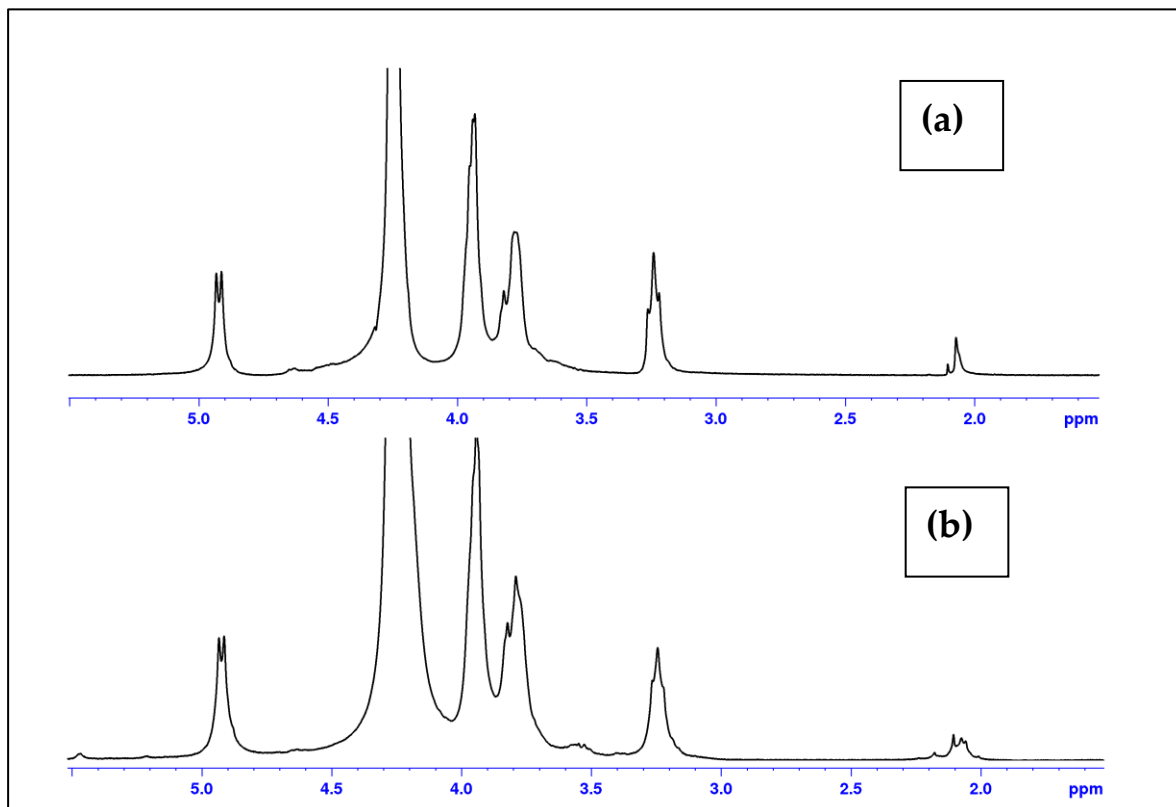


Figure 3.13. Influence of thermal treatment on ^1H NMR spectrum for film of chitosan obtained after chitosan solubilization in HCl in absence of thermal treatment (a); and after thermal treatment (b). Solvent $\text{D}_2\text{O}/\text{DCl}$ at 85°C .

After thermal treatment, the films turned brown but remained soluble in acidic conditions even if a small insoluble fraction is formed indicating few strong H-bond interchain interactions. Signal corresponding to $-\text{CH}_3$ groups around 2 ppm is modified (figure 3.13b) and new signals appear around 3.5 ppm with a decrease of the $-\text{H}_2$ signal at 3.2 ppm indicating probable H-bonds involving the small amount of $-\text{NH}-\text{CO}-\text{CH}_3$.

As carboxylic acids (formic acid and acetic acid) formed an insoluble material after thermal treatment, they probably form, as proposed previously, an amide bond with free $-\text{NH}_2$ chitosan, increasing the H-bonds network density as found with peptidic groups (Vasiliu et al., 2005).

Formic acid solvent was selected due to easier feasibility to produce nanofibers by electrospinning compared to acetic acid used previously (Garcia Garcia et al., 2018; Lemma et al., 2016). Whatever the W/FA ratio (mainly over 25/75), electrospinning allows to process chitosan alone, HA/PEO, as well as the chitosan/hyaluronan acid complex. Then, W/FA was confirmed as the most convenient solvent for processing these materials even in absence of other additives such as Dimethylformamide (DMF), N-methylpyrrolidone, or NH_4OH as proposed in literature (Brenner et al., 2012; G.

Chen et al., 2016; Pabjańczyk-Wlazło et al., 2017). Only PEO, extractible in water, was added to favor electrospinning.

2.2.2. Film Made of Complex and Influence of Thermal Treatment

In the following, a polyelectrolyte complex prepared at a charge ratio, $R_c = 0.5$, was dissolved in D_2O/DCl after thermal treatment (Figure 3.14). This sample remaining soluble in acidic conditions can be analyzed as proposed (Peniche et al., 1998).

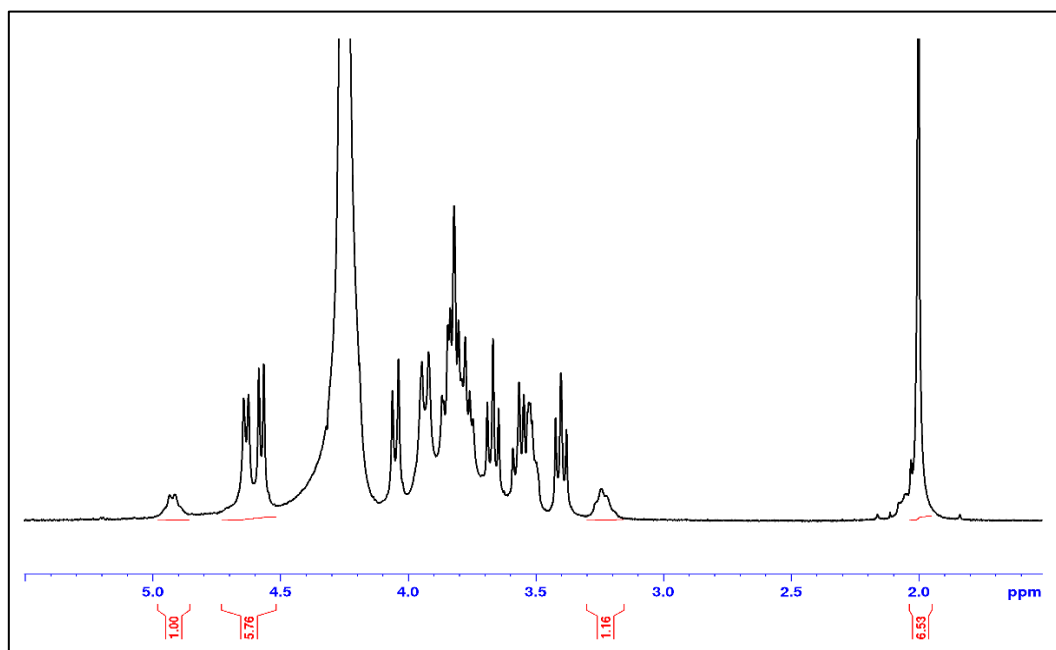


Figure 3.14. 1H NMR spectrum of a complex film prepared at a charge ratio $R_c = 0.5$ formed in W/FA 50/50 v/v after thermal treatment. Solvent D_2O/DCl at $85\text{ }^\circ\text{C}$.

Taking into consideration two H-1 of HA at 4.5–5 ppm (one of the units being carboxylated) and the H-1 of chitosan (corresponding to free $-NH_2$) at 4.9 ppm, there comes a charge ratio $CS/HA = 0.54$ in agreement with the stoichiometry of the solution prepared. A large signal occurs around 2 ppm due to $-CH_3$ from N-acetyl-D-glucosamine unit of HA (superposed with the small $-CH_3$ signal from chitosan).

To conclude, in large excess of HA, the film is still soluble in water or acidic conditions even after thermal treatment. After thermal treatment at higher charge ratio, the films are more stable and only a small amount is solubilized in acidic conditions. In this consideration, liquid NMR is only useful for material characterization at some specific CS/HA compositions, due to the insolubility in aqueous medium when the complex forms.

2.3. Behavior under uniaxial tension

2.3.1. CS and PEC for thermal stabilization

Mechanical behavior of complex and chitosan films was determined at ambient temperature before and after thermal treatment. In each case, the thickness of the material is given for the experimental curves.

From Figures 3.15 and 3.16, it is shown that thermal treatment on CS alone and PEC films, at several charge ratios, increases the stiffness and decreases strongly the plasticity of the materials. Additionally, the presence of HA increases the modulus of the films compared to CS, especially before thermal treatment when $R_c > 1.8$. The higher the material R_c , the higher stress and strain at break under traction tests.

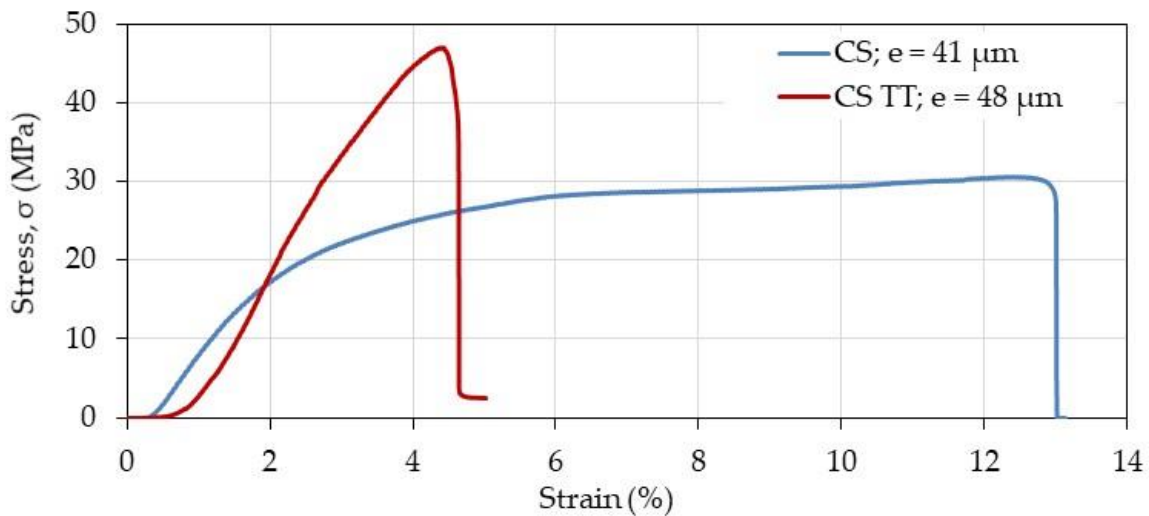


Figure 3.15. Effect of thermal treatment (TT) on mechanical chitosan film response in the dried state. The thickness (e) of the film samples was found around 40–50 μm .

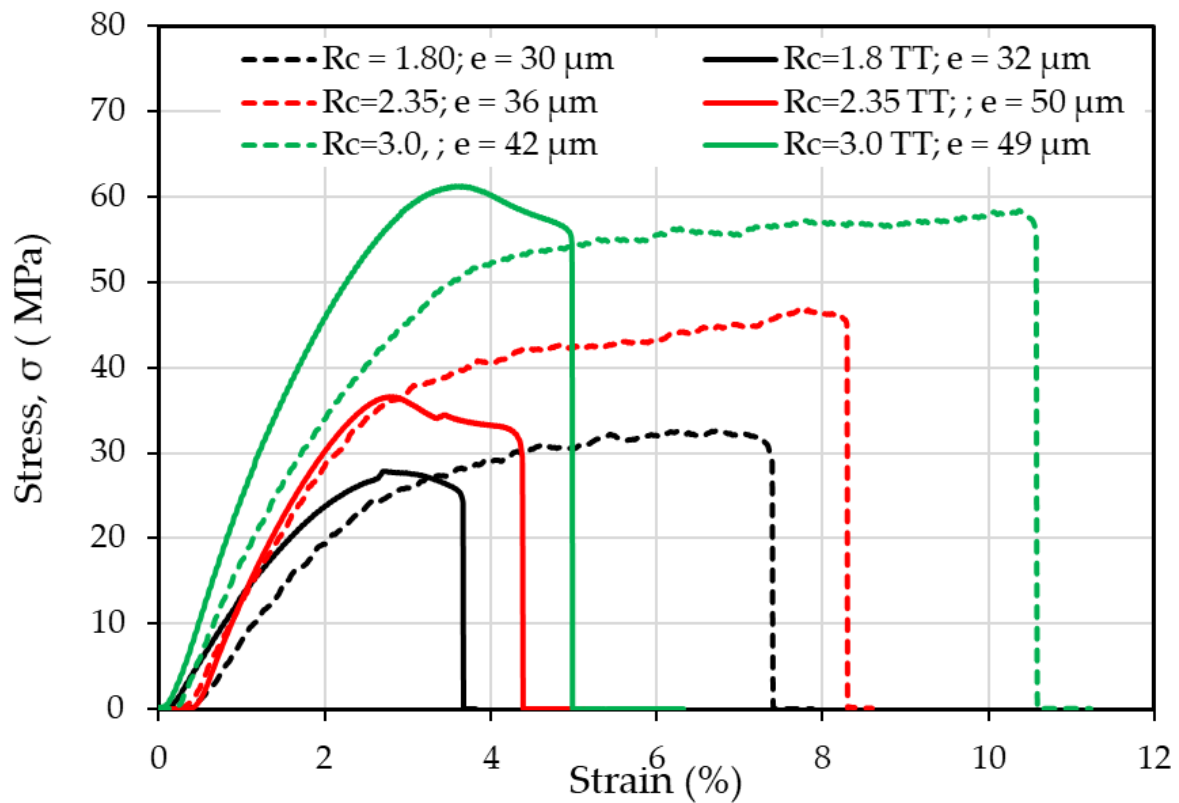


Figure 3.16. Effect of thermal treatment (TT) on mechanical response of PEC films in the dried state. Stress as a function of strain (%) before and after thermal treatment for different complexes characterized by R_c .

Considered relevant for application in physiological conditions, it was interesting to also investigate the material performances in the wet state. Some experimental data corresponding to CS (before and after TT) and PEC films (after TT) are given in Figure 3.17.

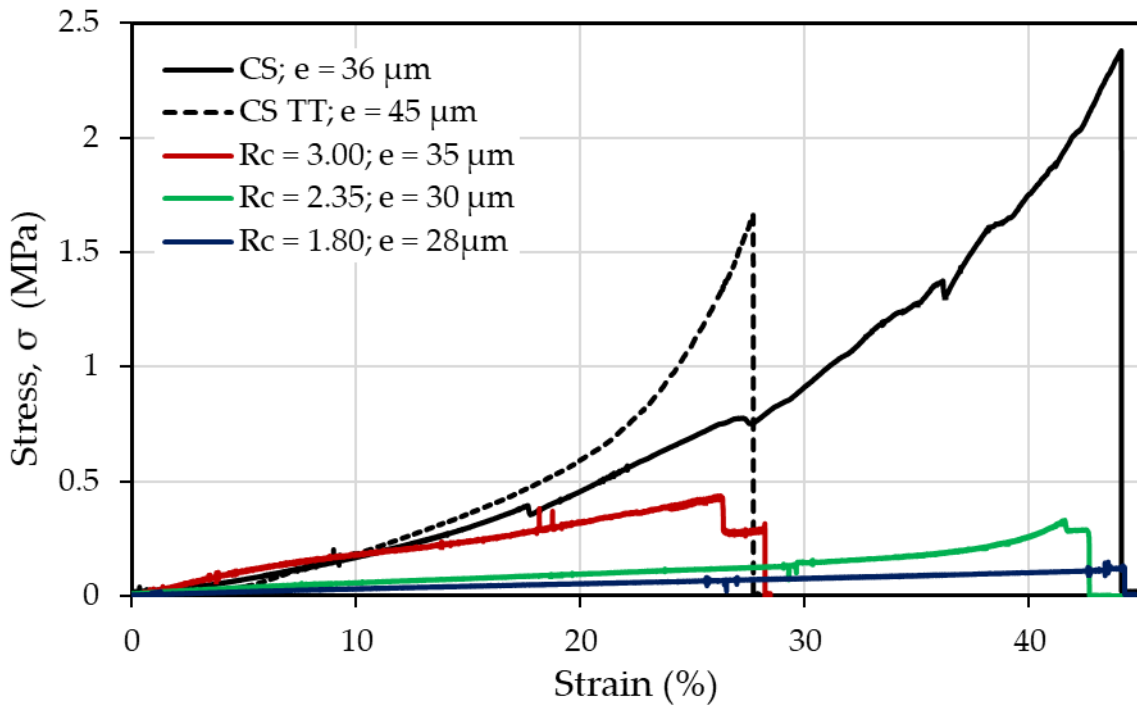


Figure 3.17. Mechanical response of chitosan and PEC films once treated at 120°C during 4 h, and in the wet state after stabilization in PBS at pH = 7.4.

For determination of the mechanical properties on films after thermal treatment, the complexes and the treated CS were directly stabilized in PBS buffer but for CS before thermal treatment, it was necessary to firstly neutralized CS in alkaline medium before PBS immersion as suggested previously (Garcia Garcia et al., 2018; Lemma et al., 2016). From data in Figure 4.13, it is concluded that the material is able to be manipulated only when $R_c \geq 1.8$ corresponding to lower values of swelling and solubility. When the charge ratio R_c increases, the stiffness increases (modulus increases and breaking strain decreases) remaining in all cases slightly lower than for CS alone for samples with the same range of thickness.

These data confirm that, for the first time to our knowledge, stable new biomaterials based on PEC involving HA and CS are obtained in PBS at pH = 7.4, for biological applications.

2.3.2. CS/PEO and PEC/PEO fiber mats

Traction experiments were performed on as-spun PEC fiber samples, having nearly the same thickness, in the absence of thermal treatment as it is presented in figure 3.18. The nanofibrous mats were collected on micro-structured collector with a regular pattern.

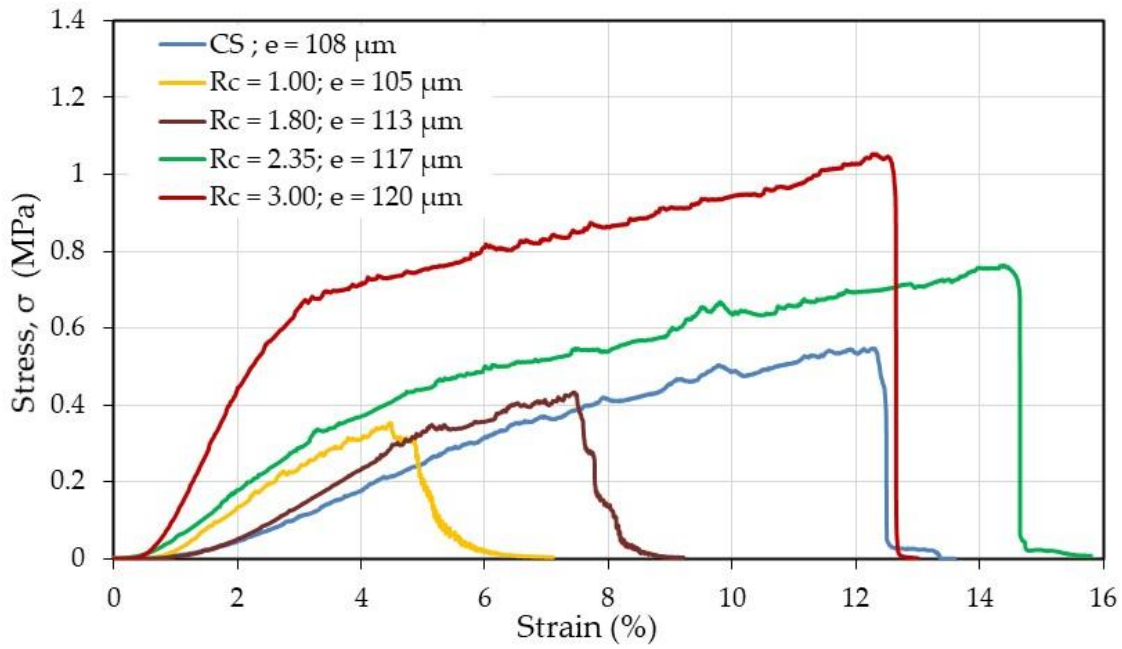


Figure 3.18. Mechanical behavior of chitosan and as-spun PEC fiber samples in dried state, obtained on square-patterned collectors.

Firstly, it is shown that the PEC fibers are stronger than CS fibers as soon as R_c is higher than 1.8, with a relatively large strain at break probably connected with the presence of PEO. The stress at break is increasing directly as a function of the chitosan content.

For fibrous materials, it must be considered that density of the mat is much lower than for films as discussed previously (Garcia Garcia et al., 2018). In this regard, the values obtained for failure stress and strain, after tensile tests, for the mat are lower. Considering the geometric characteristics of the samples (surface, weight, and thickness of the probe), the density of the mats is compared with that of the film, related with the active transverse section of the probe tested, in table 3.7.

Table 3.7. Morphological Characteristics of Films and Fibers Tested in Mechanical Experiments. Influence of the Charge ratio, R_c .

Composition	Average Density (g/cm^3)		Ratio Density Film/fibers
	Casted Film	Electrospun Nanofiber Mat	
CS	0.846	0.0295	28.7
$R_c = 1.0$	-----	0.0383	----
$R_c = 1.8$	0.949	0.0284	33.4
$R_c = 2.35$	1.127	0.0395	28.5
$R_c = 3.0$	1.163	0.0512	22.7

The cross-section ratio estimated from the material density is found around 30. In this way, the performance of nanofibers under tensile tests, is in relatively good agreement with that of films: for $R_c = 3$, stress at break is 1 MPa and 12% strain (Figure 3.18) while on compact film it is around 60 MPa and 10% (Figure 3.16), respectively. Large porosity and low density of fibers in the mats considerably decrease the effective stress.

Considering the morphology of the samples, uniaxial tensile mechanical tests on aligned fibers (electrospun on rotatory cylinder at 1500 rpm) were also performed to compare the response of nanofibers with random distribution with oriented nanofibers. On the PEC mats ($R_c = 2.35$, mass ratio = 1.0), the mechanical parameters are determined and compared with that of pure chitosan obtained in the same experimental conditions in figure 3.19.

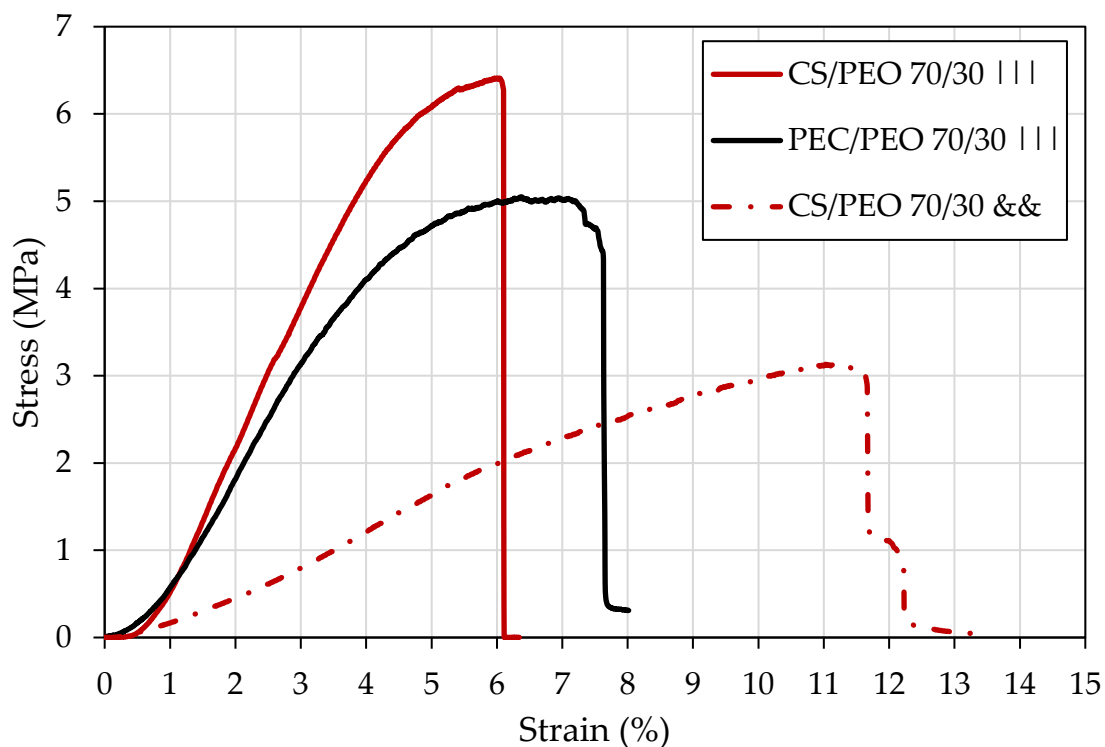


Figure 3.19. Stress at break for CS/PEO and PEC/PEO fiber mats contrasted in terms of fiber arrangement. (|||) Aligned fibers and (&&) aleatory fibers.

From figure 3.19, the role of alignment of nanofibers on their mechanical properties in the dried state is remarked, as already observed with honeycomb structures based on polycaprolactone (PCL) (Mondésert et al., 2021). The density of the material is larger for aligned PEC fibers than for randomly collected mats and larger than that of pure chitosan. Chitosan nanofibers form a highly porous mat with a density around $0.037 \pm 0.01 \text{ g/cm}^3$ (C. E. Garcia et al., 2020). Stress under uniaxial tension is increased by fiber

alignment. Aligned CS/PEO fibers present a higher stress at break, in contrast to PEC/PEO system, i.e., 6.5 MPa compared to 5 MPa. The strain at break in aligned fibers is larger for the PEC mat. In addition, it is clear that orientation increases the stress of CS fibers when contrasted to randomly orientated CS fibers (ratio = 6.5/3 MPa).

The two orientations of aligned nanofibers made of CS/PEO and PEC /PEO are also compared, under tensile tests, in figure 3.20.

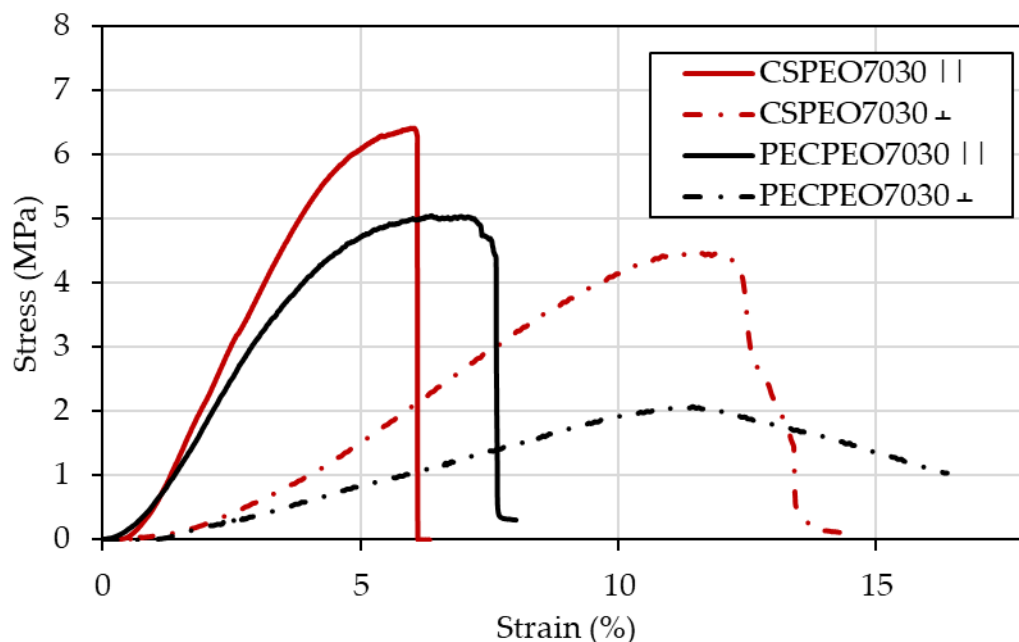


Figure 3.20. Comparison of mechanical response in dried state for aligned Chitosan/PEO and PEC/PEO 70/30 w/w nanofibers. Tensile tests of the samples on the parallel direction (||) and the transverse (⊥) direction of nanofibers.

In figure 3.20, the anisotropic response of the materials is analyzed. The tensile properties are studied for the two orientations of aligned nanofibers made of CS/PEO and PEC /PEO. It is found that, in the main direction of CS/PEO fibers, stress at break is larger than the measured value in the transversal orientation (ratio = 1.5). Performances are decreasing while strain increases. The same trend is observed for PEC fibers (ratio = 2.5). These results are the mechanical signature of the anisotropic self-organization of fibers (Thomas et al., 2006).

Relatively small differences contrasting the two directions could be in part due to connection between fibers occurring during their collection on the rotating cylinder before complete drying. Therein, deposited fibers would behave as a thin film (Thomas et al., 2006).

2.4. Substrate stability in biological solutions

In order to evaluate the stability of the produced nanofibers after neutralization, the samples were disposed in the culture solution (DMEM) and in the 0.05% Trypsin-

EDTA solution. Fibers were incubated and morphology was observed over time, the images are shown in figure 3.21.

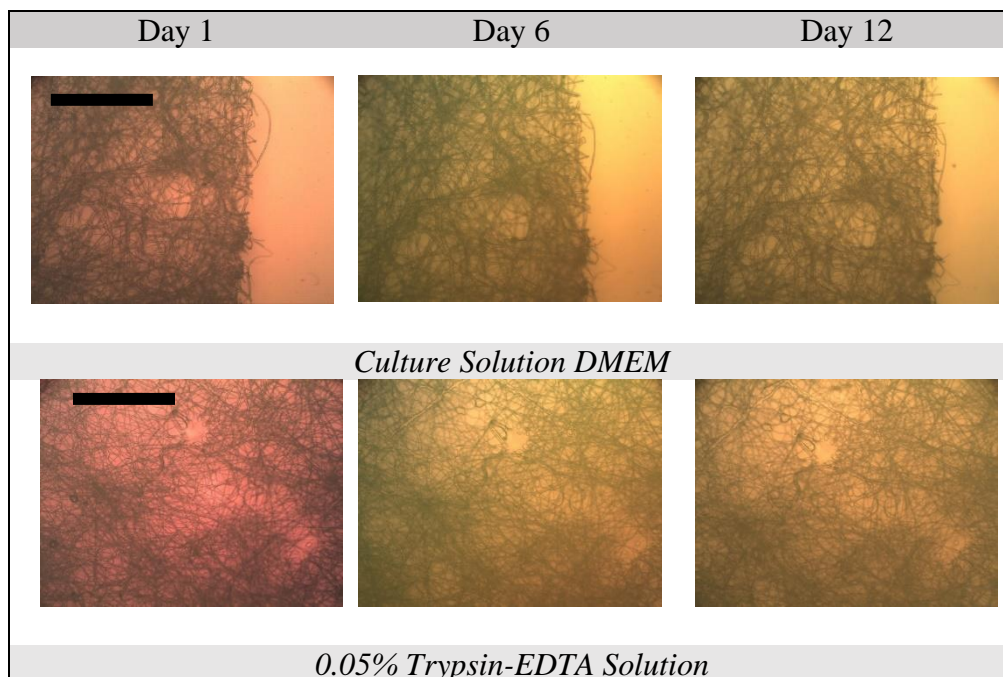


Figure 3.21. Evolution of fiber morphology in solutions adopted for cell culture (DMEM) and for cell detachment conditions (Trypsin-EDTA). Microscope images were obtained at equal magnification (10x) on the same sample location. Scale bare equals 100 μm (Garcia Garcia et al., 2021).

From these observations, it can be proved that fibers are stable in culture medium, from physiological conditions (pH=7.4) to slightly acid (pH~6.5) conditions. In this manner, biological applications are enabled and cells could be seeded and grow on the mat surface neglecting fiber dissolution or deformation at least after 12 days of culture.

2.5. Cell-substrate adhesion strength and energy

The interaction between cell and substrate is analyzed accordingly to the proposed application of the chitosan-based materials obtained in this work. AFM was applied to characterize the cell-substrate adhesion strength and energy as a function of the substrate topography and contact time.

From previous sections regarding the morphology of the fibrous substrates, an average diameter of 118 ± 36 nm was found from diameter distribution of the samples with a 70/30 CS/PEO proportion (C. E. G. Garcia et al., 2021; Garcia Garcia et al., 2018; García García et al., 2022). Smooth fibers and homogeneous mats were observed as it is shown in figure 3.5. From SEM image analyses, the porosity was determined; for the upper layers of the mat, in contact with the cell. Such fraction was found to be around 47%

(n= 10 essays) of the sample area. Due to cell dimension (around 20 μm diameter), a single cell must be in contact with several fibers but in full contact when the films and flat surfaces are used as substrates.

2.5.1. AFM response for cell detachment

After the contact time, the cantilever with the attached cell on its tip retracts back, at constant velocity, to its initial position on the vertical axis. During this step, complete detachment of the cell occurs (in figure 3.22, read from left to right). In figure 3.22, from the characteristic AFM response, the retraction curve obtained on chitosan films and fiber mats are compared with the BSA coated reference surface.

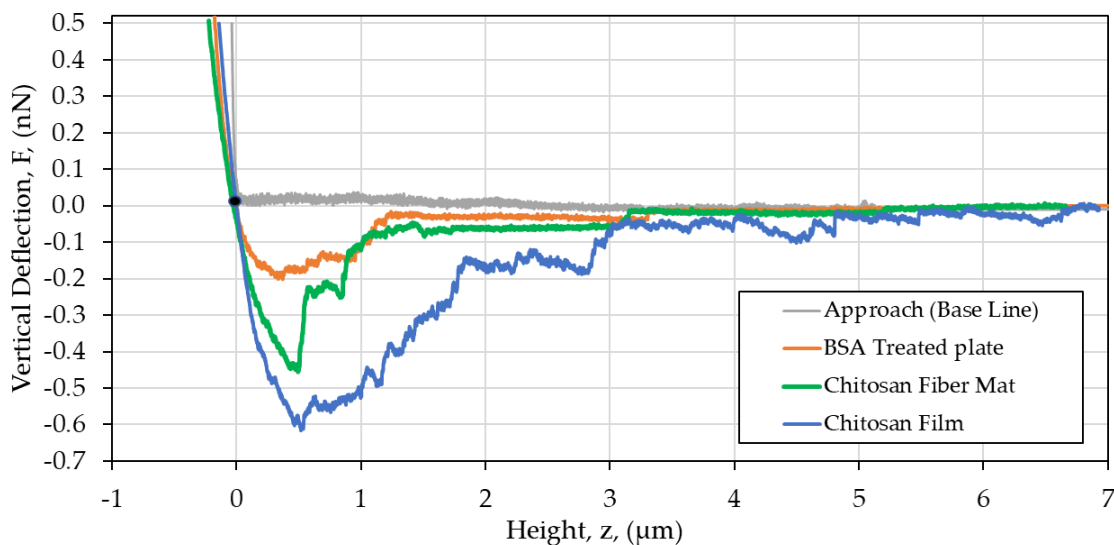


Figure 3.22. Comparative response of chondrocyte detachment on chitosan substrates (film and fiber mat) and BSA coated Petri dish. The point (0,0) on the curve F vs z represents the cell-substrate contact point. Retraction velocity is 1 $\mu\text{m}/\text{s}$ and data are shown for a contact time (t_c) of 60 s.

Once the cell is in full contact with the substrate, the former is pushed towards the surface until the force setpoint is achieved. Herein, cell indentation occurs and, depending on the substrate properties, such as porosity, roughness, and swelling, cell-substrate adsorption, a gap (in height) might appear between the approach and the retraction curves. In the same way for each material, this effect is observed in the initial slopes of the detachment response ($F > 0$) (figure 3.22). Especially, on fiber mats with high porosity and higher water retention capacity (Garcia Garcia et al., 2018), a larger deviation (around $-0.25 \mu\text{m}$ at $F = 0.5 \text{ nN}$) was detected for $t_c = 60 \text{ s}$. In contrast with flat rigid surfaces, important deviations during the contact step on CS substrates were observed for $t_c = 120 \text{ s}$. Experimental values of $t_c = 60 \text{ s}$ were considered more representative and reliable.

For all retraction curves, having a similar trend, the different steps of cell detachment are identified and provide a complementary understanding of cell adhesion

measurements. In this regard, including all phenomena occurring, three regions can be differentiated and they are defined in figure 3.23.

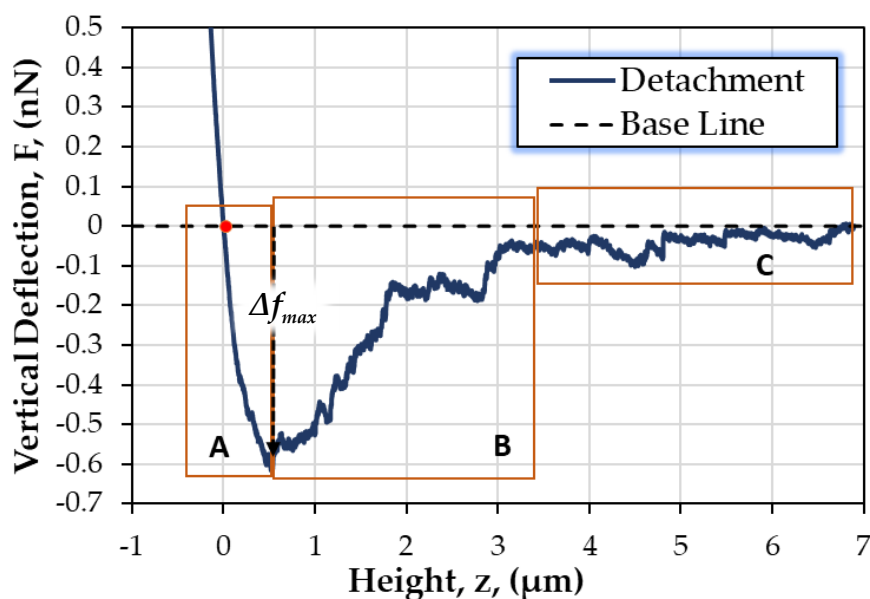


Figure 3.23. Cell force adhesion response separated in 3 regions or steps. Initial detachment in region A, rupture of secondary cell-substrate bonds in zone B and breaking of the remaining links and return to base line in region C.

The maximum force value (Δf_{max}) is detected in zone A, in the first micrometer of the cell-substrate separation measurement (figure 3.23). This peak can be associated to the cell-substrate assembly deformation and bonds being stretched at the same time.

After the highest vertical deflection value (Δf_{max}), the detachment process starts in zone B. In this region, more than 80% of the registered force jumps (Δf) occur after the first breakup. This zone is considered as the more representative part of the detachment response. It has been also observed that zone B is larger on the chitosan films than on fiber mats. Small surface interactions according to mat porosity of the fibrous substrates must affect the number and amplitude of detachment events measured in AFM, compared to the CS film.

Finally, in region C, the final links are stretched and break as long as the cell is completely separated from the substrate surface. These links being more isolated could be associated with the individual response of cell membrane tethers (Sundar Rajan et al., 2017; Titushkin & Cho, 2006). The average tether length was found between 0.5 μm and 1.5 μm for both substrates, i.e., chitosan films and fiber mats. It is important to mention that a minority of the detected events in the retraction response take place in region C.

The average of Δf_{\max} values, comparing the chitosan film and the electrospun mat for a given contact time of 60 seconds is shown in figure 3.24. From these results, a higher Δf_{\max} is observed when the chondrocytes interact with a more compact surface (the chitosan film) in contrast with the porous fiber mat for which the Δf_{\max} values are slightly smaller and more homogenous (a narrower distribution). In the same context, significant Δf_{\max} differences, when comparing CS substrates from the BSA coated surface, were found for $t_c=60$ s. This contrast between the studied substrates shows clearly that chondrocytes are around 2 times more strongly adhered to CS than when they are in contact with the coated BSA culture dish.

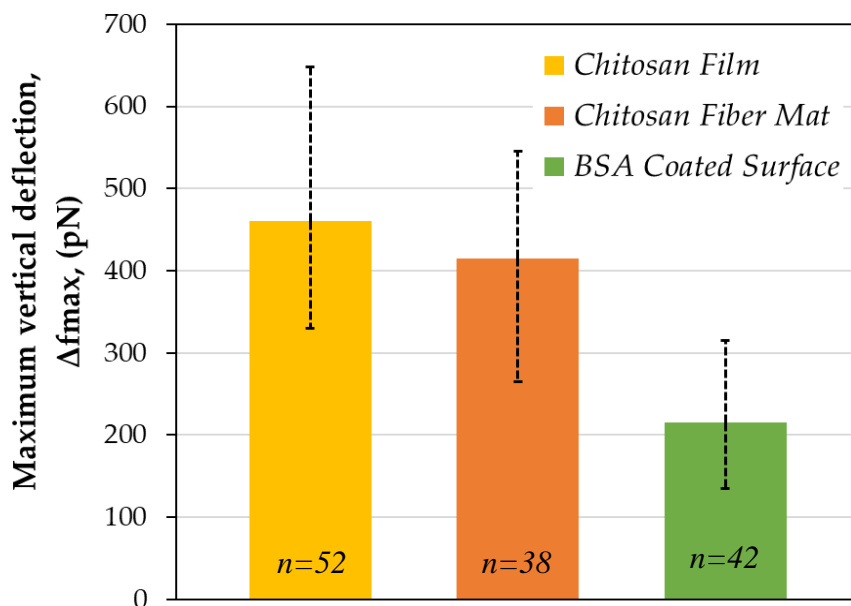


Figure 3.24. Average of maximum vertical force (Δf_{\max}) for the two substrates studied: chitosan film and chitosan nanofibers compared to the reference BSA coated surface (significant difference found, $p<0.01$), for a contact time of 60 s. SD in dotted line, number of assays = n.

Average Δf_{\max} values between 2 and 7 nN were previously observed in adhesion tests on glass for chondrocytes using a different AFM approach (Changhsun et al., 2008). This difference can be attributed mainly to the experimental AFM arrangement applied and the nature of the surface.

Because the force jump intensities are coupled with their relative position on the retraction curve, the distribution of detachment steps as a function of the location on the vertical axis (separation distance) can help understand the complete adhesion phenomenon. Towards that end, registered force jumps on chitosan substrates are presented in figure 3.25, showing an important concentration of events during the initial part of the cell adhesion response attributed to the breakup of a large quantity

of formed links and slight cell membrane deformation (zone B). Few force jumps are observed at larger distance (z) before complete detachment of the cell, those bonds could be related to a more complex interaction between the cellular membrane and the substrates. It is known that as the cell membrane is connected to the cytoskeleton, when the former detaches, cytoskeleton filaments (membrane tethers) are also elongated few micrometers until they are released (Sundar Rajan et al., 2017; Titushkin & Cho, 2006).

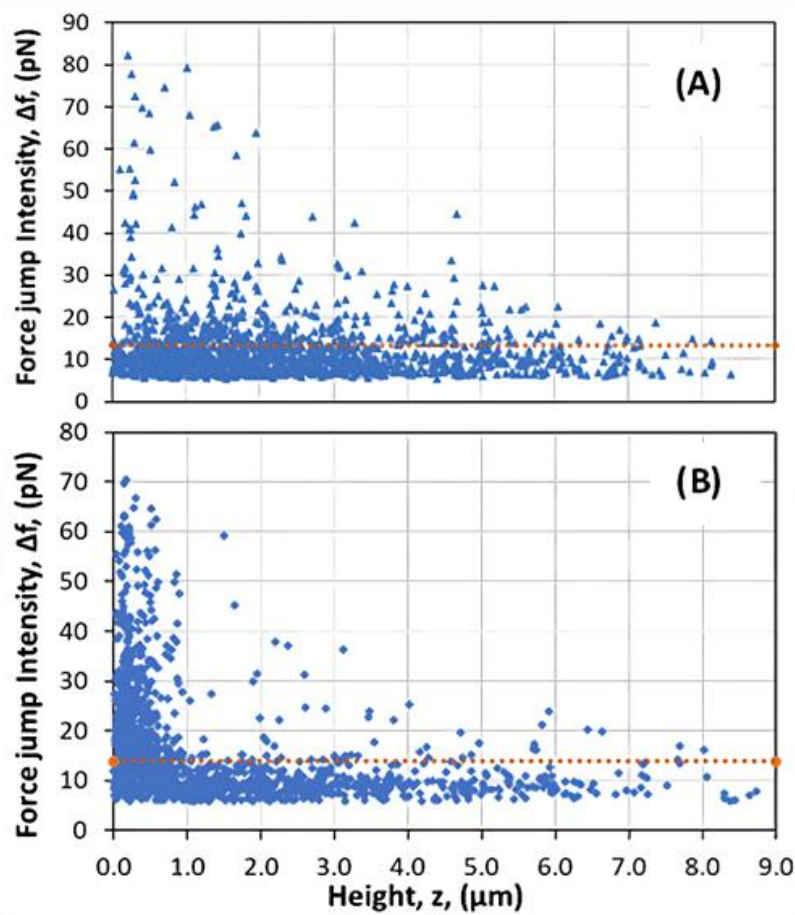


Figure 3.25. Distribution of force jumps (Δf) for chondrocyte detachment (zones B and C) from chitosan substrates vs. height (μm). Contact time of 60 seconds on the (A) chitosan film and (B) chitosan fiber mat. Dotted lines represent the average detachment force values for the film and the fibers, 13.37 pN and 13.85 pN, respectively.

As shown in figure 3.22 and described in figure 3.25, force jumps are randomly located along the retraction curve. There are no specifications about the order of every detachment step but they all can be associated with the rupture of chondrocyte-to-substrate links formed during the interval when the cell membrane enters in contact with the substrate.

The majority of force jumps are located in the first micrometers of the detachment curve for nanofibers, while they are dispersed on a wider distance on the film where the available surface for linkage is larger. This result was also observed in figure 3.22.

Considering the final straight line as the base line for data analysis (figure 3.22), the retraction response of cells (figure 3.25) enables to build a frequency step distribution curve, of force jump intensities (Δf) as a function, as shown in figure 3.26. This analysis groups all significant Δf values in intervals ranging from 2 to 3 pN, and allows to relate the force jump average and the jump intensity that could be due to an individual cell-substrate bond breaking (Sundar Rajan et al., 2017).

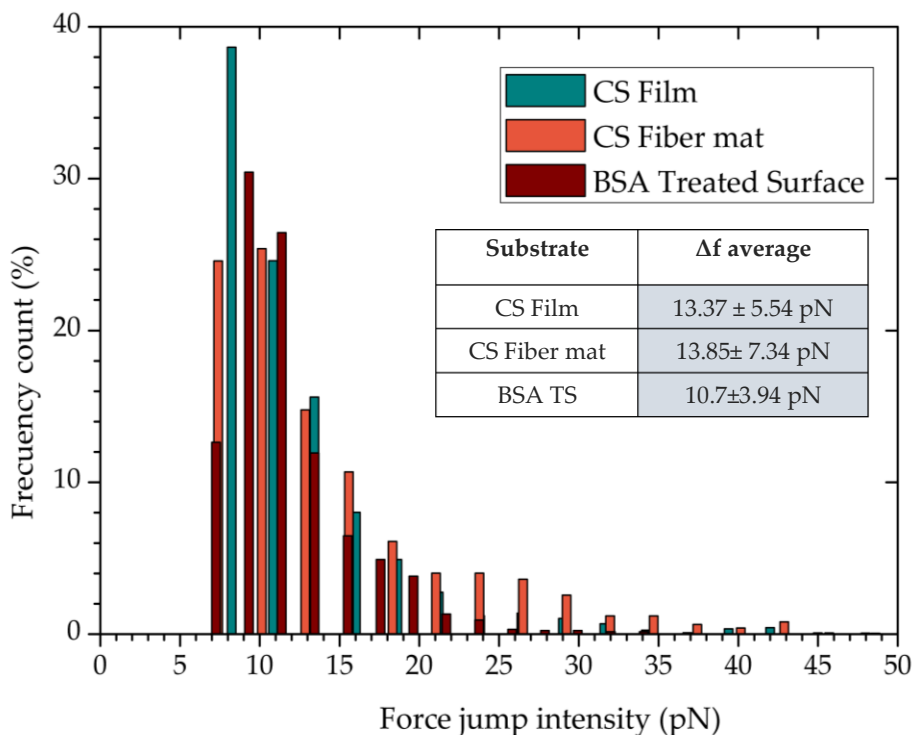


Figure 3.26. Force jump distribution for cell detachment on chitosan fiber mats and films, as well as the BSA coated surface, for a contact time of 60 seconds. Force jumps for all substrates are presented in the inserted table for a similar t_c .

From figure 3.26, it is observed that few jumps with higher intensity (over 15 pN) exist on nanofibers compared with the other substrates.

The substrate comparison is shown in the table inserted in figure 3.26, in terms of morphology (film and fiber) as well as in terms of affinity (BSA coated surface) for a contact time of 60 s. It can be also remarked that the average Δf is higher for the chitosan films and fibers compared to the BSA coated surface (as significant difference was found for a $p < 0.01$ ANOVA analysis). This effect can be attributed to the low cell-substrate selective interaction unfavored by BSA.

In the case of a contact time of 120 seconds, there were found 14.73 ± 7.58 pN and 13.97 ± 6.14 pN for CS film and fiber mat, respectively. From the obtained main values in figure 3.26, it is observed that the contact time does not reflect a significant difference ($p < 0.01$) on the average detachment steps (Δf) between the studied chitosan-based

substrates, independently of their morphology. This similarity could be explained for chitosan fibers and films, since the cell type is the same in all cases and all possible interactions have the same nature (CS-Chondrocyte).

Concerning the adhesion response, using the same technique for cell-cell adhesion strength, between an endothelial cell monolayer and tumor cells, detachment steps have been measured between 20 and 70 pN (Laurent et al., 2014; Sundar Rajan et al., 2017). These reference values are in the same range with the obtained response in the present experiments (detachment jumps between 10 and 80 pN in figure 3.25). Values acquired from different variants of AFM methods consisting of lateral displacement or detachment from a suction micropipette, after longer cell contact times (up to 90 minutes), on different types of cells are usually larger than those obtained in this work (Nagy et al., 2020; Sagvolden et al., 1999; Salá Nki et al., 2014; Sztilkovics et al., 2020; Tsang et al., 2006).

2.5.2. Adhesion Energy of chondrocytes on chitosan substrates

The adhesion energy was investigated for both cell-substrate responses, the chitosan film and the fiber mat, for a contact time of 60 seconds and compared to the BSA coated surface. As shown in figure 3.27, this parameter was affected, by the substrate morphology. The average adhesion energy value when the chitosan film was used as chondrocyte support was found 27% larger than the one observed for the nanofiber mat, 7.68×10^{-16} J and 6.05×10^{-16} J, respectively. Moreover, this difference was shown to exhibit the same trend for maximum detachment force values (Δf_{\max}) which are slightly higher for the chondrocyte-film interaction (see figure 3.24). This could be attributed to the density of cell-substrate bonds that were formed during the contact time and are expressed on the detachment response. On the other hand, we must consider the available contact surface when the chondrocyte touches the substrate. Due to fiber mat porosity, stiffness (Q. Zhang et al., 2016) and morphology, a smaller and softer direct area is available for the cell to attach during the short contact with the fibrous substrate surface.

Based on the same statement, difference in adhesion surface influences the total energy measurement on fibers as compared to films. This phenomenon results in an apparent lowering of the adhesion energy, Δf_{\max} values and, at the same time, affects the position of force jumps (Δf) (figure 3.25b) on the retraction curve.

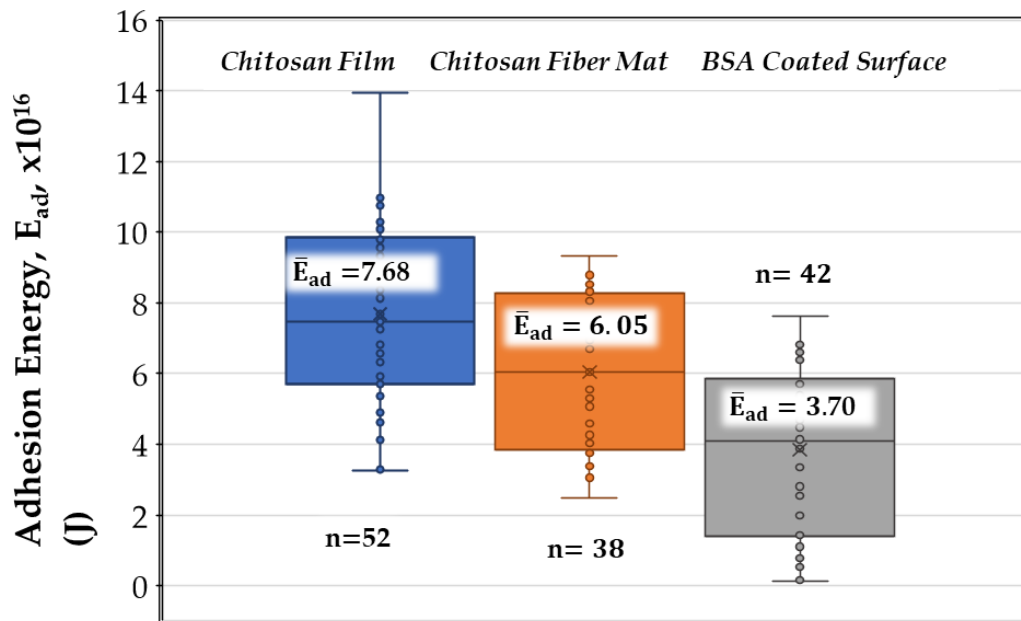


Figure 3.27. Adhesion Energy (E_{ad}) distribution for AFM adhesion test on chitosan-based substrates (chitosan film and chitosan fiber mat) compared to the BSA treated surface (significant difference found, $p < 0.01$). 25% of the data being lower and higher than first (Q1) and third (Q3) quartiles, respectively, are out of the box plot. The average value is represented with the cross in the colored area. Contact time equal to 60 s, number of assays = n.

Finally, comparison of the adhesion parameters on chitosan in contrast with the ones obtained on the surface coated with BSA is presented (figures 3.24 and 3.27). The maximum Δf for chondrocytes in contact with a BSA-treated surface had an average value of $223 \text{ pN} \pm 99 \text{ pN}$. This response is significantly lower ($p < 0.01$) as compared to the chitosan film and fibers. In addition, the adhesion energy value remains clearly lower than the response observed for the chitosan-based nanofiber mat and much lower than the detachment response in the case of the chitosan film ($p < 0.01$). The average adhesion energy determined is $3.70 \times 10^{-16} \text{ J} \pm 2.18 \times 10^{-16} \text{ J}$ for the BSA-treated surface. In fact, in the buffer used, BSA coated surface is negatively charged which promotes slight electrostatic repulsion as chondrocyte membrane has also a negative character. Cell adhesion on chitosan substrates is favored due to H-bond stabilization, hydrophilicity and polarity which serves to bind proteins on its surface. Protein adsorption and subsequent cell adhesion on biomaterial surface is the essential prerequisite for biomaterial induced tissue healing (Sukul et al., 2021).

3. Conclusion

Material characterization and production optimization are key procedures, for the sake of an appropriate design of chitosan-based substrates, with potential application on cartilage mending approaches.

In this section, the main experimental conditions for the successful electrospinning of chitosan and chitosan/hyaluronan complex, to produce nanofiber mats are reported. This process is observed to require the presence of PEO, in a yield >20%, blended with the polysaccharides for good spinnability. Polymer composition of the blends and solvent nature were studied, aiming to obtain nanofibers free of beads, using nontoxic solvents, able to easily evaporate after electrospinning. Acetic and formic acid allowed the processing of CS/PEO blends, while only formic acid enabled chitosan/hyaluronan polyelectrolyte complex preparation and electrospinning. In the case of PEC, fiber production, as well as material characterization, is studied as a function of the CS/HA charge ratio.

Stability of fibers was achieved by the use of a neutralizing ethanolic bath, which also allowed to extract PEO and solvent traces. Afterwards, CS fibers were stable under biological conditions (PBS, pH = 7.4).

In the same way, production of stable CS/HA complex nanofibers is reported with good stability of the materials. For that purpose, CS/HA fibers were thermally treated (120 °C, 4 h) to favor H-bond network, as suggested by NMR analysis. At last, samples were neutralized in alkaline non-solvent before stability measurements. Such complex nanofibers were produced allowing to take advantage of the two biologically active polymers for medical applications. Fibers with diameters in the range 100 to 200 nm were obtained from both systems.

Physicochemical characterization of CS and the complex CS/HA was enabled by the use of polymer films as model. Overall, based on water retention capacity, partial solubility and behavior of the samples under uniaxial traction, the more appropriate conditions for scaffold preparation were selected.

Electrospinning of the systems, using several micro-structured collectors allowed the obtention of randomly oriented and aligned fibers, as well as fibrous mats having squared and hexagonal patterns. The fabrication of this type of mats aims to study the impact of their topography on their biological response during cell culture.

During an initial study of chitosan/cells interactions, by the SCFS method, a single chondrocyte in contact with chitosan substrates allowed to characterize the adhesion force on chitosan films compared to fiber mats. The contact surface of cells on chitosan films revealed a slightly higher adhesion strength in contrast to fiber mats. However, cells could establish anchoring points easier on porous substrates such as nanofibrous scaffolds which present a similar topography as the extracellular matrix.

Chapter IV. Chondrocyte development on chitosan-based electrospun materials.

Cell development studies on engineered scaffolds implies, in a first step, the analysis of cell viability, cell adhesion and proliferation. In view of these aspects, the previous characterization of cell adhesion strength, on CS-based materials, helped understand the adhesion process itself coupled to the influence of the support topography on cell behavior. Chondrocytes are able to attach to a substrate with a high density of cell-substrate bonds. On chitosan films, with larger contact surface available, such an adhesion force, leads to cell morphology changes. Slightly lower forces, observed in porous fiber mats, could affect differently the cell shape as it is studied in this chapter.

Chondrocyte culture behavior on chitosan-based materials was performed by varying, mainly, the topography of the substrate. Fibrous mats produced by electrospinning of the blend CS/PEO are compared to CS films in terms of cell activity response. The influence of morphology of chitosan supports and cell characteristics are investigated by cell counting, staining and fluorescence microscopy. Similarly, chondrocyte development features, such as adhesion, morphology, viability and proliferation, on polyelectrolyte complex (PEC) fibrous materials are introduced.

1. Cell compatibility and viability

Chitosan is known as a biocompatible polymer. Its non-citotoxicity and compatibility with biological tissues is confirmed through chondrocyte culture on CS fibers and films in the next sections. Initially, adhered cells were observed in Figure 4.1 A and B on fiber mats. Comparison with cell behavior on a flat surface is shown in Figure 4.1 C and D for chitosan film and plastic culture dish respectively. Cell imaging is obtained for a fixed incubation time of 7 days and NBT cell staining is applied to ease cell identification.

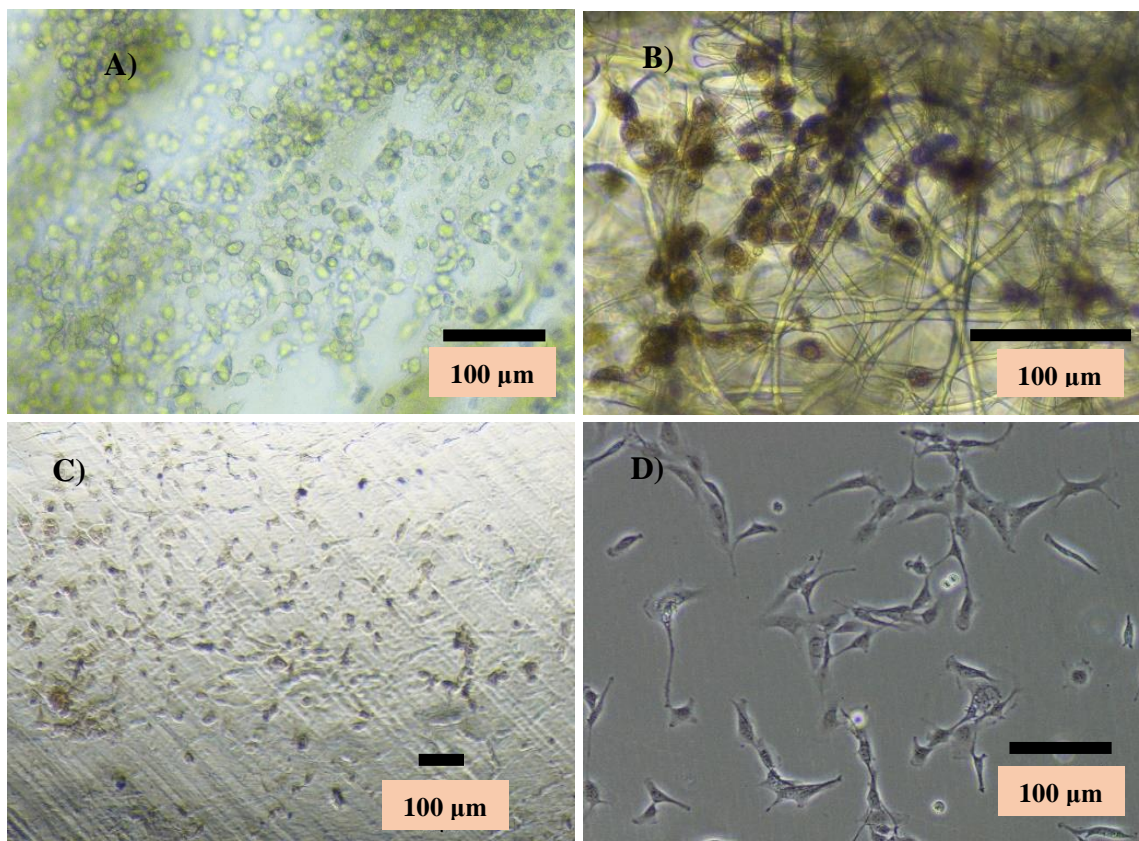


Figure 4.1. Chondrocyte proliferation on neutralized chitosan fiber mats, casted film and culture dish after 7 days of incubation. CS fibers produced from 80/20 CS/PEO blends utilizing (A) PEO MW = 1000 kg/mol and (B) PEO MW= 5000 kg/mol, (C) CS casted film and (D) culture dish (Garcia Garcia et al., 2021).

As it is established in former analysis, fiber size diameter increases with the increasing of the PEO molecular weight, contained in the mixture (figure 3.1). This difference in fiber dimensions is also noticed during cell culture observations (figures 4.1A-B), where average fiber diameter is considerably higher for electrospun fiber with 5000 kg/mol PEO compared to 1000 kg/mol PEO (Garcia Garcia et al., 2018; Lemma et al., 2016).

On CS films, as presented in figure 4.1 C, cells remain isolated and spread on the surface (characteristic of adherent cells on flat substrates). In contrast, the fibrous structure prevents changes in cell shape, cells attach all over the mat and remain spherical as found in literature (Ridolfi et al., 2017). This is claimed to preserve the native phenotype by keeping the same cell morphology as in original tissues (García-López et al., 2015; Jin et al., 2014; Rogina et al., 2021). Primary chondrocytes in mammal articular cartilage are encapsulated in individual cavities (lacunae), as it is shown in figure 4.2. Therein, the rounded shape is acquired and remains unchanged during the cell cycle.

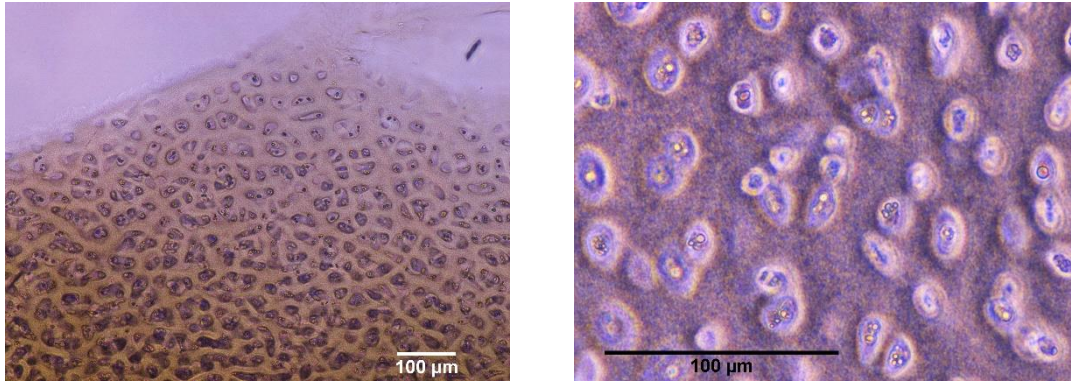


Figure 4.2. Histological slice of bovine articular cartilage stained with NBT observed at magnifications 10X and 40X.

Regarding cell size differences from Figure 4.1, once spread on flat surfaces, chondrocyte shape is importantly changed and cell size can reach up to 30-50 μm compare to their average diameter of 10 to 20 μm when the rounded shape is maintained, i.e., when adhered to CS fibers and in the native lacunae.

These initial cell culture experiments allowed the identification of the key steps needed for cell development and, considering the particular case of chondrocytes on the produced chitosan fibers, a schematic behavior is proposed is figure 4.3.

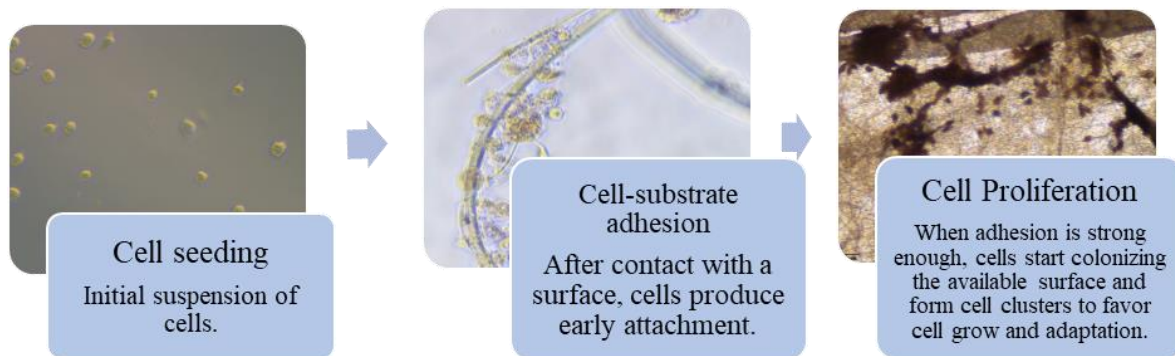


Figure 4.3. Successive steps of chondrocyte culture observed on chitosan fibers.

2. *Chondrocyte adhesion*

1.1. Chondrocyte adhesion kinetics

For the adhesion study, the thicker CS fibers were selected, facilitating sample handling. A predefined density of chondrocytes (10000 cell/ cm^2) were seeded on chitosan mats and films, then, they were collected from the substrates after different culture periods up to 24 hours. For these measurements, it is admitted that adhesion between seeded cells and supports occurred during the first hours of contact (Nguyen & Gu, 2016). Firstly, the totality of adhered cells is detached from the substrates and counted by fluorescence as described previously. It is expressed as the fraction of total adhered/seeded cells on the same surface of support (1 cm^2). Secondly, the fraction (in %) of living cells among the total cell detached were calculated based on the viability

fraction from the cell counter. In figure 4.4. the variation with time of the ratio of total adhered/seeded cells is presented.

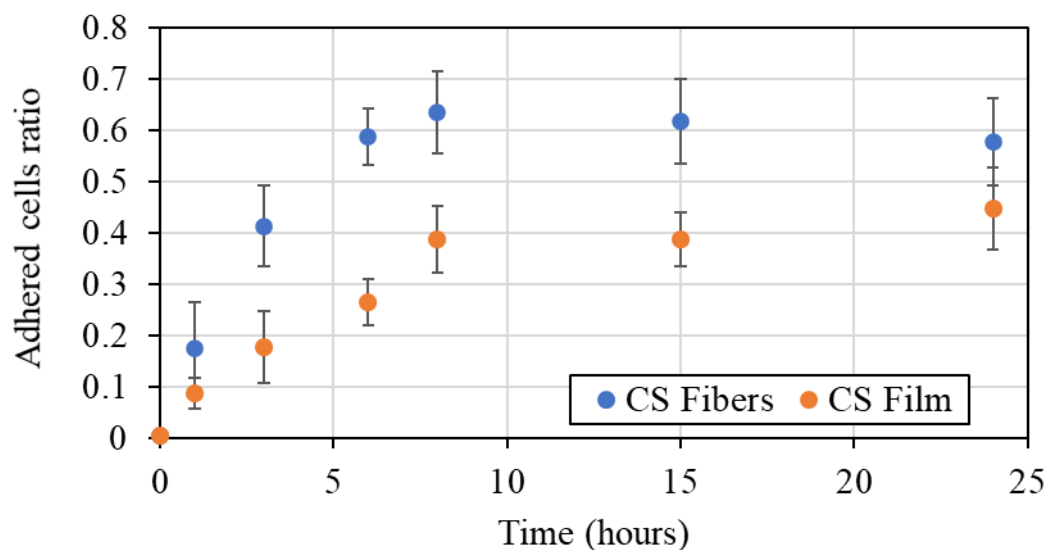


Figure 4.4. Cell adhesion kinetics of chondrocytes: adhered cell ratio as a function of seeding time, on neutralized chitosan fibers produced from CS/PEO blends using PEO MW = 5000 kg/mol compared to the adhesion response on CS film. Error bars represent mean \pm SD; n=3.

For each substrate having different morphology, it is shown in figure 4.4 that the total number of adhered chondrocytes, counted after detachment, increases as a function of seeding time. Cells were observed to develop more efficiently on fibers compared with films. This difference is attributed to the substrate topography and accessible surface for cell adhesion, which is lower on the chitosan films compared to fibrous supports. On fibers, characterized by pores having dimensions around the magnitude order of cell diameter, the cell adhesion ratio is observed constant (no significative difference) over \sim 8 hours after cell seeding. This behavior could be related to entrapment in the fibrous mat causing a lower cell detachment yield (i.e., cell quantification), but indicating a stronger adhesion. This process is confirmed since some remaining adhered cells were observed on the fiber mat by microscopy after trypsinization and PBS washings.

In the same experiment, the quantity of adhered living cells can be estimated using cell viability values (given by the cell counter). Living/total cells ratios are presented in figure 4.4 for both chitosan substrates.

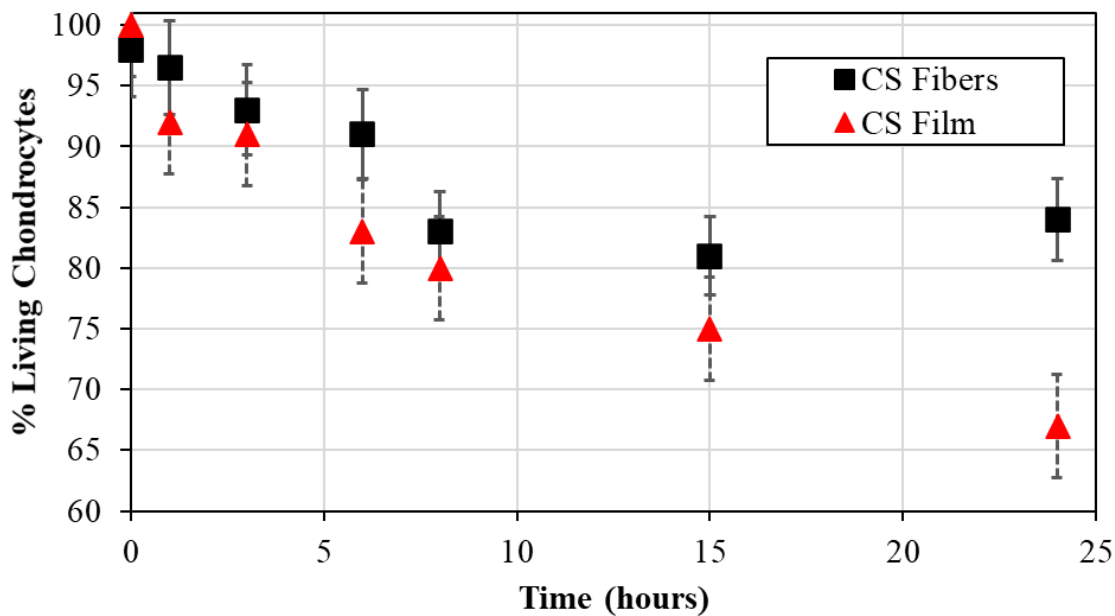


Figure 4.5. Living chondrocytes fraction as a function of seeding time, for the adhesion response on neutralized chitosan fibers (■) produced from CS/PEO (80/20) blends using PEO MW = 5000 kg/mol and CS film (▲) as control. Error bars represent mean \pm SD; n=3.

In the case of fibrous supports, no significant difference ($p < 0.01$) was found for the measurements at 8, 15 and 24 h. It indicates that cell viability is nearly constant 8 hours after cell seeding. In contrast, the fraction of living cells decreases continuously on films (statistical difference for $p < 0.01$) during the 24-hour observation, probably due to limited surface available after spreading. Actually, on chitosan film as well as on coated polymeric surface, cells adhere, expand and occupy a larger area than cells adhering to fibers which remain nearly spherical (Figure 4.1). This behavior was observed previously on nanofibers allowing chondrocyte phenotype preservation (García-López et al., 2015; Jin et al., 2014; Rogina et al., 2021). These data may also justify the decrease in cell viability as a function of time, observed on CS films since trypsinization could disrupt protein linkages and then cell properties, at least partially. Cell viability, shown in Figure 4.5, indicates a good adaptation of chondrocytes with the nanofiber mat substrate proposed. Once adhered and adapted to the substrate, cells remain alive and start colonizing the new matrix, as viability fractions increase over 15 h. Consequently, chitosan films are less convenient for chondrocytes development.

1.2. Parameters influencing cell adhesion

Dried fiber mat samples produced with both PEO molecular weights were used for chondrocyte culture allowing to compare the role of fiber diameters. Cell counting

after 24 hours of seeding helped to evaluate the influence of the neutralization step and fiber diameter on cell adhesion. A series of results is given in Table 4.1.

Table 4.1. Fraction of adhered cells on chitosan fiber mats after 24 hours of seeding and cell viability expressed as %*.

Molecular Weight of PEO in the CS/PEO blend	With neutralization step	Without neutralization step
MW = 1000 kg/mol	0.520 ± 0.244 *87%	0.714 ± 0.248 *79%
MW = 5000 kg/mol	0.495 ± 0.178 *85%	0.611 ± 0.232 *81%

In absence of neutralization, PEO fraction becomes soluble in the culture media at pH=7.4 during the first step of biomaterial conditioning. It was previously proved that chitosan remains insoluble in this case but with a slightly higher degree of swelling (Garcia Garcia et al., 2018). From table 4.1, it is demonstrated that the fraction of adhered cells shows a slight decrease as the PEO MW increases in relationship with the increasing of fiber diameter and porosity. The viability remains the same for the two types of neutralized fibers. Slightly higher values for adhered cells on as-spun fiber mats (without neutralization) could be related to electrostatic interaction between the residual protonated groups in chitosan chains and the cell membrane negatively charged. However, in this case, slightly lower viability is obtained.

Taking into account these parameters, neutralization of chitosan fibrous mats is considered necessary for substrate stability while maintaining a high living cell ratio during cell culture. In the same context, fibers containing PEO MW=1000 kg/mol are preferred as it is easier to take out from the mats during neutralization (Garcia Garcia et al., 2018).

2. Proliferation of chondrocytes on CS fibrous mats

2.1. Neutralization step and fiber diameter influence

Related to fibrous substrates, fiber size is considered an influencing factor on cell development (Bhattarai et al., 2005; Noriega et al., 2012). The materials produced from the blend CS/PEO, with both PEO MW, were used to compare the proliferation behavior of chondrocytes on fiber mats having different fiber diameter.

After detachment of cells from the chitosan fibers and films by trypsinization, the viability and quantity of total cell detached were determined. Living cells quantification on chitosan substrates for different proliferation times are shown in

Figures 4.6 and 4.7 involving the two diameter fibers compared to a film. The effect of the neutralization treatment of the chitosan fibers, being important for fiber stability is joined.

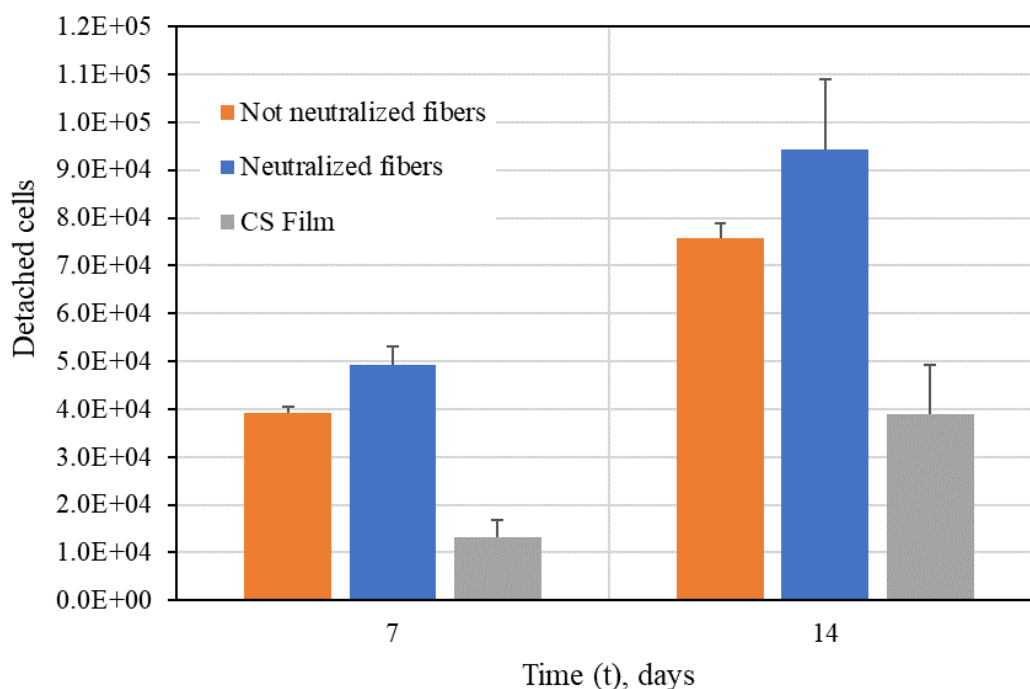


Figure 4.6. Cell proliferation for chondrocytes on chitosan substrates: total living cells detached as a function of time for PEO, MW = 1000 kg/mol on pure chitosan fibers (■), as spun-fibers (■) and CS films (■). Error bars represent mean ± SD; n=4 for fiber mats and n= 3 for CS films respectively.

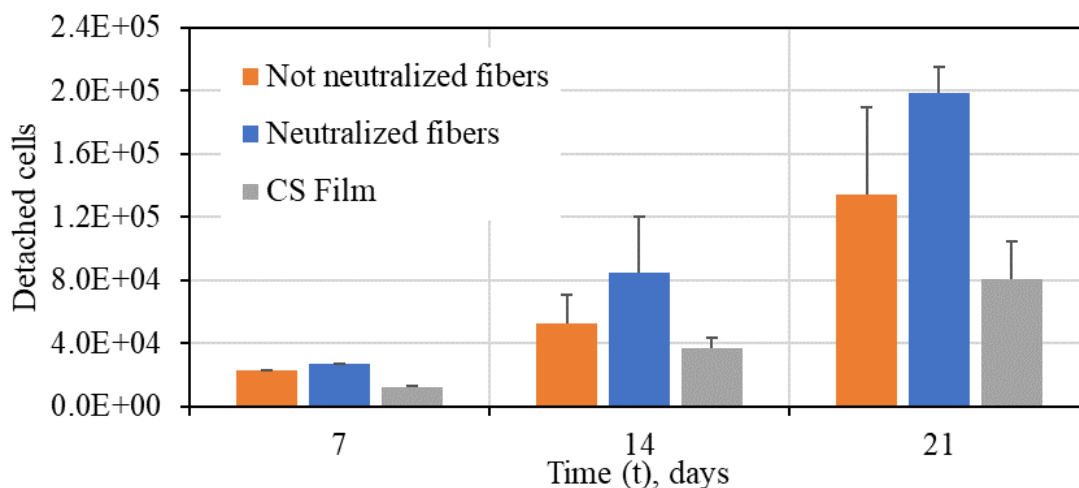


Figure 4.7. Cell proliferation for chondrocytes on chitosan substrates: total living cells detached as a function of time for PEO, MW = 5000 kg/mol on pure chitosan fibers (■), as spun-fibers (■) and CS films (■). Error bars represent mean ± SD; n=4 for fiber mats and n= 3 for CS films respectively

An increasing cell development is observed with time in Figures 4.6 and 4.7, as expected, for colonization on a compatible substrate. From Figure 4.6, on the thinner

fibers, after 7 days of culture, around 3.5 times more cells were detached from the neutralized fibrous substrates compared to films. These data also allow to conclude that fibers made of pure chitosan (after neutralization step) favor proliferation of chondrocytes in comparison with results before neutralization. In both cases, the number of detached cells is higher in contrast to the chitosan film. This could be related to the local cell confluency reached first on the cast films where cells decreased their activity and started detaching. Whereas chondrocytes on the electrospun fibers kept on growing as the available surface to create adhesion anchoring point is larger (Subramanian et al., 2005). Moreover, on mats produced with 5000 kg/mol PEO, pores are larger favoring cell penetration into the fiber network. These results from cell development on film and neutralized fibers confirmed the data obtained for the adhesion step in Figure 4.4.

A higher number of cells, at $t = 7$ and 14 days after seeding, were found on fiber mats produced from the blends with 1000 kg/mol PEO while less chondrocytes seemed to be colonizing the mats fabricated with 5000 kg/mol PEO. The later providing information with wider standard errors.

Finally, thinner chitosan fibers are more efficient for adhesion and proliferation of chondrocyte cells. Moreover, longer cell observations on chitosan nanofibers, permitted to identify the oval shape of chondrocytes, conserved up to 14 and 21 days, indicating phenotype preservation as mentioned previously.

2.2. Effect of solvent and composition of the blend

Accordingly with previous discussions, CS/PEO fiber mats have been produced using two PEO MW (5000 and 1000 kg/mol), which gives as result an important difference in fiber diameter. However, thinner fibers, produced with 1000 kg/mol PEO, were considered more efficient for cell development even though the sample handling is slightly difficult.

Related to fiber preparation with PEO MW=1000 kg/mol, formic and acetic acid have been used during electrospinning, allowing the production of fibers with close diameter values, around 120 nm and 150 nm respectively. In the same context, when composition of the blend is analyzed, 80/20 and 70/30 CS/PEO proportions enable the fabrication of fibrous mats. In order to contrast the effect of these variables on cell development, proliferation tests were performed for the different samples and proliferation profiles are shown in figure 4.8. Cells were detached from the samples and quantified by fluorescence in a cell counter.

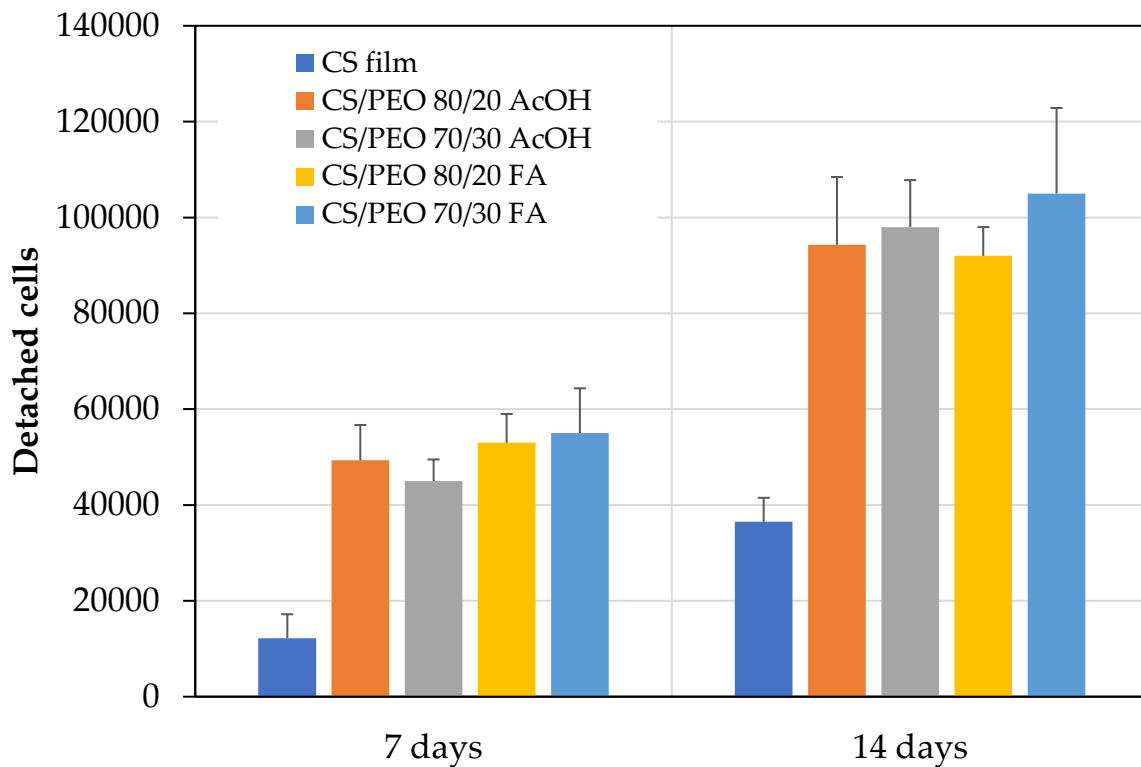


Figure 4.8. Proliferation of chondrocytes on chitosan substrates. Total living cells detached as a function of time on neutralized chitosan fibers produced from the blends: (■) CS/PEO 80/20, (■) CS/PEO 70/30 using AcOH as solvent, (■) CS/PEO 80/20, (■) CS/PEO 70/30 using FA as solvent; and (■) CS films. PEO MW= 1000 kg/mol. Error bars represent mean \pm SD; n=3.

From the culture experiment results presented in figure 4.8, cell development is confirmed for the studied substrates. Even though a situation with four different samples seems to be faced, small differences in total living cells, detached from the substrates, are found when comparing cell number at 7 and 14 days after seeding. Viability of the detached cells was registered, with living cell proportions between 90% and 100% for all fibrous supports. According to cell/substrate observations, characteristic dimension of cells ($\sim 20 \mu\text{m}$) is two orders of magnitude higher contrasted to the one of as-spun fibers ($\sim 120 \text{ nm}$ and $\sim 150 \text{ nm}$), for FA and AcOH as solvents respectively. Then, the influence of the fiber diameter difference on cell culture, due to the solvent could be neglected.

In the same context, since the neutralization step of CS/PEO mats prior to cell seeding is needed, PEO extraction can be assumed (Garcia Garcia et al., 2018). Consequently, pure CS fibers are in contact with cells whatever the PEO content after electrospinning (30 or 20%).

In conclusion, when applying CS/PEO mats with close fiber diameters and polymer content for cell development, a similar response can be expected. A slightly higher

number of cells was detached from fibers obtained from the blend CS/PEO 70/30 (FA as solvent) in comparison with the rest of substrates. This minor difference can be attributed to the sample topography since systems containing FA were observed to reduce fiber defects and fiber-fiber adhesion, during fiber collection, due to higher solvent volatility (C. E. Garcia et al., 2020). For further analysis, fiber mats produced from blends with a 70/30 CS/PEO content, in FA as solvent, are utilized.

2.3. Influence of CS fiber structuration on cell development

Similar proliferation tests were performed on fiber mats produced from the blend CS/PEO 70/30 in FA varying, in this case, the fiber arrangement. The different fiber organizations have been obtained by using several collectors during the electrospinning process. It has been discussed that solutions containing chitosan are difficult to spin, and patterned collectors are partially replicated by the spun fibers (Chapter 3, Section 3.3). Nevertheless, the relevance of fiber arrangement on cell development is worth to be covered. In figure 4.9, total living cells were quantified as a function of time for several fibrous substrates produced by electrospinning on aluminum foil, patterned and rotatory collectors. The results are compared to cell colonization on CS films.

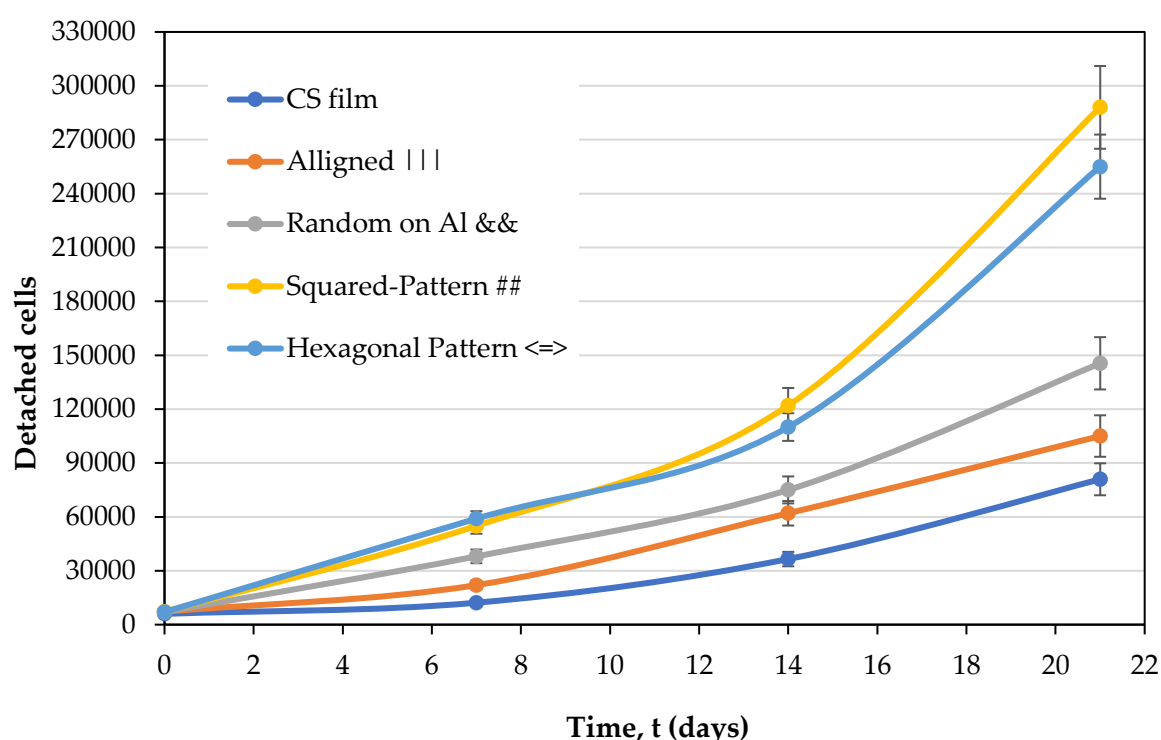


Figure 4.9. Proliferation of chondrocytes on chitosan substrates. Total living cells detached as a function of time on neutralized chitosan fibers produced from the blend CS/PEO 70/30, using different fiber collectors: (■) rotatory cylinder (at 1500 rpm), (■)

aluminum foil, (■) square-patterned collector, (▣) hexagonal-patterned collector and (■) CS films. PEO MW= 1000 kg/mol. Error bars represent mean \pm SD; n=3.

During these measurements, it is confirmed that all types of fibrous substrates have a more efficient performance for chondrocyte development than the CS film. Detached cells duplicate around every 7 days and cell viability values are found close to 90-95% in the studied fiber mats. Detached cells present an average diameter in the range of 14-22 μm . This result corresponds to primary chondrocytes reported to have an average size between 10 and 40 μm (Hirsch et al., 1997).

Cell development profiles on aligned fibers were close to the behavior on the CS film. This could be related to the high fiber density in the mat, since fibers are mostly oriented and, consequently, closely packed. Moreover, during electrospinning, the collector rotation promotes fiber stretching while alignment, approaching the substrate topography to a thin film (Thomas et al., 2006). Mass/volume ratio for aligned fiber mats was estimated in the range of 0.090-0.105 g/cm^3 . Mats of randomly collected fibers may also present higher degree of compactness compared to structured fiber mats (Table 3.7, chapter 3), with fiber mat specific mass between 0.069-0.082 g/cm^3 . More compact materials were observed to promote cell detachment, cell cluster formation and slower cell development (observed on CS films and aligned fibers).

In the case of fibrous mats recovered on the structured collectors with squared and hexagonal mesh, a significant increase in detached cells quantity is found in contrast with the rest of substrates. Structured substrates show low material density which suggests they are more porous, a key property of materials for biological applications. When squared and hexagonal patterned substrates are compared, cell proliferation seems to be favored on the former, but no relevant difference is found since detached cell quantities differ in a 10 % between both types of substrates. For further cell culture measurements, CS/PEO mats on square pattern collectors were selected.

2.4. Proliferation measured by colorimetry

Colorimetry, by intercellular INT reduction, helped to support and improve cell counting measurements performed by fluorescence. In this technique, cell detachment is not required, which is an advantage since an important number of cells could still be adhered to the fiber mat even after the trypsinization in the detachment step. The assays were performed on cells adhered to CS fibers, produced from the blend CS/PEO 70/30 (square pattern) as a function of time.

In figure 4.10, the proliferation profile of chondrocytes C20A4 on CS-based mats is presented. Since favorable repeatability was observed, absorbance measurements are related to a cell number after absorbance calibration using a known concentration of chondrocytes.

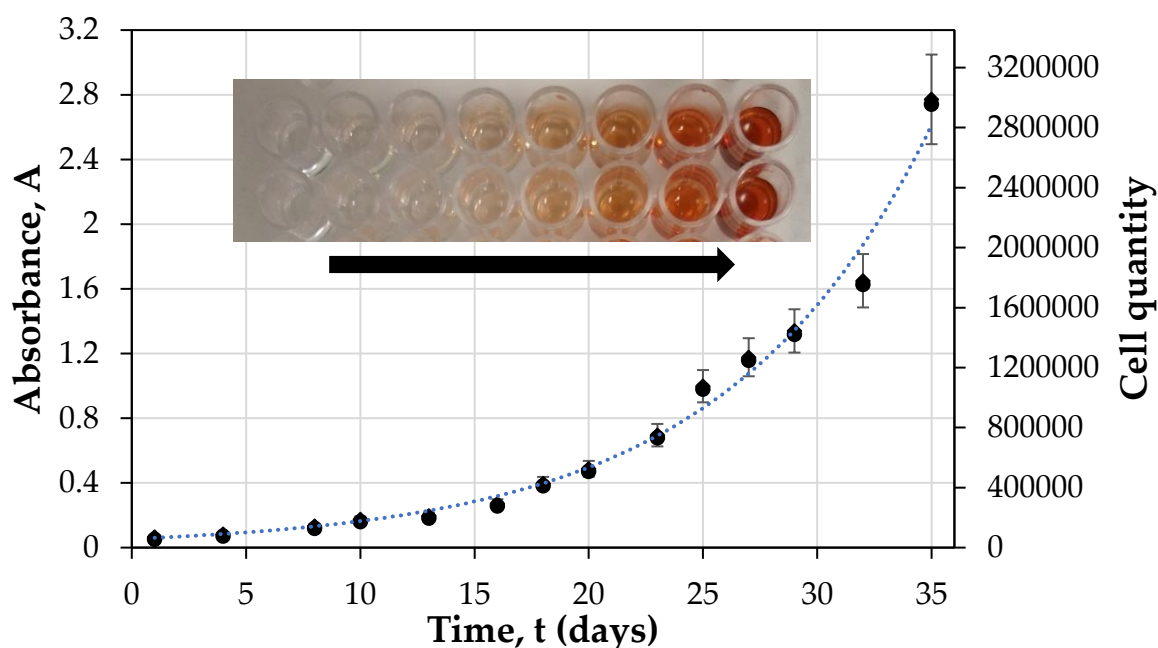


Figure 4.10. Proliferation curve obtained by INT colorimetry of C20A4 cultured on CS fiber mats (substrate surface = 1 cm²). Absorbance values were measured at 490 nm. Fit in dotted line.

From these experiments, a similar trend is observed compared fluorescence cell counting. The number of cells that develop on the mat increases exponentially with time, according to the fit, indicating an exponential growth with a characteristic growth time (τ) of 9 days. When relating the absorbance with the cell quantity, it reveals that cells could reach a proliferation ratio of 50 comparing day 1 with day 35. In terms of cell quantity, a higher number of adhered cells is identified with this method in contrast to fluorescence counting, for a similar observation time. At $t=14$ days, $\sim 120\,000$ cells counted by fluorescence while colorimetry relates the absorbance to $\sim 200\,000$ cell. The difference increases for measurements at $t=21$ days. This can be attributed to a more efficient cell determination since they are quantified without any detachment process, hence cell loss and the experimental error are reduced.

Visually, the evolution of the extract color intensity with proliferation time is clear. This method has shown adaptability, as it is applied to the cell/substrate ensemble, and helped for cell counting of adherent cells difficult to detach from CS mats. Presence of supports was observed not to affect spectrometry measurements.

2.5. Fluorescence staining

From cell proliferation studies, the influence of the substrate morphology on the cell population, colonizing the supports, was obtained. Cell visualization could apport more evidence of cell shape and adaptation to the fibrous mat during proliferation. However, cells are transparent and difficult to identify in the mat. Thus, cell staining with Red-FP defective virus and Hoechst-33342 dye was applied to chondrocyte culture, on various chitosan-based substrates.

2.5.1. Staining assessment by FACS

Hoechst-33342 staining helps to mark the nuclei of fixed cells, while Red-FP cell transfection is carried out on living cells marking the cytosol, as describe in the method. The effectiveness of the staining process was confirmed by Fluorescence-Activated Cell Sorting (FACS). This technique gives also information about cell form which could be relevant to establish the effect of staining on cell health (in the case of Red-FP).

In figure 4.11, from flux cytometry results, a representative sample is presented in terms of size, quantity of particulates inside of the cell (granularity) and fluorescence intensity for chondrocytes C20A4 before and after Red-FP transfection.

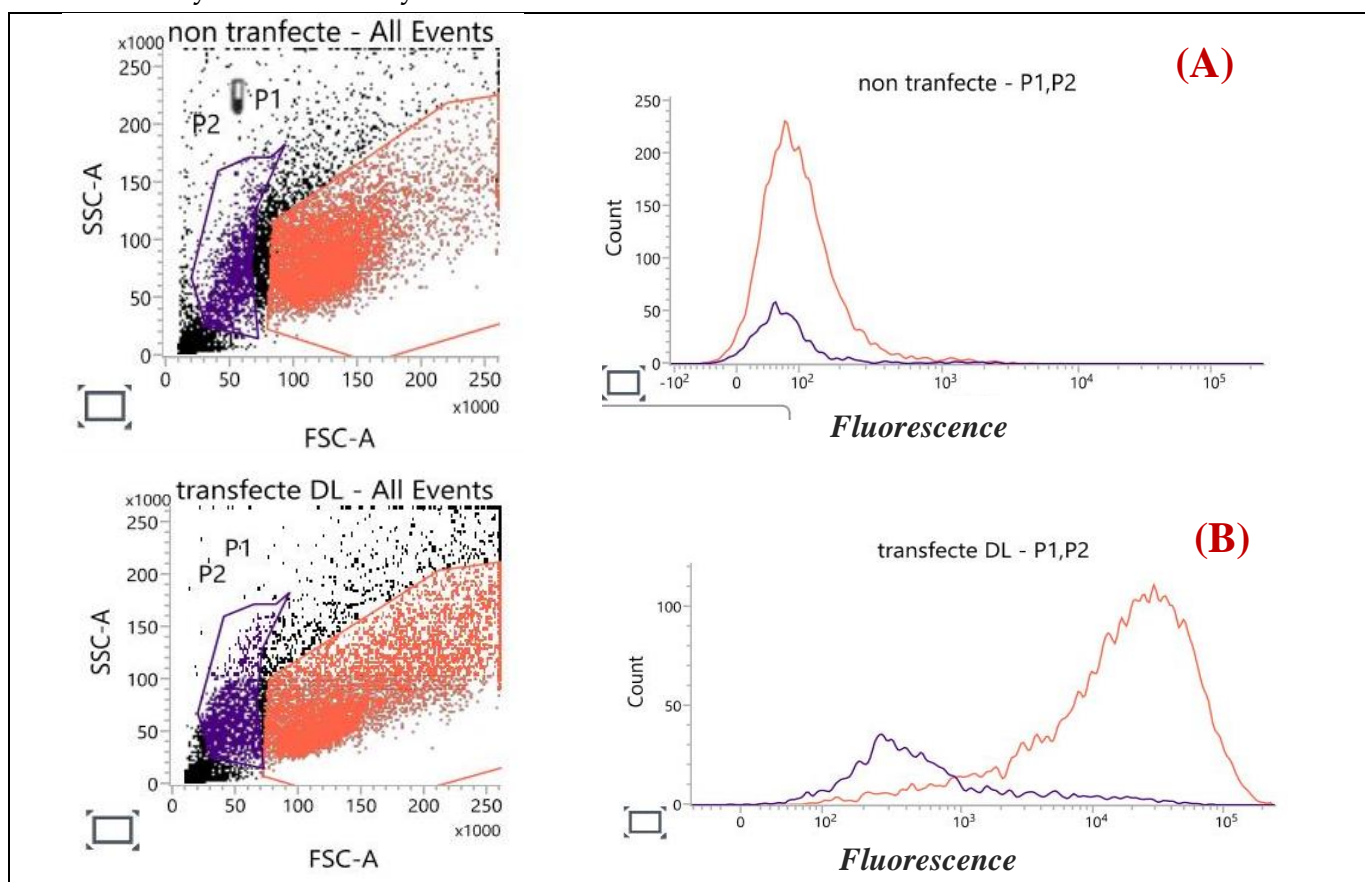


Figure 4.11. Analysis by flux cytometry of chondrocytes C20A4. On the left, cell size/granularity distribution and, on the right, fluorescence intensity distribution of cell populations P1 (orange) and P2 (violet); before (A) and after (B) Red-FP transfection. Red FP produced by transfected cell is read at 488 nm, filter 486/42.

From single-cell flux cytometry analysis, presented in figure 4.11, the differences in morphological cell parameters on the size/granularity distribution, helped to identity two populations: a major population P1 and a subpopulation P2. The subpopulation displayed a decrease in forward light scatter (FSC) and an increase in side scatter (SSC) indicative of cell shrinkage and increased granularity, respectively, both indices

representing characteristics of apoptotic cell death. The major population P1 presented an increase in FSC related to viable cells (Healy et al., 1998).

Concerning the fluorescence intensity of P1 and P2, a peak between 0-100 is observed for non-transfected cells in figure 4.11A. When transfection (staining) occurs, the fluorescence peaks are shifted to values in the range of 10^4 - 10^5 for P1 and around 400 for P2 (figure 4.11B). The lower fluorescence from unhealthy cells of P2 corresponds to a 11-13% of the total measurements. Before and after Red-FP transfection comparison for P1, clearly shows that transfected living cells emit 200 more fluorescence, at the studied wave length.

In the case of cell staining with Hoechst 33342 marker, the fluorescence peak is displaced from ~ 7000 to ~ 50000 , for a unique cell population P1, as it is shown in figure 4.12A and B.

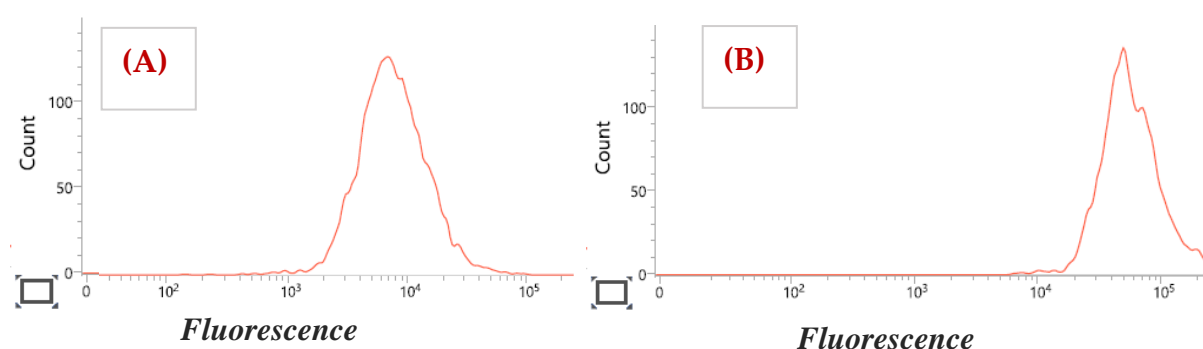


Figure 4.12. Fluorescence histograms from flux cytometry of chondrocytes C20A before (A) and after (B) staining with Hoechst 33342. The marker is read at 405nm, filter 450/40.

Globally, both markers could allow cell observation by fluorescence microscopy. Cell transfection with Red-FP is effective and cells can be stained with both fluorochromes.

2.5.2. Fluorescence Microscopy

Stained chondrocytes were more efficiently monitored by fluorescence. From this technique, the nuclei (in blue) and the cytosol (in red) can be observed for cell culture on any substrate.

Firstly, cells cultured on well plates were analyzed by fluorescence. When seeded, C20A4 chondrocytes are round with diameters between 10 and 40 μm . Once cells become adherent, after some hours accordingly to cell adhesion tests, they acquire a star-like morphology as it is observed in figure 4.13.

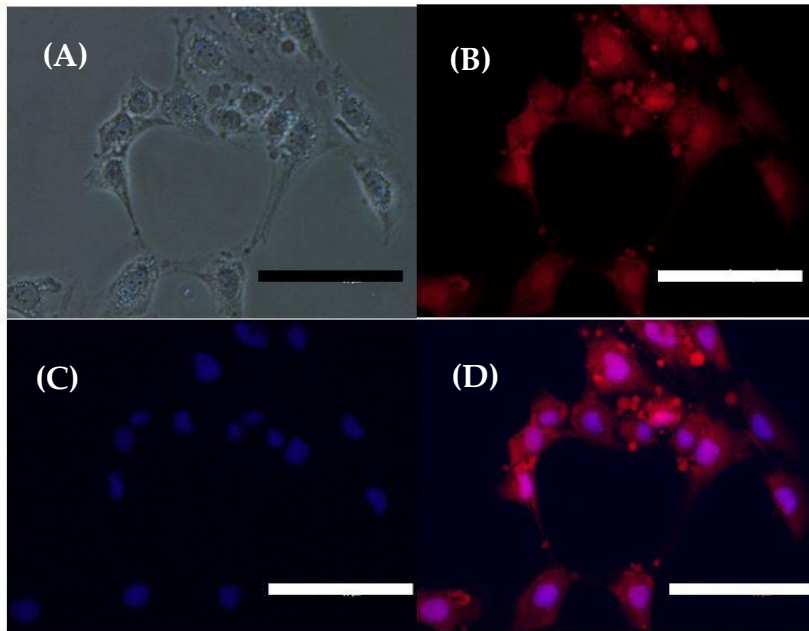


Figure 4.13. Chondrocytes C20A4 adhered to a culture dish, 24 hours after seeding, observed on an inverted fluorescence microscope. (A) normal light, (B) Red-FP transfection, (C) Hoechst-33342 staining and (D) Image overlay. Lasers: Blue, Excitation 325-375 nm/ Emission 435-485 nm and Red, Excitation 510-560 nm/Emission 590 nm. Scale bar corresponding to 150 μm .

As it is presented in figure 4.13, the combination of blue/red fluorescence allows to easily identify cell placement in the mat and possible cell arrangements. More importantly, cell staining allows to distinguish the cell morphology when adhered to a substrate. In flat surfaces, such as CS films or culture plates film, large spread cells are observed, as it has been argued in this chapter.

Consequently, fluorescence microscopy observations were performed in order to reveal the cell morphology adopted once chondrocytes developed on CS fibers. Several types of substrates were utilized for cell culture as it has been presented in proliferation measurements. Contrasting fiber orientation, cell staining was applied to culture on aligned and random fibers, as shown in figure 4.14.

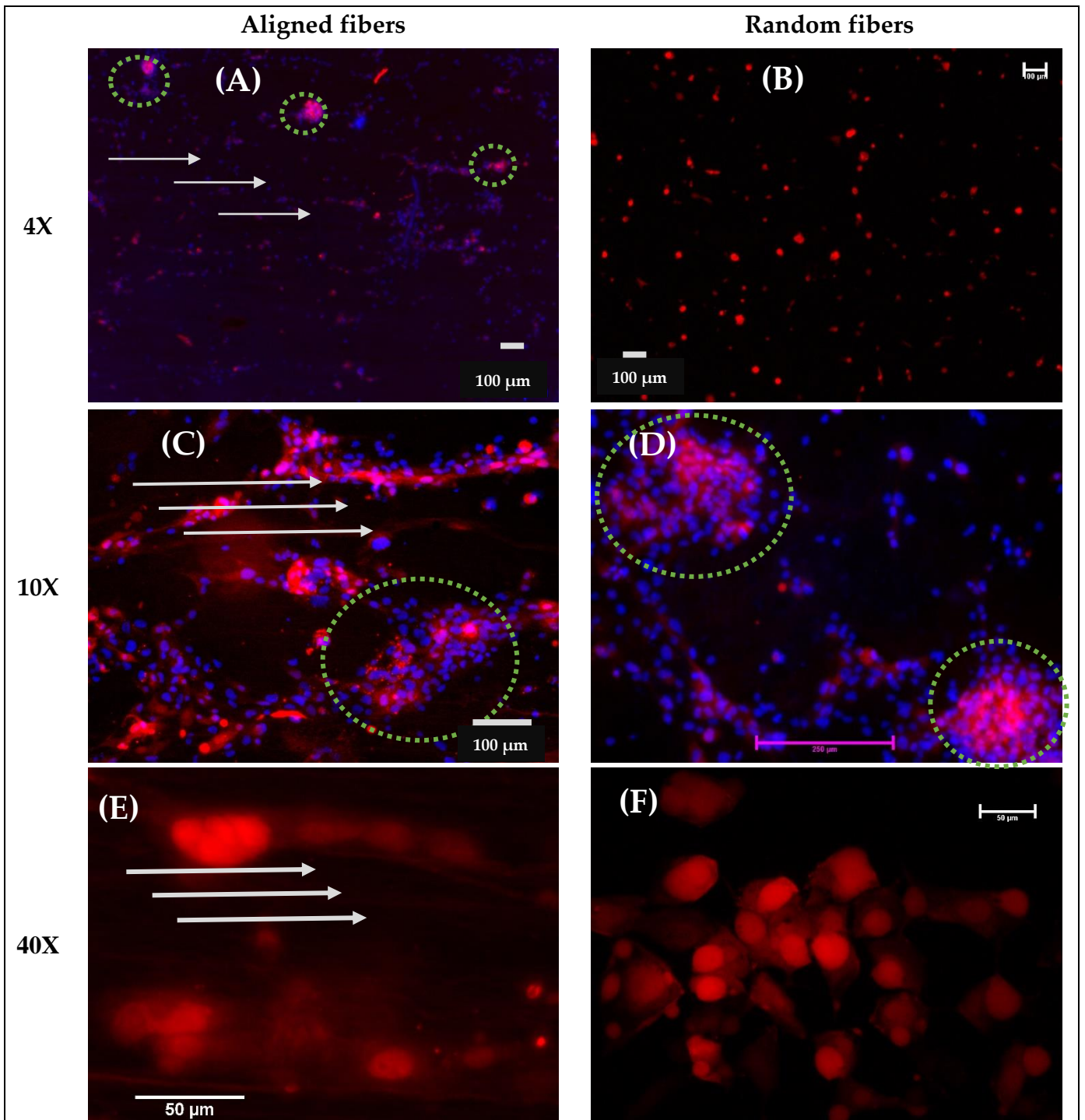
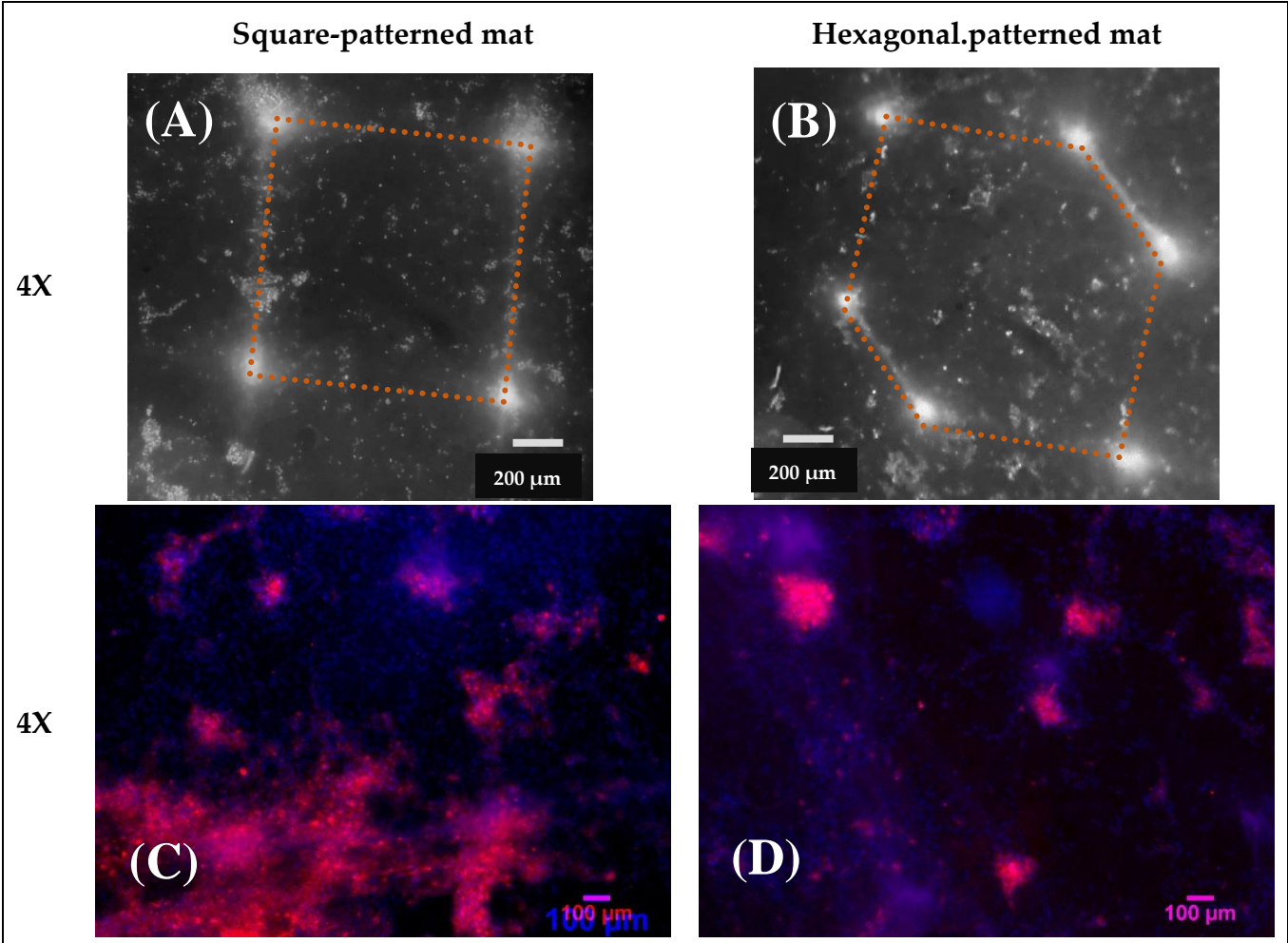


Figure 4.14. Chondrocytes C20A4 adhered to CS fibrous mats, observed on an inverted fluorescence microscope, 10 days after seeding. Substrates: aligned fibers at magnification 4X (A), 10X (C) and 40X (E); randomly oriented fibers at 4X (B), 10X (D) and 40X (F). Lasers: Blue, Excitation 325-375 nm/ Emission 435-485 nm and Red, Excitation 510-560 nm/Emission 590 nm.

From figure 4.14, it is observed that cell alignment has been partially influenced, in certain zones of the substrate, by fiber orientation. Sequences of chondrocytes, with length between 100-500 μm, are found on the mat following the same directions of

fibers (visible in figures 4.14 A, C and E). On randomly deposited fibers, cell development did not present any special arrangement; cells adhered and proliferate in small groups, distributed all over the sample. Around 10% of the substrates is occupied by cells, after microscope observations at $t = 10$ days. Moreover, cell cluster formation materialized by circles in figure 4.14, occurred on both substrates. This suggests an intrinsic tendency and capacity of cartilaginous cells, to form aggregates to shorten the diffusion distance for nutrients as well as for cell mediators. In articular cartilage chondrocyte clusters are characteristically round with no more than 20 cells (Boock & Henriksen, 2010).

In the same way, using as reference proliferation tests, fluorescence microscopy observations were performed for chondrocytes cultured on patterned mats: square and hexagonal meshed-substrates as it is presented in figure 4.15.



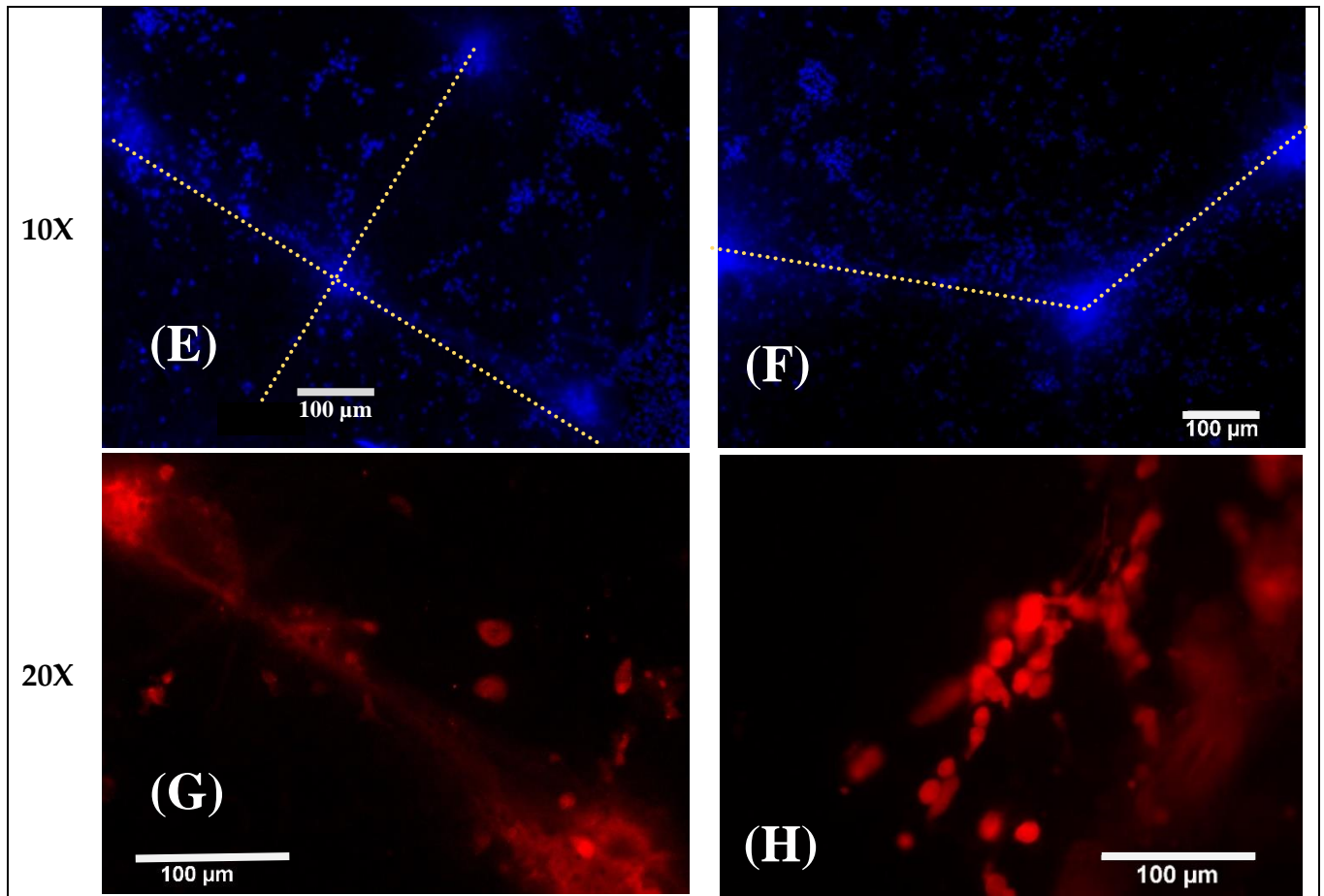


Figure 4.15. Chondrocytes C20A4 adhered to CS fibrous mats, observed on an inverted fluorescence microscope, 10 days after seeding. Direct observation on microscope (A) and (B). Substrates: Square-patterned mat, at magnifications 4x (C), 10x (E) and 20X (G); Hexagonal-patterned mat 4x (D), 10x (F) and 20X (H); Lasers: Blue, Excitation 325-375 nm/ Emission 435-485 nm and Red, Excitation 510-560 nm/Emission 590 nm.

Illustrated in figure 4.15A to 4.15H, adhered living chondrocytes, on square and hexagonal-patterned CS fibrous mats, are found along the mesh edges of the substrates but also developing in other zones of the mat. A higher concentration of cells is mainly detected on the vertices of the patterned mat (figure 4.15 E and F). This corresponds as well to a higher concentration of fibers, being the guiding points of the pattern during electrospinning, a similar conclusion was reached studying with C2C7 myoblast cultured on PLA-based structured scaffolds (Gangolphe et al., 2021).

Compared to aligned and random fibers, cell cluster is also observed on structured collectors. Microscopy indicates an occupation cell/substrate of ~14% after 10 days of culture, which is significantly higher than substrates shown in figure 4.14. Similar differences are observed when comparing substrate proliferation profiles, with lower number of cells detached from aligned and random fibers.

Regarding the cell shape, round chondrocytes are mostly observed on square and hexagonal-patterned substrates, with some oval cells aligning to the fiber mesh as it is

presented in figure 4.15 G-H. Thus, cells show adaptation to the mat topography with rounded shapes on porous substrates and cell spreading on flatter and compact surfaces (CS films). It has been observed during experimentation that cells adopt easily, more accidented substrate reliefs i.e., sample wrinkles and folding. Specific cell arrangement during culture, would be more efficient on fibrous mats having exclusively guided fibers, which is difficult to obtain with chitosan systems.

From cell development profiles, higher proliferation rates were observed for chondrocytes on square-patterned fibrous mats. Thus, observations on fluorescence microscopy at longer culture periods were carried out, as it is presented in figure 4.16.

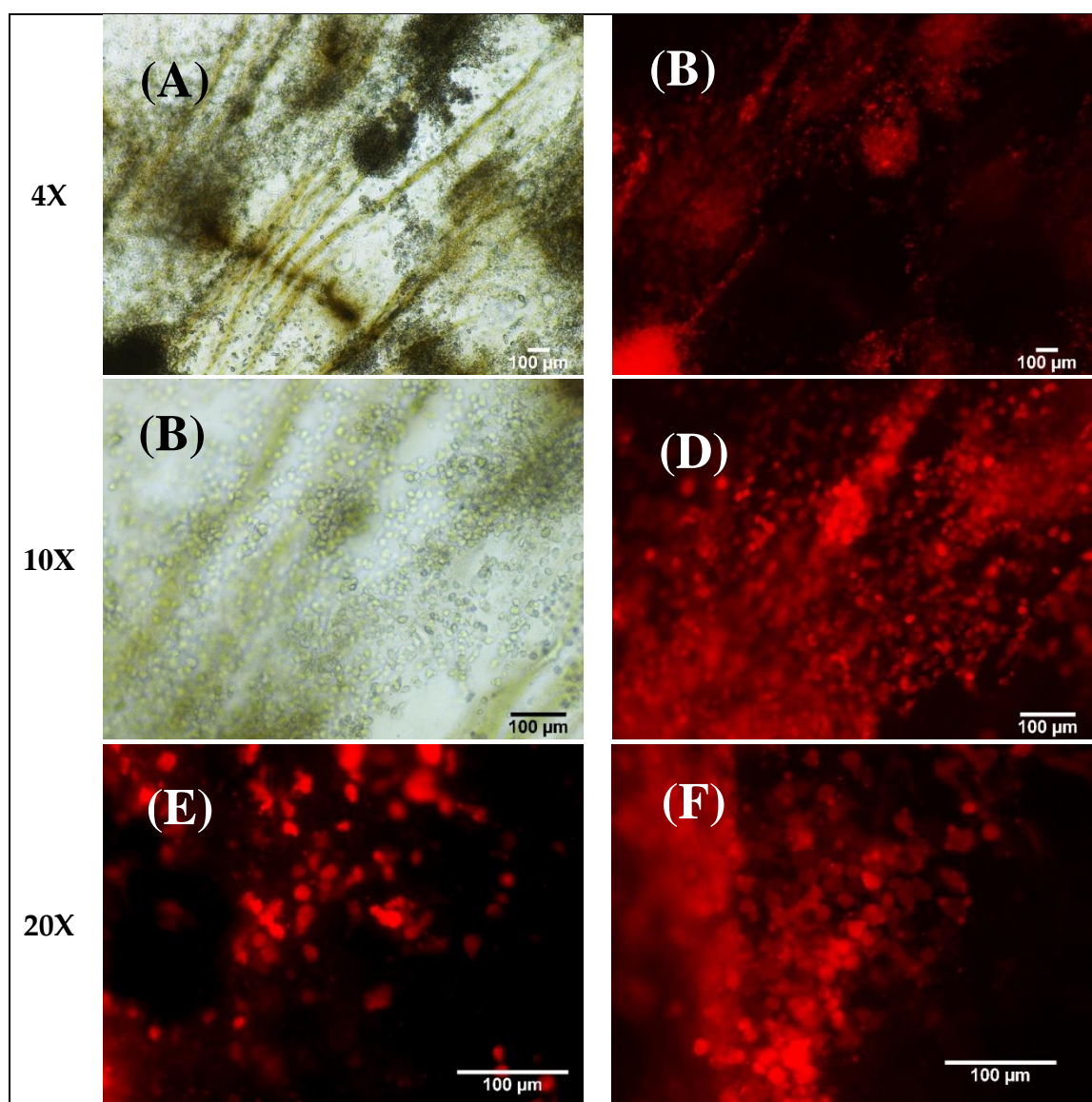


Figure 4.16. Chondrocytes C20A4 adhered to CS square-patterned fibrous mats, observed on an inverted fluorescence microscope, 28 days after seeding. In bright field at magnifications 4x (A) and 10 X(C); In fluorescence at 4x (B), 10x (D) and 20X (E)(F). Red laser: Excitation 510-560 nm/Emission 590 nm.

From this figure, it is noticed that, cell arrangement is not generalized even after 28 days of culture. Several sites in the sample presented cell cluster formation and growing, with aggregates in the range of 300-500 μm (Figure 4.16 A-B). It is also observed that cells have kept their round shape up to 4 weeks of culture (Figure 4.16 C-F), favoring phenotype preservation. Accordingly with the cell/substrate occupation, chondrocytes develop on the 30-46% of the surface of the mat.

3. Proliferation of chondrocytes on PEC fibrous mats

Hyaluronan, not only acts as a joint lubricator, but also as a significant regulator of cellular behaviors during adhesion, migration and proliferation, since it is a native component of the ECM (Solis, Chen 2012). Thus, it is expected to obtain a combination of HA and CS properties, when forming a polyelectrolyte. Electrospun nanofibers obtained from the blend PEC/PEO 70/30 w/w, at a CS/HA masse ratio = 1 ($R_c = 2.35$), were applied as substrates for chondrocyte development studies. The aim is to compare the performance of the PEC vs pure CS, evidencing the potential, in biological applications, of the complex CS/HA.

Prior to use with PEC fibers, compatibility and viability were evaluated by NBT cell marking. Chondrocytes cultured on a CS/HA film were observed 7 days after seeding, as it is illustrated in figure 4.17.

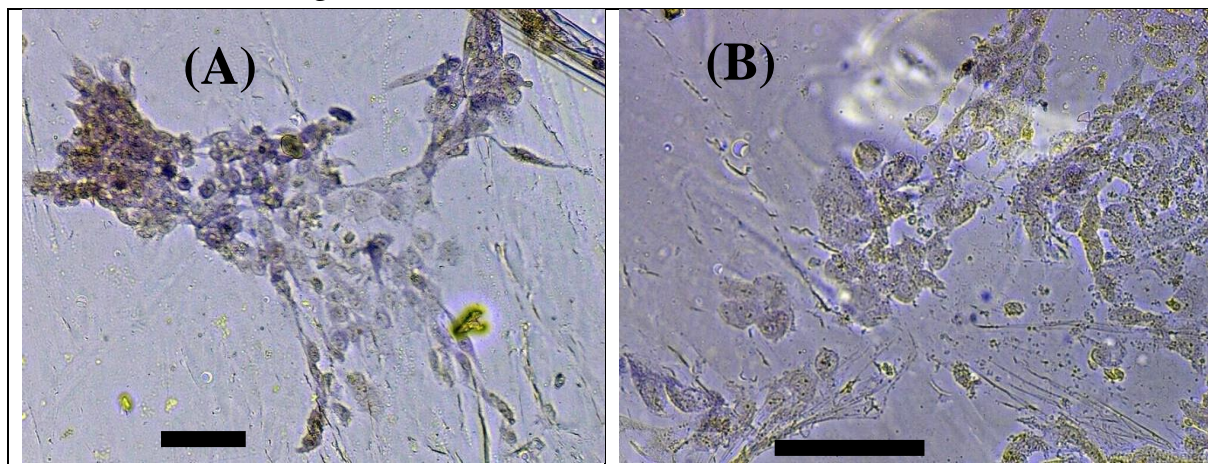


Figure 4.17. Chondrocyte proliferation on CS/HA ($R_c = 2.35$) casted films, after 7 days of incubation, at magnification 10x (A) and 20x (B). Scale bar equal to 100 μm .

On the PEC films, cells are observed to adhere and spread, covering the surface, similarly to their behavior on CS films (figure 4.1C). Formation of some cell clusters was also identified (Figure 4.17 A), with cells developing around conglomerates. More elongated chondrocytes, with an average size ranging 20-50 μm , are detected on the film surface. Cell morphology can be influenced by the presence of HA in the film which provides a high degree of swelling compared to pure CS.

In the case of fibers, proliferation profiles were also analyzed by fluorescence counting at times between 1-7 days. In table 4.2, the number of living chondrocytes, detached

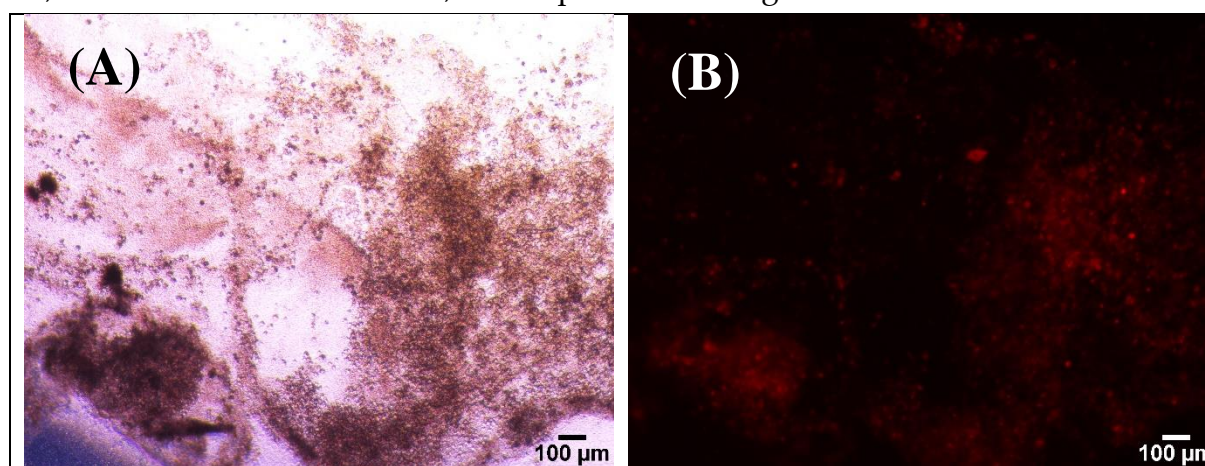
from PEC fibers, is presented. The results are compared to CS fibers for a similar incubation time; cell viability is included for each observation and the samples were neutralized and washed in PBS before cell seeding.

Table 4.2. Living cells on PEC (after thermal treatment) and CS fiber mats as a function of incubation time and cell viability expressed as *%. Samples of fibers were prepared in square patterned collector.

Electrospun system	Cell counting			
	Seeding (t=0)	Incubation = 2 days	Incubation = 4 days	Incubation = 7 days
PEC/PEO	$1.4 \times 10^4 \pm 10^3$ *96.8%	$5.5 \times 10^4 \pm 6 \times 10^3$ *100%	$1.14 \times 10^5 \pm 3 \times 10^4$ *91.4%	$1.63 \times 10^5 \pm 5 \times 10^4$ *98%
CS/PEO	$1.4 \times 10^4 \pm 10^3$ *96.8%	$2.1 \times 10^4 \pm 4 \times 10^3$ *92.8%	$3.14 \times 10^4 \pm 2 \times 10^3$ *100%	$6.5 \times 10^4 \pm 4 \times 10^3$ *95%

From these results, an increasing number of cells was detached from both substrates, considering samples with the same dimensions. Chondrocyte development is clearly favored on the PEC fibers, compared to chitosan supports. Both systems shown an elevated cell viability with values >90 %.

Measurements at longer periods were unable to make due to high substrate swelling degree, which affects sample handling and cell counting. However, fluorescence microscopy observations were performed on chondrocytes, initially stained with Red-FP, and cultured on PEC fibers, as it is presented in figure 4.18.



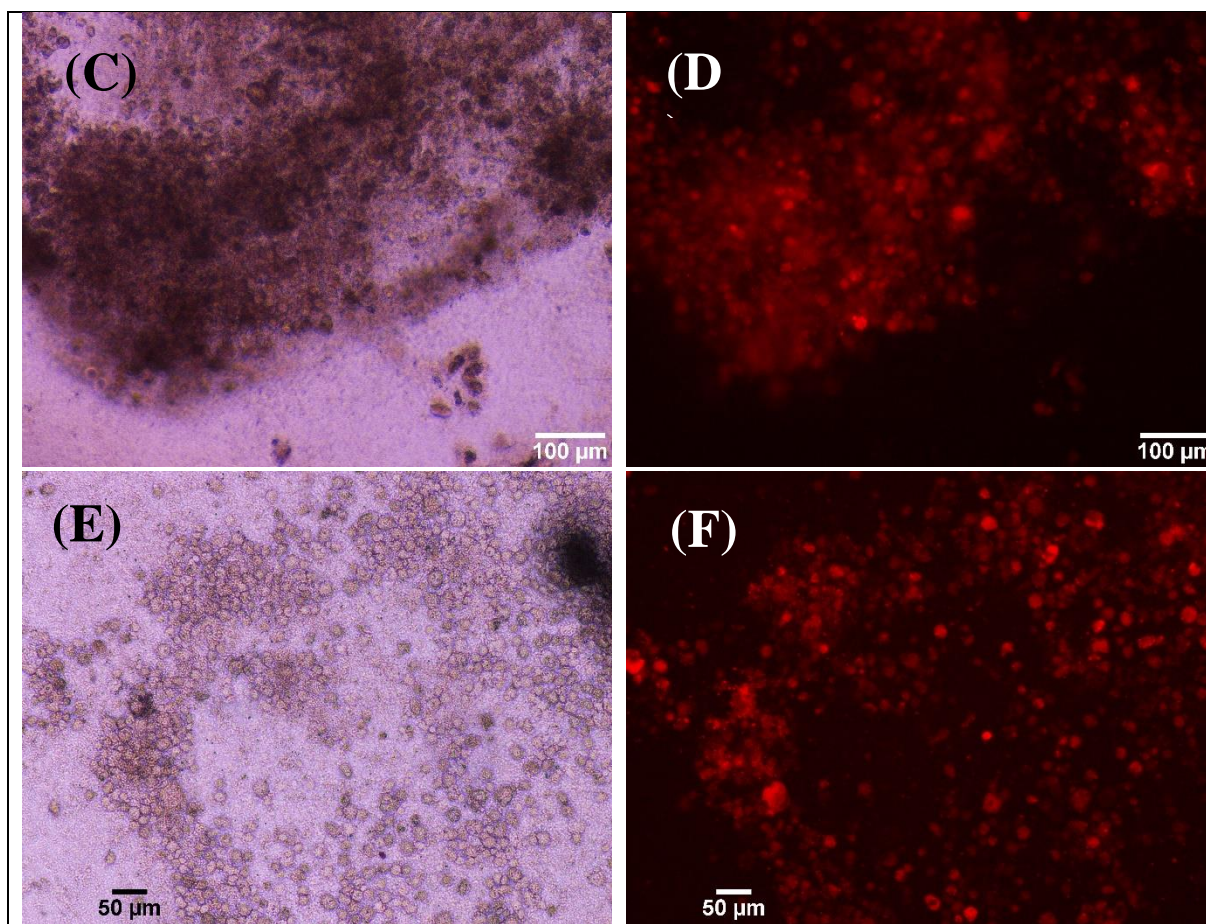


Figure 4.18. Chondrocytes C20A4 adhered to PEC fibrous mats, observed on an inverted fluorescence microscope, 14 days after seeding. In bright field and fluorescence at magnifications 4x, (A-B), and 10x (C-F). Red laser: Excitation 510-560 nm/Emission 590 nm.

Illustrated in figure 4.18, adhered living chondrocytes, detected by their red fluorescence, show adaptation to PEC fibers, occupying the sample and developing abundantly in all zones of the mat. Several sites in the substrate presented high cell concentration indicating possible cell cluster formation as it has been observed for CS fibrous mats. One of the factors, favoring cell adhesion on substrates containing HA, is the presence of specific interactions, receptor-ligand type, between the extracellular membrane and HA chains.

It is also noticed that cells have kept their round shape up to two weeks of culture (Figure 4.18 E-F) which indicates cell primary characteristics preserving. The cell/substrate occupation is estimated over 50% which is higher than values observed for proliferation on CS fibers.

As a preliminary study of chondrocyte development on PEC materials, it is important to remark the high cell affinity observed and the promising results that were obtained through cell culture. Cell adhesion and proliferation is favored by the presence of both

polymers, CS and HA. In terms of application, it is relevant to establish the appropriate incubation time to ensure substrate stability for biological purposes.

4. Conclusion

Chitosan based substrates have shown chondrocyte compatibility and non-toxicity. Accordingly with the topography of the mat, a determined cell morphology is observed. Large spread cells develop on films while rounded cell shapes are found on fibrous substrates. The difference of substrate types has also affected cell proliferation profiles. With this consideration, square-patterned mats are defined as the more efficient fibrous substrate, even though the mesh of the samples do not provoke a perfect cell arrangement in the mat. Aiming to maintain the native characteristics of chondrocytes, cell shape could be an appropriate indicator. After nearly a month in culture, oval cells were present on CS fibers and, after 15 days of incubation, on PEC fibers. The later catching our interest since more elevated proliferation rates are detected directly influenced by the composition of the mat.

Cell adhesion and proliferation studies helped to validate the application of CS fibers as substrate towards biological approaches for cartilage regeneration with primary chondrocytes. In this case, an analysis of phenotype modifications from extraction to final stage are needed.

Structuration of chitosan-based electrospun nanofibers could be applied for tissue regeneration of other tissues, such as endothelial tissue, muscles, skin and bones. In order to fulfill a desired task, fiber arrangement, promoting cell guiding, could be improved by the formation of macropores, allowing cell penetration into the scaffold.

Chapter V. Proposed clinical approach. Fiber suspension as an injectable system for cartilage regeneration treatments

The use of engineered scaffolds for tissue repairing implies, in most of the cases, the implantation of the mat, charged with cells and/or growth factors (Iwasaki et al., 2011). Even if nanomaterials based on chitosan are biodegradable in the body, a surgery is generally required to place the cell/substrate ensemble in a determined living tissue. As it has been presented and discussed in this project, fibrous scaffolds prepared by electrospinning from CS-based systems, could act as efficient tissue regeneration promoters.

In the case of articular cartilage, surgery is recommended according to the patient conditions and, when the rest of available treatments does not work. However, it could result in a higher impact to the joint, considering the low regenerative response of deteriorated cartilage.

As an alternative approach for too invasive surgical intervention, it is proposed to prepare a cell/substrate suspension, able to be injected in the damaged zone. During this research, chondrocytes cultured on CS fibrous substrates were observed to maintain their native shape, which may lead to original functions preservation contrary to monolayer cultures (B. Ma et al., 2013). In this way, it is important to confirm the viability of this approach without affecting cell development.

With this purpose, CS fibers were obtained by electrospinning using a neutralizing bath as collector. Aiming to produce an injectable system, fiber mats were fragmented and dispersed in order to obtain a fiber suspension. Chondrocytes were then seeded on the fragmented fibers, forming a cell/fiber suspension in culture medium. Incubation times up to 14 days were studied in terms of proliferation rates and cell morphology. In the same context, injectability of the system was assed, through syringes usually used for viscosupplement hyaluronan knee application. At last, the viability of the approach is discussed. Stages of the proposed method are described in the next sections.

1. Electrospinning for fiber production

Initially, the feasibility of fiber dispersion preparation was attempted using aligned CS/PEO fibers. These type of fiber mats were observed to produce fiber aggregates (big fiber mat pieces) after fiber fragmentation.

In order to reduce fiber-fiber contact during fiber collection, and therefore aggregate formation during fragmentation, CS/PEO electrospinning was performed with the help of a basic EtOH/Water bath as fiber collector. In this approach, fiber-fiber

adherence (linkage), is inhibited by a direct neutralization step during fiber collection. The basic EtOH/Water bath acts as non-solvent while -NH₂ groups in aqueous insoluble chitosan are regenerated.

The basic EtOH/Water bath is composed of EtOH/Water 80/20 v/v where K₂CO₃ is solubilized until saturation at pH~12. The resultant solution is disposed on a wide glass reservoir that acts as container and fiber collector. The glass recipient is placed on a metallic plate, connected to the needle tip of the polymer container (syringe) and electrospinning is performed on a vertical arrangement. Pure ethanol is constantly added to compensate evaporation.

Similar to previous CS-based fibrous substrates, the blend CS/PEO 70/30 w/w in W/FA 50/50 v/v was selected. In table 5.1, the processing conditions for electrospinning are presented.

Table 5.1. Conditions for electrospinning of CS/PEO on basic EtOH/Water bath.

System	Flow Rate (mL/h)	Tip to Collector Distance (cm)	Applied Voltage (kV)	Electrospun Products
CS/PEO 70/30	0.08-0.14	17	25-29	Fibers

It was observed that electrospinning of the CS/PEO blend, using the basic bath as collector, needed similar parameters compared to electrospinning on structured plates. Nevertheless, to achieve fiber formation, slight increase of the applied voltage between the needle and the metallic plate bellow bath container is required. Glass recipients are not electric conductors, this could influence the electric field needed for the process.

The collected fibers formed a white mat at the air/liquid interface of the bath, then, they adopted a form similar to small cotton balls as fibers were completely immersed in the basic ethanolic bath. The samples were maintained in EtOH/Water 80/20 up to three days after electrospinning in order to assure chitosan neutralization and mat stability before further conditioning steps.



2. Fiber stabilization and fragmentation

Fiber stabilization includes washing of neutralized fibers with deionized water, removing the rests of the basic bath, until neutral pH. Finally, the fibrous substrates were dried in environmental conditions during two days.

For fiber fragmentation, two methods were applied consecutively: liquid nitrogen freezing and fiber dispersion with an Ultra-Turrax®. The former helped to visibly

preserve the fiber morphology when mats were fragmented, and the latter to homogenize the suspension at a fixed rotation speed. Descriptively, the techniques are presented in table 5.2

Table 5.2. Methods and conditions applied for CS/PEO fiber fragmentation and dispersion.

Method	Conditions
<p data-bbox="368 483 831 521"><i>Step 1. Liquid Nitrogen Freezing</i></p> 	<p data-bbox="1026 551 1390 685">a) Addition of ~ 50 mL of liquid nitrogen to the sample.</p> <p data-bbox="1026 701 1390 786">b) Fragmentation step by friction with a pestle.</p> <p data-bbox="1031 797 1385 882"><i>The process was repeated 4 times</i></p>
<p data-bbox="368 969 831 1008"><i>Step 2- Ultra-Turrax Dispersion</i></p> 	<p data-bbox="1078 1122 1334 1160">a) 3 cycles of 15 s</p> <p data-bbox="1090 1167 1323 1238">$f = 11000 \frac{1}{min}$</p>

The selection of both methods was optimized following the observation of the fiber fragment sizes obtained. In fact, a wide fragment size distribution was noticed when only liquid N₂ (LN) freezing was carried out. With the use of the disperser, smaller fragments were produced, homogenizing in some way the dispersion even though some fiber aggregation was still observed.

In figure 5.1, size distribution and microscope images of dispersed fiber fragments are presented. The fiber suspension was observed in wet state and measurements were effectuated at each step of the preparation, i.e., once freezing and dispersing.

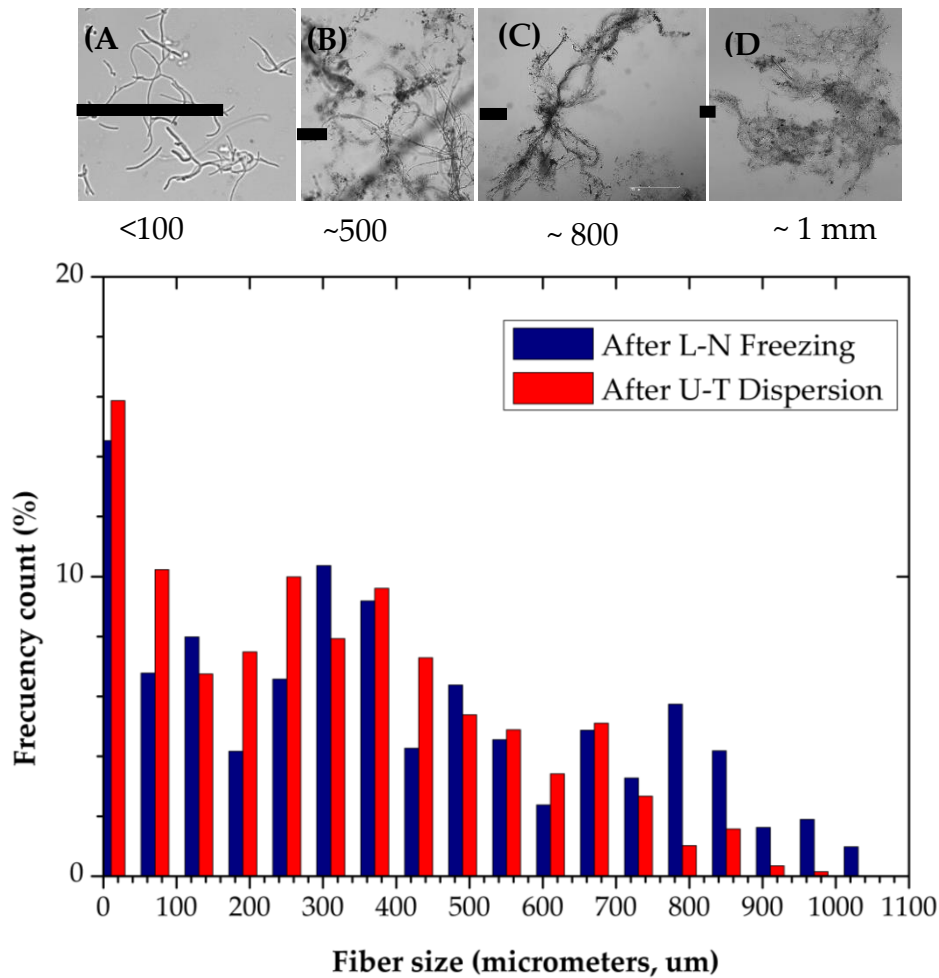


Figure 5.1. Size distribution of CS fibers, fragmented by liquid nitrogen freezing (dark blue) followed by Ultra-Turrax® dispersion (red). Comparative size of fragmented fibers suspended in PBS, in images from (A) to (D). Scale bar = 100 μm.

The established process of fiber dispersion allowed the obtention of individual fiber fragments (figure 5.1A) as well as fiber aggregates measuring up to 800 μm (figure 5.1D). Once the first step (freezing) is performed, it is observed that almost 30% of the suspended particles have dimensions larger than 500 μm. This proportion is reduced to 19% after the U-T dispersion is effectuated decreasing the size distribution. Such fiber size could affect the ability of the suspension to be injected considering the usual needle gauge for inter-articular injections between 22-25 (inner diameter in the range of 0.51-0.30 mm) (Dennis Y., Wen M. D., 2000)

3. Fiber suspension conditioning and cell culture

Besides fiber size, other parameters are relevant for the targeted application. For instance, fiber concentration is considered to directly impact the injectability of the suspension but also the way cells develop on the suspended structures. For the

biological tests, it was proposed to stablish the fiber concentration in the suspension to consequently set the concentration for cell culture in the culture plate.

3.1. Conditioning

Samples of 5 mL of neutralized fiber fragments were suspended in Phosphate buffered saline (PBS) at pH=7.4. PBS does not only serve as a washing solution but as a biological medium, avoiding possible sources of pollutants (remaining EtOH and salts from the neutralizing bath).

The suspensions were centrifugated and the pellets were dried, at air conditions, in order to determine the concentration of fiber in the dispersion by dried weight measurements using the equation:

$$C_f (mg/mL) = \frac{W_d (mg)}{V_i (mL)}$$

where C_f represents fiber concentration, W_d is the measured dried weight and V_i corresponds to the initial suspension volume.

Average fiber content was estimated around 12.03 ± 0.42 mg/mL ($n_{\text{samples}} = 5$). This value includes the remaining solutes of PBS, that might correspond to 20% of the total dried weight, leading to a $C_f \sim 10$ mg/mL.

For cell culture, the saline solution was extracted from the suspension by centrifugation. At its place, Dulbecco's Modified Eagle Medium (DMEM) was added to the fiber precipitate until a final fiber suspension ~ 6 mg/mL, in DMEM, prior to cell seeding. This value was set after the initial tests were carried-out, considering that cell observation under microscope was unable in more concentrated fiber dispersions.

3.2. Cell culture, viability and proliferation

For chondrocyte culture, 500 μ L of the fiber suspension per well, were placed in 12-well plates. For cell seeding, 10 μ L of a cell suspension, containing 10^6 cell per mL, were disposed and actively mixed by pipetting with the fiber suspension. Finally, DMEM was added to complete 3 mL per well and cells were incubated up to 14 days for further analysis. Biological solutions and equipment applied for cell culture procedures on CS/PEO and CS/HA/PEO fibrous mats (chapter IV) and fragmented fibers (chapter V) are the same.

Cell viability was evaluated by NBT staining, marking cells in black purple, after 7 days of incubation. The cell/fiber suspension was centrifugated to extract them from the suspending medium, then the protocol described in the methods was applied also to fiber suspension. From these initial tests, living chondrocytes were identify adhered to the fiber fragments and proliferate as it is presented in figure 5.2.

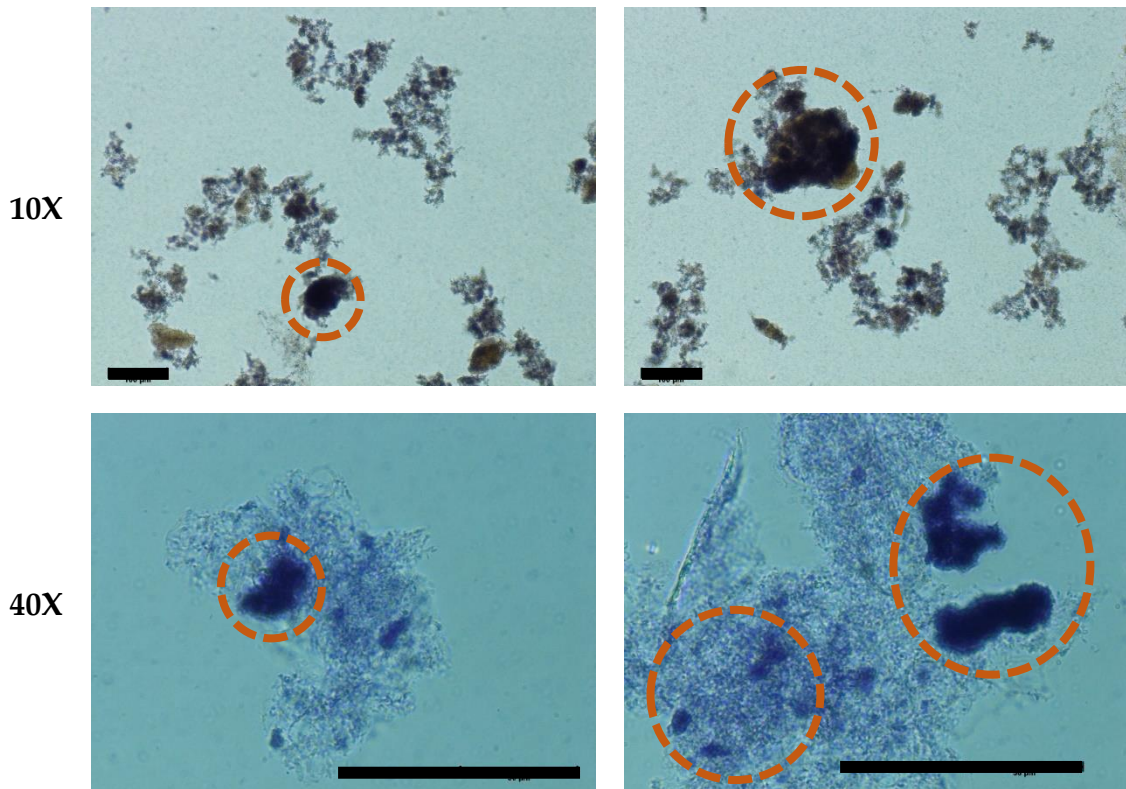
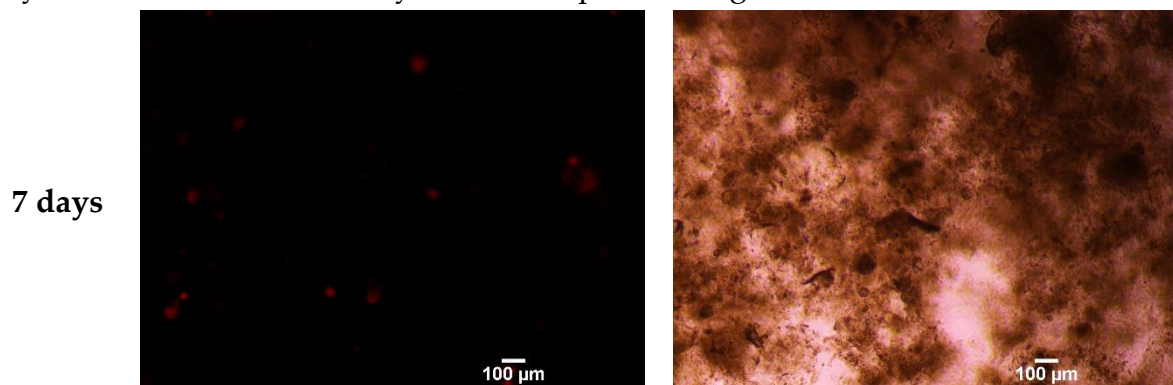


Figure 5.2. Chondrocytes on fiber fragments, stained with NBT after 7 days of incubation. Observations at magnification 10X and 40X. Scale bar = 100 μm .

From figure 5.2, it is noticed that individual cells adhere to the cut fibers suspended in culture medium. Cells started colonizing the fragments and forming cell aggregates. As it was found in fiber mats, some round cells are detected on fiber fragments, however cell shape is unclear in the clusters.

Red-FP transfected chondrocytes are easier to identify by fluorescence microscopy compared to normal C20A4 chondrocytes. The former cells were cultured on fiber suspensions aiming to visualize and verify cell viability and compatibility. By fluorescence observation, cell developing was observed as a function of time up to 14 days of incubation, in the way that it is depicted in figure 5.3.



14 days

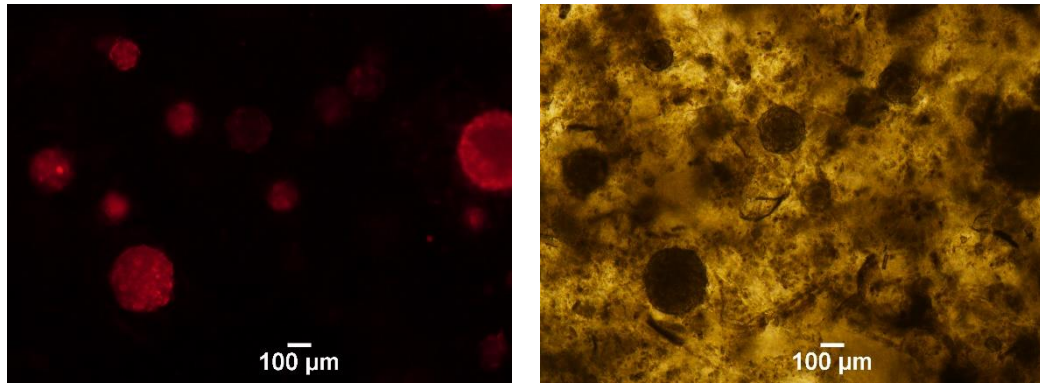


Figure 5.3. Red-FP transfected chondrocytes on fiber fragments after 7 and 14 days of incubation. Observations on inverted fluorescence microscope at magnification 4X. Red laser: Excitation 510-560 nm/Emission 590 nm. Scale bar = 100 μm .

Fluorescence microscopy allowed the observation of cell colonies in the fiber suspension. It is noticed that cells proliferate in the zone where they adhere forming a cell aggregate, which increases its size with time. Cell clusters of around 100 μm and 400 μm , are found on fiber suspension at 7 and 14 days, respectively. Cell aggregation was detected also on nanofiber mats, as well as other types of cell organization. Differently from fiber mats, cell development on suspended substrates represents a significant change for adherent cells, such as chondrocytes, which are mainly adhered to a surface or embedded in the ECM (Gao et al., 2014). For chondrocytes cultured on fiber pieces, the contact with other fragments might be restricted, then aggregation represents the most viable option for cells to adapt to the substrate and develop (Boock & Henriksen, 2010).

Proliferation profiles on suspended fibers, obtained by INT-colorimetry, was considered the most appropriate technique for cell counting. The procedure by fluorescence needs detached cells for measurement, unable to be obtained from fiber fragments. For this analysis, the protocol described in chapter II was applied for chondrocytes cultured on fiber fragments. In the same way, a calibration curve was prepared to associate absorbance values to cell quantities. In figure 5.4, the comparison between proliferation rates in CS fiber and fragmented fibers, between 1-15 days of incubation after seeding, are presented for chondrocytes C20A4.

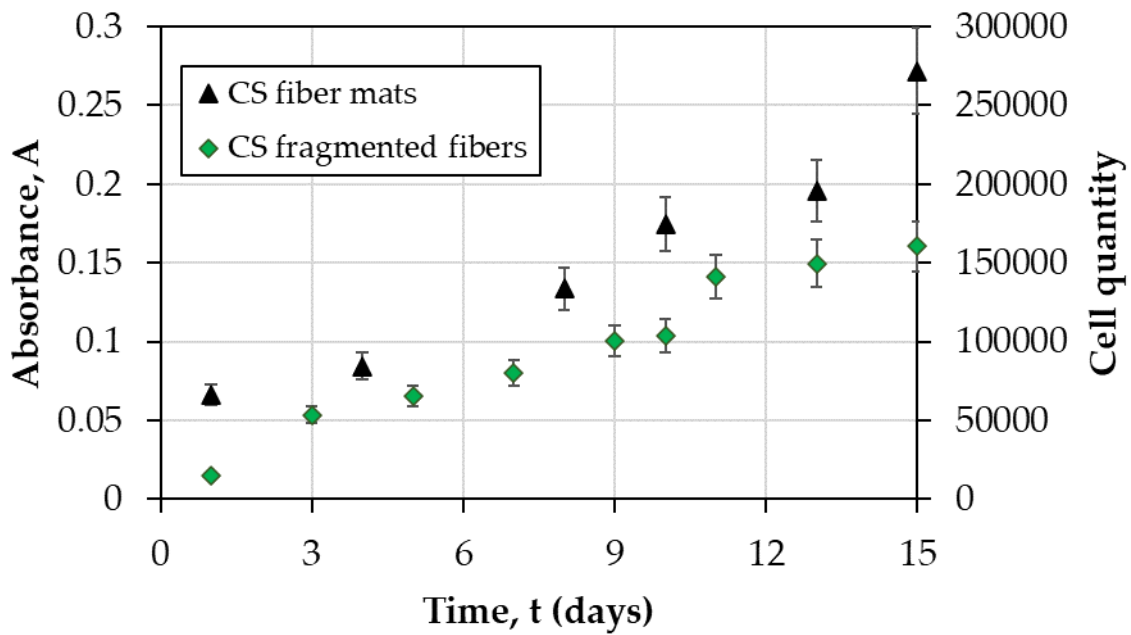


Figure 5.4. Proliferation curves obtained by INT colorimetry of C20A4 cultured on CS fiber mats (●) and fragmented fibers (●). Absorbance values were measured at 490 nm.

From the curves shown in figure 5.4, cell development is confirmed by increasing measured absorbance values, in the fiber suspension, as a function of time. Cell quantities related to optical density reveals that cells could reach proliferation ratios of ~12 comparing cell seeding ($t=0$) with day 15. After two weeks of incubation, 75% more cells are found on fiber mats in contrast to fiber fragments. However, proliferation profiles are close, and the number of cells on fragmented fiber is slightly lower than on fiber mats, for a similar incubation time.

A decrease in the proliferation rate between days 11-15 are observed on cell/fiber suspension compared to the fibrous mat, this decrease in cell activity could be influenced by the cell adhesion, organization, cluster formation and the form of the substrate (Rozario & DeSimone, 2010). Once adhered to the fibers in the suspension, cell contact to other cut fibers and possible migration might be limited. In this way, proliferating cells could be injected before cell confluency on fiber fragments is reached.

3.3. Injection characteristics

This approach is founded in the possible injection of the cell/substrate ensemble for therapeutic applications. For this purpose, an experimental test based on fiber and cell injection viability was carried out.

Fiber suspensions were loaded into a 5-mL syringe adapted with a cylindrical needle. Then, a flow rate of 0.017 mL/s was imposed using a KSD legato 200 infusion syringe pump. The suspensions were evaluated to pass through different needle diameters,

before and after cell incubation, at 7 days of culture, as it is presented in table 5.3. Needle blocking during defined injection feasibility.

Table 5.3. Evaluation of CS nanofiber suspension injection feasibility as a function of needle diameter. Usual needle gauge for knee injection marked in the shaded area.

Needle gauge	Outer diameter (mm)	Inner diameter (mm)	Fiber suspension test	Fiber + Cell suspension test
20	0.91	0.64	+	+
21	0.83	0.56	+	+
22	0.7	0.46	+	+
23	0.63	0.41	+	+
25	0.53	0.30	+	±
27	0.42	0.22	-	-

It was observed that needle diameters of 0.4 mm and larger (gauge 23) enable CS fiber injections containing living chondrocytes. It is important from an experimental point of view since first biological tests would be carried on small animals. Presence of cells in the suspension restricted injectability using needles with an inner diameter lower than 0.30 mm. It has been reported that cell injections are suitable at channel dimensions larger than 100 μm (M. Li et al., 2011).

Flow rate and needle diameter have been reported to influence cell damage estimations for Schwann cells and 3T3 fibroblasts. In summary, lower cell damage percentages are observed in wider needles and at lower suspension flow rates (M. Li et al., 2011; Walker et al., 2010). However, cell viability post-injection, and 24 h after, was found not significantly affected by the injection procedure on mesenchymal stromal cells (Walker et al., 2010).

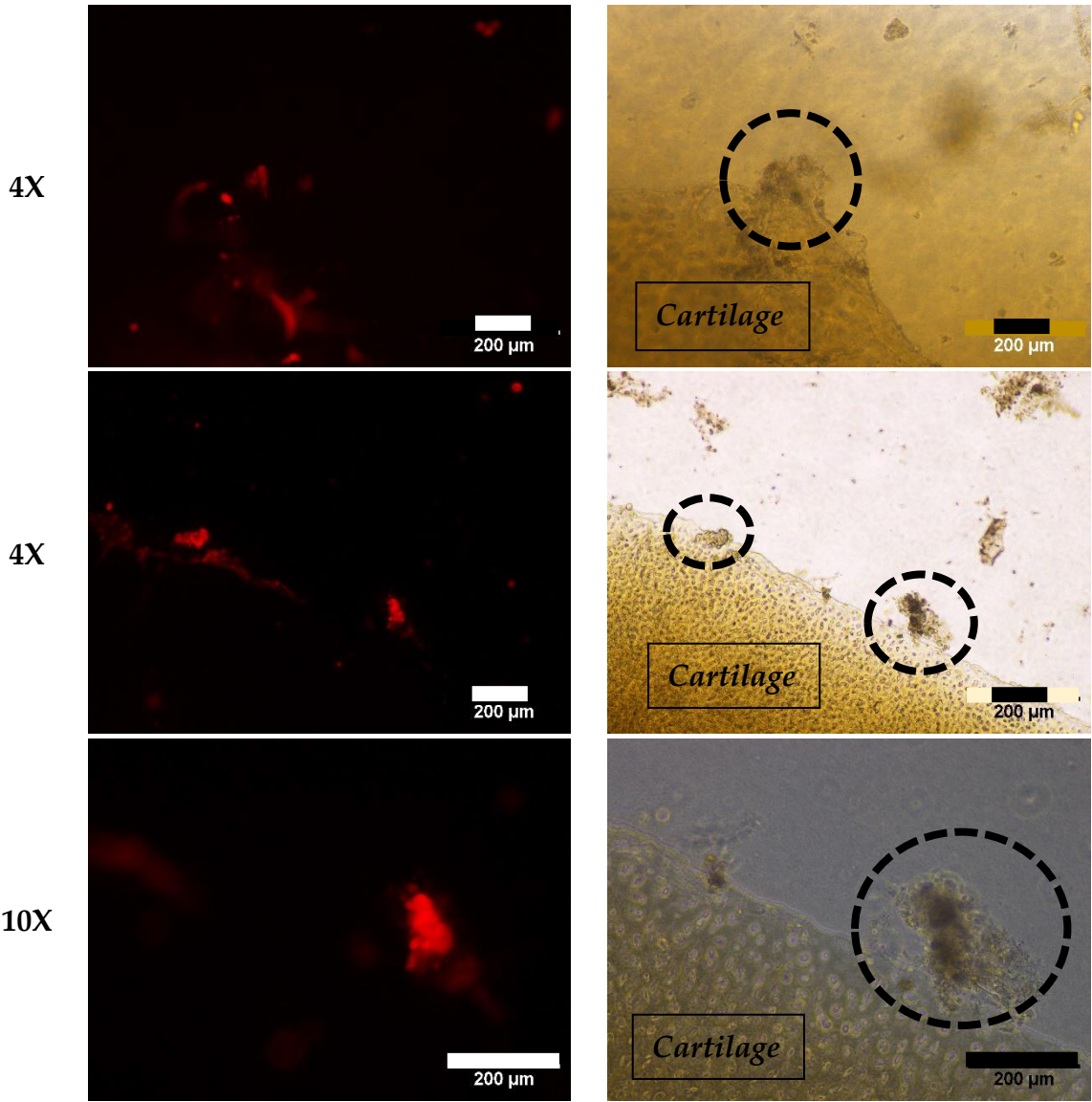
From other perspective, usual hyaluronan injections for knee cartilage treatments are effectuated with needles having internal diameter between 0.3-0.5 mm (Dennis Y., Wen M. D., 2000), which is wide enough to allow a fiber/cell suspension injection considering the carried-out tests.

4. Evaluation of the approach

The application of CS fiber suspensions as carriers for chondrocytes, to reach the damaged zones of cartilage and enhance tissue regeneration, is also based on the ability of cells to adhere and recolonized new substrates. At this stage of the research,

cell viability and development have been confirmed. For the sake of further implementations, these findings were supported by the analysis of fiber/cell/cartilage adhesion and compatibility.

The mentioned procedure was carried out by incubation of cell/fiber dispersions on histological slices of native mammal cartilage. To this end, red-FP transfected chondrocytes C20A4 were used favoring cell observation. Firstly, the suspension cell/substrate was prepared as described in sections 3a-b, and incubated during 7 days, giving cells time to adhere and proliferate. Then, cell/fibers were seeded on fresh cartilage slices, covering the bottom surface of a culture dish, and re-incubated for 3 days at 37°C. Finally, samples were observed by optical and fluorescence microscopy as it is presented in figure 5.5.



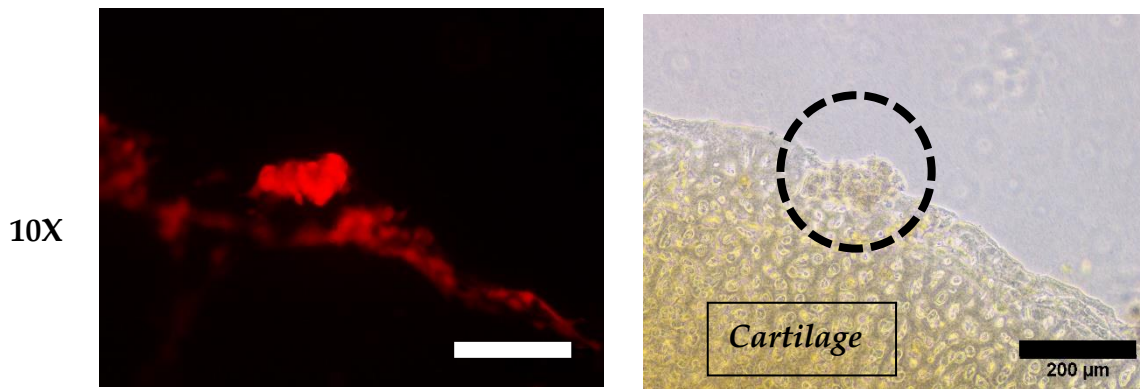


Figure 5.5. Red-FP transfected chondrocytes on fiber fragments seeded on mammal knee cartilage, after 7 days of incubation. Observations on optical and inverted fluorescence microscope at magnification 4X and 10X. Red laser: Excitation 510-560 nm/Emission 590 nm. Scale bar = 200 μm .

In figure 5.5, it is observed that fragmented fibers and cells are adhered to the native cartilage surface after being incubated during 3 days. Living chondrocytes are mainly identified by the emitted fluorescence, some cell aggregates and cut fibers are visible on optical microscopy images. As it is noticed, the adherence cell/fiber/cartilage do not occur in all cases as suspended fibers are also observed. In some cases, adhered cells on cartilage were detected, indicating possible chondrocyte migration from the fiber suspension to the histological slice. Considering the contact between cells and flat surfaces, we have observed that normal adhesion strength is high on film-type surfaces even at short contact times (C. E. G. Garcia et al., 2021). Thus, contact during seeding, could promote the adhesion of cells and cell/fibers to cartilage as a new substrate.

As a model, these results suggest that chondrocytes, attached to CS fiber fragments, could also adhere to other substrates once in contact. When injected to the articulation, the cell/fiber suspension could be able to find new adherence points, i.e., possible damaged sites in the joint. Chondrocytes, preserving their original functions and adhered to the appropriate sites, could potentially promote tissue repairing.

In conclusion, the approach represents an advantageous way to place into injured articulations the necessary agents for tissue regeneration. Considering other recent findings, the cell/fiber suspension injection can be complemented with addition of growth factors, active molecules and drugs to improve the effectiveness of the application.

Further analysis can be carried out to complete the knowledge about cell/CS-based substrate suspensions for cartilage treatments. Initially, the methods applied for fiber fragmentation could be adapted to reduce fiber size, in case of practical difficulties, mostly when working on biological tests in vivo.

Equally, the influence of the fiber content in the suspension could be studied in order to optimized cell development and injectability, as well as cell visualization. In this concern, other techniques of microscopy such as confocal microscopy may help stained cell imaging on fiber suspensions.

For this approach, cell viability modifications prior and post-injection should be carried out to confirm low cell damage. In the same way, the understanding of the effect of flow rate and needle diameter on cell characteristics could be deepen.

A major parameter to study is type-II collagen production of primary chondrocytes throughout the different stage of the approach. This analysis could help demonstrate that phenotype is preserved when cells are fixed on suspended CS-based nanofibers.

Finally, during tests *in vivo*, it is necessary to complement this approach with cell/substrate tracking methods, aiming to detect the behavior and location of the cell/fibers once introduced in the articulation.

General Conclusions and Perspectives

1. Conclusions

In tissue repairing approaches, material preparation and characterization have a key role since it defines the potential and limitations of the bio-structures proposed. All along this research, a couple of polymeric systems based on chitosan have been studied from processing conditions to application in biological domains. The relevance of chitosan intrinsic properties such as non-toxicity, non-immunogenic nature, antimicrobial activity and excellent biodegradability and biocompatibility are also highlighted.

Firstly, the electrospinning of the blend CS/PEO was optimized, in acetic and formic acid as solvents, allowing obtention of nanofibers on several collector types. Subsequently, new biomaterials based on homogeneous polyelectrolyte complex (PEC) of the blend chitosan and hyaluronan, were processed under casted films and electrospun nanofibers. PECs are considered as compelling precursors of materials with biological applications due to the specific characters of the two macromolecules involved. Thus, fibrous mats of CS/PEO and PEC/PEO were successfully produced, characterized, stabilized, and applied for cell development.

In terms of processing, spinnability of the blends increased with the PEO content. It is confirmed that the PEO molecular weight and content, have a direct impact on fiber morphology. Especially, higher PEO MW gives fibers with a larger diameter and, consequently CS/PEO supports with larger pores. High yields of chitosan and PEC (unprecedentedly prepared), in the fibers were preferred, for this reason PEO (MW=1000 kg/mol) content was fixed at 30 % w/w in the electrospun blends.

Formic acid/Water, at 50/50 v/v, was considered the most appropriate solvent, permitting electrospinning and PEC homogenization, contrary to the behavior of solutions prepared in 0.5M acetic acid. Both CS/PEO and PEC/PEO fibrous mats, were produced on square-patterned metallic plates, rotatory cylinder and aluminum foil, as collectors. The conferred fiber arrangements were observed to affect mainly mechanical and biological properties. Spun CS/PEO and PEC/PEO fibers presented close average diameters in the range of 100-200 nm and low material density between 0.040-0.100 g/cm³ compared to compact films (>0.70 g/cm³).

The stiffness and plasticity of as-spun fiber mats were observed to be affected predominantly by the composition and the fiber arrangement, as mentioned before. Samples containing larger proportions of CS in the blend, presented higher stress at break values and lower strain %. The stress/strain on uniaxial tension experiments

shows that chitosan is stronger than PEC, the latter presenting lower strain at break. In the same context, for an equal sample composition, aligned fibers, from rotatory collectors, shown higher resistance to tensile traction (with anisotropy in the two ways of measurement and induction of some crystallinity) than randomly deposited fibers and structured (square mesh) fiber mats. These tests allowed to detect the more appropriate composition for the blend not only for the final application but to facilitate sample handling.

For characterization purposes, PEC casted films were prepared as model to examine other properties of the complex at solid state. The application of thermal treatment, at 120°C during 4 h, confirms the stabilization of the material by decreasing the aqueous medium solubility and swelling degree while increasing the mechanical performances. This effect is founded on the hypothesis of amide and H-bonds formation involving -NH₂ and -COOH functions. On CS/HA charge ratios larger than 1.8, the swelling and solubility are lower after thermal treatment with 22% and 4% respectively in aqueous medium at pH>7.

In the case of fibers, CS/PEO mats were favorably stabilized by neutralization in basic EtOH/Water 80/20 v/v medium (pH~12). This is a crucial step since it permits the regeneration of protonated groups to the -NH₂ form, where chitosan is insoluble at neuter pH values. Neutralization step for protonated CS is frequently neglected leading to early material solubilization and substrate morphology modification. After this stabilization, pure chitosan material is obtained being insoluble over pH=6.5.

For PEC/PEO fiber mats, washing in the EtOH/Water alkaline bath followed by the thermal treatment, was found as the more appropriate stabilization process, obtaining the lower partial solubility proportions at pH=7.4, important for biological applications. As a non-solvent of CS and HA, the EtOH/Water solution allowed the extraction of PEO prior to biological tests.

Considering application towards cartilage repair, culture of chondrocytes from the cell line C20A4, enabled to test and understand chitosan/cell interactions, as part of the biological response of CS fibrous mats and films, at short and long observation times. Adhesion force, obtained by the SCFS method, is slightly higher for chitosan films compared to fiber mats mainly attributed to the contact available surface during the studied cell-substrate short contact times (60 and 120 s). This response can be explained considering the quantity of cell-substrate bonds that could be formed in the larger contact surface on the chitosan film in contact with the cell membrane. Such bonds lead to a slightly higher detachment force and adhesion energy values even for short contact times. The mechanism of interaction, for a single cell in contact with several nanofibers, is modified in relation with the porosity of the substrate. On nanofibers,

measured forces are more homogeneous with higher force jumps and no modification of the cell conformation. The adhesion strength, compared to a negative BSA coated surface, is favored whatever the chitosan substrate used. This difference involves H-bond and electrostatic loose contribution between chondrocyte and chitosan. The cell adhesion study revealed that the adhesive response depends largely on the topography (fibrous mat or flat films), nature, cell affinity, and electrostatic character of the chitosan-based materials.

Along with the force adhesion measurements, an approach on cell viability, fraction of adhered cells and proliferation on chitosan nanofibers was also evaluated in this work. It is shown that chitosan nanofiber mats are perfectly stable in DMEM culture solution during cell cultivation up to 5 weeks (maximum incubation time experiment). For the first step of adhesion, corresponding to the first 24 hours of incubation, it is also noticed that the adhered cell density is larger on fibers compared to film. This result is related to the larger area available, in the case of fiber mats, for a given sample size, having a lower material density compared with a compact film.

The fraction of living cells detached from the substrates, during the first day of incubation, is higher and cell viability remains at least at 85% on fibers while it decreases on films. These results are associated to the cell morphology modification when attached to film (flat) compared to pseudo spheric cell on fibers.

Concerning cell development, it has been shown that proliferation is favored on neutralized chitosan fibers, rather than on the CS/PEO as-spun mats and chitosan films. Experiments indicated higher cell viability and proliferation on nanofiber mats at 7, 14 and 21 days after seeding. As presented previously, the available surface, morphology and stability of the substrate affect significantly the cell response once cells are seeded.

Structured CS fibrous mats resulted more advantageous than randomly deposited and aligned fibers, in terms of cell proliferation rates. However, for similar time observations, high viability fractions were observed in all the studied fibrous supports. Cell visualization revealed the influence of the substrate arrangement on cell morphology. Fiber alignment partially provoked cell orientation once cells started colonizing the substrate. Equally, other types of fiber mats (square and hexagonal patterned mats), structured during electrospinning, showed that cells were more abundant on zones with higher fiber density. This ability of cells to adapt to a determined substrate topography, guiding fibers for instance, could result of important relevance for specific applications where cell orientation is required. Oval shaped chondrocytes were detected on CS fibrous mats during incubation at short and

long observation times. Chondrocyte phenotype preservation is claimed to be favored by cell morphology maintaining as they are in the native tissue.

Regarding the behavior of chondrocytes cultured on PEC fibers, cell compatibility is confirmed with positive NBT cell viability tests and living cell fractions >92% between 1-7 days of incubation. For longer incubation times, it is noticed that the supports present high swelling degrees and handling becomes difficult. However, cell colonization was verified by fluorescence microscopy up to 2 weeks, with cells occupying around a 50% of the mat surface. Additionally, on PEC fibers, chondrocytes developed preserving the round cell form. This cell behavior could be also influenced by the presence of hyaluronan which forms specific ligand-receptor bonds.

Towards a simplified clinical application, the cell/fiber suspension approach presents several advantages contrasted to complete 3D structures. By injection, the necessary agents for tissue regeneration can be placed into injured articulations avoiding surgical intervention. It was confirmed that cell adhesion and proliferation on fragmented fibers occurs as well as on cartilage. Then, healthy cells can be introduced by the suspension injection and eventually adhere to the damaged zones of the articulation, starting cell recolonization.

Overall, accordingly to the obtained results, it is clearly demonstrated that pure chitosan and PEC nanofibers have good porous support for chondrocyte development in view of application in tissue engineering. Considerably better adhesion, larger fraction of living cells and large rate of proliferation are observed on nanofibers, compared to monolayer culture on films. One advantage of the fibrous mats is the large porosity of membranes as well as its large specific surface allowing a possible high surface adsorption. The porous mat should allow cell migration, preservation of cell morphology involving phenotype maintain, nutriment transport and permeability.

In this work, original results about material preparation, cell adhesion and proliferation of chondrocytes on CS-based substrates are presented. Stable pure chitosan (biocompatible and biodegradable polymer) and CS/HA complex nanofibers were produced with good stability in PBS buffer, no phase separation was detected for the complex prepared in formic acid.

To our knowledge, no experimental data on SCFS have been published for chondrocytes on different pure CS substrates. Data from the adhesive responses presented here, allow to validate chitosan as an appropriate support for chondrocyte adhesion. Owing to material porosity, chitosan-based nanofiber mats are the most convenient supports as compared to homogeneous films for chondrocyte proliferation

applied in tissue engineering, modeling the ECM structure and allowing cartilage repairing.

2. Perspectives

This research has given several important findings towards biological applications of chitosan based fibrous substrates. In the same way, it has opened the gate to numerous perspectives and alternatives.

Part of the evaluation of the effectiveness of the CS-based fibrous substrates as a support for phenotype maintaining involves the use of primary chondrocytes and the analysis of the performance in terms of ECM production. This major feature is evaluated throughout the measurement of the type-II collagen /type-I collagen ratio. Functional chondrocytes would maintain a high collagen II production in the appropriate scaffold. The comparison with other substrates would confirm the enormous advantage of using CS (and/or PECS) for cell supports in cartilage mending. Layer-by-layer CS/PEO and PEC/PEO materials can be produced by electrospinning, as an approach to reduce PEC mats partial solubility and enhance sample handling specially during cell culture. In the same context, additives such as nanoparticles or active molecules can be incorporated to the electrospinning solution, producing fibrous mats with specific characteristics. It can be included a high mechanical resistance, enhanced bacteriostatic character, fluorescence precursors, high cell adherence, particular cell-substrate receptors and cell activity modulators.

For the approach studied in this project, fiber dispersion for injection application presented a wide size distribution. According to the practical conditions, established when experimenting with living organisms, the fragmented fiber suspension preparations can be improved and adapted to be injected directly in damaged joints avoiding too invasive surgeries. In the same context, other procedures of cell seeding, increasing the fraction of adhered cells could be implemented. Cell/fiber suspension can be complemented with growth factors, active molecules and possible polymer functionalization, to improve chondrocyte location, targeting the damaged tissues, as well as favoring tracking analysis once cell/fiber suspensions are injected in the tissue surroundings.

Related to chitosan functionalization, several studies point the potential of carboxymethyl chitosan enhancing cell adhesion and bioimaging. Lactose-modified chitosan, as an extracellular matrix for cells, particularly in cartilage repair has been mentioned, as well as fluorinated chitin derivatives for better cell viability. Finally, through a low marking rate, fluoresceine can be incorporated to chitosan, enabling

bioimaging (Pokhrel & Yadav, 2019). Specific chitosan modifications are possible in the -NH₂ group.

Validation of the CS based materials, as the more appropriate biomaterial for cartilage regeneration, involves trials on animals and on humans. Helped by the biomedical domain, the proposed methodology needs to be fully considered and adapted to medical protocols.

The injection approach of the cell/fiber suspension could be equally considered for trials on animals (mouse as model), with relatively easy injection conditions. For this purpose, different strategies of continuous analysis *in vivo* need to be developed and implemented to follow the effectiveness of the treatment, as aborded in previous paragraphs.

The characterization of the new materials prepared in this study, could allow the use of materials based on CS and CS/HA at physiological conditions towards biomedical applications, such as more efficient drug/cell delivery systems and tissue engineering scaffolds, keeping native cell functions. Additionally, as shown before, the nanofibrous structure promote the attachment of human osteoblasts and chondrocytes and maintain characteristic cell morphology and viability compared to other structures.

Bibliography

- Abramoff, B., & Caldera, F. E. (2020). Osteoarthritis: Pathology, Diagnosis, and Treatment Options. In *Medical Clinics of North America* (Vol. 104, Issue 2, pp. 293–311). <https://doi.org/10.1016/j.mcna.2019.10.007>
- Ahmed, L. A. (2013). Stem cells and cardiac repair: alternative and multifactorial approaches. *Journal of Regenerative Medicine and Tissue Engineering*, 2(1), 8. <https://doi.org/10.7243/2050-1218-2-8>
- Akai, E. R. T., Osta, K. E. D. C., Haheen, A. I. S., Ung, C. L. T. H., & Uo, X. E. D. G. (2005). Osteoblast Elastic Modulus Measured by Atomic Force Microscopy Is Substrate Dependent. 33(7), 963–971. <https://doi.org/10.1007/s10439-005-3555-3>
- Alfaro De Prá, M. A., Ribeiro-do-Valle, R. M., Maraschin, M., & Veleirinho, B. (2017). Effect of collector design on the morphological properties of polycaprolactone electrospun fibers. *Materials Letters*, 193, 154–157. <https://doi.org/10.1016/j.matlet.2017.01.102>
- Almond, A. (2007). Hyaluronan. In *Cellular and Molecular Life Sciences* (Vol. 64, Issue 13, pp. 1591–1596). <https://doi.org/10.1007/s00018-007-7032-z>
- Askari, M., Afzali Naniz, M., Kouhi, M., Saberi, A., Zolfagharian, A., & Bodaghi, M. (2020). Recent progress in extrusion 3D bioprinting of hydrogel biomaterials for tissue regeneration: a comprehensive review with a focus on advanced fabrication techniques. *Biomaterials Science*. <https://doi.org/10.1039/d0bm00973c>
- Ayhan, E., Kesmezacar, H., & Akgun, I. (2014). Intraarticular injections (corticosteroid, hyaluronic acid, platelet rich plasma) for the knee osteoarthritis. In *World Journal of Orthopedics* (Vol. 5, Issue 3, pp. 351–361). <https://doi.org/10.5312/wjo.v5.i3.351>
- Baji, A., Mai, Y. W., Wong, S. C., Abtahi, M., & Chen, P. (2010). Electrospinning of polymer nanofibers: Effects on oriented morphology, structures and tensile properties. In *Composites Science and Technology* (Vol. 70, Issue 5, pp. 703–718). Elsevier Ltd. <https://doi.org/10.1016/j.compscitech.2010.01.010>
- Bakhshandeh, B., Zarrintaj, P., Oftadeh, M. O., Keramati, F., Fouladiha, H., Sohrabi-jahromi, S., & Ziraksaz, Z. (2017). Tissue engineering; strategies, tissues, and biomaterials. *Biotechnology and Genetic Engineering Reviews*, 33(2), 144–172. <https://doi.org/10.1080/02648725.2018.1430464>
- Balagangadharan, K., Dhivya, S., & Selvamurugan, N. (2017). Chitosan based nanofibers in bone tissue engineering. *International Journal of Biological Macromolecules*, 104, 1372–1382. <https://doi.org/10.1016/j.ijbiomac.2016.12.046>
- Barbetta, A., Rizzitelli, G., Bedini, R., Pecci, R., & Dentini, M. (2010). Porous gelatin hydrogels by gas-in-liquid foam templating. *Soft Matter*, 6(8), 1785–1792. <https://doi.org/10.1039/b920049e>
- Bernabé, P., Peniche, C., & Argüelles-Monal, W. (2005). Swelling behavior of chitosan/pectin polyelectrolyte complex membranes. Effect of thermal cross-linking. *Polymer Bulletin*, 55(5), 367–375. <https://doi.org/10.1007/s00289-005-0439-5>
- Berregi, I., del Campo, G., Caracena, R., & Miranda, J. I. (2007). Quantitative

- determination of formic acid in apple juices by ¹H NMR spectrometry. *Talanta*, 72(3), 1049–1053. <https://doi.org/10.1016/j.talanta.2006.12.031>
- Bhardwaj, N., & Kundu, S. C. (2010). Electrospinning: A fascinating fiber fabrication technique. *Biotechnology Advances*, 28(3), 325–347. <https://doi.org/10.1016/j.biotechadv.2010.01.004>
- Bhattacharai, N., Edmondson, D., Veiseh, O., Matsen, F. A., & Zhang, M. (2005). Electrospun chitosan-based nanofibers and their cellular compatibility. *Biomaterials*, 26(31), 6176–6184. <https://doi.org/10.1016/j.biomaterials.2005.03.027>
- Bhosale, A. M., & Richardson, J. B. (2008). *Articular cartilage : structure , injuries and review of management*. 77–95. <https://doi.org/10.1093/bmb/ldn025>
- Biswal, T. (2019). Biopolymers for tissue engineering applications: A review. *Materials Today: Proceedings*, 41(xxxx), 397–402. <https://doi.org/10.1016/j.matpr.2020.09.628>
- Boock, P., & Henriksen, O. D. (2010). *CARTILAGE CELL CLUSTERS*. 62(1979), 2206–2218. <https://doi.org/10.1002/art.27528.CARTILAGE>
- Bosworth, L. A., & Downes, S. (2011). *Electrospinning for tissue regeneration* (L. A. Bosworth & S. Downes (eds.); First Edit). Woodhead Publishing Limited. <https://doi.org/10.1533/9780857092915>
- Brenner, E. K., Schiffman, J. D., Thompson, E. A., Toth, L. J., & Schauer, C. L. (2012). Electrospinning of hyaluronic acid nanofibers from aqueous ammonium solutions. *Carbohydrate Polymers*, 87(1), 926–929. <https://doi.org/10.1016/j.carbpol.2011.07.033>
- Bucevič, J., & Lukinavič, G. (2018). *The Use of Hoechst Dyes for DNA Staining and Beyond*. <https://doi.org/10.3390/chemosensors6020018>
- Cai, N., Hou, D., Luo, X., Han, C., Fu, J., Zeng, H., & Yu, F. (2016). Enhancing mechanical properties of polyelectrolyte complex nanofibers with graphene oxide nanofillers pretreated by polycation. *Composites Science and Technology*, 135, 128–136. <https://doi.org/10.1016/j.compscitech.2016.09.018>
- Cai, N., Zeng, H., Fu, J., Chan, V., Chen, M., Li, H., & Yu, F. (2018). *Synergistic effect of graphene oxide-silver nanofillers on engineering performances of polyelectrolyte complex nanofiber membranes*. 46238, 1–11. <https://doi.org/10.1002/app.46238>
- Casasola, R. (2016). *Electrospinning of poly (lactic) acid for biomedical applications: analysis of solution properties and process parameters, drug encapsulation and release* [Loughborough University]. <https://hdl.handle.net/2134/22949>
- Changhsun, H., Y.-H., L., Shuming, L., Jyy-Jih, T.-W., Chung Hsiun, H. W., & Ching-Chuan, J. (2008). Surface ultrastructure and mechanical property of human chondrocyte revealed by atomic force microscopy. *Osteoarthritis and Cartilage*, 16(4), 480–488. <https://doi.org/10.1016/j.joca.2007.08.004>
- Chaudhari, A. A., Vig, K., Baganizi, D. R., Sahu, R., Dixit, S., Dennis, V., Singh, S. R., & Pillai, S. R. (2016). Future prospects for scaffolding methods and biomaterials in skin tissue engineering: A review. *International Journal of Molecular Sciences*, 17(12). <https://doi.org/10.3390/ijms17121974>
- Chen, G., Guo, J., Nie, J., & Ma, G. (2016). Preparation, characterization, and application of PEO/HA core shell nanofibers based on electric field induced phase separation during electrospinning. *Polymer*, 83, 12–19.

- <https://doi.org/10.1016/j.polymer.2015.12.002>
- Chen, J.-P., Chen, S.-H., & Lai, G.-J. (2012). Preparation and characterization of biomimetic silk fibroin/chitosan composite nanofibers by electrospinning for osteoblasts culture. *Nanoscale Research Letters*, 7(1), 170. <https://doi.org/10.1186/1556-276X-7-170>
- Chen, S., Li, R., Li, X., & Xie, J. (2018). Electrospinning: An enabling nanotechnology platform for drug delivery and regenerative medicine. *Advanced Drug Delivery Reviews*, 132, 188–213. <https://doi.org/10.1016/j.addr.2018.05.001>
- Chen, Z. G., Wang, P. W., Wei, B., Mo, X. M., & Cui, F. Z. (2010). Electrospun collagen-chitosan nanofiber: A biomimetic extracellular matrix for endothelial cell and smooth muscle cell. *Acta Biomaterialia*, 6(2), 372–382. <https://doi.org/10.1016/j.actbio.2009.07.024>
- Ching, K. Y., Andriotis, O., Sengers, B., & Stolz, M. (2021). *Genipin crosslinked chitosan / PEO nanofibrous scaffolds exhibiting an improved microenvironment for the regeneration of articular cartilage*. <https://doi.org/10.1177/08853282211002015>
- Comblain, F., Rocasalbas, G., Gauthier, S., & Henrotin, Y. (2017). Chitosan: A promising polymer for cartilage repair and viscosupplementation. *Bio-Medical Materials and Engineering*, 28(s1), S209–S215. <https://doi.org/10.3233/BME-171643>
- Cooper, A., Bhattarai, N., & Kievit, F. M. (2011). *Electrospinning of chitosan derivative nanofibers with structural stability in an aqueous environment w. 9969–9972*. <https://doi.org/10.1039/c0cp02909b>
- Correlo, V. M., Pinho, E. D., Pashkuleva, I., Bhattacharya, M., Neves, N. M., & Reis, R. L. (2007). Water absorption and degradation characteristics of chitosan-based polyesters and hydroxyapatite composites. *Macromolecular Bioscience*, 7(3), 354–363. <https://doi.org/10.1002/mabi.200600233>
- Creuzet, C., Kadi, S., Rinaudo, M., & Auzély-Velty, R. (2006). New associative systems based on alkylated hyaluronic acid. Synthesis and aqueous solution properties. *Polymer*, 47(8), 2706–2713. <https://doi.org/10.1016/j.polymer.2006.02.052>
- Cui, A., Li, H., Wang, D., Zhong, J., Chen, Y., & Lu, H. (2020). Global, regional prevalence, incidence and risk factors of knee osteoarthritis in population-based studies. *EClinicalMedicine*, 29–30, 100587. <https://doi.org/10.1016/j.eclinm.2020.100587>
- Dantas, L. O., Salvini, T. de F., & McAlindon, T. E. (2021). Knee osteoarthritis: key treatments and implications for physical therapy. In *Brazilian Journal of Physical Therapy* (Vol. 25, Issue 2, pp. 135–146). Associação Brasileira de Pesquisa e Pós-Graduação em Fisioterapia. <https://doi.org/10.1016/j.bjpt.2020.08.004>
- DeFrate, L. E., Kim-Wang, S. Y., Englander, Z. A., & McNulty, A. L. (2019). Osteoarthritis year in review 2018: mechanics. *Osteoarthritis and Cartilage*, 27(3), 392–400. <https://doi.org/10.1016/j.joca.2018.12.011>
- Deitzel, J. ., Kleinmeyer, J., Harris, D., & Beck Tan, N. . (2001). The effect of processing variables on the morphology of electrospun nanofibers and textiles. *Polymer*, 42(1), 261–272. [https://doi.org/10.1016/S0032-3861\(00\)00250-0](https://doi.org/10.1016/S0032-3861(00)00250-0)
- Dersch, R., Steinhart, M., Boudriot, U., Greiner, A., & Wendorff, J. H. (2005).

- Nanoprocessing of polymers: applications in medicine, sensors, catalysis, photonics. *Polymers for Advanced Technologies*, 16(2–3), 276–282.
<https://doi.org/10.1002/pat.568>
- Deveza, L. A., Nelson, A. E., & Loeser, R. F. (2019). Phenotypes of osteoarthritis: current state and future implications. In *Clinical and experimental rheumatology* (Vol. 37, Issue 5, pp. 64–72).
- dos Santos, D. M., Correa, D. S., Medeiros, E. S., Oliveira, J. E., & Mattoso, L. H. C. (2020). Advances in Functional Polymer Nanofibers: From Spinning Fabrication Techniques to Recent Biomedical Applications. *ACS Applied Materials & Interfaces*, 12(41), 45673–45701. <https://doi.org/10.1021/acsami.0c12410>
- Doshi, J., & Reneker, D. H. (1995). Electrospinning process and applications of electrospun fibers. *Journal of Electrostatics*, 35, 151–160.
<https://doi.org/10.1109/ias.1993.299067>
- Dowsey, M. M., Nikpour, M., Dieppe, P., & Choong, P. F. M. (2012). Associations between pre-operative radiographic changes and outcomes after total knee joint replacement for osteoarthritis. *Osteoarthritis and Cartilage*, 20(10), 1095–1102.
<https://doi.org/10.1016/j.joca.2012.05.015>
- Dumont, M., Villet, R., Guirand, M., Montembault, A., Delair, T., Lack, S., Barikosky, M., Crepet, A., Alcou, P., Laurent, F., & David, L. (2018). *Processing and antibacterial properties of chitosan-coated alginate fibers*. 190(December 2016), 31–42.
<https://doi.org/10.1016/j.carbpol.2017.11.088>
- Eltom, A., Zhong, G., & Muhammad, A. (2019). Scaffold Techniques and Designs in Tissue Engineering Functions and Purposes: A Review. In *Advances in Materials Science and Engineering* (Vol. 2019). <https://doi.org/10.1155/2019/3429527>
- Emery, C. A., Whittaker, J. L., Mahmoudian, A., Lohmander, L. S., Roos, E. M., Bennell, K. L., Toomey, C. M., Reimer, R. A., Thompson, D., Ronsky, J. L., Kuntze, G., Lloyd, D. G., Andriacchi, T., Englund, M., Kraus, V. B., Losina, E., Bierma-Zeinstra, S., Runhaar, J., Peat, G., ... Arden, N. K. (2019). Establishing outcome measures in early knee osteoarthritis. *Nature Reviews Rheumatology*, 15(7), 438–448. <https://doi.org/10.1038/s41584-019-0237-3>
- Eslamian, M., Khorrami, M., Yi, N., Majd, S., & Abidian, M. R. (2019). Electrospinning of highly aligned fibers for drug delivery applications. *Journal of Materials Chemistry B*, 7(2), 224–232. <https://doi.org/10.1039/c8tb01258j>
- Filip, P., & Peer, P. (2019). *Characterization of Poly(Ethylene Oxide) Nanofibers — Mutual Relations between Mean Diameter of Electrospun Nanofibers and Solution Characteristics*. December. <https://doi.org/10.3390/pr7120948>
- Gangolphe, L., Leon-Valdivieso, C. Y., Nottelet, B., Déjean, S., Bethry, A., Pinese, C., Bossard, F., & Garric, X. (2021). Electrospun microstructured PLA-based scaffolds featuring relevant anisotropic, mechanical and degradation characteristics for soft tissue engineering. *Materials Science and Engineering C*, 129(July). <https://doi.org/10.1016/j.msec.2021.112339>
- Gao, Y., Liu, S., Huang, J., Guo, W., Chen, J., Zhang, L., Zhao, B., Peng, J., Wang, A., Wang, Y., Xu, W., Lu, S., Yuan, M., & Guo, Q. (2014). *The ECM-Cell Interaction of Cartilage Extracellular Matrix on Chondrocytes*. 2014.
- García-López, J., Garcíadiego-Cázares, D., Melgarejo-Ramírez, Y., Sánchez-Sánchez,

- R., Solís-Arrieta, L., García-Carvajal, Z., Sánchez-Betancourt, J. I., Ibarra, C., Luna-Bárcena, G., & Velasquillo, C. (2015). Chondrocyte differentiation for auricular cartilage reconstruction using a chitosan based hydrogel. *Histology and Histopathology*, 30(12), 1477–1485. <https://doi.org/10.14670/HH-11-642>
- García, C. E. G., Bossard, F., & Rinaudo, M. (2021). Electrospun biomaterials from chitosan blends applied as scaffold for tissue regeneration. *Polymers*, 13(7), 1–20. <https://doi.org/10.3390/polym13071037>
- García, C. E., Soltero, F. A., Bossard, F., & Rinaudo, M. (2020). Production of chitosan/hyaluronan complex nanofibers. Characterization and physical properties as a function of the composition. *Polymers*, 12(9). <https://doi.org/10.3390/POLYM12092004>
- García García, C. E., Lardy, B., Bossard, F., Soltero Martínez, F. A., & Rinaudo, M. (2021). Chitosan based biomaterials for cartilage tissue engineering: Chondrocyte adhesion and proliferation. *Food Hydrocolloids for Health*, 1, 100018. <https://doi.org/10.1016/j.fhfh.2021.100018>
- García García, C. E., Soltero Martínez, F. A., Bossard, F., & Rinaudo, M. (2018). Biomaterials based on electrospun chitosan. Relation between processing conditions and mechanical properties. *Polymers*, 10(3), 1–19. <https://doi.org/10.3390/polym10030257>
- García García, C. E., Verdier, C., Lardy, B., Bossard, F., Soltero Martínez, J. F. A., & Rinaudo, M. (2022). Chondrocyte cell adhesion on chitosan supports using single-cell atomic force microscopy. *International Journal of Polymer Analysis and Characterization*, 27(1), 71–85. <https://doi.org/10.1080/1023666X.2021.2008135>
- Garg, K., & Bowlin, G. L. (2011). Electrospinning jets and nanofibrous structures. *Biomicrofluidics*, 5(1), 1–19. <https://doi.org/10.1063/1.3567097>
- Gatej, I., Popa, M., & Rinaudo, M. (2005). *Role of the pH on Hyaluronan Behavior in Aqueous Solution*. 61–67.
- Goldring, M. B. (2000). Osteoarthritis and cartilage: the role of cytokines. In *Current rheumatology reports* (Vol. 2, Issue 6, pp. 459–465). Osteoarthritis Research Society International. <https://doi.org/10.1007/s11926-000-0021-y>
- Goldring, Mary B. (2000). Osteoarthritis and cartilage: the role of cytokines. In *Current rheumatology reports* (Vol. 2, Issue 6, pp. 459–465). <https://doi.org/10.1007/s11926-000-0021-y>
- Goldring, Mary B, Birkhead, J. R., Suen, L., Yamin, R., Mizuno, S., Glowacki, J., Arbiser, J. L., & Apperleyll, J. F. (1994). Interleukin-1,8-modulated Gene Expression in Immortalized Human Chondrocytes. *J Clin Invest*, 94(6), 2307–2316.
- Haghi, A. K., & Akbari, M. (2007). *Trends in electrospinning of natural nanofibers*. 1834(6), 1830–1834. <https://doi.org/10.1002/pssa.200675301>
- Haider, A., Haider, S., & Kang, I. K. (2015). A comprehensive review summarizing the effect of electrospinning parameters and potential applications of nanofibers in biomedical and biotechnology. *Arabian Journal of Chemistry*, 11(8), 1165–1188. <https://doi.org/10.1016/j.arabjc.2015.11.015>
- Haider, A., Haider, S., & Kang, I. K. (2018). A comprehensive review summarizing the effect of electrospinning parameters and potential applications of nanofibers

- in biomedical and biotechnology. In *Arabian Journal of Chemistry* (Vol. 11, Issue 8, pp. 1165–1188). Elsevier. <https://doi.org/10.1016/j.arabjc.2015.11.015>
- Healy, E., Dempsey, M., Lally, C., & Ryan, M. P. (1998). Apoptosis and necrosis: Mechanisms of cell death induced by cyclosporine A in a renal proximal tubular cell line. *Kidney International*, 54(6), 1955–1966. <https://doi.org/10.1046/j.1523-1755.1998.00202.x>
- Higashi, H., & Barendregt, J. J. (2011). Cost-effectiveness of total hip and knee replacements for the Australian population with osteoarthritis: Discrete-event simulation model. *PLoS ONE*, 6(9). <https://doi.org/10.1371/journal.pone.0025403>
- Hillel, A., Shah, P., & Elisseeff, J. (2007). Hydrogels in cell encapsulation and tissue engineering. In M. Jenkins (Ed.), *Biomedical Polymers* (Vol. 1961, pp. 57–82). Woodhead Publishing Limited. <https://doi.org/10.1533/9781845693640.57>
- Hirsch, M. S., Lunsford, L. E., Trinkaus-Randall, V., & Svoboda, K. K. H. (1997). Chondrocyte survival and differentiation in situ are integrin mediated. *Developmental Dynamics*, 210(3), 249–263. [https://doi.org/10.1002/\(SICI\)1097-0177\(199711\)210:3<249::AID-AJA6>3.0.CO;2-G](https://doi.org/10.1002/(SICI)1097-0177(199711)210:3<249::AID-AJA6>3.0.CO;2-G)
- Hoemann, C. D., Buschmann, M. D., & McKee, M. D. (2012). *Composition and method for the repair and regeneration of cartilage and other tissues*. 2(12). <https://patentimages.storage.googleapis.com/c2/a9/15/c83f9319a0814d/US8258117.pdf>
- Hosseini, H., Shahraky, M. K., Amani, A., & Landi, F. S. (2020). Electrospinning of polyvinyl alcohol/chitosan/hyaluronic acid nanofiber containing growth hormone and its release investigations. *Polymers for Advanced Technologies*, January, 1–8. <https://doi.org/10.1002/pat.5111>
- Hutter, J. L., & Bechhoefer, J. (1993). Calibration of atomic-force microscope tips. *Review of Scientific Instruments*, 64(7), 1868–1873. <https://doi.org/10.1063/1.1143970>
- In, K. S., Won, H. S., Sang, Y. L., Sang, H. L., Seong, J. H., Myung, C. L., & Lee, S. J. (2009). Chitosan nano-/microfibrous double-layered membrane with rolled-up three-dimensional structures for chondrocyte cultivation. *Journal of Biomedical Materials Research - Part A*, 90(2), 595–602. <https://doi.org/10.1002/jbm.a.32109>
- Iwasaki, N., Kasahara, Y., Yamane, S., Igarashi, T., Minami, A., & Nisimura, S. I. (2011). Chitosan-based hyaluronic acid hybrid polymer fibers as a scaffold biomaterial for cartilage tissue engineering. *Polymers*, 3(1), 100–113. <https://doi.org/10.3390/polym3010100>
- Jalaja, K., Naskar, D., Kundu, S. C., & James, N. R. (2016). Potential of electrospun core-shell structured gelatin-chitosan nanofibers for biomedical applications. *Carbohydrate Polymers*, 136, 1098–1107. <https://doi.org/10.1016/j.carbpol.2015.10.014>
- Jamshidi, A., Pelletier, J. P., & Martel-Pelletier, J. (2019). Machine-learning-based patient-specific prediction models for knee osteoarthritis. In *Nature Reviews Rheumatology* (Vol. 15, Issue 1, pp. 49–60). Springer US. <https://doi.org/10.1038/s41584-018-0130-5>
- Jayakumar, R., Prabakaran, M., Nair, S. V., & Tamura, H. (2010). Novel chitin and chitosan nanofibers in biomedical applications. *Biotechnology Advances*, 28(1),

- 142–150. <https://doi.org/10.1016/j.biotechadv.2009.11.001>
- Jevsevar, D. S. (2013). Treatment of osteoarthritis of the knee: Evidence-based guideline, 2nd edition. In *Journal of the American Academy of Orthopaedic Surgeons* (Vol. 21, Issue 9, pp. 571–576). <https://doi.org/10.5435/JAAOS-21-09-571>
- Ji, D. Y., Kuo, T. F., Wu, H. Da, Yang, J. C., & Lee, S. Y. (2012). A novel injectable chitosan/polyglutamate polyelectrolyte complex hydrogel with hydroxyapatite for soft-tissue augmentation. *Carbohydrate Polymers*, 89(4), 1123–1130. <https://doi.org/10.1016/j.carbpol.2012.03.083>
- Jiang, H., Hu, Y., Li, Y., Zhao, P., Zhu, K., & Chen, W. (2005). A facile technique to prepare biodegradable coaxial electrospun nanofibers for controlled release of bioactive agents. *Journal of Controlled Release*, 108(2–3), 237–243. <https://doi.org/10.1016/j.jconrel.2005.08.006>
- Jin, R., Lin, C., & Cao, A. (2014). Enzyme-mediated fast injectable hydrogels based on chitosan-glycolic acid/tyrosine: Preparation, characterization, and chondrocyte culture. *Polymer Chemistry*, 5(2), 391–398. <https://doi.org/10.1039/c3py00864a>
- Kasahara, Y., Iwasaki, N., Yamane, S., Igarashi, T., Majima, T., Nonaka, S., Harada, K., Nishimura, S. I., & Minami, A. (2008). Development of mature cartilage constructs using novel three-dimensional porous scaffolds for enhanced repair of osteochondral defects. *Journal of Biomedical Materials Research - Part A*, 86(1), 127–136. <https://doi.org/10.1002/jbm.a.31259>
- Kloppenburger, M., & Berenbaum, F. (2020). Osteoarthritis year in review 2019: epidemiology and therapy. *Osteoarthritis and Cartilage*, 28(3), 242–248. <https://doi.org/10.1016/j.joca.2020.01.002>
- Kolasinski, S. L., Neogi, T., Hochberg, M. C., Oatis, C., Guyatt, G., Block, J., Callahan, L., Copenhaver, C., Dodge, C., Felson, D., Gellar, K., Harvey, W. F., Hawker, G., Herzig, E., Kwoh, C. K., Nelson, A. E., Samuels, J., Scanzello, C., White, D., ... Reston, J. (2020). 2019 American College of Rheumatology/Arthritis Foundation Guideline for the Management of Osteoarthritis of the Hand, Hip, and Knee. *Arthritis Care and Research*, 72(2), 149–162. <https://doi.org/10.1002/acr.24131>
- Krishnan, Y., & Grodzinsky, A. J. (2018). Cartilage diseases. In *Matrix Biology* (Vols. 71–72, Issue 3, pp. 51–69). <https://doi.org/10.1016/j.matbio.2018.05.005>
- Lancuski, A. (2013). *Mise en forme et caractérisation de nano-fibres fonctionnalisées par chimie click pour l'ingénierie tissulaire*. Université Grenoble Alpes.
- Laudenslager, M.J., Sigmund, W. M. (2012). Electrospinning. *Encyclopedia of Nanotechnology*, 769–775.
- Laurent, V. M., Duperray, A., Sundar Rajan, V., & Verdier, C. (2014). Atomic Force Microscopy Reveals a Role for Endothelial Cell ICAM-1 Expression in Bladder Cancer Cell Adherence. *PLOS ONE*, 9(5), 1–11. <https://doi.org/10.1371/journal.pone.0098034>
- Lawson, T. B., Mäkelä, J. T. A., Klein, T., Snyder, B. D., & Grinstaff, M. W. (2020a). Nanotechnology and osteoarthritis; part 1: Clinical landscape and opportunities for advanced diagnostics. *Journal of Orthopaedic Research*, April. <https://doi.org/10.1002/jor.24817>
- Lawson, T. B., Mäkelä, J. T. A., Klein, T., Snyder, B. D., & Grinstaff, M. W. (2020b). Nanotechnology and Osteoarthritis. Part 2: Opportunities for advanced devices

- and therapeutics. *Journal of Orthopaedic Research*, August, 1–12.
<https://doi.org/10.1002/jor.24842>
- Lehmann, P., Symietz, C., Brezesinski, G., Kraß, H., & Kurth, D. G. (2005). Langmuir and langmuir-blodgett films of metallosupramolecular polyelectrolyte-amphiphile complexes. *Langmuir*, 21(13), 5901–5906.
<https://doi.org/10.1021/la050841p>
- Lemma, S. M., Bossard, F. F., & Rinaudo, M. (2016). Preparation of pure and stable chitosan nanofibers by electrospinning in the presence of poly(ethylene oxide). *International Journal of Molecular Sciences*, 17(11).
<https://doi.org/10.3390/ijms17111790>
- Li, M., Tian, X., Schreyer, D. J., & Chen, X. (2011). Effect of needle geometry on flow rate and cell damage in the dispensing-based biofabrication process. *Biotechnology Progress*, 27(6), 1777–1784. <https://doi.org/10.1002/btpr.679>
- Li, W. J., Danielson, K. G., Alexander, P. G., & Tuan, R. S. (2003). Biological response of chondrocytes cultured in three-dimensional nanofibrous poly(ϵ -caprolactone) scaffolds. *Journal of Biomedical Materials Research - Part A*, 67(4), 1105–1114.
<https://doi.org/10.1002/jbm.a.10101>
- Li, Z., & Wang, C. (2013). *Effects of Working Parameters on Electrospinning* (pp. 15–28). Springer, Berlin, Heidelberg. https://doi.org/10.1007/978-3-642-36427-3_2
- Liu, H., Li, W., Wen, W., Luo, B., Liu, M., Ding, S., & Zhou, C. (2017). Mechanical properties and osteogenic activity of poly(L-lactide) fibrous membrane synergistically enhanced by chitosan nanofibers and polydopamine layer. *Materials Science and Engineering C*, 81(August), 280–290.
<https://doi.org/10.1016/j.msec.2017.08.010>
- Liu, Y., Ma, G., Fang, D., Xu, J., Zhang, H., & Nie, J. (2011). Effects of solution properties and electric field on the electrospinning of hyaluronic acid. *Carbohydrate Polymers*, 83(2), 1011–1015.
<https://doi.org/10.1016/j.carbpol.2010.08.061>
- Loeser, R. F., Goldring, S. R., Scanzello, C. R., & Goldring, M. B. (2012). Osteoarthritis: A disease of the joint as an organ. In *Arthritis and Rheumatism* (Vol. 64, Issue 6, pp. 1697–1707). <https://doi.org/10.1002/art.34453>
- Ma, B., Leijten, J. C. H., Wu, L., Kip, M., Blitterswijk, C. A. Van, Post, J. N., & Karperien, M. (2013). *Gene expression profile of dedifferentiated human articular chondrocytes in monolayer culture*. 21, 599–603.
<https://doi.org/10.1016/j.joca.2013.01.014>
- Ma, G., Liu, Y., Fang, D., Chen, J., Peng, C., Fei, X., & Nie, J. (2012). Hyaluronic acid/chitosan polyelectrolyte complexes nanofibers prepared by electrospinning. *Materials Letters*, 74, 78–80. <https://doi.org/10.1016/j.matlet.2012.01.012>
- Ma, H., Chen, G., Zhang, J., Liu, Y., Nie, J., & Ma, G. (2017). Facile fabrication of core-shell polyelectrolyte complexes nanofibers based on electric field induced phase separation. *Polymer*, 110, 80–86. <https://doi.org/10.1016/j.polymer.2016.12.062>
- Majima, T., Irie, T., Sawaguchi, N., Funakoshi, T., Iwasaki, N., Harada, K., Minami, A., & Nishimura, S. I. (2007). Chitosan-based hyaluronan hybrid polymer fibre scaffold for ligament and tendon tissue engineering. *Proceedings of the Institution of Mechanical Engineers, Part H: Journal of Engineering in Medicine*, 221(5), 537–546.

- <https://doi.org/10.1243/09544119JEIM203>
- Malik, S., Sundarrajan, S., Hussain, T., Nazir, A., Ayyoob, M., Berto, F., & Ramakrishna, S. (2020). Sustainable nanofibers in tissue engineering and biomedical applications. *Material Design & Processing Communications*, August, 1–22. <https://doi.org/10.1002/mdp2.202>
- Maly, M. R., Marriott, K. A., & Chopp-Hurley, J. N. (2020). Osteoarthritis year in review 2019: rehabilitation and outcomes. *Osteoarthritis and Cartilage*, 28(3), 249–266. <https://doi.org/10.1016/j.joca.2019.11.008>
- Mandl, L. A. (2019). Osteoarthritis year in review 2018: clinical. *Osteoarthritis and Cartilage*, 27(3), 359–364. <https://doi.org/10.1016/j.joca.2018.11.001>
- Maumus, M., Pers, Y. M., Ruiz, M., Jorgensen, C., & Noël, D. (2018). Mesenchymal stem cells and regenerative medicine: Future perspectives in osteoarthritis. *Medecine/Sciences*, 34(12), 1092–1099. <https://doi.org/10.1051/medsci/2018294>
- Mazzoni, E., Iaquina, M. R., Lanzillotti, C., Mazziotta, C., Maritati, M., Montesi, M., Sprio, S., Tampieri, A., Tognon, M., & Martini, F. (2021). Bioactive Materials for Soft Tissue Repair. In *Frontiers in Bioengineering and Biotechnology* (Vol. 9, Issue February, pp. 1–17). <https://doi.org/10.3389/fbioe.2021.613787>
- McAlindon, T. E., Bannuru, R. R., Sullivan, M. C., Arden, N. K., Berenbaum, F., Bierma-Zeinstra, S. M., Hawker, G. A., Henrotin, Y., Hunter, D. J., Kawaguchi, H., Kwoh, K., Lohmander, S., Rannou, F., Roos, E. M., & Underwood, M. (2014). OARSI guidelines for the non-surgical management of knee osteoarthritis. *Osteoarthritis and Cartilage*, 22(3), 363–388. <https://doi.org/10.1016/j.joca.2014.01.003>
- Meng, X., Perry, S. L., & Schiffman, J. D. (2017). Complex Coacervation: Chemically Stable Fibers Electrospun from Aqueous Polyelectrolyte Solutions. *ACS Macro Letters*, 6(5), 505–511. <https://doi.org/10.1021/acsmacrolett.7b00173>
- Mohan, N., Mohanan, P. V., Sabareeswaran, A., & Nair, P. (2017). Chitosan-hyaluronic acid hydrogel for cartilage repair. *International Journal of Biological Macromolecules*, 104, 1936–1945. <https://doi.org/10.1016/j.ijbiomac.2017.03.142>
- Mondésert, H., Bossard, F., & Favier, D. (2021). Anisotropic electrospun honeycomb polycaprolactone scaffolds: Elaboration, morphological and mechanical properties. *Journal of the Mechanical Behavior of Biomedical Materials*, 113(October 2020). <https://doi.org/10.1016/j.jmbbm.2020.104124>
- Mora, J. C., Przkora, R., & Cruz-Almeida, Y. (2018). Knee osteoarthritis: Pathophysiology and current treatment modalities. In *Journal of Pain Research* (Vol. 11, pp. 2189–2196). <https://doi.org/10.2147/JPR.S154002>
- Murano, E., Perin, D., Khan, R., & Bergamin, M. (2011). Hyaluronan: From biomimetic to industrial business strategy. *Natural Product Communications*, 6(4), 555–572. <https://doi.org/10.1177/1934578x1100600415>
- Murray, K. J., & Azari, M. F. (2015). Leg length discrepancy and osteoarthritis in the knee, hip and lumbar spine. *Journal of the Canadian Chiropractic Association*, 59(3), 226–237.
- Muzzarelli, R. A. A., Greco, F., Busilacchi, A., Sollazzo, V., & Gigante, A. (2012). Chitosan, hyaluronan and chondroitin sulfate in tissue engineering for cartilage regeneration: A review. *Carbohydrate Polymers*, 89(3), 723–739.

- <https://doi.org/10.1016/j.carbpol.2012.04.057>
- Na, H., Chen, P., Wong, S. C., Hague, S., & Li, Q. (2012). Fabrication of PVDF/PVA microtubules by coaxial electrospinning. *Polymer (United Kingdom)*, 53(13), 2736–2743. <https://doi.org/10.1016/j.polymer.2012.04.021>
- Nagy, A. G., Bonyar, A., Szekacs, I., & Horvath, R. (2020). Analysis of single-cell force-spectroscopy data of Vero cells recorded by FluidFM BOT. *2020 IEEE 26th International Symposium for Design and Technology in Electronic Packaging, SIITME 2020 - Conference Proceedings*, 21–25. <https://doi.org/10.1109/SIITME50350.2020.9292265>
- Nam, Y. S., & Park, T. G. (1999). Porous biodegradable polymeric scaffolds prepared by thermally induced phase separation. *Journal of Biomedical Materials Research*, 47(1), 8–17. [https://doi.org/10.1002/\(SICI\)1097-4636\(199910\)47:1<8::AID-JBM2>3.0.CO;2-L](https://doi.org/10.1002/(SICI)1097-4636(199910)47:1<8::AID-JBM2>3.0.CO;2-L)
- Nguyen, T. D., & Gu, Y. (2016). Investigation of Cell-Substrate Adhesion Properties of Living Chondrocyte by Measuring Adhesive Shear Force and Detachment Using AFM and Inverse FEA. *Scientific Reports*, 6(38059), 1–13. <https://doi.org/10.1038/srep38059>
- Noriega, S. E., Hasanova, G. I., Schneider, M. J., Larsen, G. F., & Subramanian, A. (2012). Effect of fiber diameter on the spreading, proliferation and differentiation of chondrocytes on electrospun chitosan matrices. *Cells Tissues Organs*, 195(3), 207–221. <https://doi.org/10.1159/000325144>
- Pabjańczyk-Wlazło, E., Krucińska, I., Chrzanowski, M., Szparaga, G., Chaberska, A., Kolesińska, B., Komisarzyk, A., & Boguń, M. (2017). Fabrication of Pure Electrospun Materials from Hyaluronic Acid. *Fibres and Textiles in Eastern Europe*, 25(123), 45–52. <https://doi.org/10.5604/01.3001.0010.1688>
- Pakravan, M., Heuzey, M., & Aji, A. (2011). A fundamental study of chitosan / PEO electrospinning. *Polymer*, 52(21), 4813–4824. <https://doi.org/10.1016/j.polymer.2011.08.034>
- Peniche, C., Argüelles-Monal, W., Davidenko, N., Sastre, R., Gallardo, A., & San Román, J. (1999). Self-curing membranes of chitosan/PAA IPNs obtained by radical polymerization: Preparation, characterization and interpolymer complexation. *Biomaterials*, 20(20), 1869–1878. [https://doi.org/10.1016/S0142-9612\(99\)00048-4](https://doi.org/10.1016/S0142-9612(99)00048-4)
- Peniche, C., Elvira, C., & San Roman, J. (1998). Interpolymer complexes of chitosan and polymethacrylic derivatives of salicylic acid: Preparation, characterization and modification by thermal treatment. *Polymer*, 39(25), 6549–6554. [https://doi.org/10.1016/S0032-3861\(98\)00059-7](https://doi.org/10.1016/S0032-3861(98)00059-7)
- Petrova, V. A., Chernyakov, D. D., Poshina, D. N., Gofman, I. V, Romanov, D. P., Mishanin, A. I., Golovkin, A. S., & Skorik, Y. A. (2019). Electrospun bilayer chitosan/hyaluronan material and its compatibility with mesenchymal stem cells. *Materials*, 12(12). <https://doi.org/10.3390/ma12122016>
- Pillay, V., Dott, C., Choonara, Y. E., Tyagi, C., Tomar, L., Kumar, P., du Toit, L. C., & Ndesendo, V. M. K. (2013). A Review of the Effect of Processing Variables on the Fabrication of Electrospun Nanofibers for Drug Delivery Applications. *Journal of Nanomaterials*, 2013, 1–22. <https://doi.org/10.1155/2013/789289>

- Pokhrel, S., & Yadav, P. N. (2019). Functionalization of chitosan polymer and their applications. *Journal of Macromolecular Science, Part A: Pure and Applied Chemistry*, 56(5), 450–475. <https://doi.org/10.1080/10601325.2019.1581576>
- Pratap, S. Y., Sudip, D., Suprabha, N., & Rakesh, B. (2020). Optimization of electrospinning process & parameters for producing defect-free chitosan/polyethylene oxide nanofibers for bone tissue engineering. *Journal of Biomaterials Science, Polymer Edition*, 31(6), 781–803. <https://doi.org/10.1080/09205063.2020.1718824>
- Puech, P. H., Taubenberger, A., Ulrich, F., Krieg, M., Muller, D. J., & Heisenberg, C. P. (2005). Measuring cell adhesion forces of primary gastrulating cells from zebrafish using atomic force microscopy. *Journal of Cell Science*, 118(18), 4199–4206. <https://doi.org/10.1242/jcs.02547>
- Rai, V., Dilisio, M. F., Dietz, N. E., & Agrawal, D. K. (2017). Recent strategies in cartilage repair: A systemic review of the scaffold development and tissue engineering. *Journal of Biomedical Materials Research - Part A*, 105(8), 2343–2354. <https://doi.org/10.1002/jbm.a.36087>
- Rajpoot, K., Safavi, M., Sreeharsha, N., & Tekade, R. K. (2020). Recent advances in regenerative medicine. *The Future of Pharmaceutical Product Development and Research*, 367–412. <https://doi.org/10.1016/b978-0-12-814455-8.00011-6>
- Recillas, M., Silva, L. L., Peniche, C., Goycoolea, F. M., Rinaudo, M., Román, J. S., & Argüelles-Monal, W. M. (2011). Thermo- and pH-responsive polyelectrolyte complex membranes from chitosan-g-N-isopropylacrylamide and pectin. *Carbohydrate Polymers*, 86(3), 1336–1343. <https://doi.org/10.1016/j.carbpol.2011.06.047>
- Reichenbach, S., Rutjes, A. W., Nuesch, E., Trelle, S., & Jüni, P. (2010). Joint lavage for osteoarthritis of the knee. *Cochrane Database of Systematic Reviews*, 5. <https://doi.org/10.1002/14651858.cd007320.pub2>
- Ridolfi, D. M., Lemes, A. P., de Oliveira, S., Justo, G. Z., Palladino, M. V., & Durán, N. (2017). Electrospun poly(ethylene oxide)/chitosan nanofibers with cellulose nanocrystals as support for cell culture of 3T3 fibroblasts. *Cellulose*, 24(8), 3353–3365. <https://doi.org/10.1007/s10570-017-1362-2>
- Rinaudo, M. (2006). Chitin and chitosan: Properties and applications. *Progress in Polymer Science (Oxford)*, 31(7), 603–632. <https://doi.org/10.1016/j.progpolymsci.2006.06.001>
- Rogers, K. (2018). Tissue engineering. In *Encyclopedia Britannica*. <https://www.britannica.com/science/tissue-engineering>
- Rogina, A., Pušić, M., Štefan, L., Ivković, A., Urlić, I., Ivanković, M., & Ivanković, H. (2021). Characterization of Chitosan-Based Scaffolds Seeded with Sheep Nasal Chondrocytes for Cartilage Tissue Engineering. *Annals of Biomedical Engineering*, 49(6), 1572–1586. <https://doi.org/10.1007/s10439-020-02712-9>
- Rongen, J. J., Rovers, M. M., van Tienen, T. G., Buma, P., & Hannink, G. (2017). Increased risk for knee replacement surgery after arthroscopic surgery for degenerative meniscal tears: a multi-center longitudinal observational study using data from the osteoarthritis initiative. *Osteoarthritis and Cartilage*, 25(1), 23–29. <https://doi.org/10.1016/j.joca.2016.09.013>

- Rozario, T., & DeSimone, D. W. (2010). The extracellular matrix in development and morphogenesis: A dynamic view. *Developmental Biology*, 341(1), 126–140. <https://doi.org/10.1016/j.ydbio.2009.10.026>
- Rusu-Balaita, L., Desbrières, J., & Rinaudo, M. (2003). Formation of a biocompatible polyelectrolyte complex: Chitosan-hyaluronan complex stability. *Polymer Bulletin*, 50(1–2), 91–98. <https://doi.org/10.1007/s00289-003-0144-1>
- Sadeghi, A. M. M., Dorkoosh, F. A., Avadi, M. R., Saadat, P., Rafiee-Tehrani, M., & Junginger, H. E. (2008). Preparation, characterization and antibacterial activities of chitosan, N-trimethyl chitosan (TMC) and N-diethylmethyl chitosan (DEMC) nanoparticles loaded with insulin using both the ionotropic gelation and polyelectrolyte complexation methods. *International Journal of Pharmaceutics*, 355(1–2), 299–306. <https://doi.org/10.1016/j.ijpharm.2007.11.052>
- Sagvolden, G., Giaever, I., Pettersen, E. O., & Feder, J. (1999). Cell adhesion force microscopy. *Proceedings of the National Academy of Sciences of the United States of America*, 96(2), 471–476. <https://doi.org/10.1073/pnas.96.2.471>
- Salá Nki, R., Hos, C., Orgovan, N., Pé Ter, B., Sá Ndor, N., Bajtay, Z., Erdei, A., Horvath, R., & Szabo, B. (2014). Single cell adhesion assay using computer controlled Micropipette. *PLoS ONE*, 9(10). <https://doi.org/10.1371/journal.pone.0111450>
- Sandri, G., Rossi, S., Bonferoni, M. C., Miele, D., Faccendini, A., Del Favero, E., Di Cola, E., Icaro Cornaglia, A., Boselli, C., Luxbacher, T., Malavasi, L., Cantu, L., & Ferrari, F. (2019). Chitosan/glycosaminoglycan scaffolds for skin repairation. *Carbohydrate Polymers*, 220(May), 219–227. <https://doi.org/10.1016/j.carbpol.2019.05.069>
- Sapkota, S., & Chou, S. (2020). Electrospun Chitosan-based Fibers for Wound Healing Applications. *Journal of Biomaterials*, 4(2), 51. <https://doi.org/10.11648/j.jb.20200402.13>
- Schaefer, L., & Schaefer, R. M. (2010). *Proteoglycans : from structural compounds to signaling molecules*. 237–246. <https://doi.org/10.1007/s00441-009-0821-y>
- Shafei, S., Foroughi, J., Stevens, L., Wong, C. S., Zabihi, O., & Naebe, M. (2017). Electroactive nanostructured scaffold produced by controlled deposition of PPy on electrospun PCL fibres. *Research on Chemical Intermediates*, 43(2), 1235–1251. <https://doi.org/10.1007/s11164-016-2695-4>
- Shim, I. K., Suh, W. H., Lee, S. Y., Lee, S. H., Heo, S. J., Lee, M. C., & Lee, S. J. (2008). Chitosan nano-/microfibrous double-layered membrane with rolled-up three-dimensional structures for chondrocyte cultivation. *Journal of Biomedical Materials Research Part A*, 595–602. <https://doi.org/10.1002/jbm.a.32109>
- Siemieniuk, R. A. C., Harris, I. A., Agoritsas, T., Poolman, R. W., Brignardello-Petersen, R., Van De Velde, S., Buchbinder, R., Englund, M., Lytvyn, L., Quinlan, C., Helsing, L., Knutsen, G., Olsen, N. R., MacDonald, H., Hailey, L., Wilson, H. M., Lydiatt, A., & Kristiansen, A. (2017). Arthroscopic surgery for degenerative knee arthritis and meniscal tears: A clinical practice guideline. *BMJ (Online)*, 357, 1–8. <https://doi.org/10.1136/bmj.j1982>
- Sill, T. J., & von Recum, H. A. (2008). Electrospinning: Applications in drug delivery and tissue engineering. *Biomaterials*, 29(13), 1989–2006.

- <http://www.ncbi.nlm.nih.gov/pubmed/18281090>
- Smith, L. A., & Ma, P. X. (2004). Nano-fibrous scaffolds for tissue engineering. *Colloids and Surfaces B: Biointerfaces*, 39(3), 125–131. <https://doi.org/10.1016/j.colsurfb.2003.12.004>
- Subramanian, A., Vu, D., Larsen, G. F., & Lin, H. Y. (2005). Preparation and evaluation of the electrospun chitosan/PEO fibers for potential applications in cartilage tissue engineering. *Journal of Biomaterials Science, Polymer Edition*, 16(7), 861–873. <https://doi.org/10.1163/1568562054255682>
- Sukul, M., Sahariah, P., Lauzon, H. L., Borges, J., Másson, M., Mano, J. F., Haugen, H. J., & Reseland, J. E. (2021). In vitro biological response of human osteoblasts in 3D chitosan sponges with controlled degree of deacetylation and molecular weight. *Carbohydrate Polymers*, 254(November). <https://doi.org/10.1016/j.carbpol.2020.117434>
- Sundar Rajan, V., Laurent, V. M., Verdier, C., & Duperray, A. (2017). Unraveling the Receptor-Ligand Interactions between Bladder Cancer Cells and the Endothelium Using AFM. *Biophysical Journal*, 112(6), 1246–1257. <https://doi.org/10.1016/j.bpj.2017.01.033>
- Sztilkovichs, M., Gerecsei, T., Peter, B., Saftics, A., Kurunczi, S., Szekacs, I., Szabo, B., & Horvath, R. (2020). Single-cell adhesion force kinetics of cell populations from combined label-free optical biosensor and robotic fluidic force microscopy. *Scientific Reports*, 10(1), 1–13. <https://doi.org/10.1038/s41598-019-56898-7>
- Tan, H., Gong, Y., Lao, L., Mao, Z., & Gao, C. (2007). Gelatin/chitosan/hyaluronan ternary complex scaffold containing basic fibroblast growth factor for cartilage tissue engineering. *Journal of Materials Science: Materials in Medicine*, 18(10), 1961–1968. <https://doi.org/10.1007/s10856-007-3095-5>
- Theron, S. A., Zussman, E., & Yarin, A. L. (2004). Experimental investigation of the governing parameters in the electrospinning of polymer solutions. *Polymer*, 45(6), 2017–2030. <https://doi.org/10.1016/J.POLYMER.2004.01.024>
- Thomas, V., Jose, M. V, Chowdhury, S., Sullivan, J. F., Dean, D. R., & Vohra, Y. K. (2006). Mechano-morphological studies of aligned nanofibrous scaffolds of polycaprolactone fabricated by electrospinning. *Journal of Biomaterials Science, Polymer Edition*, 17(9), 969–984. <https://doi.org/10.1163/156856206778366022>
- Thorlund, J. B., Juhl, C. B., Roos, E. M., & Lohmander, L. S. (2015). Arthroscopic surgery for degenerative knee: systematic review and meta-analysis of benefits and harms. *BMJ*, 350, 1–9. <https://doi.org/10.1136/bmj.h2747>
- TIĞLI, R. S., & Gumüşderelioğlu, M. (2009). Evaluation of alginate-chitosan semi IPNs as cartilage scaffolds. *Journal of Materials Science: Materials in Medicine*, 20(3), 699–709. <https://doi.org/10.1007/s10856-008-3624-x>
- Titushkin, I., & Cho, M. (2006). Distinct Membrane Mechanical Properties of Human Mesenchymal Stem Cells Determined Using Laser Optical Tweezers. *Biophysical Journal*, 90(7), 2582–2591. <https://doi.org/10.1529/biophysj.105.073775>
- Toegel, S., Bieder, D., André, S., Altmann, F., Walzer, S. M., Kaltner, H., Hofstaetter, J. G., Windhager, R., & Gabius, H. J. (2013). Glycophenotyping of osteoarthritic cartilage and chondrocytes by RT-qPCR, mass spectrometry, histochemistry with plant/human lectins and lectin localization with a glycoprotein. *Arthritis*

- Research and Therapy*, 15(5). <https://doi.org/10.1186/ar4330>
- Tonda-Turo, C., Ruini, F., Ramella, M., Boccafoschi, F., Gentile, P., Gioffredi, E., Falvo D'Urso Labate, G., & Ciardelli, G. (2017). Non-covalently crosslinked chitosan nanofibrous mats prepared by electrospinning as substrates for soft tissue regeneration. *Carbohydrate Polymers*, 162, 82–92. <https://doi.org/10.1016/j.carbpol.2017.01.050>
- Tong, H. W., Zhang, X., & Wang, M. (2012). A new nanofiber fabrication technique based on coaxial electrospinning. *Materials Letters*, 66(1), 257–260. <https://doi.org/10.1016/j.matlet.2011.08.095>
- Toole, B. P. (2001). Hyaluronan in morphogenesis. *Seminars in Cell and Developmental Biology*, 12(2), 79–87. <https://doi.org/10.1006/scdb.2000.0244>
- Tsang, P. H., Li, G., Brun, Y. V., Freund, L. Ben, & Tang, J. X. (2006). Adhesion of single bacterial cells in the micronewton range. *Proceedings of the National Academy of Sciences of the United States of America*, 103(15), 5764–5768. <https://doi.org/10.1073/pnas.0601705103>
- Tsao, C. T., Chang, C. H., Lin, Y. Y., Wu, M. F., Wang, J. L., Young, T. H., Han, J. L., & Hsieh, K. H. (2011). Evaluation of chitosan/ γ -poly(glutamic acid) polyelectrolyte complex for wound dressing materials. *Carbohydrate Polymers*, 84(2), 812–819. <https://doi.org/10.1016/j.carbpol.2010.04.034>
- Umlauf, D., Frank, S., Pap, T., & Bertrand, J. (2010). Cartilage biology, pathology, and repair. In *Cellular and Molecular Life Sciences* (Vol. 67, Issue 24, pp. 4197–4211). <https://doi.org/10.1007/s00018-010-0498-0>
- Ungai-Salánki, R., Peter, B., Gerecsei, T., Orgovan, N., Horvath, R., & Szabó, B. (2019). A practical review on the measurement tools for cellular adhesion force. In *Advances in Colloid and Interface Science* (Vol. 269, pp. 309–333). <https://doi.org/10.1016/j.cis.2019.05.005>
- Varady, N. H., & Grodzinsky, A. J. (2016). Osteoarthritis year in review 2015: Mechanics. *Osteoarthritis and Cartilage*, 24(1), 27–35. <https://doi.org/10.1016/j.joca.2015.08.018>
- Varnaitė-Žuravliova, S., Savest, N., Baltušnikaitė-Guzaitienė, J., Abraitienė, A., & Krumme, A. (2019). Electrospinning of Chitosan Biopolymer and Polyethylene Oxide Blends. *Autex Research Journal*, 0(0). <https://doi.org/10.2478/aut-2019-0031>
- Vasiliu, S., Popa, M., & Rinaudo, M. (2005). Polyelectrolyte capsules made of two biocompatible natural polymers. *European Polymer Journal*, 41(5), 923–932. <https://doi.org/10.1016/j.eurpolymj.2004.11.017>
- Wade, R. J., & Burdick, J. A. (2014). Advances in nanofibrous scaffolds for biomedical applications: From electrospinning to self-assembly. *Nano Today*, 9(6), 722–742. <https://doi.org/10.1016/j.nantod.2014.10.002>
- Walker, P. A., Jimenez, F., Aroom, K., Gill, B. S., Savitz, S. I., & Cox, C. S. (2010). Effect of Needle Diameter and Flow Rate on Mesenchymal Stromal Cell (MSC) Cell Characterization and Viability. *Journal of Surgical Research*, 158(2), 382. <https://doi.org/10.1016/j.jss.2009.11.581>
- Wang, Chi, Cheng, Y.-W., Hsu, C.-H., Chien, H.-S., & Tsou, S.-Y. (2011). How to manipulate the electrospinning jet with controlled properties to obtain uniform fibers with the smallest diameter?—a brief discussion of solution electrospinning

- process. *Journal of Polymer Research*, 18(1), 111–123.
<https://doi.org/10.1007/s10965-010-9397-1>
- Wang, Chongyang, Hou, W., Guo, X., Li, J., Hu, T., Qiu, M., Liu, S., Mo, X., & Liu, X. (2017). Two-phase electrospinning to incorporate growth factors loaded chitosan nanoparticles into electrospun fibrous scaffolds for bioactivity retention and cartilage regeneration. *79*, 507–515. <https://doi.org/10.1016/j.msec.2017.05.075>
- Wang, X. S., Ji, Y. L., Zheng, P. Y., An, Q. F., Zhao, Q., Lee, K. R., Qian, J. W., & Gao, C. J. (2015). Engineering novel polyelectrolyte complex membranes with improved mechanical properties and separation performance. *Journal of Materials Chemistry A*, 3(14), 7296–7303. <https://doi.org/10.1039/c4ta06477a>
- Wang, X., Zhao, H., Turng, L. S., & Li, Q. (2013). Crystalline morphology of electrospun poly(ϵ -caprolactone) (PCL) nanofibers. *Industrial and Engineering Chemistry Research*, 52(13), 4939–4949. <https://doi.org/10.1021/ie302185e>
- Wang, Y., Yuan, M., Guo, Q. Y., Lu, S. B., & Peng, J. (2015). Mesenchymal stem cells for treating articular cartilage defects and osteoarthritis. *Cell Transplantation*, 24(9), 1661–1678. <https://doi.org/10.3727/096368914X683485>
- Wei, W., Ma, Y., Yao, X., Zhou, W., Wang, X., Li, C., Lin, J., He, Q., Leptihn, S., & Ouyang, H. (2021). Advanced hydrogels for the repair of cartilage defects and regeneration. *Bioactive Materials*, 6(4), 998–1011.
<https://doi.org/10.1016/j.bioactmat.2020.09.030>
- Wu, C. H., Ko, C. S., Huang, J. W., Huang, H. J., & Chu, I. M. (2010). Effects of exogenous glycosaminoglycans on human chondrocytes cultivated on type II collagen scaffolds. *Journal of Materials Science: Materials in Medicine*, 21(2), 725–729. <https://doi.org/10.1007/s10856-009-3889-8>
- Wu, D., Zhu, L., Li, Y., Zhang, X., Xu, S., Yang, G., & Delair, T. (2020). Chitosan-based Colloidal Polyelectrolyte Complexes for Drug Delivery: A Review. In *Carbohydrate Polymers* (Vol. 238). <https://doi.org/10.1016/j.carbpol.2020.116126>
- Wylde, V., Hewlett, S., Learmonth, I. D., & Dieppe, P. (2011). Persistent pain after joint replacement: Prevalence, sensory qualities, and postoperative determinants. *Pain*, 152(3), 566–572. <https://doi.org/10.1016/j.pain.2010.11.023>
- Xie, X., Chen, Y., Wang, X., Xu, X., Shen, Y., Khan, A. ur R., Aldalbah, A., Fetz, A. E., Bowlin, G. L., El-Newehy, M., & Mo, X. (2020). Electrospinning nanofiber scaffolds for soft and hard tissue regeneration. *Journal of Materials Science and Technology*, 59, 243–261. <https://doi.org/10.1016/j.jmst.2020.04.037>
- Xu, C. Y., Inai, R., Kotaki, M., & Ramakrishna, S. (2004). Aligned biodegradable nanofibrous structure: A potential scaffold for blood vessel engineering. *Biomaterials*, 25(5), 877–886. [https://doi.org/10.1016/S0142-9612\(03\)00593-3](https://doi.org/10.1016/S0142-9612(03)00593-3)
- Xu, J., Cai, N., Xu, W., Xue, Y., Wang, Z., Dai, Q., & Yu, F. (2013). Mechanical enhancement of nanofibrous scaffolds through polyelectrolyte complexation. *Nanotechnology*, 24(2). <https://doi.org/10.1088/0957-4484/24/2/025701>
- Yamane, S., Iwasaki, N., Kasahara, Y., Harada, K., Majima, T., Monde, K., Nishimura, S. I., & Minami, A. (2007). Effect of pore size on in vitro cartilage formation using chitosan-based hyaluronic acid hybrid polymer fibers. *Journal of Biomedical Materials Research - Part A*, 81(3), 586–593. <https://doi.org/10.1002/jbm.a.31095>
- Yamane, S., Iwasaki, N., Majima, T., Funakoshi, T., Masuko, T., Harada, K., Minami,

- A., Monde, K., & Nishimura, S. I. (2005). Feasibility of chitosan-based hyaluronic acid hybrid biomaterial for a novel scaffold in cartilage tissue engineering. *Biomaterials*, 26(6), 611–619. <https://doi.org/10.1016/j.biomaterials.2004.03.013>
- Yang, Y. M., Hu, W., Wang, X. D., & Gu, X. S. (2007). The controlling biodegradation of chitosan fibers by N-acetylation in vitro and in vivo. *Journal of Materials Science: Materials in Medicine*, 18(11), 2117–2121. <https://doi.org/10.1007/s10856-007-3013-x>
- Yao, S., Wang, X., Liu, X., Wang, R., Deng, C., & Cui, F. (2013). *Effects of Ambient Relative Humidity and Solvent Properties on the Electrospinning of Pure Hyaluronic Acid Nanofibers*. 13(xx), 1–7. <https://doi.org/10.1166/jnn.2013.7197>
- Younes, I., & Rinaudo, M. (2015). Chitin and chitosan preparation from marine sources. Structure, properties and applications. *Marine Drugs*, 13(3), 1133–1174. <https://doi.org/10.3390/md13031133>
- Yu, D. G., Wang, M., Li, X., Liu, X., Zhu, L. M., & Annie Bligh, S. W. (2020). Multifluid electrospinning for the generation of complex nanostructures. *Wiley Interdisciplinary Reviews: Nanomedicine and Nanobiotechnology*, 12(3), 1–11. <https://doi.org/10.1002/wnan.1601>
- Zeiger, A. S., Hinton, B., & Van Vliet, K. J. (2013). Why the dish makes a difference: Quantitative comparison of polystyrene culture surfaces. *Acta Biomaterialia*, 9(7), 7354–7361. <https://doi.org/10.1016/j.actbio.2013.02.035>
- Zhang, Q., Yu, Y., & Zhao, H. (2016). The effect of matrix stiffness on biomechanical properties of chondrocytes. *Acta Biochimica et Biophysica Sinica*, 48(10), 958–965. <https://doi.org/10.1093/abbs/gmw087>
- Zhang, Y., Reddy, V. J., Wong, S. Y., Li, X., Su, B., Ramakrishna, S., & Lim, C. T. (2010). Enhanced biomineralization in osteoblasts on a novel electrospun biocomposite nanofibrous substrate of hydroxyapatite/collagen/chitosan. *Tissue Engineering. Part A*, 16(6), 1949–1960. <https://doi.org/10.1089/ten.tea.2009.0221>
- Zotkin, M. A., Vikhoreva, G. A., Smotrina, T. V., & Derbenev, M. A. (2004). Thermal modification and study of the structure of chitosan films. *Fibre Chemistry*, 36(1), 16–20. <https://doi.org/10.1023/B:FICH.0000025532.80007.49>
- Zuo, W., Zhu, M., Yang, W., Yu, H., Chen, Y., & Zhang, Y. (2005). Experimental study on relationship between jet instability and formation of beaded fibers during electrospinning. *Polymer Engineering and Science*, 45(5), 704–709. <https://doi.org/10.1002/pen.20304>